

# Global flood hazard reduction by foreshore vegetation

MSc. thesis

V.T.M. van Zelst

Technische Universiteit Delft







The cover photo shows a wetland at the Powderhorn Ranch, the United States of America. This land along the Gulf coast provides a critical and fast-disappearing habitat for a variety of species. In addition, it is the perfect backdrop for a campground. "*It is hard to find a better place on the coast to wake up and watch the sunrise and put the sun to bed*", Carter Smith, executive director of the Texas Parks and Wildlife. Besides habitat for wild life, wetlands can mitigate flood hazard by damping incoming waves. Global wave damping by foreshore vegetation, including salt marshes and mangroves, is the subject of this thesis. The photo was found on: <https://www.nature.org/> (last accessed 1 May 2018)







# Global flood hazard reduction by foreshore vegetation

MSc. thesis

by

V.T.M. van Zelst

to obtain the degree of Master of Science  
at the Delft University of Technology,  
to be defended publicly on Monday July 2, 2018 at 09:30 AM.

Student number: 4169980

Thesis committee:	Prof. dr. ir. S.G.J. Aarninkhof,	TU Delft (chairman)
	Dr. ir. B. Hofland,	TU Delft
	Dr. B.K. van Wesenbeeck,	TU Delft / Deltares
	Dr. ir. J.T. Dijkstra,	Deltares







# Preface

This thesis concludes the Master of Science programme in hydraulic engineering at Delft University of Technology. The thesis is conducted at Deltares.

During my Multidisciplinary project in Sri Lanka, as part of the Master programme, I saw mangroves for the first time in real life. Studying the effect of foreshore vegetation for locations all around the globe, sometimes felt as planning a vacation. I am very glad to see, that eventually the wave damping effect of foreshore vegetation is mapped on a global scale.

First, I would like to thank my thesis committee for their support throughout the thesis. Big thanks to Jasper Dijkstra, my daily supervisor, who gave me often very useful feedback, shared his experience and helped among others to construct the look-up table. I would like to thank Bregje van Wesenbeeck for the opportunity to graduate in co-operation with Deltares, for scoping my research at the start, but also for her focus on the social impact of the global assessment. I would like to thank Bas Hofland especially for his feedback regarding hydrodynamics and in general for his fruitful comments during the committee meetings. Last, I would like to thank Stefan Aarninkhof, the chairman of the committee, for his trust in me to start this global adventure and his enthusiasm towards nature based solutions.

I would like to thank Vincent Vuik, which helped me in the first few months to choose a direction and his comments regarding the sensitivity analysis methodology. I would like to thank Hessel Winsemius, for the preliminary interview which took place in the city center of Delft, as it was Hessel's first vacation day. Furthermore, thanks for the comments during the Aqueduct days. I would like to thank Dirk Eilander, for all the help and the fruitful cooperation during the programming stage. I also would like to thank Gerit Hendriksen for his help setting up the local Geoserver. Furthermore I would like to thank all other colleagues at Deltares and the fellow interns, who often gave good advice.

At last, I would like to thank my family, in particular my parents for their support throughout my study. Special thanks to my girlfriend who always gave some extra support close to deadlines. Finally, I would like to thank my friends for the fruitful discussions regarding each others work.

*V.T.M. (Vincent) van Zelst  
Delft, June 2018*



# Summary

Global flood exposure simulations show that about 600 million people, of which 320 million in urban areas, are at risk to the impacts of global sea-level rise and changing storm intensity and frequency. Increasing availability of data and computational efficiency enables to assess flood hazard on a global scale. Implementation of salt marshes and mangroves as nature based flood defences has gained strong interest in the field of hydraulic engineering during the last decade, because these ecosystems can be an innovative, sustainable and cost-effective supplement to man-made traditional coastal protection measures. Foreshore vegetation can reduce wave heights substantially, resulting in reduced loads on coastal structures. This results in lower required dike heights, which leads to reduced investment and maintenance costs. In addition, foreshore vegetation can counter erosion, by accumulating sediments.

This thesis focuses on wave damping by salt marshes and mangroves and aims to map flood hazard reduction by foreshore vegetation on a global scale. It reveals areas where wave attenuation by foreshore vegetation is the most beneficial in terms of absolute wave reduction and reduced wave transmission. In addition, the research shows in which areas worldwide people could benefit the most from foreshore vegetation.

Wave attenuation by foreshore vegetation is studied on a global scale using transects which are aligned perpendicular to the Open Street Map (OSM) coastline, which is a common approach used in global studies. The position of the OSM coastline is sometimes situated in front of e.g. a marsh and sometimes at the back end of a marsh. In this study the transects have a length of 8 km, in order to capture the most foreshores. Because of data availability, the study area is bounded between the pole circle and a latitude of 60° S. The study area contains in total 495361 transects, which have an intermediate distance of roughly 1 km and are individually assessed. The assessment of each transect involves construction of the foreshore profile, derivation of vegetation presence and the corresponding vegetation type, determination of the governing hydrodynamic conditions and computation of wave propagation over the foreshore.

Wave damping by foreshore vegetation is determined by comparing the wave height at the end of the vegetated zone with bare foreshore situation. In general, foreshore vegetation does not prevent flooding, because the capacity to decrease surge levels is limited. For this reason a dike profile is assumed to be present at the end of the foreshore, as no global database of flood protection structures exists and e.g. dikes are too small to be visible on global topography maps. The assumed dike profile has an inner and outer slope of 1:3, no berm and no protective cover. A critical overtopping rate of 1 l/s/m is used, which is realistic for the assumed profile, but induces an overestimation of the effect of vegetation if in reality e.g. a well maintained grass cover is present. Dike height reduction by foreshore vegetation is obtained by subtracting the required freeboard for a vegetated foreshore from the required freeboard for a bare foreshore.

For each transect a foreshore profile is derived based on topobathymetric data from the Global Intertidal Elevation (GIE) map (20-30 m resolution, ~1 m vertical accuracy) or MERIT-GEBCO (MG). MG is a merged set of MERIT elevation (3 arc-seconds resolution, ~2 m vertical accuracy) and GEBCO bathymetry (30 arc-seconds resolution, ~10 m vertical accuracy). GIE data is based on the time-ensemble averaged probability of inundation and is combined with tidal statistics from the global tide model FES2012. Due to higher accuracy and resolution foreshore derivation based on GIE is preferred, however the GIE set is lacking in some instances as it falsely identifies land or open sea as part of the intertidal zone. In these cases the foreshore is derived based on MG.

Vegetation presence is based on the VegGEE map (resolution 10-30m) which uses the Normalized Difference Vegetation Index (NDVI) on images of Sentinel-2A and Landsat-8. Once vegetation is present, the corresponding cover type is derived from the salt marsh map and mangroves map. In case the former have no data, for a specific transect, GlobCover and Corine Land Cover (CLC) are consulted for locations outside and inside Europe respectively. Global wave characteristics are derived from ERA-Interim reanalysis and extreme water levels from the Global Tide and Surge Model (GTSM). The developed algorithm is unique, as it combines GIE, MG, the salt marshes and mangroves map, GlobCover, CLC and GTSM in order to derive vegetated foreshore profiles on a global scale for a variation of possible transect configurations.

The nearshore wave height is based on a depth limited criterion at the start of the (vegetated) foreshore. Results from case studies on the Western Scheldt, The Netherlands, and Chesapeake Bay, United States, show an overestimation of the nearshore wave height in sheltered areas due to this approach. The induced error is the largest for sheltered areas which have high extreme water levels, because the incoming wave is not or only partly depth limited. The significant wave height at the start of the vegetated zone was overestimated on average by 1.1 m with a standard

deviation of 0.6 m for vegetated transects in the Western Scheldt. For the same location, the wave height reduction by foreshore vegetation is overestimated with a RMSE of 0.15 m, which is solely induced by the depth limited approach.

Wave propagation over the vegetated foreshore is determined based on a dataset of XBeach pre-runs, referred to as the look-up table. This approach is chosen over individual XBeach runs for two reasons: (1) due to the high amount of transects a computational attractive method is preferred, (2) individual XBeach runs might give the impression of accurate results, which is impossible taking into account the use of global datasets. The look-up table is constructed based on 32000 XBeach runs and contains data for various combinations of wave heights, water levels, wave steepnesses, foreshore slopes and vegetation widths and cover types (bare foreshore, salt marshes, mangroves).

The datasets used in the global assessment can be split into three categories: (1) bathymetry and elevation data, (2) hydrodynamic data and (3) vegetation data. Most input data uncertainty is induced by the global bathymetry and elevation data, due to the lack of vertical accuracy of GIE and MG. The depth limited approach induces model uncertainty. However, the bed profile uncertainty is dominant because the nearshore wave height determination and foreshore wave propagation highly depends on the derived profile.

A Morris sensitivity analysis (SA) is performed for two transects in the Western Scheldt using the global datasets and approach (SA global), but also using local topo-bathymetric data, SWAN and XBeach simulations (SA local). The wave period appeared as the most influential parameter in sheltered areas based on the global SA results. The use of the offshore wave period in sheltered areas, results in lower wave attenuation as longer waves are harder to attenuate. While the schematization is wrong, the use of the offshore wave period compensates partly for the overestimation induced by the depth limited approach. Next the profile characteristics are the most influential, followed by uncertainty in the water level (vegetation width) in case of an extensive (small) vegetated foreshore profile. Most wave attenuation takes place in the first hundreds of meters, which explains the minor role of vegetation width for an extensive vegetated transect. In SA local are also the salt marsh characterization parameters included. The stem density, stem height and stem diameter are the most influential parameters, because they come with large uncertainties due to seasonal influences.

In addition, the influence of vegetation characteristics is studied based on a case study for the East coast of Australia covering about 1100 km of coastline along which both salt marshes and mangroves are present. Variation exists between different salt marsh and mangrove types. In addition, salt marshes are heavily affected by seasonal influences as biomass can reduce by 80 % during winter at higher latitudes. The schematization for salt marshes and mangroves in the global assessment are conservative and more optimistic properties can be found in literature. The case study results show that decreased biomass has a strong impact on wave attenuation by salt marshes, as the mean wave transmission reduction decreased from roughly 22 % to 4 %. The young pioneer mangroves used in the global assessment give the most conservative results of all studied mangroves types. For the other studied mangrove types, maximum increase in wave transmission reduction of 15 % is observed with respect to the global run type.

The results of the global assessment show that 31 % of the coastline in the study area is vegetated, of which more than half has a vegetation width that is larger than 100 m and 5% has a vegetation width exceeding 1000 m. Along 5% (15%) of the studied (vegetated) coastline is a significant wave height reduction observed of at least 30 centimeters, giving 1 in 100 years storm conditions. Hot spots where wave attenuation in absolute terms exceeds 75 cm are found at James Bay in Canada, the coasts of Columbia, Brazil, Guinea, Tanzania, Mozambique, Madagascar, India, Bangladesh, Myanmar, Thailand, Vietnam, China, Indonesia, Papua New Guinea, Australia and a few locations in the UK and France.

The reduction in wave transmission along the vegetated field of a transect is used as measure of wave attenuation in relative terms. This measure indicates hotspots along the Gulf of Mexico and overall highlights areas in South-East Asia where extensive mangrove fields can be found. Evaluation of more than 150 000 vegetated transects showed that mangroves and salt marshes are able to reduce wave transmission by a maximum of roughly 60 % and 40 % respectively. These results were found for both an exposed environment and a sheltered environment, but depends on the vegetation characterization in the model. In other words, for a denser vegetation characterization larger wave transmission reduction results would be obtained. In addition, the results are limited by the maximum vegetation width (2000 m) and foreshore slope (1:2000) in the look-up table.

The linkage between the global assessment results and the Low Elevation Coastal Zone Urban-Rural population map shows that 28 % (10 %) of the vegetated transects in rural (urban) areas reduce the incoming wave height by at least 20 centimeters. Correlation of the results with the human development index (HDI) show that especially in countries at the South-East coast of Africa and in Asia, coastal vegetation can have an important role, as countries with a low or medium HDI are likely to have less governmental strength, knowledge or financial resources to take effective measures against flooding.

The dike height reduction results are summed per country and are translated to monetary values using an unit price per meter dike height per kilometer which is related to the HDI per country. The results show that Tanzania, Guinea-Bissau and Burma are the top 3 countries experiencing the largest wave damping by foreshore vegetation relative to

their coastline length, with a maximum of 0.75 m/km dike height reduction. Together Australia, The United States of America and Canada can potentially save 208 billion USA dollar, due to reduced dike investment or maintenance costs. The total potential dike coast reduction per country has a bias towards high developed countries with a long coastline. The total dike reduction cost relative to the Gross Domestic Product (GDP) underlines the importance of coastal vegetation for Small Islands Development States (SIDS). Countries such as the Solomon Islands and the Federated States of Micronesia deal with limited resources and remoteness. For this reason, taking flood prevention measures is unattractive from an economic point of view. Under this assumption present coastal vegetation will, at least, lower wave impact.

The performed global flood hazard reduction assessment is unique, as it uses global open source data to express quantitatively wave damping by salt marshes and mangroves on a global scale. The results show the effect of foreshore vegetation in terms of wave attenuation, reduced dike height and the potential social impact. This research solely focused on wave damping by foreshore vegetation, however salt marshes and mangroves have more positive effects. Including these effects in a global assessment, e.g. accumulation of sediments, will probably further underline the importance of coastal vegetation. Before implementation of foreshore vegetation in dike assessments, behavior of vegetation during extreme conditions, e.g. influence of uprooting, should be further investigated. In addition, seasonal changes and long term resilience of vegetation should be tackled. Despite these knowledge gaps, based on the performed analysis can be concluded that foreshore vegetation has a high potential to mitigate flood hazard at various areas around the globe.

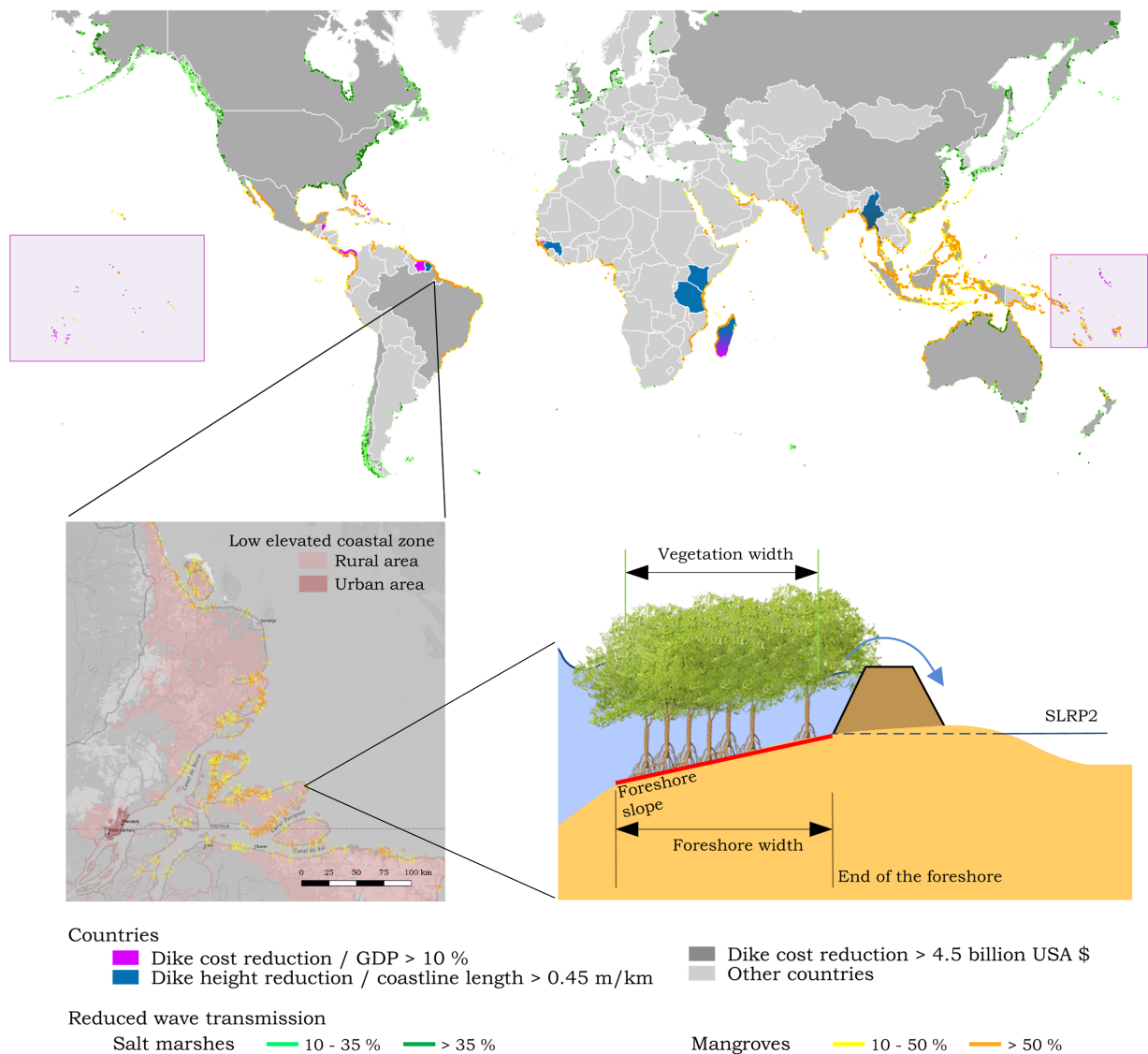


Figure 1: Overview figure global flood hazard reduction by foreshore vegetation

# Contents

<b>Preface</b>	<b>iii</b>
<b>Summary</b>	<b>v</b>
<b>I Initiation</b>	<b>1</b>
<b>1 Introduction</b>	<b>3</b>
<b>2 Vegetated foreshore dike systems</b>	<b>7</b>
2.1 Foreshore vegetation . . . . .	7
2.2 Hydrodynamics . . . . .	11
2.2.1 Wave propagation . . . . .	11
2.2.2 Wave propagation over vegetated fields . . . . .	11
2.3 Dike failure due to wave overtopping . . . . .	17
2.3.1 Wave run-up . . . . .	17
2.3.2 Wave overtopping . . . . .	17
2.4 Wave modelling. . . . .	19
2.4.1 Nearshore wave transformation . . . . .	19
2.4.2 Wave-vegetation interaction . . . . .	19
2.5 Foreshore vegetation characterization parameters . . . . .	21
<b>II Global framework</b>	<b>25</b>
<b>3 Conditions</b>	<b>27</b>
3.1 Global bathymetry and elevation data . . . . .	27
3.2 Global hydrodynamic data . . . . .	28
3.3 Global vegetation data . . . . .	28
3.4 Global transect data. . . . .	30
<b>4 Model approach</b>	<b>31</b>
4.1 Transect definitions . . . . .	32
4.2 Step 1-2: Loading data from global datasets for transect . . . . .	32
4.3 Step 3: Definition of foreshore parameters . . . . .	33
4.4 Step 4: Definition of vegetation parameters . . . . .	36
4.5 Step 5: Determination of wave attenuation . . . . .	39
4.6 Step 6: Calculation of required dike freeboard . . . . .	40
<b>5 Results</b>	<b>41</b>
5.1 Wave height reduction . . . . .	42
5.1.1 Wave attenuation by foreshore vegetation in absolute terms. . . . .	42
5.1.2 Wave attenuation by foreshore vegetation in relative terms . . . . .	43
5.1.3 Model behavior . . . . .	44
5.2 Crest height reduction . . . . .	50
5.3 Social impact of flood hazard reduction by foreshore vegetation . . . . .	53



<b>III</b>	<b>Local framework</b>	<b>57</b>
<b>6</b>	<b>Case study Eastern and Western Scheldt</b>	<b>59</b>
6.1	Site characteristics . . . . .	59
6.1.1	Bathymetry and elevation . . . . .	60
6.1.2	Hydrodynamic boundary conditions . . . . .	60
6.2	Model approach . . . . .	60
6.2.1	Nearshore wave propagation. . . . .	60
6.2.2	Derivation of foreshore location . . . . .	61
6.2.3	Foreshore wave propagation. . . . .	62
6.3	Results . . . . .	62
6.3.1	Wave attenuation by foreshore vegetation . . . . .	63
6.3.2	Wave attenuation by foreshore vegetation in relative terms . . . . .	64
6.4	Morris sensitivity analysis. . . . .	65
6.4.1	Model approach . . . . .	65
6.4.2	Results . . . . .	66
6.4.3	Conclusion. . . . .	67
<b>IV</b>	<b>Interpretation</b>	<b>69</b>
<b>7</b>	<b>Discussion</b>	<b>71</b>
7.1	Determination of foreshore profiles. . . . .	71
7.1.1	Input data . . . . .	71
7.1.2	Foreshore methods . . . . .	72
7.2	Determination of the vegetated zone . . . . .	74
7.3	Hydrodynamics. . . . .	75
7.3.1	Extreme water levels . . . . .	75
7.3.2	Wave propagation . . . . .	75
7.4	Dike location and schematization. . . . .	76
<b>8</b>	<b>Conclusion</b>	<b>77</b>
<b>9</b>	<b>Recommendations</b>	<b>79</b>
<b>V</b>	<b>References</b>	<b>83</b>
	<b>Bibliography</b>	<b>85</b>
<b>VI</b>	<b>Appendices</b>	<b>93</b>
<b>A</b>	<b>Vegetated foreshore dike systems</b>	<b>95</b>
<b>B</b>	<b>Sensitivity analysis methods</b>	<b>97</b>
<b>C</b>	<b>Offshore to nearshore wave transformation methods</b>	<b>101</b>
<b>D</b>	<b>Global flood hazard assessment</b>	<b>109</b>
D.1	Hydrodynamic boundary conditions . . . . .	110
D.2	Vegetation width . . . . .	117
D.3	Foreshore slope . . . . .	120
D.3.1	Foreshore slopes in global flood hazard assessment . . . . .	120
D.3.2	Foreshore slopes in Mediterranean sea. . . . .	122
D.4	Wave attenuation . . . . .	124
D.5	Crest height reduction . . . . .	126
D.6	Crest height reduction results per country . . . . .	127
D.7	Pilot study results for look-up table . . . . .	148
<b>E</b>	<b>Case studies</b>	<b>151</b>
E.1	Western Scheldt, The Netherlands . . . . .	152
E.2	Queensland, Australia. . . . .	160
<b>F</b>	<b>Vegetation characterization in numerical models</b>	<b>161</b>



# I

## Initiation



# Introduction

## Project context

Global flood exposure simulations show that about 600 million people, of which 320 million in urban areas, are at risk to the impacts of coastal flooding ([McGranahan et al., 2007](#)). Rapid urbanization has created tens of megacities in coastal settings, these areas are at risk to impacts of global sea-level rise and changing storm frequencies ([Nicholls, 1995](#)). The Low Elevation Coastal Zone (LECZ) is defined as the contiguous area along the coast that is situated less than 10 m above sea level. Almost two-thirds of urban settlements, with populations greater than 5 million fall in this zone ([McGranahan et al., 2007](#)). Analysis on urban expansion indicated that urban land expansion has been occurring faster in this zone than in other areas. Continuing population growth and urbanization will add 2.5 billion to the world's urban population, of which nearly 90 % is concentrated in Asia and Africa ([UNDESA, 2014](#)). Global flood exposure simulations show that an enormous amount of people and assets will be exposed to coastal flooding in coming decades ([Güneralp et al., 2015](#); [Jongman et al., 2012](#)).

Increasing availability of data and computational efficiency makes it possible to assess coastal flood risk on a global scale, although with large uncertainties, e.g. due to relatively low spatial resolution ([Hinkel et al., 2014](#); [Muis et al., 2015a](#)). Estimating flood risk and assessing possible interventions requires proper understanding of the local environment and the natural and socio-economic conditions. The risk depends largely on presence of flood protection measures, of which no global database exist ([Jongman et al., 2012](#)). Besides man-made constructions, ecosystems can be a supplement to man-made coastal protection measures [Van Wesenbeeck et al. \(2014\)](#). The latter, concerning salt marshes and mangroves, has gained strong interest in the last decade. The main reason for this trend is the strong need for innovative, sustainable and cost-effective coastal protection measures which can cope with climate change ([Borsje et al., 2011](#)).

Recently quite some research is executed on wave reduction by salt marshes and mangroves which can potentially be used as complementary flood protection measure. Outcomes show that vegetated foreshores can reduce wave loads significantly ([Anderson et al., 2011](#); [Brinkman, 2006](#); [Horstman et al., 2014](#); [Möller et al., 1996](#)). This indicates the potential of vegetation as additional coastal flood defence measure. Large deltas can also benefit of storm surge mitigation by mangroves and salt marshes ([Coppenolle et al., 2018](#)), however extensive wetlands are needed to reduce surge levels and flooding is hard to prevent completely. Integrating nature in coastal defence systems counters some knowledge gaps. Two main pointed knowledge gaps are: 1. the protective value of vegetation during extreme storm conditions, 2. knowledge on long-term resilience ([Bouma et al., 2014](#)). The first gap aims to deal with i.e. swaying, breaking of vegetation during extreme conditions. Most studies focus on wave attenuation rates by vegetation during moderate wave conditions, these rates cannot be applied directly to storm conditions ([Vuik et al., 2016](#)).

Ecosystem based designs should be developed and tested as engineering solutions according to standards for probability of failure ([Van Wesenbeeck et al., 2014](#)). Probabilistic calculations can only be performed in case enough data is available to estimate uncertainties. Less is known about these uncertainties and their influence on the failure probability or design of a foreshore-dike system. Additionally, the interrelationship between uncertainty by vegetation and other uncertainties, i.e. hydraulic conditions, in a (global) flood hazard assessment framework are still undiscovered.

Mapping the potential of wave damping by salt marshes and mangroves on a global scale and assessing uncertainties can point out the possible benefit of including vegetation in flood hazard assessments. This information can be very useful for decision makers, in relation to nature conservation and flood prevention in coastal areas, i.e. green belt policies.

## Research framework

### Objective

The research objective is getting insight in the potential of flood hazard reduction by foreshore vegetation worldwide. The corresponding uncertainty and the interrelation with uncertainty induced by other factors in a global and local coastal flood hazard assessment framework is assessed by performing a sensitivity analysis using global and local data.

### Main research questions

1. In which areas worldwide is wave attenuation by foreshore vegetation the largest?
2. Where do people worldwide potentially benefit the most of wave attenuation by foreshore vegetation?
3. How is uncertainty in flood hazard reduction due to wave attenuation by foreshore vegetation apportioned over the input parameters?

### Sub questions

- How are important parameters for wave propagation in a vegetated foreshore dike system distributed?
- Which method is appropriate to include the effect of foreshore vegetation in flood hazard assessments in case of dike failure due to wave overtopping?
- What is the interrelation between uncertainties which are induced in a *local* and *global* flood hazard assessment which includes wave damping by vegetation?
- What is the difference in uncertainty distribution in a *local* and *global* flood hazard assessment framework?

### Spatial framework

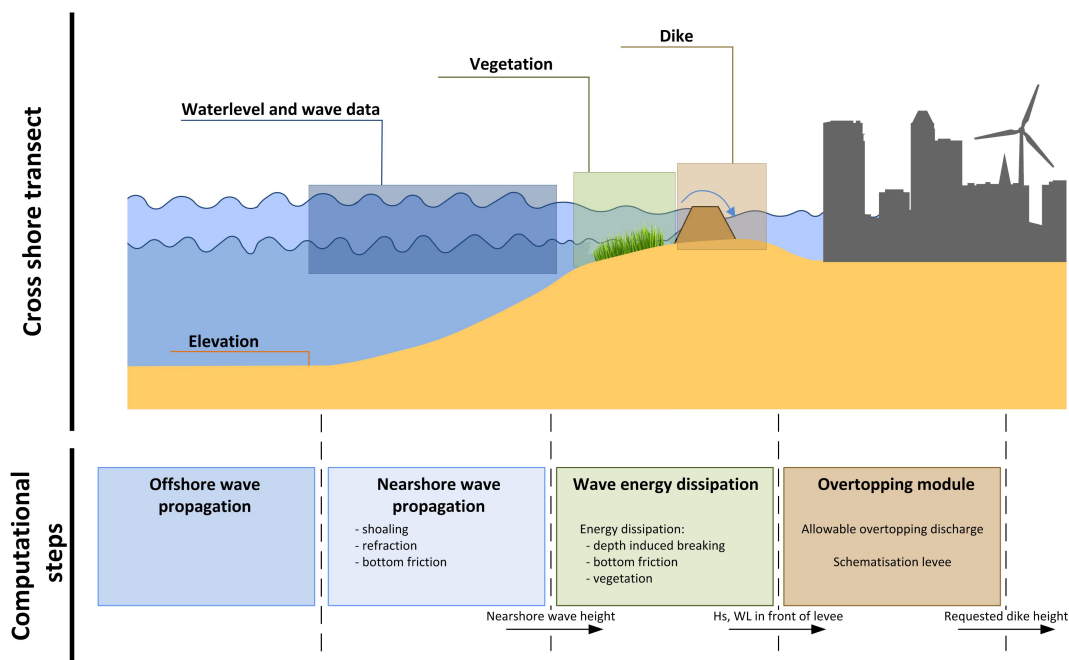


Figure 1.1: Research framework: flood hazard reduction by foreshore vegetation

In order to assess flood hazard reduction by foreshore vegetation several steps have to be taken. An arbitrary cross section is given in figure 1.1. A deep water wave entering shallow water is affected by the decreasing water depth. Closer to shore wave energy is dissipated by bottom friction, wave breaking or interaction with vegetation. Eventually the wave can overtop the dike resulting in water entering the hinterland. A maximum wave overtopping discharge results in a requested dike height.

### Constraints

The research focuses on wave propagation, wave-vegetation interaction and dike overtopping. Possible storm surge reduction by foreshore vegetation is neglected. The bed level is assumed as static and no morphological processes are included. Dike failure due to wave overtopping is assumed and no other failure methods are considered. Additionally, inundation depths and risk of the hinterland are out of the scope of this research. Last, global data sources are coarse and for this reason outcomes of this research should not be used for design purposes.

## Methodology

A global hazard assessment is performed to assess the potential of wave damping by foreshore vegetation on a global scale. Wave damping is determined by comparing the wave height at the end of the vegetated zone with a bare foreshore situation. The effect of foreshore vegetation is determined using shore normal transects for which possible wave damping by vegetation is calculated individually. The use of global datasets makes it challenging to determine a correct foreshore location. In order to derive an accurate foreshore profile and corresponding vegetation parameters different methods are developed. As the use of a numerical model is not feasible for this spatial scale a different method, which approximates the outcomes of a numerical model, is further developed.

The results of the global assessment are compared with known relations from earlier research to check correct model behavior. In the global framework several different coastal regimes are countered, for instance different water levels, bed slopes, wave heights and wave periods, which gives insight in sensitivity to different conditions. The social impact of flood hazard reduction by foreshore vegetation is indicated by projecting the wave damping results on an urban population map for the low elevation coastal zone (LECZ), by making a link to the human development index and by calculating potential dike cost reduction per country.

In a local framework the results of the global assessment are compared with results for a case study location in the Netherlands. This comparison gives insight in the error of the global model and shows which input uncertainties and model uncertainties are responsible for the observed deviation. The sensitivity to input uncertainty is studied using both the global and local approach.

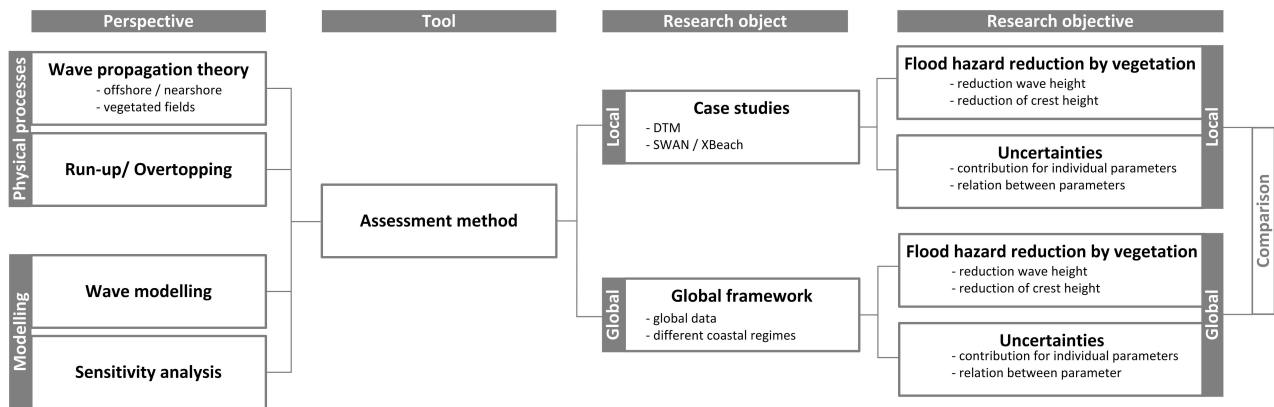


Figure 1.2: Research methodology

## Outline

A transect in the global flood hazard assessment runs to several consecutive steps as shown in figure 1.1. Information about the processes included in these steps are presented in Chapter 2. In order to develop and perform a global assessment additional information is required about datasets with global coverage. The datasets used in the global assessment are introduced in Chapter 3. In Chapter 4 is described how the global model calculates wave attenuation by foreshore vegetation for an individual transect. In addition are intermediate results of the global study presented in this chapter. The results in terms of wave damping and reduced crest height are presented in Chapter 5. In this chapter is also the model behavior evaluated. Chapters ?? and 6 are part of the local framework, in which the performance of the global model is compared with numerical simulations using detailed bathymetry and elevation data. Furthermore the sensitivity to input uncertainty and model uncertainty is presented in this section. Finally the discussion, conclusion and recommendations are presented Chapters 7, 8 and 9.





## Vegetated foreshore dike systems

### 2.1. Foreshore vegetation

A salt marsh is a wetland that is defined as a flat poorly drained area that is subject to frequent flooding by salt water and usually covered with a thick mat of grassy salt tolerant plants (NRCS, 2007). Wetland plants are located around the globe in marshes, at the margins of bays and estuaries and along protected oceans shorelines. Salt marshes form along coastlines where disturbances from water motion and ice are moderate. In the tropics, between 30 ° N and 30 ° S, salt marshes are mostly replaced by mangrove forests (Pennings and Bertness, 2001). Most of the salt marshes can be found in Asia (Giri et al., 2011). Foreshore vegetation is subjected to water level changes on a daily and seasonal basis due to tides and fresh water run-off. Sea water flows in and out the area via a network of tidal channels.

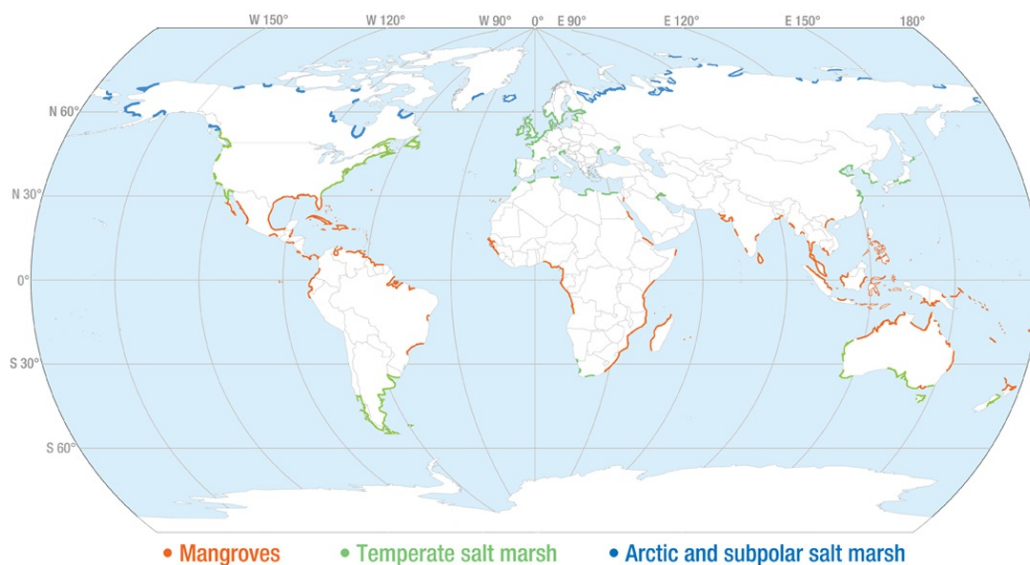


Figure 2.1: Distribution of coastal wetlands of the world (Scott et al., 2014)

#### Salt marsh species and distribution

Globally different salt marsh species can be distinguished. *Spartina* species (cordgrass) dominate many temperate coastal salt marshes. *Spartina alterniflora* occurs mostly at the seaward edge and is the dominant plant of many U.S. east coast and Gulf of Mexico salt marshes. A zone of *Spartina patens* is often found inland from the *S. alterniflora* zone in the U.S. and along the Gulf Coast. (Gordon and Cranford, 1995). Other salt marsh species with less frequent presence along the U.S. East coast are: *Juncus gerardii* (rush), *Distichlis spicata* (spike grass) and *Salicornia europaea* (glasswort). At the U.S. West coast salt marshes are less extensive, but show more diverse species. In Europe salt marshes are located along the Atlantic coasts, the North Sea, the Baltic Sea and the Mediterranean Sea. The most seaward areas are dominated by *Spartina anglica*, *Salicornia europaea*, *Spartina maritima* and *Salicornia dolichostachya* (Cronk and Fennessy, 2001). Besides areas in North America and Europe, salt marshes can be found in South America, Australia and in parts of Asia.

Continent	Coastline	Extension [km <sup>2</sup> ]	Dominant vegetation
North America	North Atlantic	500	<i>Spartina</i> , <i>Phragmites</i>
	South Atlantic, Gulf Coast	15.000	<i>Spartina</i> , <i>Juncus</i>
	Pacific	440	<i>Salicornia</i> , <i>Spartina</i>
	Atlantic	2300	<i>Spartina</i> , <i>Juncus</i>
Europe	All	1400	<i>Spartina</i> , <i>Salicornia</i>
Asia (Japan, Korea, China)	Pacific	25.000	<i>Chenopods</i> , <i>Phragmites</i>
Australia, New Zealand	Southern (temperate)	772	<i>Sarcocornia</i> , <i>shrubs</i>
South Africa	Southern	70	<i>Sarcocornia</i> , <i>Spartina</i>

Table 2.1: Global salt marsh surface area and dominant species

### Salt marsh zonation

Salt marsh species show a zonation based on their tolerance to e.g. salinity levels, tidal regime and soil oxygen availability (Cronk and Fennessy, 2001). Salt marshes are normally found on mud flats, but also occur on sand flats. Based on topography and plant characteristics, salt marshes are divided in zones, e.g. in the lower, medium and high marsh area. These zones are related to the number of tidal submergences per year (Adam, 1990). In literature sometimes a pioneer zone is distinguished situated at the most seaward edge. In figure 2.2 a typical zonation and corresponding tidal levels are shown including some dominant species. Two types of e.g. *S. alterniflora* can exist in the same marsh: a tall and short form. The tall form (1-3m) dominates along banks of channels and the most seaward area. The shorter form (10-80 cm) is found more inland. The height difference can be explained by the differences in conditions (Anderson and Treshow, 1980), e.g. higher salinity and lower oxygen levels.

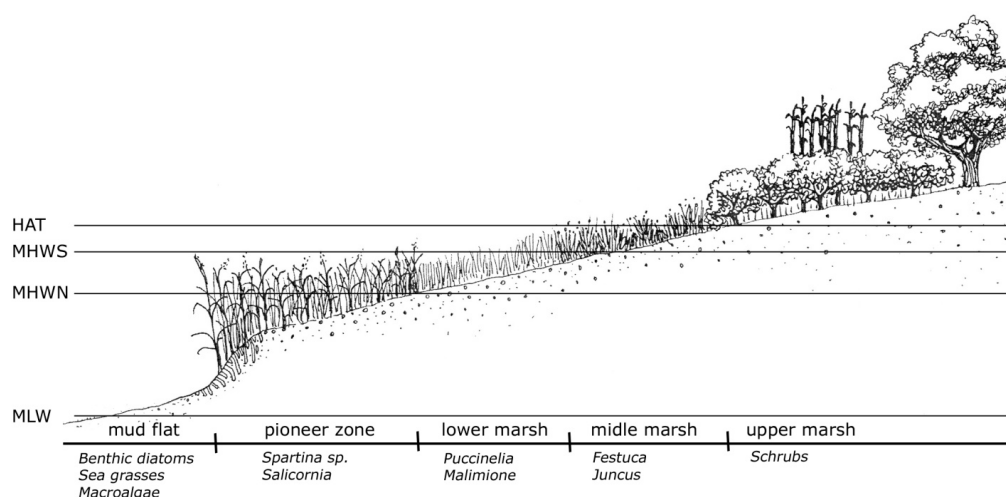


Figure 2.2: Typical salt marsh zonation (van Belzen, 2013)

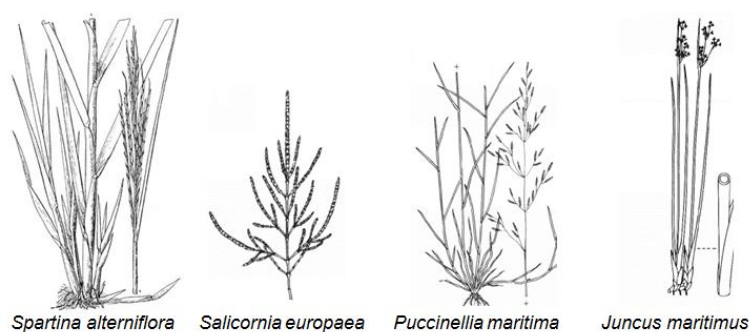


Figure 2.3: Frequent occurring salt marsh species (Rothmaler, 2001)

### Geomorphological classification

Overtime several geomorphological classifications for marsh systems are made (Dijkema, 1987; Pye and French, 1993). Ranging from open coast formations with exposed sand flats to more protected back-barrier systems in estuaries. Marshes within estuaries tend to be muddy in case of relative high river influence, for insignificant river discharge marshes tend to be sandy (Allen, 2000).

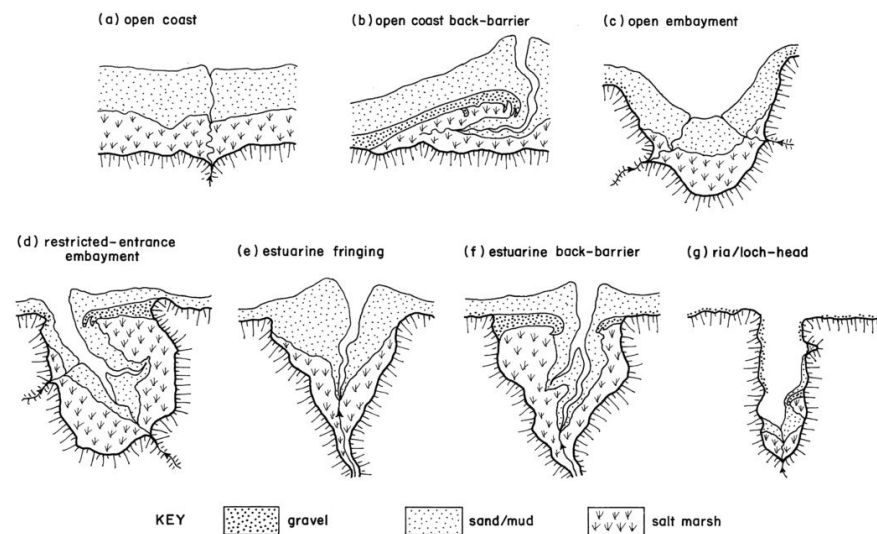


Figure 2.4: Geomorphological classification of salt marshes (Allen, 2000)

### Temporal and latitudinal variation

In temperate areas seasonal changes have a large impact on the vegetation density and biomass. The growing season in Europe starts in March/April and ends in September/November (Möller and Spencer, 2002; Neumeier, 2005; Vuik et al., 2017). During the winter a decline in biomass is observed with a minimum in February/March, with a maximum density decrease of roughly 85%. In North America the same trend is observed (Chaisson, 2012; Dame and Kenny, 1986; Rogers et al., 2016). The productivity is mainly influenced by salinity, elevation, nutrition and temperature. (Chaisson, 2012) states that inter annual density variation in *Spartina alterniflora* stands in the USA are mainly explained by precipitation differences. Higher precipitation results in lower salt stress, which leads to increased growth (Crain et al., 2004). (Kirwan et al., 2009) studied latitudinal variation among coastal wetlands in North America. The study found a strong latitudinal gradient in productivity, with a  $27 \text{ gm}^{-2}\text{yr}^{-1}$  biomass increase with an increase of mean annual temperature by  $1^\circ\text{C}$ .

### Long term resilience

One of the knowledge gaps pointed out by (Bouma et al., 2014) is long term resilience of vegetation. Results of regional assessments show, based on static landscape assumptions, that 20-45 % of coastal salt marshes will be submerged at the end of this century due to sea level rise (Craft et al., 2009; McFadden et al., 2007). This static landscape approach results in an unrealistic estimation, because coastal ecosystems are highly dynamic and have significant capability to adjust to changing sea levels via several non-linear feedback mechanisms. In order to prevent erosion vertical accretion should be at least equal to the rate of relative sea level rise. To a certain extend increasing inundation depths will result in higher sediment deposition rates (Reed, 1995). Furthermore, vegetation growth is higher at lower elevations than higher in the marsh (Morris et al., 2002). These mechanisms can play a key role in the preservation of salt marshes.

In contrast to earlier work, (Kirwan et al., 2010) used numerical simulations which include non-linear feedback mechanisms to predict the ability of salt marshes to cope with rising sea levels. Results show that marshes are to a certain degree capable to adapt to changing sea levels. However, beyond a depth capable of supporting vegetation, elevation is quickly lost relative to the rising sea level. Several maximum sea level rise (SLR) rates are defined depending on the tidal range and the suspended sediment concentration. Areas with low sediment concentrations and a small tidal range are vulnerable to sea level rise. In these areas a sea level rise of several mm per year can already result in loss of land. High sediment rates and a larger tidal range make a salt marsh more resilient against SLR. Besides these natural processes, human activity e.g. water extraction also influences the vulnerability of marshes to sea level rise, because it can result in increasing subsidence rates (Kirwan and Megonigal, 2013).

### Mangrove species and distribution

Mangrove trees are solely found in the tropics, between 30° N and 30° S. The study of [Giri et al. \(2011\)](#) showed that only 15 countries are containing approximately 75 % of world's mangroves. Most mangroves can be found in a small band between 5° N and 5° S. Asia holds about 42 % of world's mangroves, of which about 22 % is situated in Indonesia. In Africa 20% of the mangroves can be found. The mangroves are mainly situated in Guinea, Guinea-Bissau, Mozambique and Madagascar. In America, mainly in the countries Brazil, Mexico and Cuba mangroves can be found. In total America holds about 20 % of world's mangroves.

Mangrove types are commonly divided in three main categories: *Rhizophora*, *Avicennia* and *Laguncularia*.

*Rhizophora* mangroves are recognized by their long prop roots, which start from the trunk and diverge in many individual roots towards bed. This dense network of roots enables this type of mangrove to efficiently attenuate incoming waves. *Avicennia* mangroves have vertical roots, pneumatophores, which stick out the bed. These vertical roots enable the mangrove to get oxygen, even when partially submerged. *Laguncularia* mangroves can be found higher in the coastal zone, e.g. around lagoons. This mangrove type can have both prop roots or pneumatophores.

### Mangrove zonation

Comparable to salt marshes, mangroves also show zonation based on the governing conditions in the coastal zone. In the most common zonation, *Rhizophora* mangroves dominate the lower coastal zone and the *Avicennia* the higher zone. This is explained by the root network of the *Rhizophora* which is able to resist incoming waves. Most seaward, young *Rhizophora* mangroves can be found, commonly called *Pioneer* mangroves. These mangroves have a dense root network, however they are prone to uprooting due to their young age.

### Vertical layering

Opposite to salt marshes, mangroves have a clear vertical layering, which influences their ability to attenuate waves. A mangrove tree can be divided into three sections: (1) the root layer, (2) the trunk and (3) the canopy. The root layer results in effective wave damping in shallow water. However, wave attenuating capacity lowers for higher water levels, till eventually the canopy is reached. The last is uncommon as most mangroves can have considerable heights, e.g. 10 m is not rare. An diverse mangrove forest is preferred, taking into account the effect of vertical layering on wave attenuation.

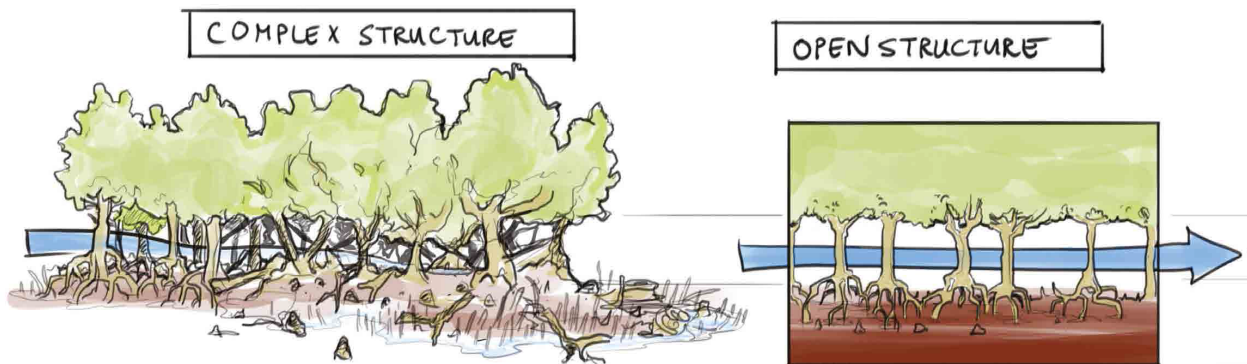


Figure 2.5: The effect of vertical layering on wave attenuation capacity of mangroves. *Rhizophora* (left), *Avicennia* (right) ([Spalding et al., 2014](#))

### Wave attenuation by mangroves

Past decades various field studies are performed, mainly in Asia, in order to get better understanding of wave attenuation by mangroves. In the research of [Brinkman \(2006\)](#), an overview of previous studies is presented. Wave attenuation rates range between 1 % to 15 % per 100 m for young mangroves and 10's % for older mangroves, in which wave attenuation is described by:

$$\text{Wave attenuation} = \Delta H / H_{\text{incident}} \quad (2.1)$$

## 2.2. Hydrodynamics

### 2.2.1. Wave propagation

#### Waves in deep water

Waves are generated by air-pressure fluctuations at the sea surface, these fluctuations are mainly due to wave-induced wind variations. In deep water, where waves are unaffected by the seabed, quadruplet wave-wave interactions redistribute energy among the spectrum (Holthuijsen, 2010). For wind waves this results in a downward shift of the spectral peak, which gives the JONSWAP spectrum. Outside the generation area wind waves turn into swell waves due to directional and frequency dispersion. The steepness of swell waves is, in contradiction to wind waves, too low for effective redistribution of energy. For this reason a swell spectrum is not a JONSWAP spectrum, but has a narrow frequency and directional band. In deep water energy dissipation occurs only due to white capping, which occurs when the wave steepness becomes to large.

#### Waves in coastal waters

As waves propagate to coastal waters they are affected by the bottom. Depth induced processes are *shoaling*, *refraction*, (increased ) *bottom friction* and *depth-induced breaking*. The next descriptions are from (Holthuijsen, 2010). *Shoaling* is variation of waves in the direction of wave propagation due to depth-induced changes of group velocity. As the group velocity slows down, the amplitude is increased to conserve energy. *Refraction* is turning of waves towards more shallow areas, due to depth -or current induced change of the phase speed. *Depth-induced breaking* occurs close to shore in the surfzone where the wave height becomes to large relative to the water depth, which induces breaking. *Diffraction* is not directly induced by decreasing depth. *Diffraction* is turning of waves towards areas with lower amplitudes along the wave crest. This phenomenon can in particular be observed in presents of headlands or breakwaters. Below the water surface particles are in motion linked to the motion of the water surface. In shallow water the orbital paths have an ellipsoidal shape which flattens towards the bottom. It is this particle motion which interacts with vegetation. The amplitude of the horizontal orbital velocity is described by:

$$\hat{u}(z) = \omega \frac{H}{2} \frac{\cosh(k(z+h))}{\sinh(kh)} \quad (2.2)$$

### 2.2.2. Wave propagation over vegetated fields

Waves which propagate over vegetated fields lose energy due to wave-vegetation interaction. A dynamic coupling exists between underwater vegetation and water flow. The vegetation's structure is influenced by hydraulic loads, while the wave attenuation is a function of the vegetation's structure as well. Furthermore the state of vegetation changes, e.g. seasonally changes overtime or breaking/bending under high hydraulic loads (Seymour et al., 1989).

Wave damping by vegetation depends on plant characteristics, e.g. geometry, buoyancy, density, stiffness and spatial configuration and on wave characteristics, mainly wave height, period and direction (Mendez and Losada, 2004). Finding a general formulation for wave attenuation over vegetated fields is difficult, due to large variability in plant and wave characteristics. Despite these difficulties several researchers formulated different methods for wave attenuation by vegetation.

#### Drag force approach

A formulation is presented by (Dalrymple et al., 1984) to describe dissipation of wave energy over a vegetated field (marsh grass, seaweed, trees). The vegetation was modelled as an array of rigid cylinders, which is often still the approach nowadays. His derivation, presented in Appendix A, assumes linear wave theory and a flat bottom and starts with the conservation of wave energy, equation 2.3, which includes a dissipation term solely due to wave-vegetation interaction. Work done by waves acting on the cylinders is described by a quadratic drag formulation described in equation 2.4. He noted that the choice of the drag coefficient,  $C_D$ , is highly dependable on the flexibility of the considered plant.

$$\frac{\partial(Ec_g)}{\partial x} = -\epsilon_D \quad (2.3)$$

$$\epsilon_D = \int \overline{F_x u} dz = \int_{-h}^{s-h} \frac{1}{2} \rho C_D A u |u| \cdot u dz \cdot N \quad (2.4)$$

Where  $F_x$  = horizontal drag force,  $u$  = horizontal orbital velocity,  $A$  = drag area and  $N$  = amount of stems per unit area.

In the above presented approach the effects of vegetation are only included in the dissipation term. This method is not valid in case vegetation influences the local flow field significantly. (Kobayashi et al., 1993) proposed a different approach based on continuity and momentum equations for small amplitude waves propagating over submerged vegetation. The rigid cylinder approach is again used. The drag force is linearized and formulated as:

$$F_x \approx \frac{1}{2} \rho C_D b N |u| u \approx \rho D u \quad (2.5)$$

In which  $D$  indicates the degree of damping of wave energy by drag force  $F_x$ .



### Swaying vegetation motion

The previous presented approaches neglect the decrease in drag resistance due to swaying of vegetation. More realistic is to model the wave-vegetation interaction by calculating the drag force based on the relative velocity taking into account swaying vegetation motion. (Asano et al., 1992) described the relative velocity as:  $u_r = u - u_{veg}$ . A schematization of wave-vegetation interaction is given in figure 2.6. Vegetation motion is modelled as a forced vibration with one degree of freedom. In case of large swaying motions the proposed formulations no longer holds, because the vertical component,  $F_z$ , can no longer be neglected. (Dubi and Tørum, 1995) performed experiments in a wave tank in order to find a linear relation of the damping force with velocity. In addition to previous research, (Méndez et al., 1999), extended the solutions for random non-breaking waves. The results give insight in wave height evolution, vegetation and fluid motion and forces as well moments on the vegetation in irregular wave conditions. (Dijkstra and Uittenbogaard, 2010) created a generically applicable tool useful for modelling the interaction between flow and (very) flexible vegetation. Very flexible vegetation can have a position which is almost parallel to the flow direction, neglecting lift force,  $F_z$ , is not allowed in this case. In the model all plants are considered to behave alike, so only applicable to spatial uniform vegetation fields. (Maza et al., 2013) continues on the work of (Méndez et al., 1999) by formulating a new numerical coupled model which solves the Navier-Stokes equations and includes turbulence. For flexible swaying plants best results are given when flow and plant motion are coupled. In contrast to previous models, the model performs well for low range Reynolds numbers.

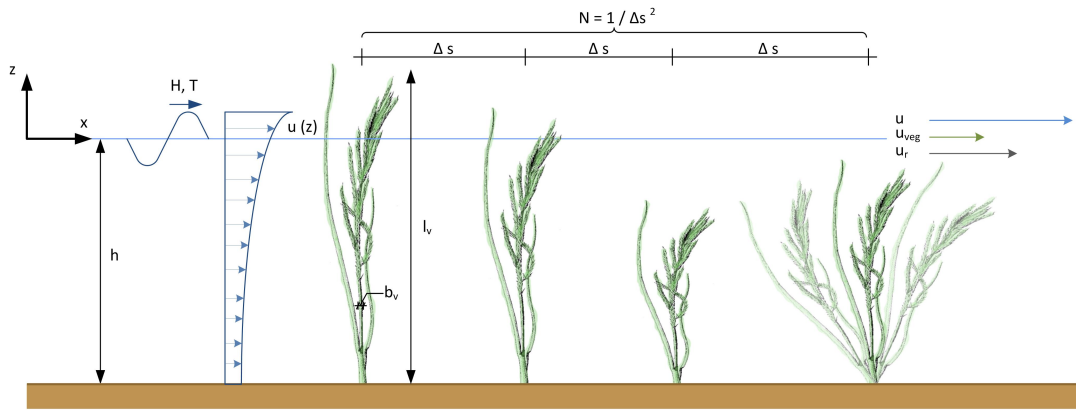


Figure 2.6: Wave-vegetation interaction and modelling parameters

### Propagation of random (non)breaking waves

A wave attenuation formulation including wave breaking which can be applied to monochromatic or random wave fields is formulated by (Mendez and Losada, 2004). Plant motion and reflection are neglected and the major assumption regards the linear summation of dissipation induced by vegetation and breaking. The approach continues on the work of (Dalrymple et al., 1984) and also uses a nonlinear drag force. Wave energy conservation is given by:

$$\frac{\partial(Ec_g)}{\partial x} = -\langle \epsilon_b \rangle - \langle \epsilon_v \rangle \quad (2.6)$$

In which:

$$\langle \epsilon_b \rangle = \frac{3\sqrt{\pi}}{16} \rho g \frac{B^3 f_p}{\gamma_b^4 h^5} H_{rms}^7 \quad (2.7)$$

$$\langle \epsilon_v \rangle = \frac{1}{2\sqrt{\pi}} \rho \tilde{C}_D b_v N_v \left( \frac{kg}{2\sigma} \right)^3 \cdot \frac{\sinh^3 kah + 3 \sinh kah}{3k \cosh^3 kh} H_{rms}^3 \quad (2.8)$$

Where  $E$  = wave energy/unit area,  $c_g$  = wave group velocity,  $\langle \epsilon_b \rangle$  = time averaged rate of energy dissipation induced by breaking,  $\langle \epsilon_v \rangle$  = time averaged rate of energy dissipation induced by vegetation,  $B$  and  $\gamma_b$  are adjusting parameters,  $f_p$  is the average frequency corresponding to the peak period  $T_p$ ,  $H_{rms}$  = root-mean-square wave height,  $\rho$  = fluid density,  $\tilde{C}_D$  = bulk drag coefficient,  $b_v$  = plant area per unit height,  $N_v$  = number of stems per unit horizontal area,  $k$  = wave number,  $\sigma$  = wave frequency,  $\alpha$  = relative vegetation height.

Vegetation properties are represented by  $b_v$ ,  $N_v$  and  $h_v = \alpha/h$ . The accuracy of the solution depends on knowledge of the bulk drag coefficient. Studies on this coefficient are covered in table 2.3.



### Spectral distribution of wave energy damping

Wave-wave interaction may play an important role in wave energy dissipation by vegetation. A changed spectral shape can for instance result in different wave run-up values. (Paul and Amos, 2011) performed a field study for sea grass and included seasonal influences. Higher frequencies showed increased attenuation by vegetation under random waves. (Jadhav et al., 2013) studied salt marsh (*Spartina alterniflora*) behaviour based on field data gathered during a tropical storm along the Louisiana coast. More wave dissipation is observed at frequencies close to the peak frequency. Results from laboratory tests by (Anderson and Smith, 2014) show wave attenuation is most dependent on stem density and the ratio stem length to water depth. Increased wave dissipation is observed for frequencies above the peak frequency for tests performed with double peaked irregular waves. (Wu and Cox, 2015) found also that wave damping is frequency dependent. They found higher dissipation rates above the peak frequency,  $f_p$ , and lower damping below  $f_p$ . Frequency dependency was only observed for shallow water conditions. Damping in general increased for increased relative water depth and wave steepness.

### Submerged and emerged vegetation

According linear wave theory the particle velocities are highest near the water surface. For this reason it is expected that emergent vegetation results in larger wave energy dissipation than submerged vegetation. Higher velocities result in a higher drag force and more wave damping. (Augustin et al., 2009; Dubi and Tørum, 1995) found during experiments substantially more wave reduction for emergent vegetation. This indicates that the amount of wave energy dissipation is clearly dependent on the relative water depth. (Yang et al., 2011) studied wave attenuation by salt marshes at the Yangtze Estuary, China. The results showed an inversely correlated attenuation rate to water depth, explained by shoaling and a higher stem density closer to the bed. Geometric properties of vegetation,  $l_v$ ,  $b_v$ ,  $N$ , as well as physical properties such as flexibility vary with elevation. For this reason estimation of wave energy dissipation should include vegetation properties and the relative vegetation length to water depth ratio (Ozeren et al., 2014).

### Salt marsh behaviour during storm conditions

Empirical evidence for the capacity of salt marsh species to act during extreme water level and wave conditions is lacking. Furthermore their ability to survive these extreme conditions is not well understood. Most studies are limited to low water depths (<1m) and low wave heights (<0.3m) (Yang et al., 2011), because field studies coop with the variability in nature and laboratory flume studies are hampered by limits to conditions which can be generated. (Möller et al., 2014) tested in a large scale flume wave dissipation and the response to high incident wave energy of transported live plants (*Elymus athericus*, *Puccinellia maritima* and *Altriplex prostrata*). Wave dissipation of about 20% over a 40m stretch is observed for wave heights up to 0.9 m in 2 m water depth. Repeated bending of vegetation during energetic conditions results eventually in plant breakage. According to (Puijalon et al., 2011) plants show two strategies to deal with forces: an avoidance strategy, especially for flexible species which minimize the encountered forces by reconfiguring. The more stiffer species show a tolerance strategy by maximizing their resistance to breakage. Cumulatively, breakage lead to a biomass loss of 31% after two days of tests under high conditions. The surface remained stable, with neglecting lowering (order of few mm) over the entire experiment.

(Rupprecht et al., 2017) analysed results of (Möller et al., 2014) focusing on orbital velocities ( $2-91 \text{ cm s}^{-1}$ ) and difference in damage between species. Under wave forcing two types of motion can occur: Swaying, oscillatory plant motion over the wave cycle with symmetric bending angles in both flow directions and whip-like motion, fast flipping from short backward bending to extended forward bending in wave direction 2.7. Especially the whip-like motion results in loss of resistance and high orbital velocities. Which type of movement occurs depends on biophysical and hydrodynamic properties. Three orbital velocity regimes were considered: (1) low orbital velocity

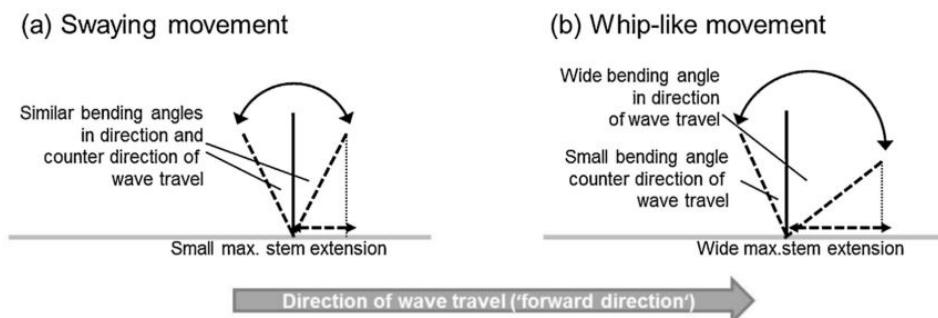


Figure 2.7: Schematic of plant motion under wave loading. (a) Bending angles and stem extension under swaying movement characteristic for low to medium orbital velocities, (b) bending angles and stem extension under whip-like motion characteristic for high orbital velocities. (Rupprecht et al., 2017)

with  $U_{peakf} \leq 32 \text{ cm s}^{-1}$ , (2) medium orbital velocity with  $42 \leq U_{peakf} \leq 63 \text{ cm s}^{-1}$ , (3) high orbital velocity with  $U_{peakf} \geq 74 \text{ cm s}^{-1}$ . For the first regime *Puccinellia* and *Elymus* showed swaying movement with similar measured mean peak forward/backward orbital velocities ( $U_{peakf}$ ,  $U_{peakb}$ ). At medium orbital velocity large difference were observed between the two species. *Puccinellia* showed a transition from swaying to whip-like motion for  $U_{peak} = 62 \text{ cm s}^{-1}$ . *Elymus* showed swaying motion with stem folding and breaking. At high orbital velocities both species showed whip-like motion. Eventually the *Puccinellia*, with higher stem flexibility, survived the extreme conditions well. For *Elymus* severe physical damage was observed with a total biomass loss of 80%.

(Vuik et al., 2017) implemented a breakage model for vegetation in a wave energy balance, as described in equation 2.8 in order to develop a relation between orbital velocity and biomass loss. The plant stability is again expressed in terms of critical orbital velocity, which combines several factors: i.e. flexural strength, stem diameter, vegetation height, flexibility. The flexural strength of the stems is expressed in terms of maximum bending stress, which is obtained via three-point-bending tests on samples of *Spartina anglica* and *Scirpus maritimus* collected at Bath and Hellegat, the Netherlands. The critical orbital velocity for circular stems of *Spartina* is defined by (Vuik et al., 2017) as:

$$u_{crit,cir} = \sqrt{\frac{\sigma_{max} \pi (b_v^4 - b_{v,in}^4)}{8A_c \rho C_D b_v^2 (\alpha h)^2 \cos^2 \theta}} \quad (2.9)$$

and for triangular stems of *Scirpus* as

$$u_{crit,tri} = \sqrt{\frac{\sigma_{max} (b_v^2)}{4A_c \rho C_D (\alpha h)^2 \cos^2 \theta}} \quad (2.10)$$

In which:  $\sigma_{max}$  = flexural strength,  $b_v$  = stem diameter,  $A_c$  = correction factor,  $C_D$  = drag coefficient,  $h_v = \alpha h$  = vegetation height and  $\theta$  = leaning angle

The model is validated on data from (Rupprecht et al., 2017) for *Elymus*. The results show a critical orbital velocity for *Spartina* of  $0.86 \pm 0.28 \text{ m/s}$ , which seems more stable than *Scirpus*,  $u_{crit} = 0.59 \pm 0.22 \text{ m/s}$ .

Stem breakage can result in severe loss of biomass, which is more likely to occur for energetic wave events and relatively stiff and long vegetation. The threshold differs between species because of different biophysical characteristics. Neglecting breakage will overestimate the wave dissipation effect of vegetation during storm conditions. UPROOTING MANGROVES?

	Maximum orbital velocity [m s <sup>-1</sup> ]	Flexural rigidity [Nm <sup>2</sup> 10 <sup>-5</sup> ]	Stem diameter [mm]	Stem height [mm]	Flexural strength [MPa]
<i>Elymus</i>	1.06 ± 0.34	29.9 ± 18.4	1.3 ± 0.3	700 ± 10	40 ± 28
<i>Scirpus maritimus</i>	0.59 ± 0.22	5200 ± 3500	7.3 ± 1.6	722 ± 183	9.2 ± 4.3
<i>Spartina anglica</i>	0.86 ± 0.28	210 ± 100	3.5 ± 0.6	441 ± 87	12.5 ± 5.6

Table 2.2: Characteristics of *Elymus*, *Scirpus maritimus* and *Spartina anglica* (mean ± standard deviation) according to (Rupprecht et al., 2017; Vuik et al., 2017)

### Drag coefficient

In most model approaches work done by vegetation is schematized via a drag formulation. The bulk drag coefficient,  $C_D$ , is the representative drag coefficient for the contribution for the individual stems in a vegetation field. The  $C_D$  factor is used as calibration parameter to minimize the difference between model outcomes and measurements. The drag coefficient  $C_D$  represents drag due to skin friction and pressure differences, but also includes processes which are not included in the model, i.e. swaying, attenuation of orbital motion and interaction between individual wakes in dense vegetation fields (Vuik et al., 2016). A generalized value does not exist, because the factor is dependent on biophysical characters as well on hydrodynamics. Different authors formulated empirical formulas for  $C_D$ , often depending on the Reynolds number ( $Re$ ) or the Keulegan-Carpenter number ( $KC$ ). (Mendez and Losada, 2004) plotted results to both  $Re$  and  $KC$  and showed that  $KC$  was performing better. Results of (Bradley and Houser, 2009) show almost equal results for  $Re$  and  $KC$ . (Anderson and Smith, 2014) found that  $Re$  gives a better prediction for submerged vegetation, but induces large variations for emerged vegetation. (Wu and Cox, 2015) concludes that  $KC$  gives a better prediction considering wave nonlinearity. These different results show that not one generalized approach exists and that performance of  $KC$  or  $Re$  is maybe site/test specific.

The  $C_D$  is often written in the following forms depending on  $Re$  or  $KC$ :

$$C_D = \alpha + \left( \frac{\beta}{Re} \right)^\gamma \quad (2.11)$$

$$C_D = \alpha + \left( \frac{\beta}{KC} \right)^\gamma \quad (2.12)$$

$$Re = \frac{u_c d}{\nu} \quad (2.13)$$

$$KC = \frac{u_c T}{d} \quad (2.14)$$

Where,  $d$  is the stem diameter,  $\nu$  is the kinematic viscosity ( $1 \times 10^{-6} \text{ m}^2 \text{ s}^{-1}$ ),  $T$  is the wave period and  $u_c$  is the orbital velocity at the bottom in front of the vegetated zone (2.2).

In figure 2.8 different drag coefficient formulations are plotted. The differences between studies is especially large for low  $Re$  values. As indication numerical values are presented for  $Re = 1000$ . The variation between the formulations originate probably partly from different test circumstances, for example: regular or irregular waves, vegetation characteristics, submerged or emerged vegetation, uniformity of vegetation field. The corresponding studies and formulations are presented in table 2.3.

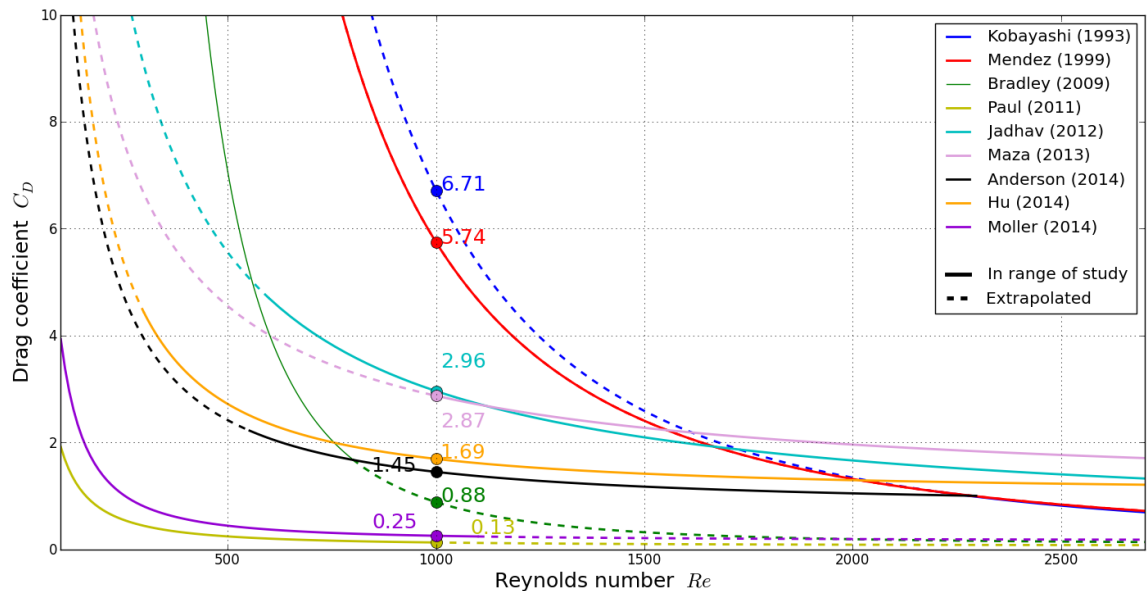


Figure 2.8: Overview of  $C_D$  formulations depending on  $Re$ .

Author	Vegetation characteristics	$C_D$ formulation	Range		
Dependent on $Re$					
(Kobayashi et al., 1993)	Polypropylene strips as artificial kelp $l_v=25$ cm, $52\times0.03$ mm, $N=1110-1490$ m <sup>-2</sup> $h\approx0.50$ m, $H=0,036-0,19$ m, (Asano et al., 1992)	$C_D=0.08+\left(\frac{2200}{Re}\right)^{2.4}$	2200	$<Re<$	18000
(Méndez et al., 1999)	(Asano et al., 1992) non-sway veg	$C_D=0.08+\left(\frac{2200}{Re}\right)^{2.2}$	200	$<Re<$	15500
(Méndez et al., 1999)	(Asano et al., 1992) swaying veg	$C_D=0.40+\left(\frac{4600}{Re}\right)^{2.90}$	2300	$<Re<$	22000
(Bradley and Houser, 2009)	<i>Thalassia testudinum</i> $l_v=0.25-0.30$ m, $b_v\approx0.33$ mm, $N\approx1100$ m <sup>-2</sup> $h\approx1-1.5$ m, $H_s\approx0.09$ m	$C_D=0.10+\left(\frac{925}{Re}\right)^{-3.16}$	200	$<Re<$	800
(Paul and Amos, 2011)	<i>Zostera noltii</i> , sea grass $l_v=13\pm3$ cm, $N_{average}=625\pm225$ m <sup>-2</sup> $h\approx0.75-3.5$ m, $H_s\approx0.1-0.18$ m <sup>-2</sup>	$C_D=0.06+\left(\frac{153}{Re}\right)^{1.45}$	100	$<Re<$	1000
(Jadhav and Chen, 2012)	<i>Spartina alterniflora</i> $l_v\approx0.63$ m, $b_v\approx8$ mm, $N\approx422$ $h\approx0.55$ m, $H_s<0.4$ m	$C_D=0.36+\left(\frac{2600}{Re}\right)$	600	$<Re<$	3200
(Maza et al., 2013)	Polypropylene strips as <i>Posidonia oceanica</i> $l_v=35$ and $55$ cm, $\phi1$ mm, $N=360$ and $180$ m <sup>-2</sup> $h=1.8,2,2.2,2.4$ m, $H=0.4-0.5$ m	$C_D=0.87+\left(\frac{2200}{Re}\right)^{0.88}$	1000	$<Re<$	3500
(Maza et al., 2013)	PVC strips as artificial seagrass $l_v=27.5$ and $45$ cm, $10\times1$ mm, $N=360$ and $180$ m <sup>-2</sup> $h=0.80$ m, $H=0.05-0.2$ m	$C_D=1.61+\left(\frac{4600}{Re}\right)^{1.9}$	1000	$<Re<$	3500
(Anderson and Smith, 2014)	Polyolefin tubes as <i>Spartina alterniflora</i> $l_v=41.5$ cm, $b_v=6.4$ mm, $N=200$ and $400$ m <sup>-2</sup> $h=0.31-0.53$ m, $H_s=0.05-0.19$ m	$C_D=0.76+\left(\frac{744.2}{Re}\right)^{1.27}$	553	$<Re<$	2296
(Hu et al., 2014)	Stiff wooden rods as vegetation mimics $l_v=36$ cm, $b_v=10$ mm, $N=62,139,556$ m <sup>-2</sup> $h=0.25$ and $0.50$ m, $H=0.04-0.20$ m	$C_D=1.04+\left(\frac{730}{Re}\right)^{1.37}$	300	$<Re<$	4700
(Möller et al., 2014)	<i>Puccinellia maritima</i> , $l_v=22\pm3$ cm, $b_v=1.1\pm0.3$ mm <i>Elymus athericus</i> , $l_v=70\pm1$ cm, $b_v=1.3\pm0.3$ mm $h=2.0$ m, $H_s=0.2-0.7$ m	$C_D=0.16+\left(\frac{227.3}{Re}\right)^{1.615}$	100	$<Re<$	1100
Dependent on $KC$					
(Mendez and Losada, 2004)	Artificial kelp as <i>L. hyperborea</i> $l_v=20$ cm, $b_v=25$ mm, $N=1200$ m <sup>-2</sup> $h=0.4-1.0$ m, $H=0.045-0.17$ m found better correlation using $Q=\left(\frac{KC}{\alpha}\right)^{0.76}$	$C_D=0.47\exp(-0.052KC)$ $C_D=\frac{\exp(-0.0138Q)}{Q^{0.3}}$	3 7	$<KC<$ $<Q<$	59 172
(Bradley and Houser, 2009)	see above	$C_D=126.45KC^{-2.7}$	1	$<KC<$	6
(Anderson and Smith, 2014)	see above	$C_D=1.10\left(\frac{27.4}{KC}\right)^{3.08}$	26	$<KC<$	112

Table 2.3: Drag coefficient,  $C_D$ , formulations depending on  $Re$  and  $KC$  in literature based on tests with artificial or live plants. In which:  $l_v$ =stem length,  $b_v$ = stem diameter,  $\alpha$ = relative plant height,  $h$ =water depth,  $H$ =wave height (regular waves,  $H_s$ = wave height (irregular waves).

## 2.3. Dike failure due to wave overtopping

The dike body is the last link between the sea and the hinterland in a vegetated foreshore dike system. Wave overtopping can result in damage of the inner slope, which can eventually induce dike breaching resulting in flooding of the hinterland. In this section formulations from literature describing wave run-up and wave overtopping are presented.

### 2.3.1. Wave run-up

Run-up is defined as the maximum water level on a slope during a wave period. The wave run-up is influenced by the geometry of the dike (and forshore) and properties of incoming waves. Wave run-up is expressed as  $R_{u2\%}$ , the wave run-up height exceeded by 2% of the incoming waves. Which is in (EurOtop, 2016) given by:

$$\frac{R_{u2\%}}{H_{m0}} = 1.65 \cdot \gamma_b \cdot \gamma_f \cdot \gamma_\beta \cdot \xi_{m-1,0} \quad (2.15)$$

with a maximum of:

$$\frac{R_{u2\%}}{H_{m0}} = 1.0 \cdot \gamma_f \cdot \gamma_\beta \left( 4 - \frac{1.5}{\sqrt{\gamma_b \cdot \xi_{m-1,0}}} \right) \quad (2.16)$$

where:

$$\xi_{m-1,0} = \frac{\tan \alpha}{\sqrt{H_{m0}/L_{m-1,0}}} \quad (2.17)$$

Where  $H_{m0}$  = significant wave height estimated from spectral analysis,  $\gamma_b$  = influence factor for a berm,  $\gamma_f$  = influence factor for roughness elements on a slope,  $\gamma_\beta$  = influence factor for oblique wave attack and  $\xi_{m-1,0}$  = the breaker parameter based on  $T_{m-1,0}$  which is the spectral wave period based on  $m_{-1}/m_0$ . The coefficients in (2.15), (2.16) are normal distributed stochastic variables with respectively:  $\mu = 1.65, \sigma = 0.10$  and  $\mu = 1.0, \sigma = 0.07$ .

### 2.3.2. Wave overtopping

#### General

The quantity of water which overtops the dike determines the load on the inner slope, which is often the weakest part of the dike. The quantity is expressed as the mean overtopping volume in  $m^3/s$  or  $l/s$ . Using an average value, neglects the fact that a cover is more affected by a large instantaneous volume than a set of small quantities. A range of formulas to calculate overtopping rates are present in literature. Most have a form based on work of (Owen, 1980):

$$\frac{q}{\sqrt{gH_{m0}^3}} = a \exp\left(-b \frac{R_c}{H_{m0}}\right) \quad (2.18)$$

Research has resulted in equation (2.19) and (2.20) as presented in (EurOtop, 2016). The formula is based on adaptations by (van der Meer, 2014) on the overtopping formula presented in (EurOtop, 2007). Equation (2.19) mainly describes gentle slopes with plunging or breaking waves, equation (2.20) is used for waves with higher surf similarity parameters,  $\xi_{m-1,0}$ , thus surging -and collapsing waves. The new formulation performs better for low relative freeboards,  $R_c/H_{m0} < 0.5-1.0$ .

$$\frac{q}{\sqrt{g \cdot H_{m0}^3}} = \frac{0.023}{\sqrt{\tan \alpha}} \gamma_b \cdot \xi_{m-1,0} \cdot \exp\left[-\left(2.7 \frac{R_c}{\xi_{m-1,0} \cdot H_{m0} \cdot \gamma_\beta \cdot \gamma_f \cdot \gamma_b \cdot \gamma_v}\right)^{1.3}\right] \quad (2.19)$$

with a maximum of:

$$\frac{q}{\sqrt{g \cdot H_{m0}^3}} = 0.09 \cdot \exp\left[-\left(1.5 \frac{R_c}{H_{m0} \cdot \gamma_f \cdot \gamma_\beta \cdot \gamma^*}\right)^{1.3}\right] \quad (2.20)$$

Where  $q$  = mean overtopping discharge per meter structure width,  $\alpha$  = structure slope,  $R_c$  = freeboard,  $\gamma_v$  = influence factor for a wall at the end of the slope,  $\gamma^*$  = influence factor for non-breaking waves for a storm wall on a slope. The coefficients in (2.19), are normal distributed stochastic variables with respectively:  $\mu = 0.023, \sigma = 0.003$  and  $\mu = 2.7, \sigma = 0.20$ , for (2.20):  $\mu = 0.09, \sigma = 0.013$  and  $\mu = 1.5, \sigma = 0.15$ .

### Shallow foreshores

A (vegetated) foreshore can be horizontal or have a slope up to a maximum of 1:10 and has a minimum length by definition of one wave length,  $L_{m-1,0}$  (EurOtop, 2016). At shallow foreshore waves tend to break, but the spectrum will keep the same shape which is not the case for very shallow foreshores. The transition between shallow and very shallow foreshores is given by the point where the original wave height has decreased by depth-induced wave breaking to 50% or more.

Incoming waves can be characterized by wave height, wave period and wave steepness. Most wave conditions have a steepness between  $s_{m-1,0} = 0.01-0.06$ . Larger values are found for local generated wind waves and lower values correspond to swell waves. On a long very shallow foreshore waves may break and reduce to 10%-20% of their original height (Van Gent, 1999). If this happens the spectral shape changes towards a flat spectrum with no significant peak. The spectral period  $T_{m-1,0}$  increases significantly. (Hofland et al., 2017) derived an empirical prediction formula for  $T_{m-1,0}$  and found an increase of  $T_{m-1,0}$  up to about 8 times the offshore value. This change results in surface motions in the infra-gravity waves regime. The increased breaker parameter  $\xi_{m-1,0}$  is probably outside the range of the general governing wave run-up and wave overtopping formulations, which are approximately valid for  $\xi_{m-1,0} < 5$  (EurOtop, 2016). Using equations (2.19) and (2.20) result in underestimation of the overtopping discharges. Instead formulations by (Altomare et al., 2016) should be used.

### Critical overtopping rates

Overtopping can result in damage to a flood defence structure, but can also cause a direct hazard to people or properties directly behind the structure. Two types of overtopping can be distinguished, firstly 'green water' overtopping in which water runs up to the slope and over the crest and secondly 'spray' which occurs when waves break at the outer dike slope. The spray may be carried over the dike by momentum or by an onshore directed wind.

Considering a dike foreshore system it is most likely that during extreme wave conditions the wave height,  $H_{m0}$  ranges between 1-3m. Maximum allowable overtopping considering structural design is based on the quality of the crest and inner slope. Most sea dikes have a crest and inner slope covered by grass. A well-maintained grass cover is defined as a closed grass cover without open patches, transitions and obstacles. In general the grass cover strength depends on coverage and type of grass cover, these characteristics can differ significantly worldwide. Besides structural allowable overtopping limits, more strict limit exist for property, vehicles and people. Table 2.4 gives a brief overview of allowable overtopping rates, for more details is referred to (EurOtop, 2016).

Structural design		Damage to property		Safe passage	
no restrictions to quality slope	$q < 0.1 \text{ l/s/m}$	no damage to buildings	$q < 0.01 \text{ l/s/m}$	safe passage of cars	$q < 0.001 \text{ l/s/m}$
normal quality slope	$q < 1.0 \text{ l/s/m}$	acceptable damage	$q < 0.02 \text{ l/s/m}$	safe passage of pedestrians	$q < 0.005 \text{ l/s/m}$
high quality slope	$q < 10 \text{ l/s/m}$				

Table 2.4: Overview of allowable overtopping rates in (l/s/m) (Schierreck, 2012)

## 2.4. Wave modelling

Figure 1.1 shows the computational steps spatially over the different areas. In this section the models suitable to calculate nearshore wave transformation, wave-vegetation interaction and wave overtopping are discussed.

### 2.4.1. Nearshore wave transformation

When waves leave oceanic waters and enter coastal waters, they enter an area which is shallow enough to affect the waves. Bottom friction starts to play a role and closer to shore triad wave-wave interactions and depth-induced breaking are the dominant processes for wave evolution.

#### SWAN

The third-generation spectral numerical wave model SWAN (Simulating WAVes Nearshore) computes propagation of random, short-crest wind generated waves in coastal regions. The model is fit to model the propagation of short waves from oceanic to coastal waters by including relevant processes, e.g. shoaling, refraction, bottom friction and depth-induced breaking (SWAN, 2017). The wave spectrum transformation is described by the spectral action balance equation. The model can be run in 1D/2D and in stationary or non-stationary mode.

#### Breaker criterium

Nearshore wave height change is mainly dominated by depth-induced wave breaking. If only the wave height transformation is of interest, a first estimation of the nearshore wave height can be given by the breaker criterium (Holthuijsen, 2010):

$$\frac{H_{max}}{h_b} = \gamma \quad (2.21)$$

The value of the breaker index,  $\gamma$ , differs in literature. A common approach is developed by (Battjes and Stive, 1985),  $\gamma = 0.5 \cdot 0.4 \tanh(33s_0)$ . (Nairn, 1990) modified the former formula and proposed:  $\gamma = 0.39 + 0.56 \tanh(33s_0)$ . Where  $s_0 = H_{rms}/L_{peak,deepwater}$ . A formulation based on water depth and wave number is proposed by (Ruessink et al., 2003)  $\gamma = 0.76kh + 0.29$ . The breaker index has clearly no universal value, but can provide an estimate with low computational effort.

### 2.4.2. Wave-vegetation interaction

Several different numerical models which include energy dissipation by vegetation are available. Although the numerical models are in essence different, the vegetation module implemented in SWAN, but also in SWASH and XBeach is similar. The rigid cylinder approach as presented by (Dalrymple et al., 1984) is used. Wave damping is included by adding an energy sink term to the wave energy balance using the model of (Mendez and Losada, 2004).

$$D_{veg} = \frac{1}{2g\sqrt{\pi}} \tilde{C}_D b_v N_v \left( \frac{gk}{2\sigma} \right)^3 \frac{\sinh^3 kah + 3 \sinh kah}{3k \cosh^3 kh} H_{rms}^3 \quad (2.22)$$

Vertical variation in vegetation properties can be included using (Suzuki et al., 2011):

$$S_{ds,veg} = \sum_{i=1}^I S_{ds,veg,i} \quad (2.23)$$

The numerical models schematize vegetation stems as rigid cylinders, characterized by the input parameters  $N_v$ ,  $b_v$ ,  $l_v$ . The sum of these three factors is the vegetation factor. In table 2.3 is shown that the drag coefficient is depend on hydrodynamic conditions and vegetation characteristics. The numerical models work with an static input for  $C_D$ , which neglects the fact that  $C_D$  varies through the vegetated area due to changing hydrodynamic conditions.



### SWASH

The non-hydrostatic multi-dimensional wave-flow model SWASH is created to describe unsteady, rotational flow and transport in coastal waters. It solves the continuity and momentum equations and is able to include equations for conservative transport of salinity, temperature and suspended sediment load. Wave damping by vegetation is again implemented as described earlier, only optionally inertia can be included which is specified by means of the virtual mass coefficient (SWASH, 2017). The non-hydrostatic mode makes this model computational expensive.

### XBeach

The depth-averaged process based numerical model XBeach was initially developed to model storm impact on dunes. Besides the 2D mode, it is possible to run the model in 1D mode, cross-shore (Roelvink et al., 2009; Roelvink, 2010). XBeach facilitates three hydrodynamic modes:

- **Stationary mode** a constant amount of wave energy is imposed, individual waves and long waves are neglected.
- **Surfbeat (instationary mode)** wave height variation on wave group scale are resolved giving rise to infragravity waves and corresponding processes, e.g. wave set-up.
- **Non-hydrostatic mode** individual waves are resolved by calculating the non-linear shallow water equations including non-hydrostatic pressure. Processes on individual wave scale are included, e.g. overwash.

Although the model was originally aimed on hydrodynamic and morphodynamic responses in the nearshore, recently the model is extended with a vegetation module (van Rooijen et al., 2015). In 1D mode (cross-shore, depth-averaged) XBeach solves the short wave action balance:

$$\frac{\partial A}{\partial t} + \frac{\partial c_g A}{\partial x} = -\frac{D_{break} + D_{veg}}{\sigma} \quad (2.24)$$

Where  $A = E_w / \sigma$ ,  $E_w$  = wave energy =  $\frac{1}{8} \rho g H_{rms}^2$ ,  $c_g$  = wave group velocity and  $\sigma$  = wave frequency.

In addition to the vegetation module of the previous models, XBeach optionally calculates damping of long (infragravity) waves and mean flow by vegetation. XBeach uses the depth-averaged shallow water equations in a Generalized Lagrangian Mean (GLM) framework to solve infragravity waves and flow. The velocity is directly calculated, which is used as input for the vegetation drag force formulation:

$$F_{veg,i}(t) = \int_{\alpha_{i-1}h}^{\alpha_i h} \frac{1}{2} \rho \tilde{C}_{D,i} b_{v,i} N_i u^L(t) |u^L(t)| dz \quad (2.25)$$

The ability of the model is tested on a flume experiment by Kansy using submerged kelp vegetation mimics (van Rooijen et al., 2015). During the experiment several wave periods and wave heights are imposed on the vegetation bed, giving a good base for calibration. Effects of infragravity waves, emerged vegetation and nonlinear wave effects are not tested yet.

### Conclusion

In table 2.5 the different models and the included processes are listed. Wave-vegetation interaction modelling is limited, e.g. swaying and breaking of vegetation is not included. For this reason wave-vegetation interaction model outputs for extreme events be interpreted with care.

Models	Short wave height transformation	Short wave period transformation	Infragravity waves	Short wave vegetation-interaction	Long wave vegetation-interaction	Computational time
SWAN	+	+	-	+	-	medium
XBeach stationary	+	-	-	+	-	low
surfbeat	+	-	+	+	+	medium
non-hydrostatic	+	+	+	+	+	high
SWASH	+	+	+	+	+	high

Table 2.5: Overview models to compute wave propagation and wave-vegetation interaction

### Wave overtopping calculation

The quantity of wave overtopping can be computed using a process-based numerical model in non-hydrostatic mode, e.g. SWASH or XBeach. Using these models requires large computational effort, which is undesirable considering the global character of the research. The formulations presented in section 2.3 can also be used against less computational effort.

## 2.5. Foreshore vegetation characterization parameters

In this section an overview of vegetational parameters vegetation are presented based on published results of field studies. In addition two vegetation indicators based on satellite imagery are introduced.

Wave attenuation capacity by vegetation depends largely on vegetational characteristics. Vegetation modelling requires the characteristic input:  $l_v$ ,  $b_v$ ,  $N_v$ . These variables show spatial and temporal variability in the field. Knowledge of these variations is necessary to come up with a robust flood hazard assessment which includes vegetation. Temporal variation can be split in annual (short term) and inter annual (long term) variation. The first considers seasonal variations, as long term variation takes into account erosion/accretion of vegetation area and climate change. Dike designs and evaluations are made for dike stretches of several hundreds of meters. Spatial vegetation variability should be known to consider the normative cross-section.

### Salt marsh characterization parameters

#### Global distribution of salt marsh plant height

Results from field studies are used to establish an overview of the parameters which might be countered in the field. An overview of plant height variation is presented in Figure 2.9. Vegetation types and seasonal influences are included for different continents. The most data is available for Europe, due to an increased amount of field studies in the recent past. Africa and Oceania are not included due to lack of data. A high variation of species is reported in Europe. Overall the results show a higher mean and maximum stem height in America and Asia. The few data sources for Asia reported only summer state results, which makes it impossible to get insight in seasonal variations. For the other continents it is clear that seasonal changes can have large influence on stem height. In Figure 2.9 the mean stem height values are given. Although the amount of data points are not equally distributed over the different seasons, still it gives a good indication for Europe and America. The salt marsh type *Spartina alterniflora* shows large variability among different studies. This is probably due to the different study locations, i.e. more sheltered areas versus sites to open sea.

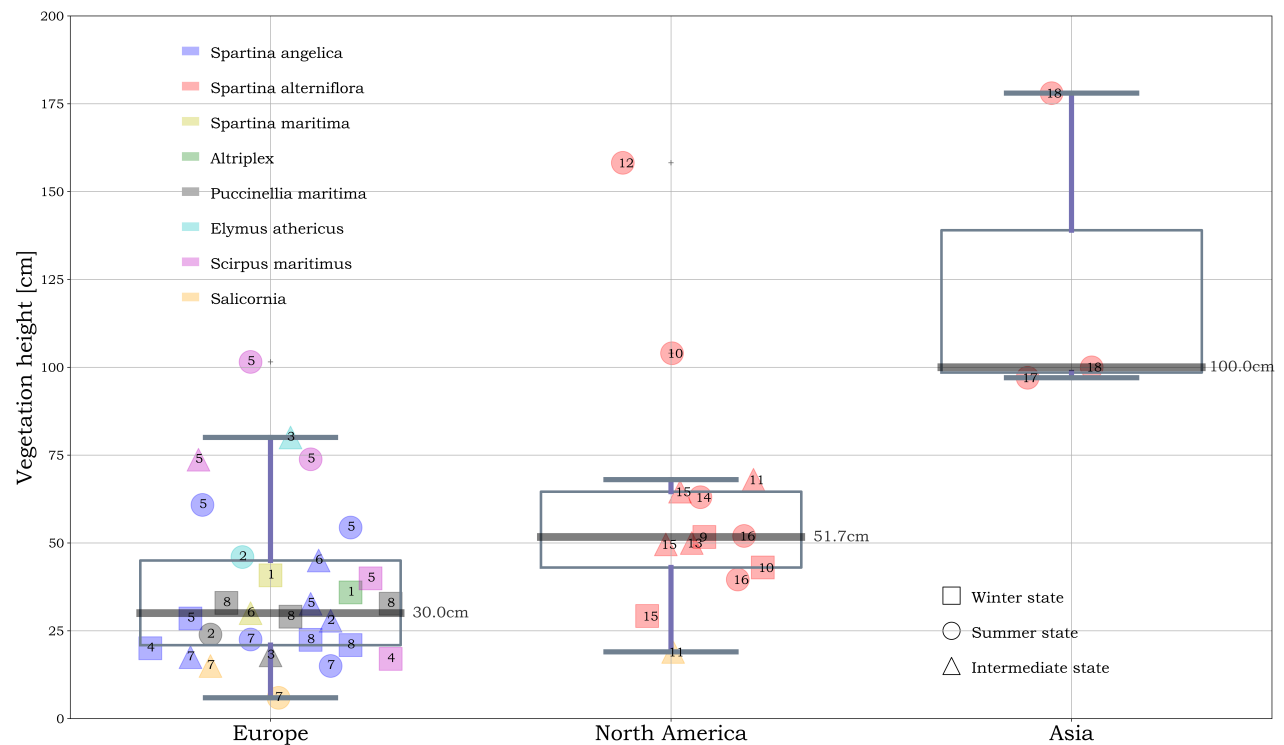


Figure 2.9: Overview of plant heights for different salt marsh species in Europe, America and Asia.

The numbers in the plot refer to the particular study: 1. (Feagin et al., 2011), 2. (Rupprecht et al., 2015), 3. (Rupprecht et al., 2017), 4. (Vuik et al., 2016), 5. (Vuik et al., 2017), 6. (Neumeier, 2005), 7. (Moller, 2006), 8. (van der Wal et al., 2016), 9. (Feagin et al., 2011), 10. (Lana et al., 1991), 11. (Rogers et al., 2016), 12. (Dame and Kenny, 1986), 13. (Cunha et al., 2005), 14. (Jadhav et al., 2013), 15. (Cain and Cohen, 2014), 16. (Knutson et al., 1982), 17. (Yang et al., 2011), 18. (Zhang et al., 2004). Winter state includes data obtained in January, February, March or April. Summer state refers to the months August, September, October or November. Intermediate state covers the other months.

### Distribution of salt marsh parameters in Europe

In Figure 2.10 an overview of the distribution of the stem density, stem diameter and stem height is presented based on studied areas in Europe. The collection of stem density data is quite labour expensive, this is probably the reason for the fewer data points. The Figure shows that seasonal variability is probably largest for stem densities. The stem diameter shows no strong seasonal behaviour, but shows great variability among the salt marsh types with largest diameters for *Scirpus maritimus*.

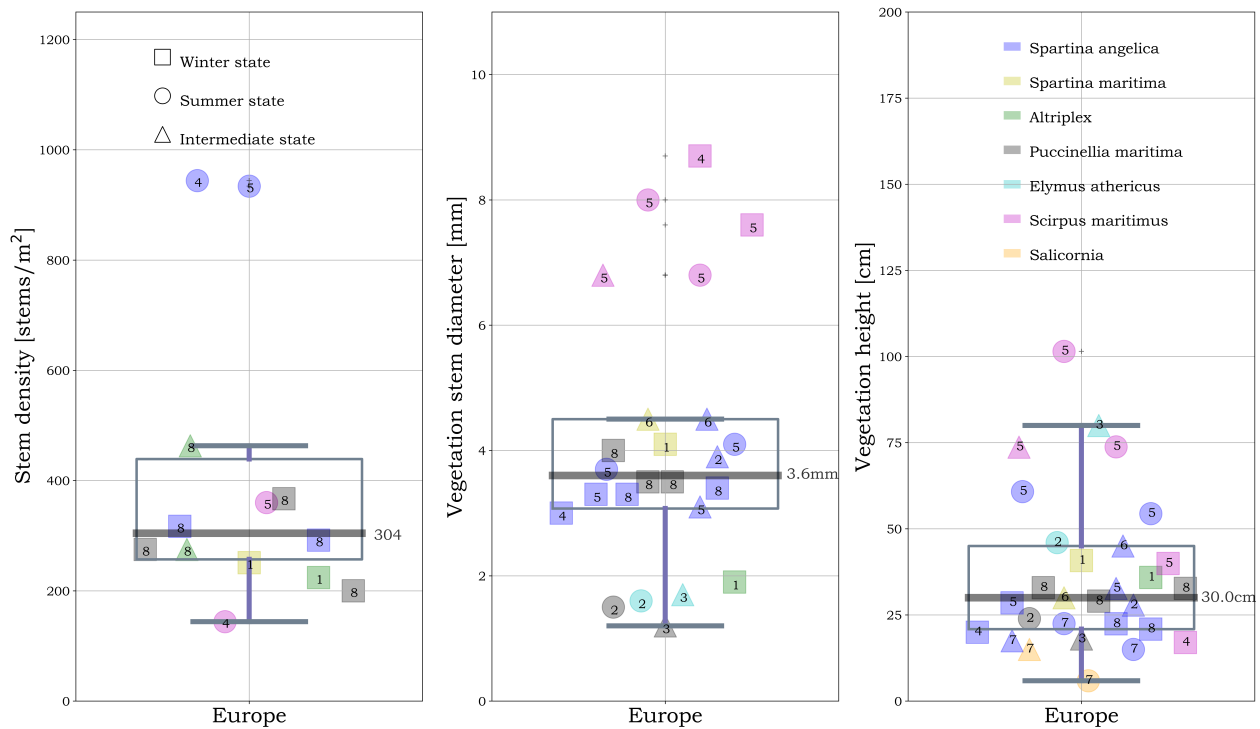


Figure 2.10: Overview of salt marsh parameters in Europe.

The numbers in the plot refer to studies by: 1. (Feagin et al., 2011), 2. (Rupperecht et al., 2015), 3. (Rupperecht et al., 2017), 4. (Vuik et al., 2016), 5. (Vuik et al., 2017), 6. (Neumeier, 2005), 7. (Moller, 2006), 8. (van der Wal et al., 2016). Winter state includes data obtained in January, February, March or April. Summer state refers to the months August, September, October or November. Intermediate state covers the other months.

### Mangrove characterization parameters

In the study of Janssen (2016) an overview of mangrove characteristics is presented based on extensive literature research. The results are presented in Figure 2.11. Natural variability results in a large spreading among trees of the same mangrove type.

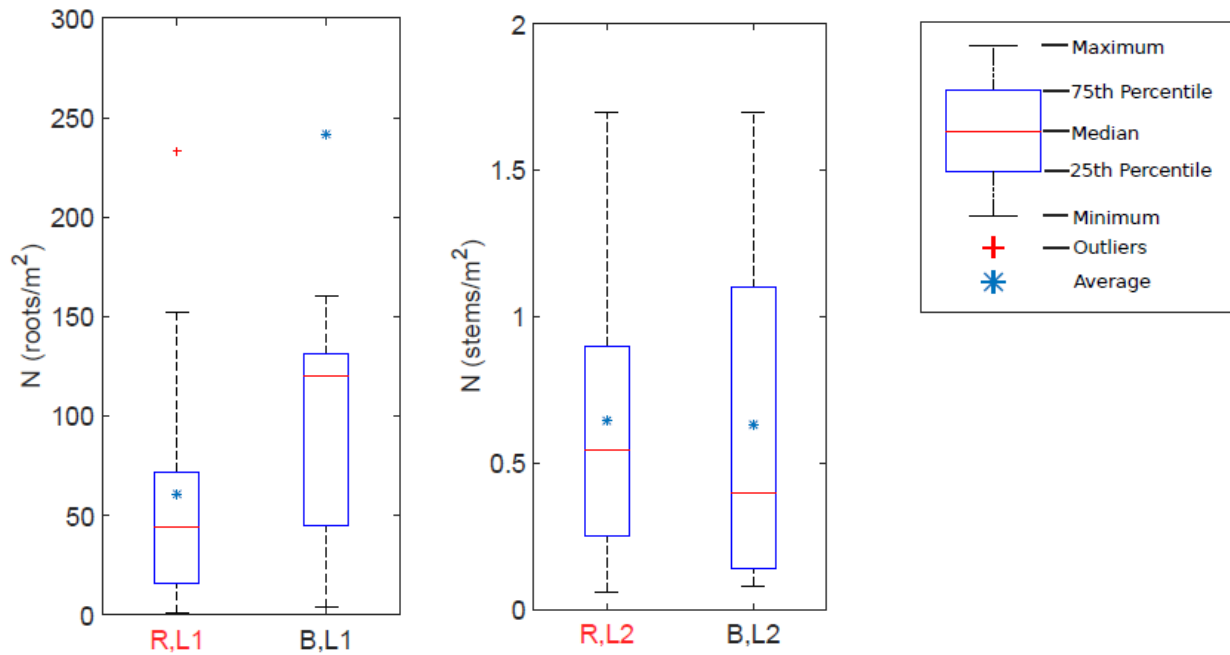


Figure 2.11: Boxplot for mangrove root densities (left) and for the stem density (right) for Red mangroves (*Rhizophora*) and Black mangroves (*Avicennia*) (Janssen, 2016)

### Vegetational parameters observed from air or space

Vegetation characteristics can also be determined using earth observation (EO) data. This data is derived from satellite images of the Sentinel-2A mission by ESA, which is a polar-orbiting, multispectral high-resolution imaging mission. Two indicators are derived:

#### Normalized Difference Vegetation Index

The indicator Normalized Difference Vegetation Index (NDVI) describes the "greenness" of an area. With this indicator it is possible to map e.g. salt marsh vegetation and tidal flats. The NDVI is calculated from surface reflectance in the red (RR) -and near-infrared (RNIR) band. The NDVI is dimensionless and is calculated by  $NDVI = (RNIR - RR) / (RNIR + RR)$ . It ranges from -1 to 1 in which  $NDVI < 0$  indicates water and NDVI increases to 1 for increasing vegetation cover. The NDVI value which corresponds to salt marsh vegetation, or even more specific a specific salt marsh type, is hard to determine. There is simply no general value to make this distinction.

#### Local leaf area index of the marsh

The Leaf Area Index (LAI) refers to the green leaf area per unit ground area. The LAI is given by an algorithm which is trained based on local vegetation characteristics and corresponding reflectance obtained by the satellite. By comparing the LAI for different months an estimate can be made of seasonal variations. The LAI cannot directly be used for numerical modelling. For modelling application it is generally assumed that the LAI is equivalent to the vegetation factor, which is the product:  $l_v \cdot b_v \cdot N$ . Based on field data a representative value for  $l_v$  and  $b_v$  is chosen, next the corresponding density  $N$  can be derived from the LAI.



# II

## Global framework



This chapter gives an overview of the different datasets which are used as input for the global study.

### 3.1. Global bathymetry and elevation data

Performing a global analysis in the coastal zone requires accurate global bathymetry and elevation data. Two products are used in the global hazard assessment: MERIT-GEBCO (MG) and Global Intertidal Elevation (GIE).

#### MERIT - GEBCO (MG)

Over recent years several satellite derived digital elevation models (DEMs) are published. Although the resolution is increasing the vertical accuracy is often lacking. The accuracy is mainly influenced by stripe and speckle noise, absolute biases and by positive biases originated from measuring tree canopies. During the development of the MERIT elevation model is aimed to remove these four main error sources by among others applying several filtering algorithms and using global forest data sets (Yamazaki et al., 2017). The result is a DEM on a 3 arc-seconds grid with a vertical accuracy of about 2 m. The vertical accuracy is highest in relatively flat and bare areas. In these areas the 90% confidence interval for the mean error is 7 m. In forested areas this error increases to 9 m.

General Bathymetric Chart of the Oceans (GEBCO) published by a group of scientists who continuously develop bathymetry data products. The product used in this study is GEBCO 2014 on a 30 arc-second grid (Becker et al., 2009). In order to achieve global coverage GEBCO uses a heterogeneous set of sounding data complemented with satellite derived gravity data. First obvious errors are removed from the sounding data by comparison with the satellite derived data. The final dataset matches the sounding data and uses interpolation towards satellite derived data in data scarce regions. The vertical accuracy has a mean error in the order of tens of meters.

In order to achieve a dataset which covers the entire coastal zone the two datasets described above are merged. As the two sets have a different resolution GEBCO data is first downsampled linearly towards a resolution of 3 arc-seconds (90 m). Next the sets are merged using the OSM's coastline, assuming it represents MSL.

#### Global intertidal elevation map (GIE)

The global intertidal elevation map is based on the time-ensemble averaged (TEA) probability of inundation technique, which can be used to create intertidal elevation maps (Murray et al., 2012; Niedermeier et al., 2005). The global coastline is divided into 25000 tiles of 40 x 40 km<sup>2</sup>. For these tiles data is collected from NASA/USGS Landsat EO data and ESA/Copernicus Sentinel 2 EO data for a period ranging from 1997-2017. The median number of images per tile was 315 with a total range between 2 and 2223 images. For pixels in these tiles the modified normalised difference water index (MNDWI) is calculated:

$$MNDWI = \frac{SWIR1 - G}{SWIR1 + G} \quad (3.1)$$

In which *SWIR1* and *G* are the short-wave infra red bands and green bands respectively (Van Wesenbeeck and Dijkstra, 2017). Tidal statistics from the global tide model FES2012 are used to couple the derived inundation probability to an elevation. The GIE data points represent points which are situated between LAT and HAT.

Errors are induced due to identification of water in the hinterland as part of the intertidal zone e.g. volcanic substrates, or water on roofs. Furthermore this error can be induced by snow or shadows. An example is given in Figure 3.1. At the left side the GIE map and at the right satellite imagery of the city Buckie, Scotland. The whole city and a



large part of the sea is falsely identified as intertidal zone. In morphological dynamic regions the technique failed to identify e.g. tidal flats as intertidal zone. The global set is tested for sites in the Western Scheldt in the Netherlands, the East coast of the United Kingdom and Cadiz Bay in Spain. The coefficient of determination  $R^2$  ranged from 0,45 to 0,77 (Van Wesenbeeck and Dijkstra, 2017). Foreshore derivation techniques which use the described global datasets are presented in Section 4.3.



Figure 3.1: GIE map misidentifying land as intertidal zone at Buckie, Scotland

### 3.2. Global hydrodynamic data

Wave and water level characteristics are derived using two sources with global coverage. The global distribution of the wave height, wave period and extreme water levels can be found in Appendix D.1.

#### Off-shore wave boundary conditions (ERA-I)

Off-shore wave boundary conditions are derived from the ERA-Interim (ERA-I) dataset. This set is a global reanalysis based on data from 1979 till present day and covers from 81 ° South to 90 ° North. The set is derived from the ECMWF wave model with a grid of 0.75 ° x 0.75 ° and 6 hours time interval which is coupled with an atmospheric model. Several studies concluded that the set underestimates tropical cyclone waves, mainly due to the rough grid size Muis et al. (2015b), (Shanas and Kumar, 2015). The FAST project team selected ERA points nearest to the coast, which resulted in a set of 4307 points. The Peak Over Threshold method is performed to derive representative values for the significant wave height  $H_s$  and peak wave period  $T_p$  for the return periods 1, 2, 5, 10, 25, 50, 100, 250, 500 and 1000 years. The results are mapped on Dynamic and Interactive Vulnerability Assessment (DIVA) points.

#### Extreme water levels (GTSM)

Representative water levels for above mentioned return periods are derived from a D-Flow Flexible Mesh model, the Global Surge and Tide Model (GTSM), by (Muis et al., 2016) which are mapped on DIVA points. The output of the GTSM are extreme water levels which include tide and surge. The model is forced with wind speed and atmospheric pressure from the ERA-I dataset and tides are included based on FES2012. Extreme water levels are estimated using a Gumbel distribution fit using the maximum-likelihood method. The uncertainty of the fit is below 10% for half of world's coastline and is only larger than 25 % for 4% of the coastline. The largest uncertainty is found in regions with relatively low extreme water levels, e.g. the Mediterranean Sea.

### 3.3. Global vegetation data

Representation of vegetation presence and corresponding biophysical characteristics is crucial for reliable wave damping calculations. Several data products are used to obtain vegetation presence and vegetation type during the global assessment.

#### Corine Land Cover (CLC)

The CORINE Land Cover (CLC) inventory is a product initiated by the European Union in 1985 as prototype project for several environmental studies. At present the inventory is taken over by the European Economic Area (EEA), which publishes an update every six years (EEA, 2016). The map contains 44 different land cover classes and has a minimum feature width of 100 m. A total of 12 countries is covered, ranging from 14° W to 29°E and 62°N to 28°S. CLC is mainly based on visual interpretation of Earth Observation (EO) images. The latest map originates from 2012 and is validated with an overall accuracy of 83.3 % (Van der Wal et al., 2016). The FAST project team derived five main classes from the 44 different layers: 1. Intertidal vegetation, 2. Intertidal flats, 3. Water, 4. Inland marsh and

5. Broadleaved forest. In this study the CLC map is used to determine the vegetation cover type for assessments in Europe. The intertidal vegetation class includes intertidal sand/silt or mud-based halophytic grasses, flowering plants which are submerged during high tides and coastal and intertidal salt meadows.

#### GlobCover

GlobCover is a land cover map published by ESA which covers the entire world. The GlobCover project is initiated in 2005 with the aim to develop a land cover map using EO from the 300m resolution Medium Resolution Imaging Spectrometer (MERIS) sensor onboard of the ENVISAT satellite. The map published in December 2008 contains 22 land cover classes and is based on data gathered between December 2004 and June 2006. The data is validated against several thousand reference points, resulting in an overall accuracy of 73%. The FAST project team reclassified GlobCover into four classes suitable for the project: 1. Intertidal vegetation, 2. Intertidal flats, 3. Inland marsh and 4. Broadleaved forest. The reclassified map is used as complementary map for assessments outside Europe. The global coverage of the set is at the expense of resolution and accuracy. Data from GlobCover sometimes misidentifies the cover type. An example in Figure 3.2 in which salt marsh vegetation is identified as a combination of inland marsh and broad leaved forest.

#### Global salt marsh map

The Global salt marsh map gives an overview of the extent of salt marshes on a global scale by presenting 350.985 individual occurrences (Mcowen et al., 2017). The dataset is based on data from different articles, databases and reports from several (non) governmental organizations and EO data ranging from the years 1973 to 2015. The authors not intended to produce an accurate salt marsh presence map, but an overview of data availability. Visual inspection using QGIS and Google satellite shows however a high accurate match in Europe and North America with an resolution similar or higher than the CLC map.

#### Global mangroves map

The Global mangroves map shows the extent and distribution of mangroves worldwide. The map is based on about 1000 Landsat satellite images which are processed using classification techniques. The values are normalized based on in-situ data, existing maps and databases. The study showed that only 15 countries containing approximately 75% of world's mangroves (Giri et al., 2011). Furthermore the largest percentage of mangroves is found in a small band between 5 ° North and 5 ° South. The map has a resolution of 30 m, which is far better than GlobCover and CLC.

#### Vegetation presence (VegGEE)

The resolution of the land cover maps is not sufficient for an accurate wave attenuation calculation. The FAST project team derived a vegetation absence/presence map using Google Earth Engine (GEE) based on Sentinel-2A and Landsat-8 data, resolution of 10 m and 30 m respectively. Vegetation presence is derived based on an individual NDVI threshold per cell based on the yearly NDVI average and NDVI amplitude. The final data product is the GEE vegetation presence (VegGEE) map, which has almost global coverage, excluding North Canada, North Russia and the arctics.

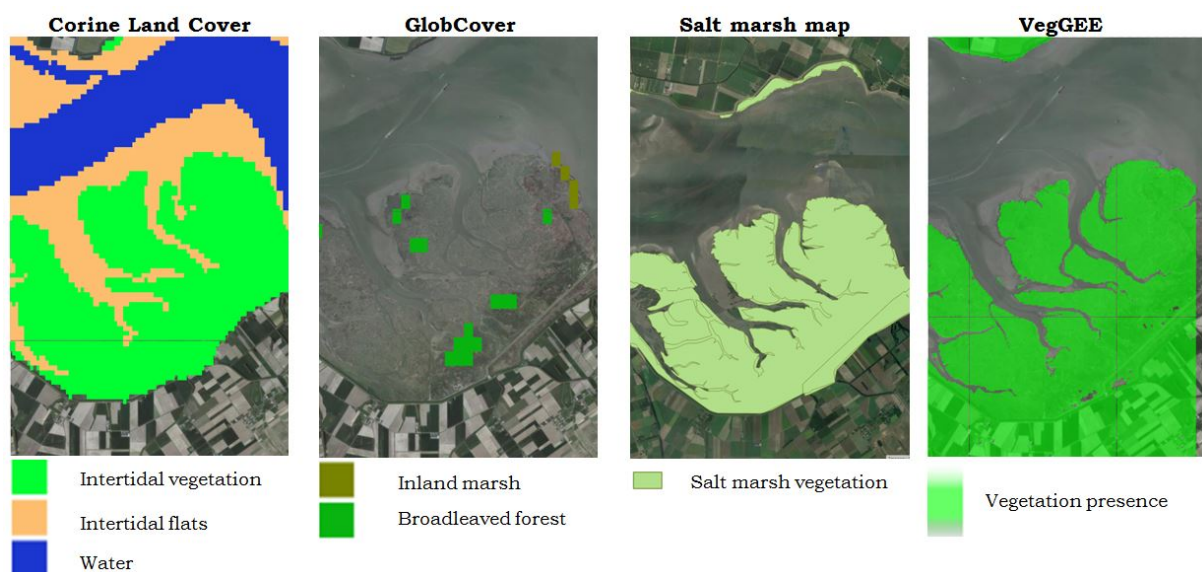


Figure 3.2: Performance of different vegetation datasets for the drowned land of Saeftinghe in Zeeland, The Netherlands

### 3.4. Global transect data

For this study shore normal transects are used to assess wave damping by foreshore vegetation. These transects are generated for the Aqueduct project. The Aqueduct project launched the Aqueduct Global Flood Analyzer which gives insight in river flood risk on a global scale. The tool is developed by a consortium of the American World Resources Institute (WRI), together with Deltares, VU University of Amsterdam, Utrecht University and the Netherlands Environmental Assessment Agency. The project aims to extend the analysis by implementing coastal flood risk. The global coastline is approximated by a polynomial which is derived based on Open Street Map (OSM). Along this coastline shore normal transects are derived based on a 30 arc-second grid with a transect length of 8 km, of which the middle is situated on the OSM coastline. The distance between the transects is roughly 1 km. The transects are all combined in a shape file containing a total of 766034 individual transects. Absolute values in literature for the world's coastline length vary significantly. This is mainly due to the fact that the resolution of the measurement influences the final estimation to a great extent ([Mandelbrot, 1967](#)).

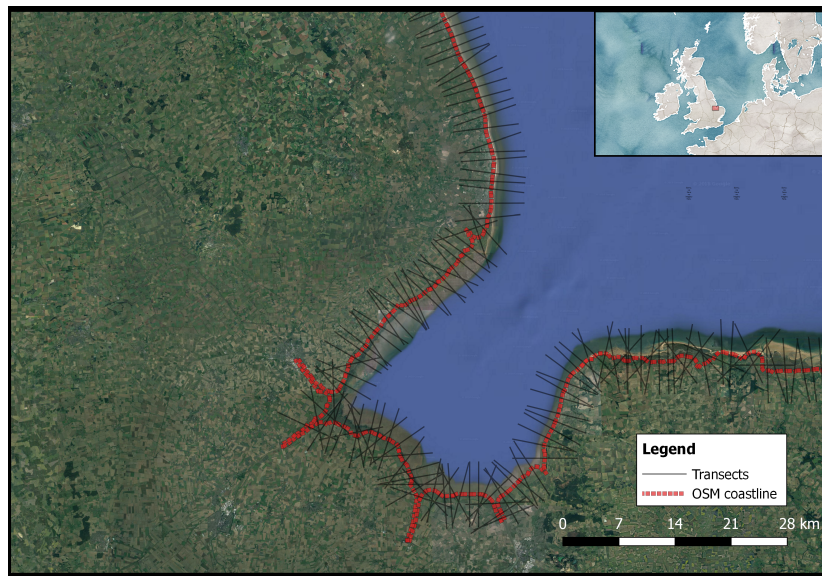


Figure 3.3: Open Street Map (OSM) coastline estimation and transects at Freiston, UK

The GIE and VegGEE datasets have limited to no coverage above the pole circle and below a latitude of  $60^{\circ}$  S. The study area is bounded by these limits and contains in total 495361 transects. The study area is shown in Figure 3.4.

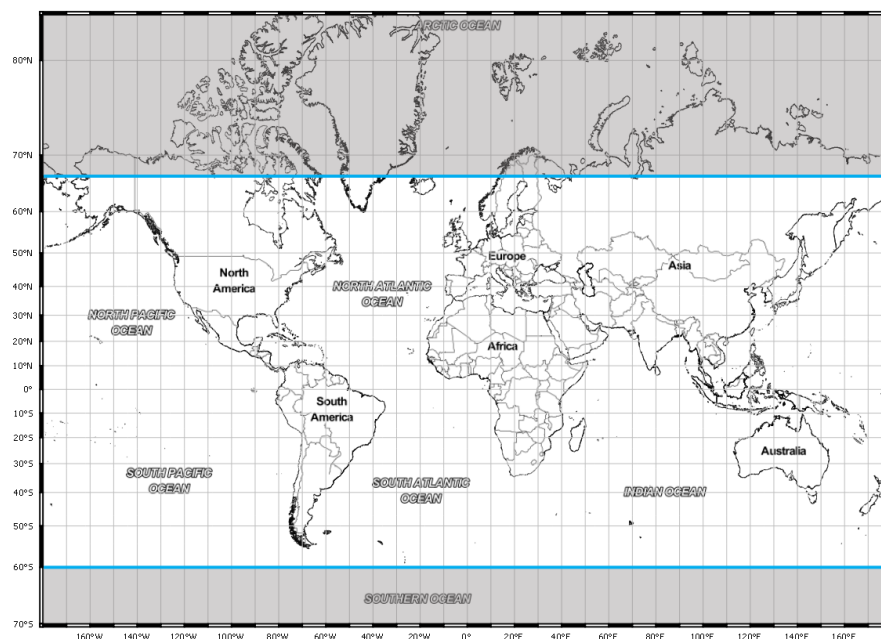


Figure 3.4: The study area between  $60^{\circ}$  S and  $66^{\circ} 33' 47.1$  N (Arctic Circle)

## Model approach

In order to assess the influence of foreshore vegetation on a global scale an algorithm is constructed which follows six consecutive steps for each individual transect:

- Step 1: Reading transect coordinates
- Step 2: Loading profile, vegetation and hydrodynamic data from global datasets
- Step 3: Definition of foreshore parameters
- Step 4: Definition of vegetation parameters
- Step 5: Determination of wave attenuation
- Step 6: Calculation of the required dike freeboard

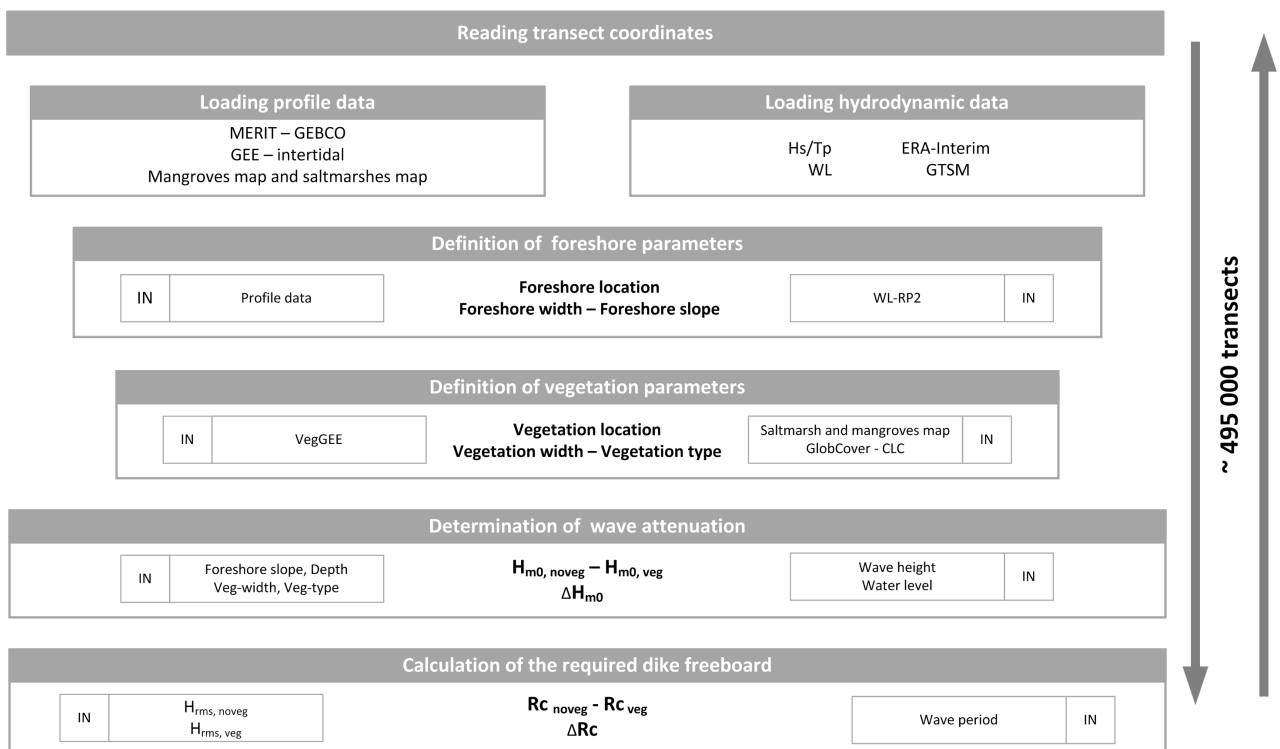


Figure 4.1: Overview of steps in Global Flood Hazard Assessment



#### 4.1. Transect definitions

The foreshore is generally defined in this study as the area between LAT and HAT in case of foreshore determination based on the GIE map. The foreshore is bounded between  $-2\text{ m} + \text{MSL}$  and the extreme water level for a return period of 2 years (SLRP2) if determination is based on MG. The derived foreshore bounds can differ among transects based on the available data and the used foreshore determination method, which are described in this chapter.

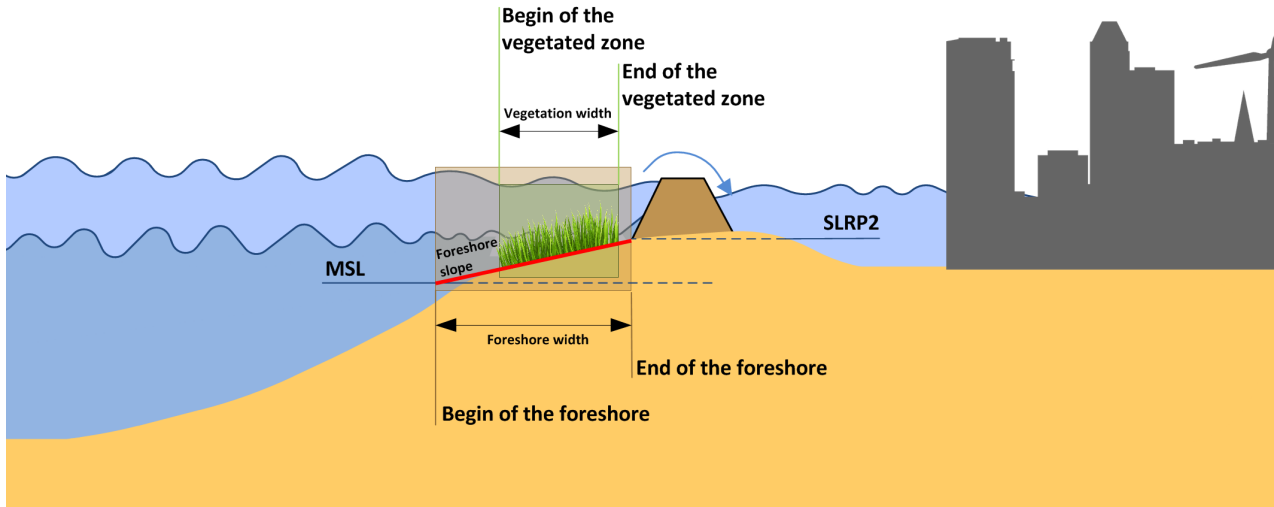


Figure 4.2: Overview of definitions on the foreshore

#### 4.2. Step 1-2: Loading data from global datasets for transect

First the coordinates of the start and end point of the assessed transect are read. Next hydrodynamic and profile data is obtained via a server request to get surge data (GTSM), wave characteristics (ERA-I) and profile data (MG and GIE). Hydrodynamic data is loaded for the following return periods: 2, 5, 10, 25, 50, 100, 250, 500 and 1000 years. The characteristics of the sources are described in Chapter 3. Profile data is obtained along a line between the start and end coordinates of the specific transect with a step size of 25 m. A first scan is performed to assess if the retrieved topo-bathymetric data is situated completely above or below MSL. This scan filters erroneous transects, which are located e.g. completely on land or on open water. Next, data from the mangroves map and salt marshes map is loaded along the transect using the same step size.

### 4.3. Step 3: Definition of foreshore parameters

The goal of this step is to define the location, width and slope of the foreshore along the transects using global topobathymetric data. The 1D coastal profile corresponding to a transect is derived using different data sets, introduced in Chapter 3. The combined set MG has coverage over the full profile, but has a coarse resolution and is based on linear interpolation near the shoreline. On the other hand the GIE map has a high resolution, but covers only parts of the profile and often falsely identifies inland waters or land as intertidal zone.

#### GIE validity checks

Validity checks are performed on the obtained GIE data for each transects, as the quality of the data is lacking in some environments. The main goal is to remove false indications of intertidal area in the GIE set.

Individual data points from the GIE set are marked invalid in case: (1) MG points are situated above the governing surge level and the GIE point at this grid point is situated below the MG. (2) GIE data points are situated at open sea. (3) the GIE range is below the minimum range threshold.

Besides these three checks a fourth criterion is used based on continuity of the data. The GIE set contains discontinuities, because the data is derived using the MNDWI from satellite imagery. The fourth check aims to remove speckle noise and fill up missing data. The data length is defined as the length of continuous GIE data points along the transect. Gap length on the other hand is defined as the length of the empty data points between data patches. If the data length of a patch is smaller than the data length threshold the patch is marked invalid and removed from the profile. The gap is filled by linear interpolation, if the gap length between two patches is smaller than the critical gap length.

#### Derivation of foreshore location

Based on the validity of the elevation data four foreshore determination methods were formulated. The methods are listed below based on expected accuracy. The algorithm used in the global assessment uses the same sequence.

##### Method 1 (GIE)

The foreshore characteristics are derived from the last valid GIE patch, which is often the only patch. The last patch is selected, because e.g. if a transect starts at the other bank in an estuary two patches will be present. The start of the foreshore coincides with the first valid GIE point and the end of the foreshore is defined by the last valid GIE point. An example is presented in Figure 4.3.

##### Method 2 (MG)

In case no valid GIE data points are found the profile characteristics are based on MG. First, data points between a minimum threshold of -2 m +MSL and a maximum threshold equal to SLRP2 are selected from MG. For these points the direction of the slope is determined for each grid point, by comparison based on elevation between the point concerned and the next point. In this way patches are created, which are comparable with the patches in the GIE data. Using data length, gap length and the corresponding thresholds validity of the patches is checked similar as the method used for GIE. Based on the remaining data points the start and end of the foreshore are determined as the first and last valid point respectively of the last patch. An example is presented in Figure 4.4.

##### Method 3 (MG)

The third method is used if not sufficient foreshore data is available to satisfy the minimum data length threshold. The start of the foreshore is defined as the first up crossing intersection with -2m +MSL along the transect. The end of the foreshore is the intersection between the MG profile and SLRP2. An example is shown in Figure 4.5.

##### Method 4 (MG)

In case no begin and/or start of the foreshore is found using method 3, these locations are determined differently. The start and/or end of the foreshore are defined as the first point and last data point respectively along the transect based on MG.

#### Extension of the foreshore based on vegetation maps

It might be possible that intertidal vegetation is present outside the derived foreshore.

First, for the most upper and lower part of the intertidal zone relatively less data is available to characterize this area as intertidal zone using satellite data, because i.e. the upper part might be flooded only a few days a month. This is a known uncertainty in the GIE map (van Wesenbeeck and Dijkstra, 2017). Second, it is hard to define the bed elevation in mangroves forests based on satellite imagery. So in some cases the actual intertidal zone stretches further inland than the derived foreshore using global elevation maps. In order to counter this problem data is

obtained from the mangroves and saltmarsh map using the same coordinates and step size. If vegetation is present according one of these maps the foreshore is extended until the end of the vegetated zone. As elevation for these extrapolated points SLRP2 is chosen, because elevation from MERIT overestimates the elevation probably, because it indicates tree canopies as the surface as described in Chapter 3.

### Derived foreshore parameters

Once the foreshore is derived using one of the methods the foreshore width and foreshore slope are derived as foreshore characterizing parameters. The foreshore width is determined by calculating the distance between the start and the end of the foreshore. The slope is estimated using a linear regression based on the data points in the foreshore.

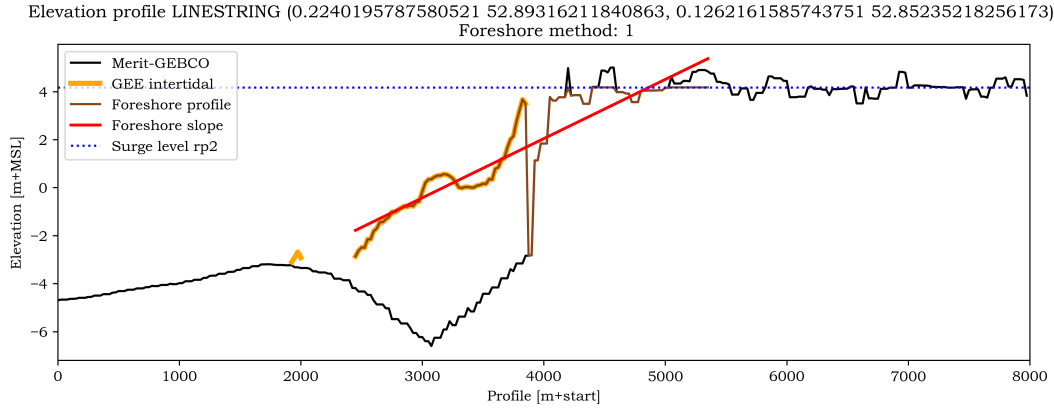


Figure 4.3: Derived profile at Freiston (UK) according foreshore method 1  
Profile is built using GIE and extended based on the salt marshes map

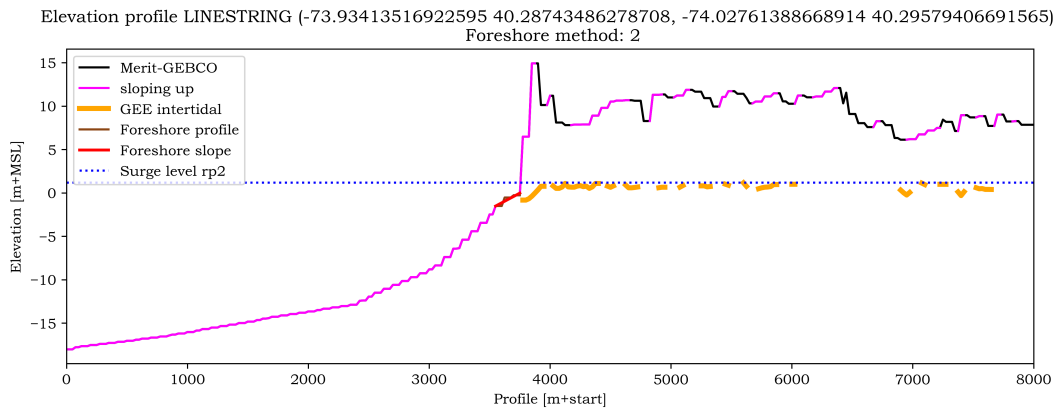


Figure 4.4: Derived profile just south of New York (USA) according foreshore method 2  
GIE data is marked invalid, thus profile is built based on MG

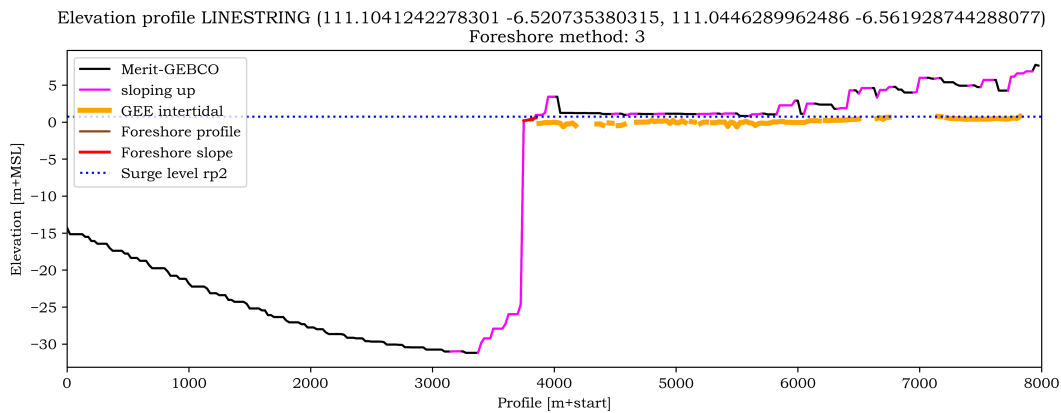


Figure 4.5: Derived profile at North Coast of Indonesia according foreshore method 3  
GIE data is marked invalid and not enough MG data is available between the minimum and maximum threshold to meet the minimum data length requirement, thus method 3 is used

### Foreshore derivation methods in global assessment

In the assessment four different methods are used to determine the foreshore location. An overview of the global distribution of foreshore determination methods is presented in Figure 4.6. The first method which uses only GIE data has the best resolution, but often falsely indicates intertidal zones in urban areas and areas with a small tidal range. Taking this into account, the spatial distribution of the methods is an indicator of the accuracy of the assessment. Especially method 4 indicates potential erroneous transects. The GIE data does not cover North Russia, Greenland and large extents of Canada, which explains the absence of method 1 in these regions. Notable is the high percentage of foreshore method 1 in the Mediterranean Sea, which is characterized by a small tidal range. Results for this area have potentially a larger error than in other areas. This subject is further discussed in Appendix D.3.2. In Table 4.1 the distribution in terms of percentage is given for all transects, salt marshes and mangroves. Foreshore vegetation is likely to be present in areas with a higher tidal range. At the same time, is the performance GIE map better in areas with a higher tidal range, which explains the shift to a higher percentage of foreshore method 1 for the vegetated transects.

Foreshore method	1	2	3	4
All transects	24.5 %	56.5 %	17.1 %	0.02 %
Salt marshes	30.6 %	43.7 %	25.7 %	0.02 %
Mangroves	46.0 %	44.5 %	9.5 %	0.004 %

Table 4.1: Distribution of foreshore methods over all transects and vegetated transects

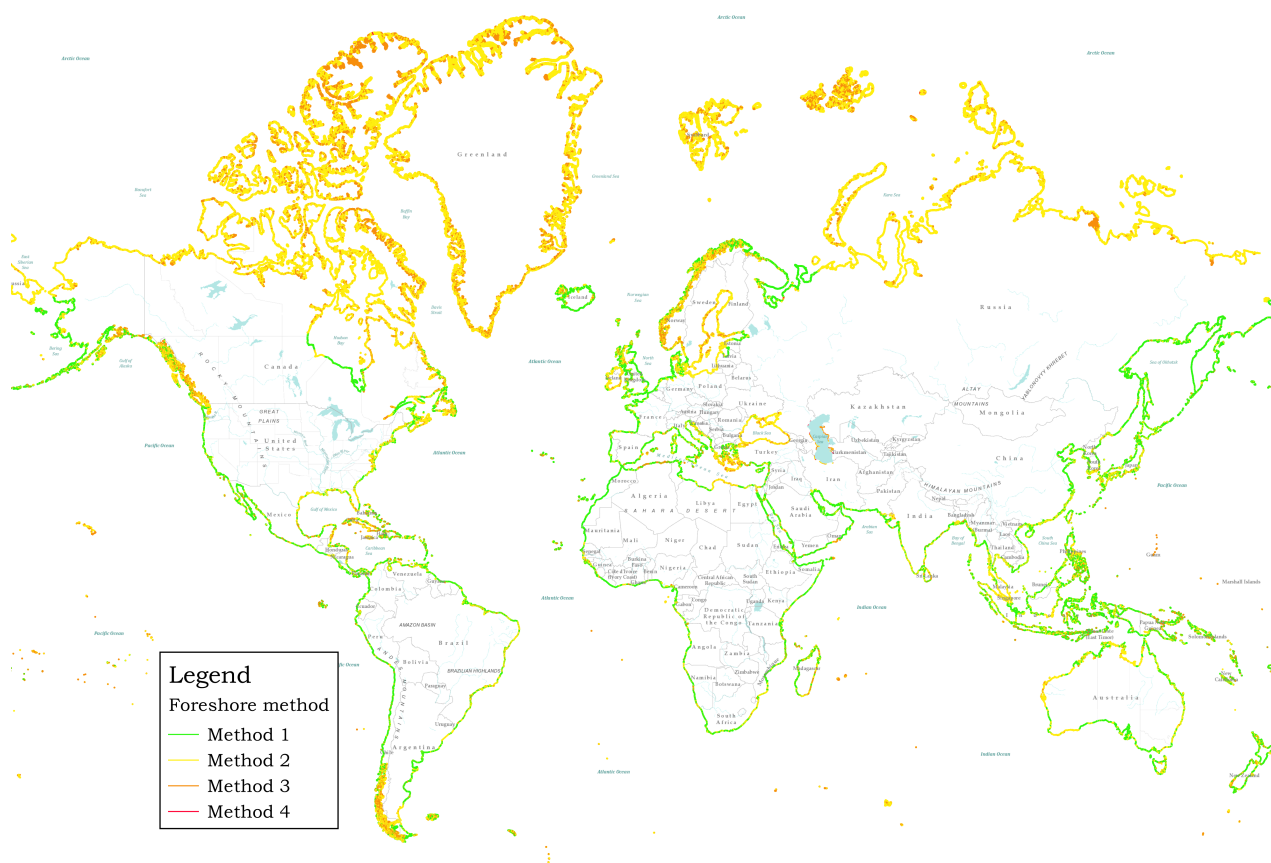


Figure 4.6: World map with overview of used foreshore derivation method



#### 4.4. Step 4: Definition of vegetation parameters

Once the foreshore is determined the vegGEE map is accessed to construct a vegetation presence profile. This vegetation profile shows at which grid points along the profile vegetation is present. The VegGEE set has a high resolution, but does not contain information about the vegetation cover type. The salt marsh and mangroves map, GlobCover and CLC are used to get the corresponding cover type. In total three different vegetation cover type methods can be distinguished. Similar to the foreshore methods, these methods are called in sequence based on expected accuracy.

##### Vegetation cover method 1: Salt marsh map and Mangroves map

Data is obtained from the salt marshes and mangroves map along the profile. Data from the salt marshes map is first placed on the vegetation profile. Second, data from the mangroves map is placed, which might overwrite the earlier salt marsh data at some grid points. The mangroves data is able to overwrite the salt marsh data, because the wave attenuation capability of mangroves is larger. In Figure 4.7 the profile from Figure 4.3 is again presented, but including vegetation. The vegetation for this extended profile is obtained using vegetation cover method 1, see Figure 4.8 for the intersection with the salt marsh map.

##### Vegetation cover method 2: Corine Land Cover

If the transect is situated in Europe and no data is found in the salt marsh map the Corine Land Cover (CLC) map is consulted. At the grid points where the CLC map indicates intertidal vegetation salt marshes are placed on the vegetation profile. Any other cover types, e.g. inland marsh or tidal flats are handled as no vegetation.

##### Vegetation cover method 3: GlobCover

If the transect is situated outside Europe and no data is found in the salt marshes and mangroves map the GlobCover map is accessed. The GlobCover map has a lower resolution and the data is very sparse in comparison to the other sources. If the transect is situated between  $\pm 30^\circ$  latitude the cover types 'broadleaved forest' and 'nodata' are assigned as mangroves. This approach gives a reasonable result, keeping in mind that only a vegetation type is assigned to grid points which are indicated vegetated by the VegGEE map. Outside the tropics GlobCover types 'broad leaved forest', 'inland marsh' and 'no data' are assigned as salt marsh vegetation.

#### Derived vegetation parameters

After constructing the vegetation profile the vegetation width and vegetation type are derived. The vegetation width is defined by the sum of vegetated grid cells between the start and end of the vegetated zone. The vegetation type is the most dominant type among the vegetated grid points, because no mixed types are possible in the global model.

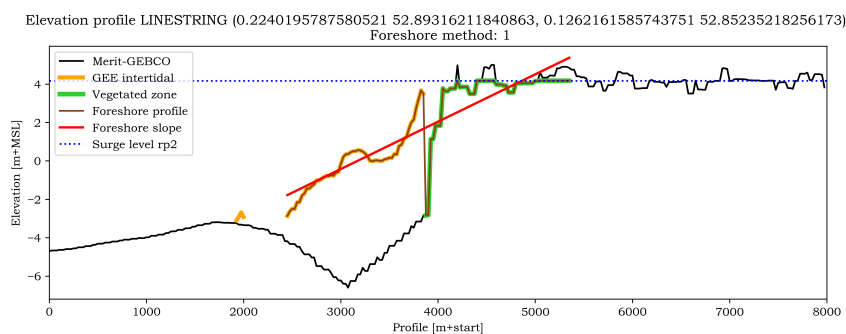


Figure 4.7: Derived profile with vegetation based on salt marsh map



Figure 4.8: Intersection with salt marsh map

## Derived vegetation parameters in global assessment

### Vegetation cover source

The vegetation cover source per transect is presented in Figure 4.9. It shows clearly at which locations the salt marsh map and mangroves map have limited to no coverage. In Table 4.2 the distribution in terms of percentage is shown.

### GlobCover

Coverage gaps in the salt marsh map and mangroves map are mainly observed outside Europe in Northern Canada, Northern Africa, Southern Chile, Korea, Japan and Russia. These areas are situated outside the tropics, which explains the higher percentage of salt marshes from GlobCover in Table 4.2. Russia, Greenland and the most Northern part of Canada are not part of the study, because the VegGEE map does not cover these areas. Data of GlobCover is very sparse in the coastal zone. Often VegGEE indicates vegetation presence, but the transect does not directly intersect data from the GlobCover map. In these cases the cover type is determined based on latitude, as explained in section 4.4. Indication of vegetation presence is trustworthy, due to the high resolution and accuracy of VegGEE, only the corresponding cover type is doubtful. For example algae might be indicated as vegetation by VegGEE and further processed as salt marshes or mangroves.

### Corine Land Cover (CLC)

CLC is hardly used in Europe, due to excellent coverage of the salt marsh map. Notable countries for which CLC is consulted are Greece and Finland. The resolution of CLC might be relatively coarse, but it gives a good indication. Furthermore no false indications are observed in the CLC map during the study.

Cover type source	Salt marsh / Mangroves map	GlobCover	CLC
Salt marshes	30.2 %	69.4 %	0.4 %
Mangroves	70.7 %	29.3 %	0.0 %

Table 4.2: Distribution of cover type sources for vegetated transects

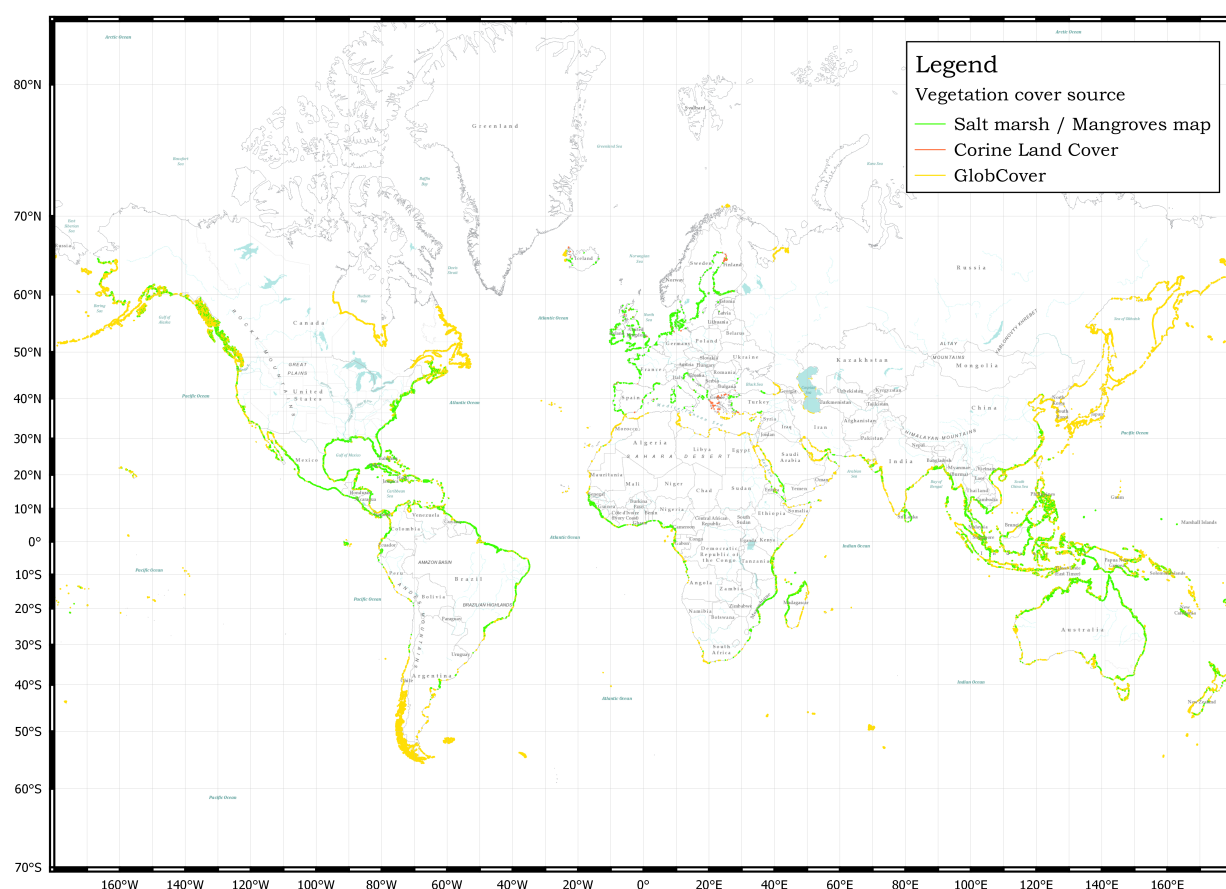


Figure 4.9: World map with overview of used vegetation cover sources

### Vegetation type

An overview of the most occurring vegetation type per transect is given in Figure 4.10. Mainly in Australia, China, South Africa and Peru salt marshes as well mangroves are found closely together.

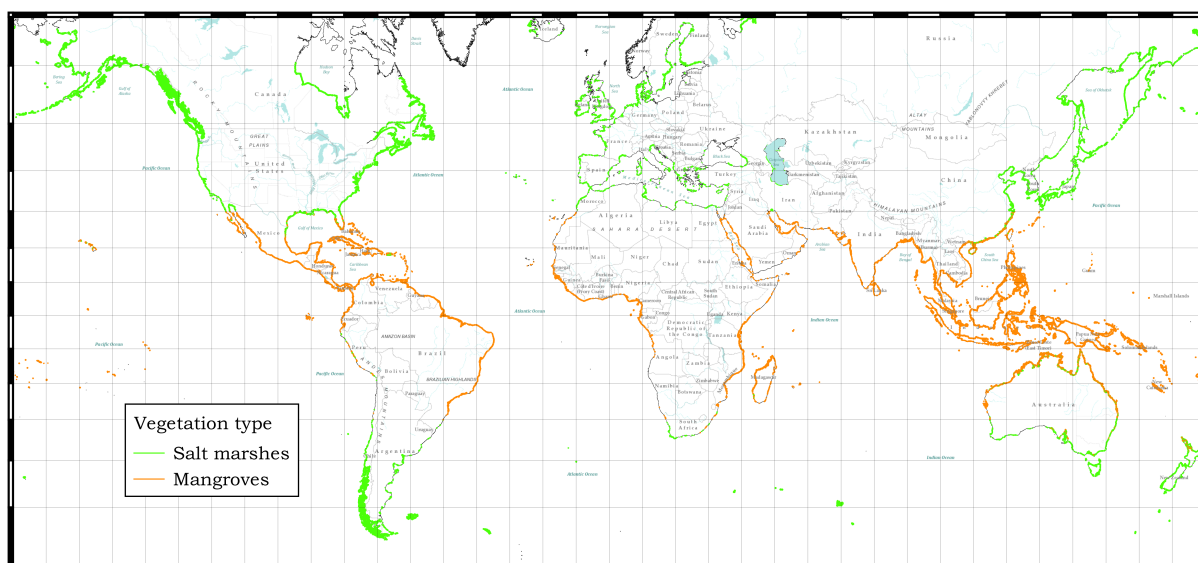


Figure 4.10: World map with overview of vegetation presence -and type

### Vegetation width

In Table 4.3 areas and countries are listed in which transects are found with extensive vegetation widths. The intermediate results show that most vegetated transects have a vegetation width between 0 and 100 m, as presented in Figure 4.11. In total 31 % of the studied coastline is vegetated. Furthermore, less extensive vegetated transects are likely vegetated by salt marshes and among extensive vegetation widths more mangroves are observed.

America	Europe	Africa	Asia	Oceania
Hudson-Bay Gulf of Mexico Brazil Colombia	United-Kingdom Denmark Netherlands France East-Spain	Guinea Nigeria Cameroon Mozambique Madagascar	Indonesia Bangladesh Myanmar Thailand Vietnam	Australia Papua-New Guinea

Table 4.3: Areas and countries with notable amount of extensive vegetated transects

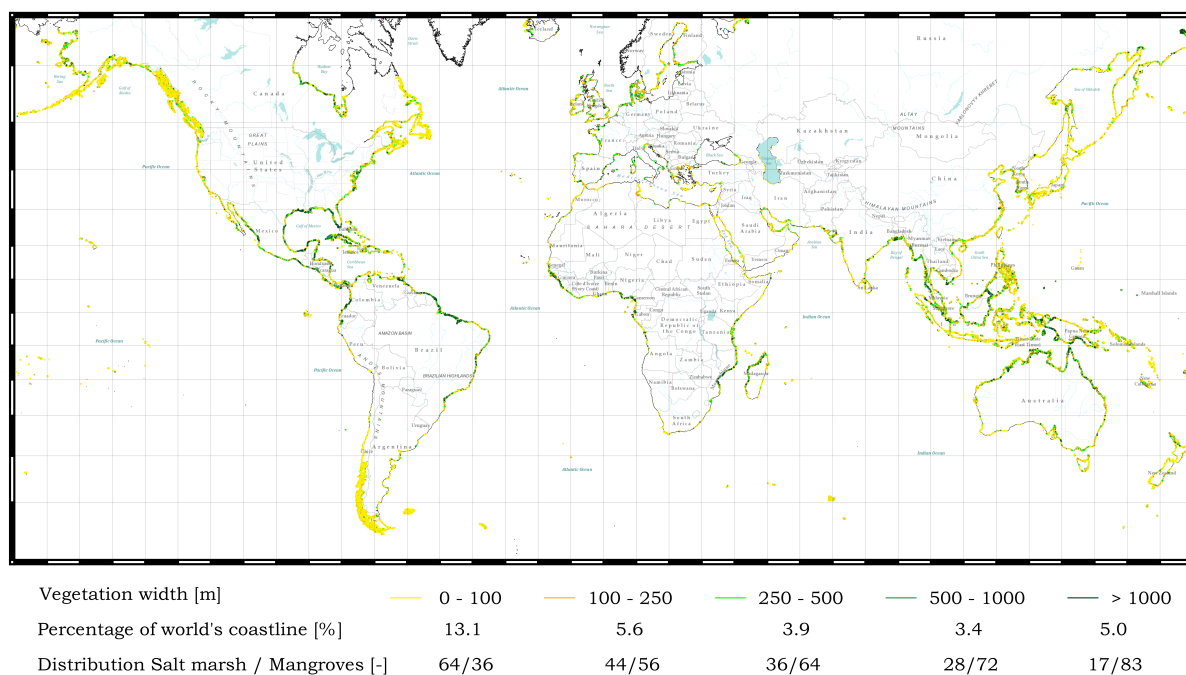


Figure 4.11: World map with overview of vegetation width

## 4.5. Step 5: Determination of wave attenuation

Once the foreshore and vegetation parameters are determined, wave propagation over the foreshore is calculated. Wave propagation is preferably calculated by a numerical model. This approach is not feasible, due to the high number of transects. For this reason a large set based on XBeach surfbeat pre-runs is constructed, referred to as the look-up table. From the different wave propagation models described in Section 2.4.2 XBeach surfbeat is chosen, because of the inclusion of infragravity waves.

### Look-up table

In this study the look-up table mimics a XBeach calculation and returns wave attenuation over the foreshore based on several input parameters. For each transect is searched for the closed match between the input conditions and a dataset of XBeach pre-runs. Theoretically if all possible situations are covered in the look-up table the same answer as the numerical model result will be returned. However, in practice only a limited amount of conditions are covered in this dataset.

The dataset is constructed based on various wave heights, wave steepnesses, water depths, vegetation types and foreshore slopes. The wave direction is assumed to be shore normal, which results in the most conservative situation. The choice of input parameters is based on a preliminary input conditions study which focused mainly on the UK due to its large range of coastal features, but also based on a preliminary global run. Output of these pilot studies can be found in Appendix D.7. An overview of the conditions is given in Table 4.4. XBeach runs are performed for all possible input combinations, resulting in about 32000 individual runs. Output is written at multiple grid points resulting in coverage for different foreshore and vegetation widths. In total the dataset consists of 668 304 data points.

Parameter	Values
Significant wave height [m]	0.5, 1.0, 1.5, 2.0, 2.5, 3.0, 3.5, 4.0, 4.5, 5.0, 6.0, 7.0, 10.0
Water level [m +MSL]	1.0, 1.5, 2.0, 2.5, 3.0, 3.5, 4.0, 4.5, 5, 5.5, 6.0, 6.5, 7.0, 7.5, 8.0, 10.0
Wave steepness [-]	0.14, 0.067, 0.033
Foreshore slope [1/slope]	10, 20, 40, 70, 100, 150, 200, 250, 300, 400, 500, 600, 700, 800, 1000, 1500, 2000
Vegetation width [m]	25, 50, 75, 100, 150, 200, 250, 300, 400, 500, 600, 700, 800, 900 1000, 1200, 1400, 1600, 1800, 2000

Table 4.4: Conditions used for XBeach pre-runs

The combinations are run for two vegetation types and for a bare foreshore. The vegetation characterization is presented in Table 4.5.

Parameter		Salt marshes	Mangroves
$N$	[m <sup>-2</sup> ]	1225	30
$b_v$	[mm]	1.25	35
$h$	[m]	0.30	3.0
$C_D$	[-]	0.19	1.0

Table 4.5: Biophysical parameters used during XBeach pre-runs

### Wave attenuation

The wave height at the end of the foreshore or vegetated zone is determined based on six parameters: (1) Significant wave height, (2) Water depth, (3) Peak wave period, (4) Foreshore slope, (5) Vegetation width, (6) Cover type. The input values for the significant wave height and the water depth should be determined at the start of the foreshore or at the start of the vegetated zone, depending on the presence of vegetation. The water depth is defined as the difference between the extreme water level and the bed level. The governing wave height is determined based on a depth breaking criterion of 0.55 and the previously explained water depth. For the wave period the offshore conditions are used.

In case of a bare foreshore the governing input location is begin of the foreshore. This scenario will obviously not result in wave attenuation by vegetation, but gives the wave height at the end of the foreshore. In case of a vegetated foreshore the governing input location is begin of the vegetated zone. The output consists of the wave height for the situation with and without vegetation cover. Wave attenuation by foreshore vegetation is calculated by comparison of the wave height at the end of the foreshore for a bare foreshore and vegetated foreshore.

#### 4.6. Step 6: Calculation of required dike freeboard

Wave damping is determined by comparing the wave height at the end of the vegetated zone with bare foreshore situation. In general foreshore vegetation does not prevent flooding, because the capacity to decrease surge levels is limited. For this reason a dike profile is assumed to be present at the end of the foreshore, as no global database of flood protection structures exists and e.g. dikes are not visible on global topography maps. The assumed dike profile has an inner and outer slope of 1:3, no berm and no protective cover. A critical overtopping rate of 1 l/s/m is used, which is realistic for the assumed profile, but induces an overestimation of the effect of vegetation if in reality e.g. a well maintained grass cover is present. The goal is not to come up with a dike design, but with an indicator for the effectiveness of vegetation on the foreshore. This indicator, dike height reduction by foreshore vegetation, is obtained by subtracting the required freeboard for a bare foreshore and vegetated foreshore, as described in Equation (4.1).

$$\Delta R_c = R_{c,noveg} - R_{c,veg} \quad (4.1)$$

First the root-mean-square wave height and the peak wave period are transformed to the spectral wave height and spectral wave period, as described in Equation (4.2) and Equation (4.3).

$$H_{m0} = H_{rms} \cdot 2\sqrt{2} \quad (4.2)$$

$$T_{m-1,0} = T_p / 1.1 \quad (4.3)$$

Next the required crest height for the situation with and without vegetated foreshore is calculated. The required freeboard for the various return periods is calculated based on the overtopping formulas (EurOtop, 2007). The formulations can be found in Section 2.3 and Appendix A.

# 5

## Results

In Chapter 4 the model approach is described and intermediate results are presented. In this chapter the final results of the global assessment in terms of wave height reduction and crest height reduction by foreshore vegetation are presented. The assessment is performed for nine return periods, but the values in the chapter's figures correspond to a return period of 100 years.

This chapter consists of three main sections:

- 1. Wave height reduction
- 2. Crest height reduction
- 3. Social impact of flood hazard reduction by foreshore vegetation

In the first section extra attention is paid to the behavior of the model by linking the behavior to observations in previous research. Here a general distinction is made between mangroves and salt marshes, because they differ in biophysical properties and living environment. Next a further distinction is made based on the hydrodynamic boundary conditions. Last, the influence of the vegetation characterization is evaluated based on a case study for the East coast of Australia. A complete overview of group boxplots, histograms and scatter plots for the studied variables can be found in appendix D. The second section shows the results of the translation from wave damping to crest height reduction. The last section aims on the social impact of vegetated foreshores.

The world maps are hosted online and can be accessed via:

<https://easyzoom.com/albumaccess/1aa634dc333e445f9c03f72823cc5605>

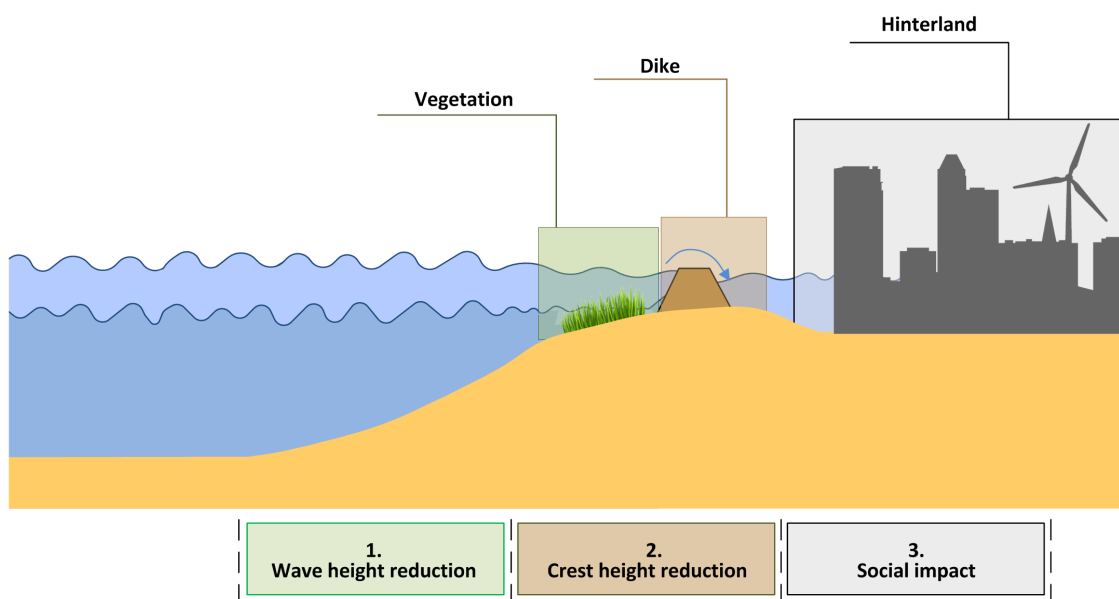


Figure 5.1: Results of the global flood hazard assessment

## 5.1. Wave height reduction

In the global assessment 495361 transects are evaluated of which 154062 are vegetated. This section treats the wave damping results on these transects. In the results a distinction is made between wave damping in absolute terms and relative terms.

### 5.1.1. Wave attenuation by foreshore vegetation in absolute terms

Wave attenuation is obtained by comparison of the wave height results for a bare foreshore and vegetated foreshore. The difference in wave height at the end of the foreshore gives the wave attenuation in absolute terms, described in Equation (5.1).

$$\Delta H_{m0} = H_{m0, \text{end noveg}} - H_{m0, \text{end veg}} \quad (5.1)$$

In Table 5.1 wave attenuation results are presented for various bins. Roughly 70 % of the vegetated transects showed a significant wave height reduction below 30 centimeters. Along 5 % of world's coastline, 15% of the vegetated transects, a wave height reduction of at least 30 centimeters is observed. The highest attenuation results are clearly obtained for transects vegetated by mangroves.

$\Delta H_{m0}$ [m]	0.0 - 0.10	0.10 - 0.20	0.20 - 0.30	0.30 - 0.40	0.40 - 0.50	0.50 - 0.75	0.75 - 1.00	> 1
Amount of transects [-]	47958	31389	26630	9748	4787	5950	2325	1398
Percentage of all transects [%]	9.7	6.3	5.4	2.0	1.0	1.2	0.5	0.3
Percentage of vegetated transects [%]	31.1	20.4	17.3	6.3	3.1	3.9	1.5	0.9
Salt marshes [%]	19.6	7.2	3.8	1.4	0.8	1.1	0.4	0.1
Mangroves [%]	11.5	13.2	13.5	4.9	2.3	2.8	1.2	0.8

Table 5.1: Distribution of transects over wave attenuation bins

In Figure 5.2 the results are shown visually for the higher wave attenuation bins. The earlier mentioned areas based on their extensive vegetated transects, are all marked in the world map.

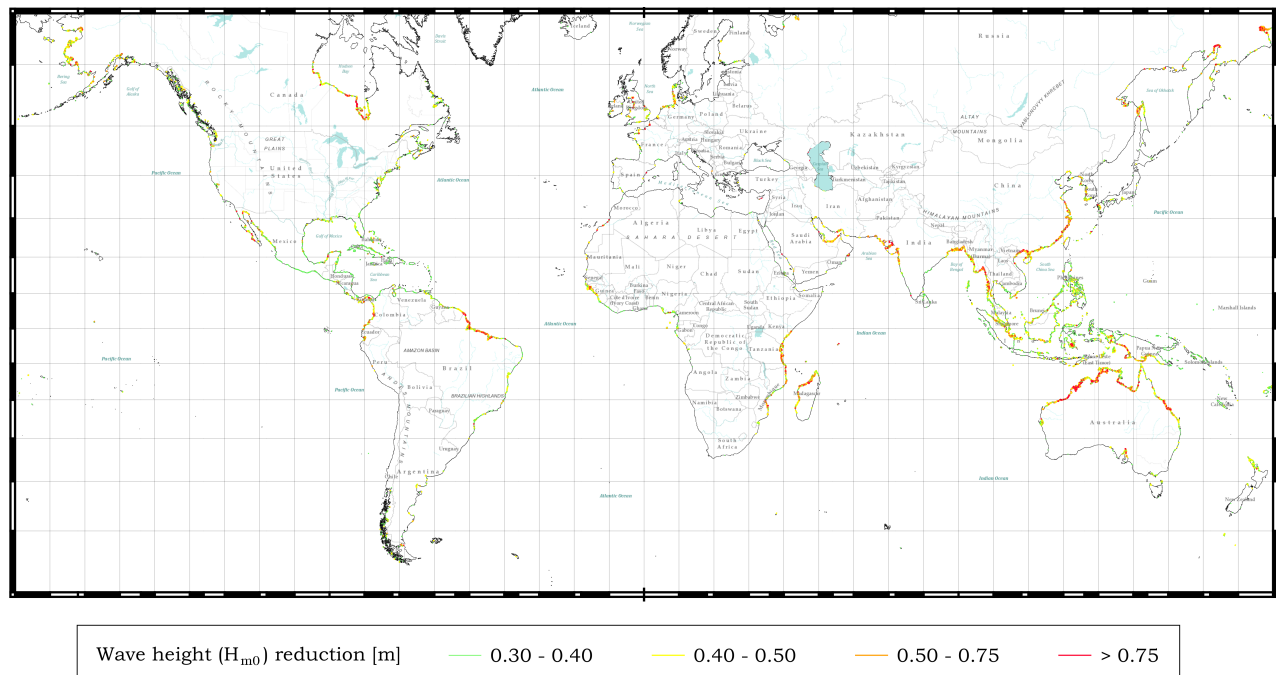


Figure 5.2: Global potential of wave damping by foreshore vegetation for a return period of 100 years



### 5.1.2. Wave attenuation by foreshore vegetation in relative terms

The use of absolute wave attenuation,  $\Delta H_{m0}$ , gives a bias towards areas which cope with high significant wave heights, because it is e.g. almost impossible to achieve a  $\Delta H_{m0}$  of 0.80 m on a wave with a  $H_{m0}$  of 1.00 m. In order to get better insight in the wave attenuation process a relative measure of wave attenuation is used, described in Equation (5.2).

$$\text{Reduced wave transmission} = \Delta H_{m0} / H_{m0, \text{start veg}} \quad (5.2)$$

In Table 5.2 wave attenuation in relative terms is presented over various bins. Overall about 7 % of all transects, 21 % of the vegetated transects, showed wave damping relative to the incoming wave height higher than 20%. The results show that on average, the incoming wave height is more damped on transects vegetated by mangroves. This is explained by the different territory of the two vegetation types and their biophysical properties. Based on Figure D.1, Figure D.17 and Figure 4.10 can be seen that salt marshes are observed in areas with higher offshore wave heights and in areas with higher extreme water levels. In addition, salt marshes have a far lower stem height. The disadvantageous relative stem height to water depth ratio for salt marshes result in less attenuation for marshes, which is in line with research of [Yang et al. \(2011\)](#). The choice of the value of the last bin in Table 5.2 is not arbitrary, because only in a few cases more than 60 % of the incoming wave height was damped by vegetation.

$\Delta H_{m0} / H_{m0, \text{start veg}} [-]$	0.0 - 0.10	0.10 - 0.20	0.20 - 0.30	0.30 - 0.40	0.40 - 0.50	0.50 - 0.60	> 0.60
Amount of transects [-]	27434	14368	9605	9342	7281	5435	1437
Percentage of all transects [%]	5.5	2.9	1.9	1.9	1.5	1.1	0.3
Percentage of vegetated transects [%]	17.8	9.3	6.2	6.1	4.7	3.5	0.9
Salt marshes [%]	14.8	5.2	2.6	2.0	0.7	0.1	0.0
Mangroves [%]	3.0	4.1	3.6	4.1	4.0	3.4	0.9

Table 5.2: Distribution of transects over relative wave attenuation bins

In Figure 5.3 the wave attenuation results in relative terms are shown. Mainly areas in the tropics, e.g. Indonesia and the Philippines stand out in comparison with the results in absolute terms presented in Figure 5.2.

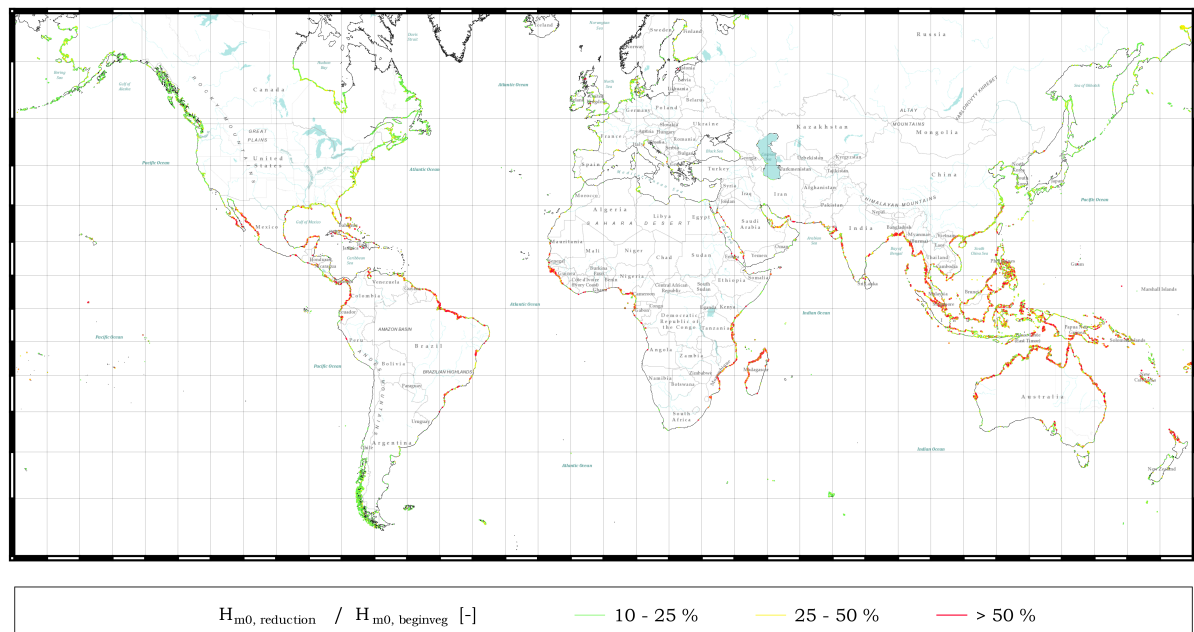


Figure 5.3: Global potential of wave damping in relative terms by foreshore vegetation for a return period of 100 years



### 5.1.3. Model behavior

The relation between wave attenuation by foreshore vegetation and several parameters is studied based on the assessed transects. The studied variables are: wave height, extreme water level, depth at begin of the vegetated zone, foreshore slope and vegetation width. Wave attenuation is expressed in absolute terms, but also relative to the incoming wave height and relative to the depth at the start of the foreshore. The model behavior is studied to check if the outcomes of the global assessment are in line with results from earlier research.

#### Wave attenuation patterns in global assessment

The relation between wave attenuation and the studied parameters is made visually using group boxplots. In these boxplots the amount of transects per bin differs between about 30.000 and 150 transects. A distinction is made between salt marshes and mangroves, due to their difference in living environment and biophysical properties.

#### Wave height

During the research no very clear trend is observed between the offshore significant wave height and wave reduction. This is observed because, the offshore wave height is more an indication of the general wave climate and differs from the wave height in front of the vegetated zone. The relation between the wave height at the start of the vegetated zone and wave reduction is presented in Figure 5.4 and 5.5. Wave attenuation in absolute terms increases for increasing wave height, which is line with research of (Tschirky et al., 2001). Wave attenuation in relative terms in Figure 5.6 and 5.7 shows a different trend. The maximum wave transmission reduction declines for increasing wave height at begin of the vegetated zone for salt marsh vegetation. For mangroves this same trend is observed for the medians of the boxplots. This might be explained by the relation between wave height and water depth. In most occasions the wave height at begin of the vegetated zone is depth limited. Thus a higher wave height is likely to correspond to a larger water depth. A strong dependency on water depth would explain the decreasing wave transmission reduction for increasing wave heights.

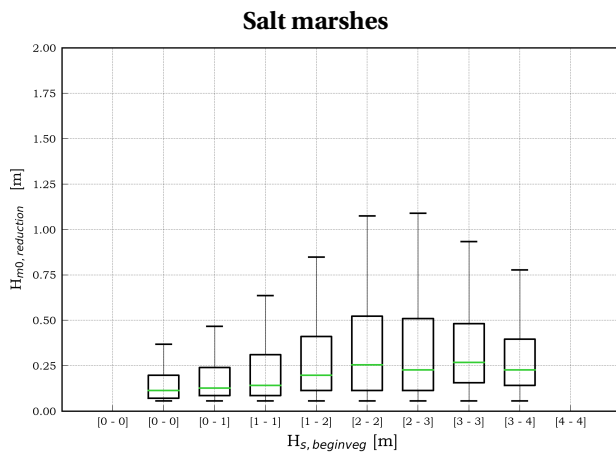


Figure 5.4: Effect of significant wave height at begin of vegetated zone on wave attenuation in absolute terms by salt marshes

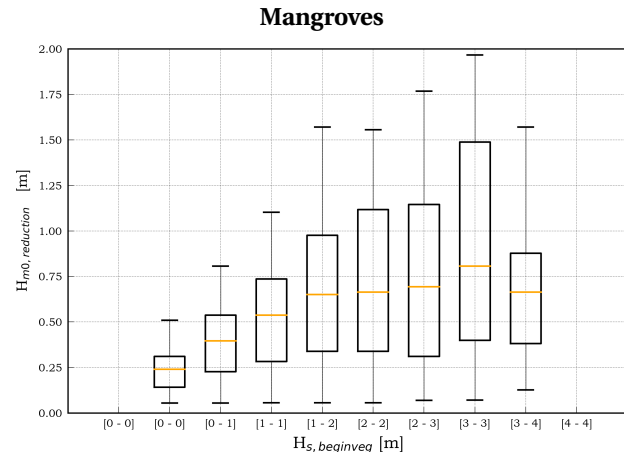


Figure 5.5: Effect of significant wave height at begin of vegetated zone on wave attenuation in absolute terms by mangroves

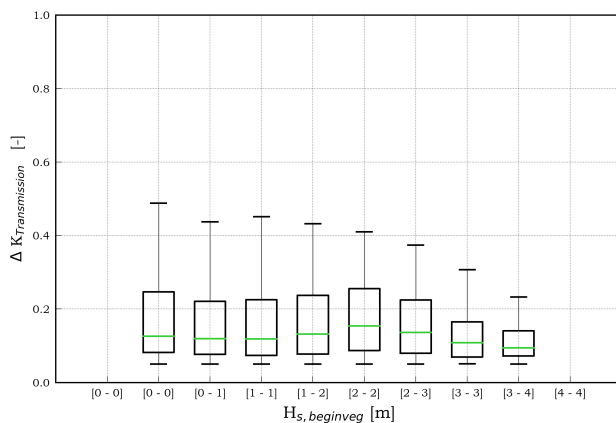


Figure 5.6: Effect of significant wave height at begin of vegetated zone on wave transmission reduction by salt marshes

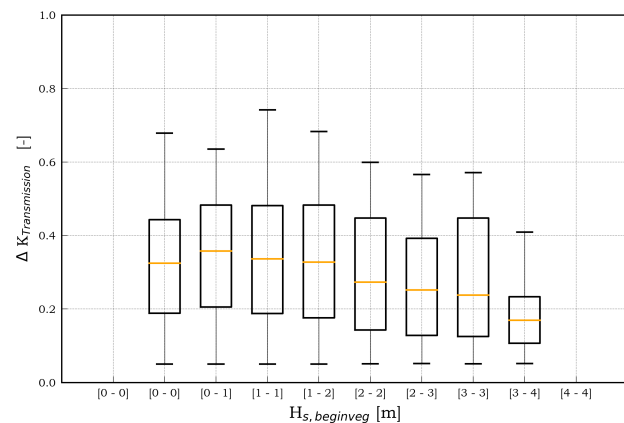


Figure 5.7: Effect of significant wave height at begin of vegetated zone on wave transmission reduction by mangroves

### Water level

The extreme water levels from the GTSM model represent a combination of tide and surge. Both vegetation groups show an increase in attenuation for larger extreme water levels. This is directly opposite to earlier performed research e.g. by (Yang et al., 2011). The results shown in Figure 5.8 and 5.9 are not wrong, but should be interpreted differently. The trends in these figures show the combined results of thousands of transects. One should keep in mind that the other parameters are not static, but have various values and are interrelated. In this case it is likely that a higher depth correspond to higher wave heights, which make it more easier to achieve higher attenuation results in absolute terms. Furthermore the combination of tide and surge suggests that conditions for vegetation growth are probably better in areas with higher extreme water levels. As more extensive vegetation fields are expected for locations with a large tidal range.

The wave transmission reduction related to the depth at begin of the foreshore show a different trend. For salt marshes a decrease in wave transmission is observed for increasing extreme water levels. For mangroves this trend is less clearly visible. This result is comparable with the relation observed between vegetation width and wave attenuation relative to the depth at the start of the vegetated zone. These differences can be explained partly by the relative short height of salt marshes in comparison to mangroves, because with a smaller stem height the chance of submergence increases. Another aspect which contributes to this effect is the environment in which salt marshes are found. Salt marshes are often situated in areas where large extreme water levels can occur, which also increases the chance of submergence.

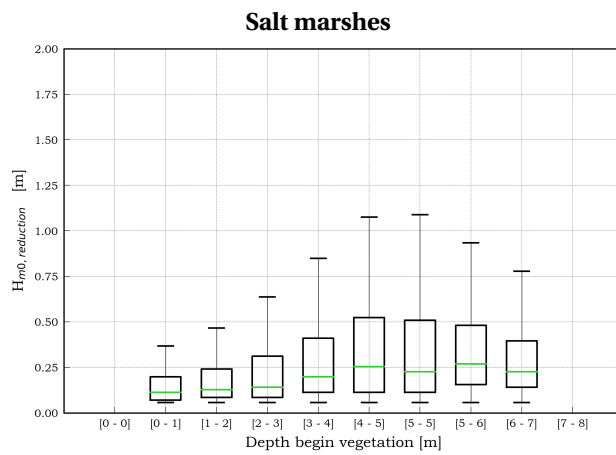


Figure 5.8: Effect of water depth in front of vegetated zone on wave attenuation in absolute terms by salt marshes

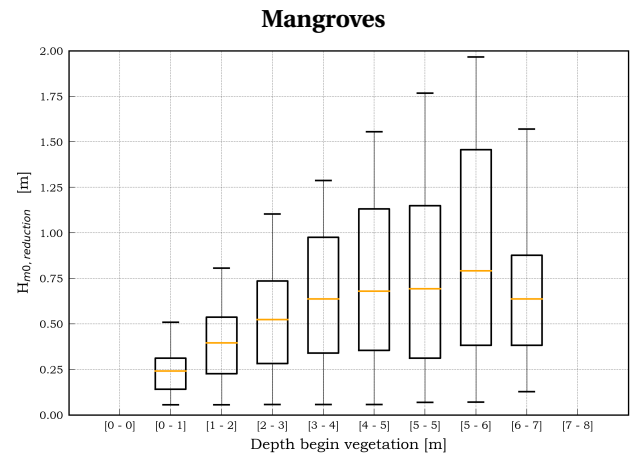


Figure 5.9: Effect of water depth in front of vegetated zone on wave attenuation in absolute terms by mangroves

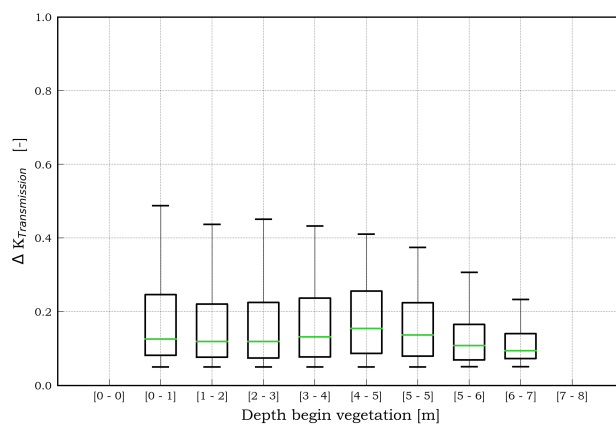


Figure 5.10: Effect of water depth in front of vegetated zone on wave transmission reduction by salt marshes

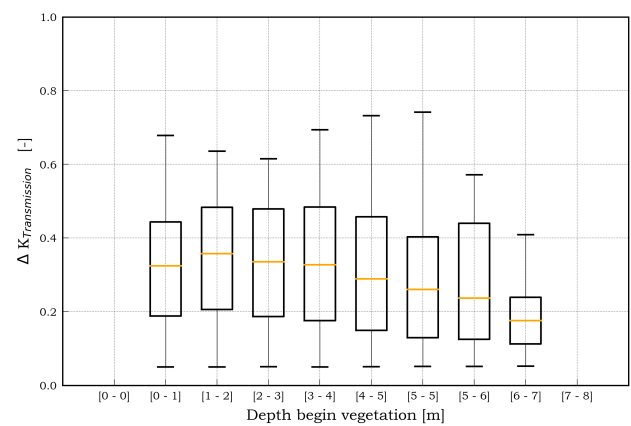


Figure 5.11: Effect of water depth in front of vegetated zone on wave transmission reduction by mangroves

### Foreshore slope

For both vegetation groups wave damping in absolute terms increases for milder slopes as can be seen in Appendix D.3. Wave attenuation relative to the depth in front of the vegetated zone in Figure 5.12 and 5.13 shows a clear upwards trend. This indicates that wave attenuation increases for milder slopes and for decreasing water depths.

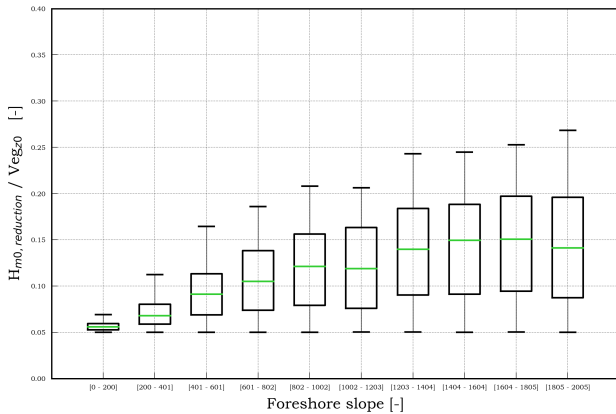


Figure 5.12: Effect of foreshore slope on wave attenuation by salt marshes relative to depth in front of vegetated zone

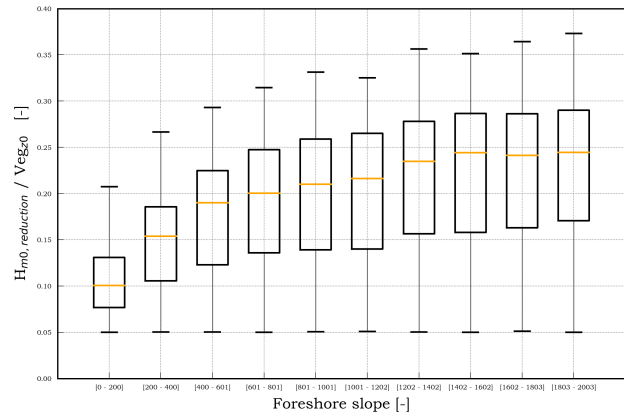


Figure 5.13: Effect of foreshore slope on wave attenuation by mangroves relative to depth in front of vegetated zone

### Vegetation width

Globally more foreshores are vegetated by mangroves than by salt marshes. Furthermore the width of the mangrove belts exceeds the salt marsh field width which can be seen in Appendix D.2. A salt marsh vegetation width above 4000m is hardly found during the study. On the other hand, for a few thousand transects vegetated with mangroves a vegetation width above 4000 m is observed.

Wave attenuation in absolute and relative terms increases for increasing vegetation width. The strongest relation is observed for the reduced wave transmission. The largest damping takes place in the first hundreds of meters of the vegetated zone for mangroves. In the first 450 meters the median reduced wave transmission is about 25 %. For some transects in this bin the observed maximum of roughly 60 % reduction is already obtained. After 900 m the median reduction remains relatively constant. For salt marshes slightly lower rates are observed. About 10 % and 25 % in the first 450 m and 900 m respectively. The maximum observed median wave attenuation rate for salt marshes is about 40 %. A maximum vegetation width of 2000 m is used in the look-up table. Without this limit, a higher attenuation rate would probably be observed for transects with a vegetation width greater than 2000 m. The full results are presented to show the decrease in uncertainty in wave attenuation for increasing vegetation width, which is especially notable for salt marshes.

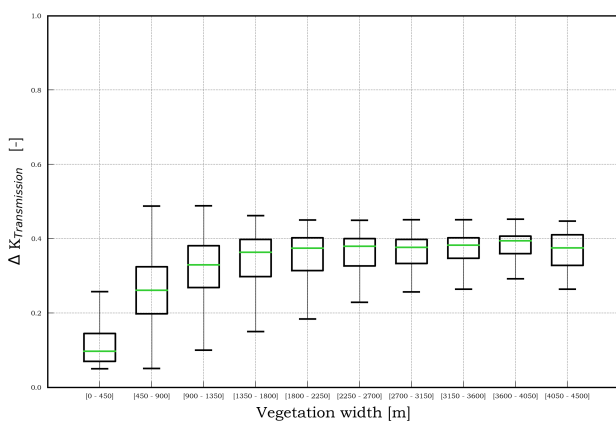


Figure 5.14: Effect of vegetation width on wave transmission reduction by salt marshes

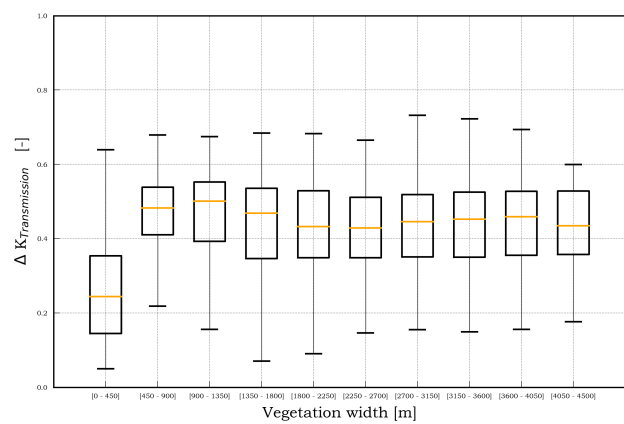


Figure 5.15: Effect of vegetation width on wave transmission reduction by mangroves

### Wave attenuation patterns in exposed and sheltered environments

Besides vegetation type another distinction is made, in order to get better insight in the wave damping process and the relation to hydrodynamic conditions. The second distinction is made based on difference in hydraulic boundary conditions. A exposed environment characterized by large offshore wave heights and extreme water levels e.g. USA's West coast versus a more sheltered environment like the coast of Malaysia. The boundaries for these two environments are presented in Table 5.3. The reader should keep in mind that the distinction is made based on offshore conditions. This implies that the results for the different environments are mainly induced by difference in water level, because the offshore wave height is no direct measure of the wave height in front of the vegetated zone.

Environment	$H_{s, offshore}$ [m]	$T_p$ [s]	Extreme water level [m +MSL]
Exposed environment	> 4	> 12	> 4
Sheltered environment	< 6	< 12	< 3

Table 5.3: Characterization of exposed environment and sheltered environment

The wave damping results in absolute terms for both environments are shown in Appendix D.2. It stands out that the most mangroves can be found in the defined sheltered environment. In addition, wave attenuation in absolute terms is larger in an exposed environment. [Songy \(2016\)](#) found a strong dependency on the foreshore slope and for this reason two slope bins are plotted. For both vegetation types and environments more wave attenuation is observed for milder slopes.

In Figure 5.16 and Figure 5.17 the wave transmission over the vegetation fields is plotted for both environments. The wave transmission in these figures is a combination of wave height reduction by depth induced breaking, bottom friction and wave vegetation interaction. For steeper slopes wave energy is reduced faster than for mild slopes. This explained by the decreasing depth, by which wave breaking is induced. So one could say that for a steep vegetated slope there is less potential for damping by vegetation, because most waves losing energy by depth induced breaking. This hypothesis is supported by Figure 5.18 and Figure 5.19 in which wave reduction by vegetation relative to the incoming wave height is plotted. Less damping by vegetation is observed for steeper slopes, independent of the vegetation type or environment. The observations indicate a shift from depth induced wave energy dissipation towards vegetation induced energy dissipation for milder slopes.

More clearly visible is the maximum wave damping rate induced by vegetation, described earlier in Section 5.1.3. For mangroves the limit is roughly 60 % and for salt marshes 40 %, but this percentages will change for different vegetation characterizations. In addition, the percentages are limited by the vegetation widths and foreshore slopes covered in the look-up table. The maximum rates are equal for the defined environments, but the difference in slope of the scatter cloud indicates that the limit is reached faster in sheltered environments. This is explained by the water level difference between the two environments.

### Influence of vegetation characteristics

In the global assessment two vegetation types are used, salt marshes and mangroves. These vegetation types are modeled using the biophysical characterization presented in Section 4.5. In reality various configurations can be found, e.g. different stem densities. For salt marshes the variations depend on the salt marsh type, but also on temporal changes in e.g. temperature. The temporal influences are more important at higher latitudes, because colder temperatures occur e.g. in Northern Europe than in Southern Europe. During this research an overview of biophysical salt marsh properties found in literature are bundled, with special attention for differences between species and differences between summer and winter state. These results are presented earlier in Section 2.5. For mangroves temporal influences are less important, but differences exist between mangrove types. In the research of [Janssen \(2016\)](#) an extensive study is performed in order to come up with various biophysical schematizations which can be used to include mangroves in hydrodynamic numerical models. Based on the above described sources extra XBeach pre-runs are performed for new vegetation characterizations. In total data is added to the look-up table for four new vegetation characterizations, two for each vegetation type. The vegetation characterizations can be found in Appendix F.

The new characterizations are used to get insight in the influence of vegetation characteristics on the results of the global assessment. A case study is performed for a part of the east coast of Australia, where both salt marsh and mangroves are present. An overview of the case study area can be found in Appendix E.2. The case study area contains in total 1172 transects, of which 34 vegetated by salt marsh vegetation and 277 by mangroves. Wave attenuation is calculated for various return periods, similar to the global assessment. The results for a return period of 10, 100 and 1000 years are compared to get insight in the sensitivity to both the hydraulic boundary conditions and vegetation characterizations. The hydraulic conditions are presented in Table 5.4.

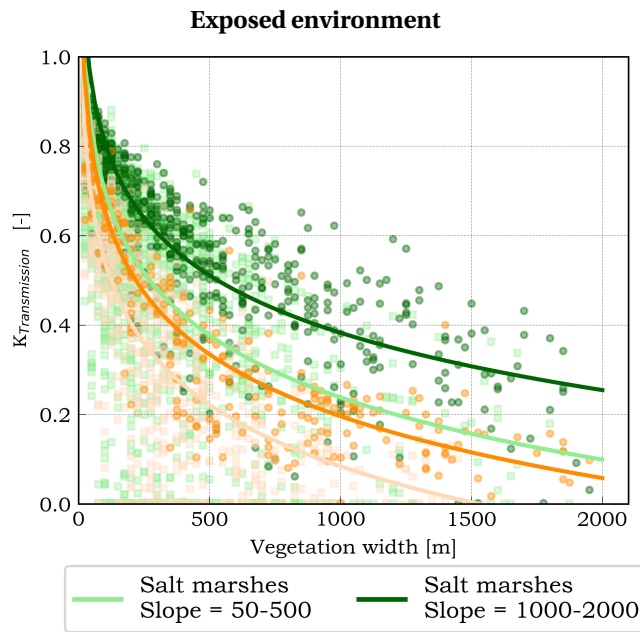


Figure 5.16: Wave transmission over vegetated field in exposed environment

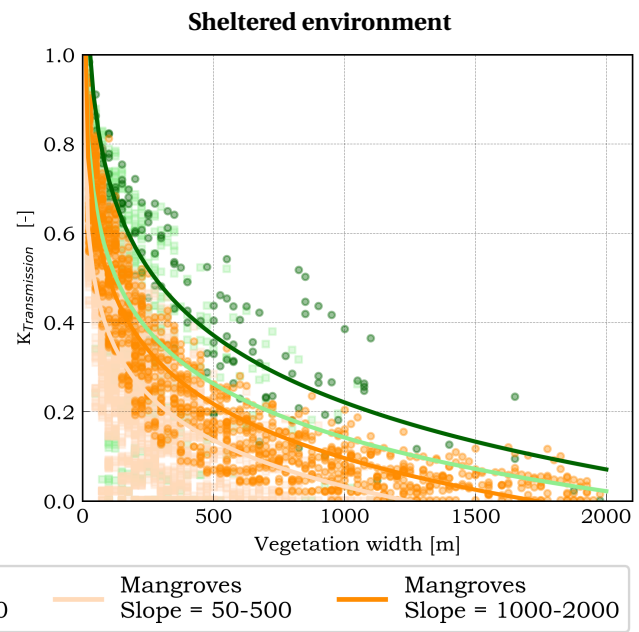


Figure 5.17: Wave transmission over vegetated field in sheltered environment

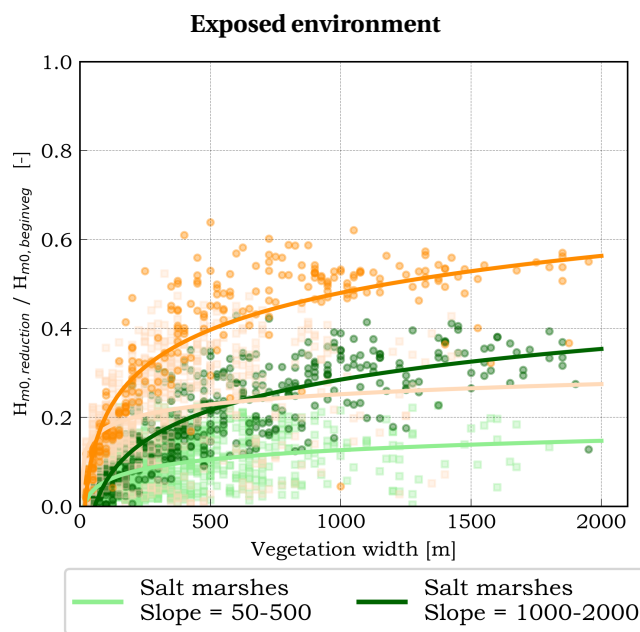


Figure 5.18: Wave attenuation relative to incoming wave height in exposed environment

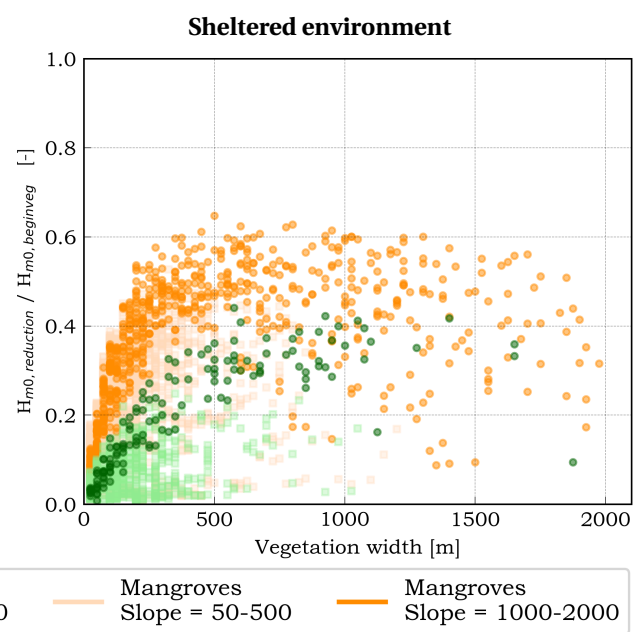


Figure 5.19: Wave attenuation relative to incoming wave height in sheltered environment

Return period	$H_{s, offshore}$ [m]	$T_p$ [s]	$H_{s, start veg}$ [m]	Water level [m +MSL]
10 years	4.0	11.4	0.98	2.04
100 years	5.1	12.5	1.07	2.20
1000 years	6.3	13.4	1.17	2.36

Table 5.4: Hydraulic boundary conditions for case study at the East coast of Australia

## Results

The results of the case study are plotted in Figure 5.20 and Figure 5.21 in which wave transmission reduction is used as measure of the effect of vegetation. Wave transmission reduction for the studied return periods is very small, so only the results corresponding to a 100 years return period are plotted. This would suggest that the wave transmission rates are quite independent on the hydraulic conditions, which seems unlikely. These results are probably obtained due to the resolution of the look-up table. In other words the small deviations among the return periods are too small to be represented well using the look-up table. An overview of the results for the three return periods are presented in Table 5.5.

For salt marsh vegetation the difference between the *Very sparse* type and other types is significant. The characterization mainly differs in stem density. The factor 4 decrease in stem density combined with a change in  $C_D$  and stem height results in a decrease of the wave transmission reduction from 22.5 % to 4.1 % in comparison to the *Global run* type. The results are in line with research of Songy (2016) who concluded that stem density was one of the most influential parameters. The stem density, stem diameter and drag coefficient have all the same linear relation in Equation (2.8) by Mendez and Losada (2004), but the large stem density differences make this parameter the most influential. The *Global run* type and *Denser* type mainly differ in stem height, 30 cm and 50 cm respectively. An overall increase in reduced wave transmission of about 9 % is observed between both types.

For mangroves the spread in results is smaller, with the largest difference of roughly 15 % between the *Pioneer* type and the *Global run* type. The pioneers are situated most seaward and have a very dense root layer, which results in very effective wave damping especially for low water depths. The *Global run* type is also schematized as pioneer mangrove, but a very young pioneer with less biomass. The *Rhizophora* type has a less dense root layer, but the roots are much thicker. Furthermore the stem height can easily exceed ten meters. This is a significant difference to the pioneers which are only a few meters in height. The *Rhizophora* type is normally not found at the seaward edge, but this situation can occur e.g. due to seaward erosion.

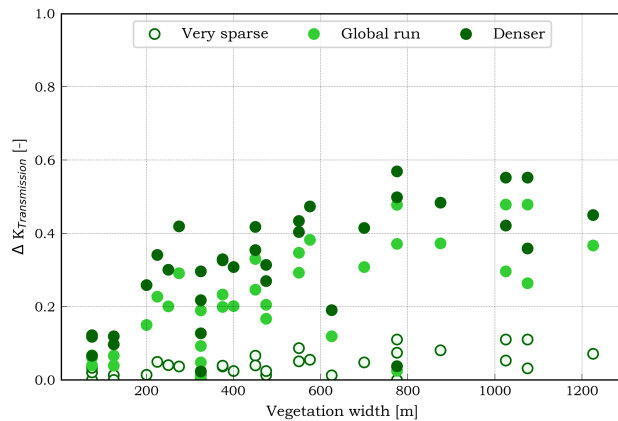


Figure 5.20: Reduced wave transmission for different salt marshes characterizations

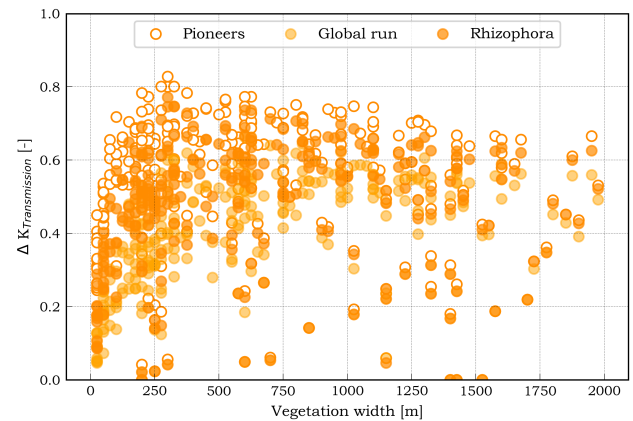


Figure 5.21: Reduced wave transmission for different mangrove types

Return period	Salt marshes			Mangroves		
	Very sparse	Global run	Denser	Pioneers	Global run	Rhizophora
10 years	0.040	0.225	0.313	0.528	0.381	0.465
100 years	0.041	0.225	0.314	0.543	0.387	0.476
1000 years	0.041	0.229	0.322	0.561	0.396	0.489

Table 5.5: Mean wave transmission reduction for various vegetation characterizations over three return periods

## Conclusion

Different salt marsh characterizations and mangroves types are compared. The schematization for salt marshes and mangroves used in the global assessment are conservative and far more optimistic properties can be found globally, e.g. large salt marsh stem heights in China. The *Very sparse* salt marsh state is hardly found in reality and will only occur during harsh winters at higher latitudes. However, the results show that the impact of decreased biomass can be enormous and has to be kept in mind.



## 5.2. Crest height reduction

The crest height reduction results from the global assessment are plotted in Figure 5.22. The results are indicative, because they are obtained by assuming the presence of a dike as described in Section 4.6. Logically, the same areas as presented in Figure 5.2 are marked. Only the areas with the largest crest height reduction in meters are plotted. A plot of the other bins can be found in Appendix D.5. The results show that for more than 10 % of the transects in the study area, roughly 59 000 km of coastline, a crest height reduction of at least 50 centimeters can be achieved due to foreshore vegetation.

$\Delta R_c$ [m]	0.0 - 0.10	0.10 - 0.25	0.25 - 0.50	0.50 - 1.00	1.00 - 2.00	>2.00
Amount of transects [-]	10189	21789	28870	40269	12542	6037
Percentage of all transects [%]	2.1	4.4	5.8	8.1	2.5	1.2
Percentage of vegetated transects [%]	6.6	14.1	18.7	26.1	8.1	3.9
Salt marshes [%]	5.6	9.4	8.7	6.1	2.7	1.0
Mangroves [%]	1.0	4.7	10.1	20.0	5.5	2.9

Table 5.6: Distribution of transects over crest height reduction bins

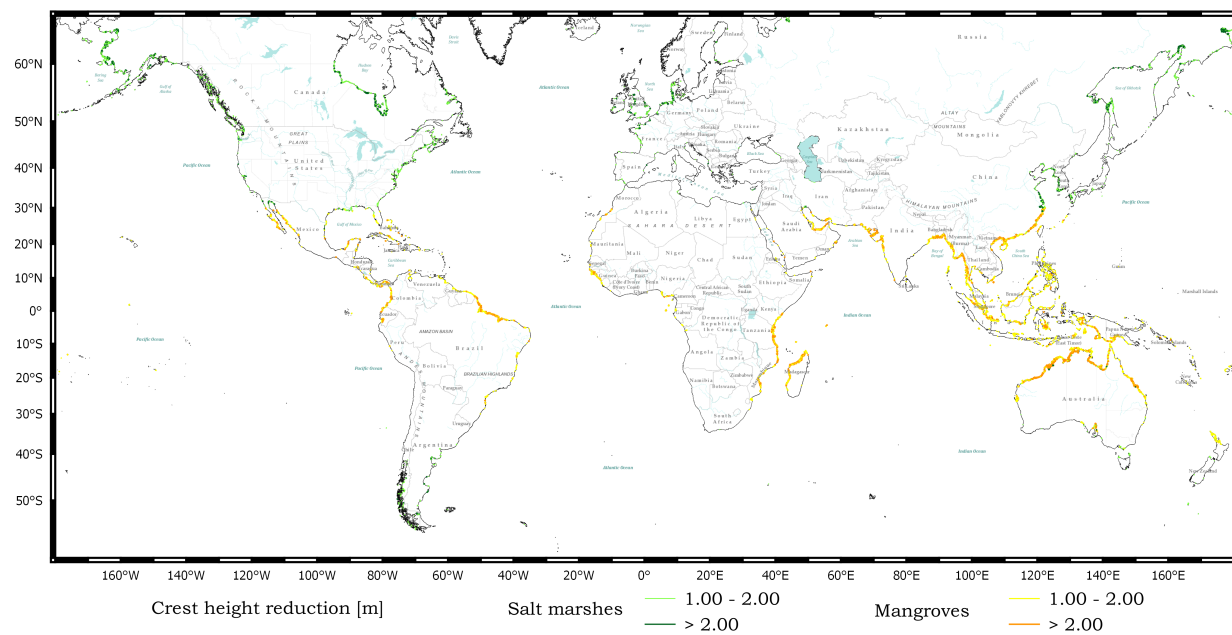


Figure 5.22: World map with overview of transects with a crest height reduction starting from 1 m by foreshore vegetation

### Influence of maximum overtopping criterion

In the global assessment a maximum overtopping criterion of 1 l/s/m is used. However, a dike with e.g. a well maintained grass cover will fail at a higher overtopping rate. The influence of the overtopping rate is studied by reanalysis of the results of the global assessment for three different overtopping rates. In Figure 5.23 is the relation between  $\Delta R_c$  and  $\Delta H_{m0}$  presented for  $q = 0.1$  l/s/m,  $q = 1$  l/s/m (global assessment) and  $q = 10$  l/s/m. For small wave height reductions the absolute difference among the results is not substantial. However, starting around  $\Delta H_{m0} = 0.6$ , the difference between the results for the different overtopping rates has a magnitude of roughly 1 m. The results show that the use of a maximum overtopping criterion of 1 l/s/m tends to overestimate the potential dike height reduction, if in reality a dike is present that can handle more than 1 l/s/m. In addition, the graph shows that the induced error is the largest for higher wave attenuation rates. Furthermore, the results are quite similar for different breaker parameters. This indicates that the influence of different slopes and different wave lengths, is less important than the choice for the overtopping criterion.

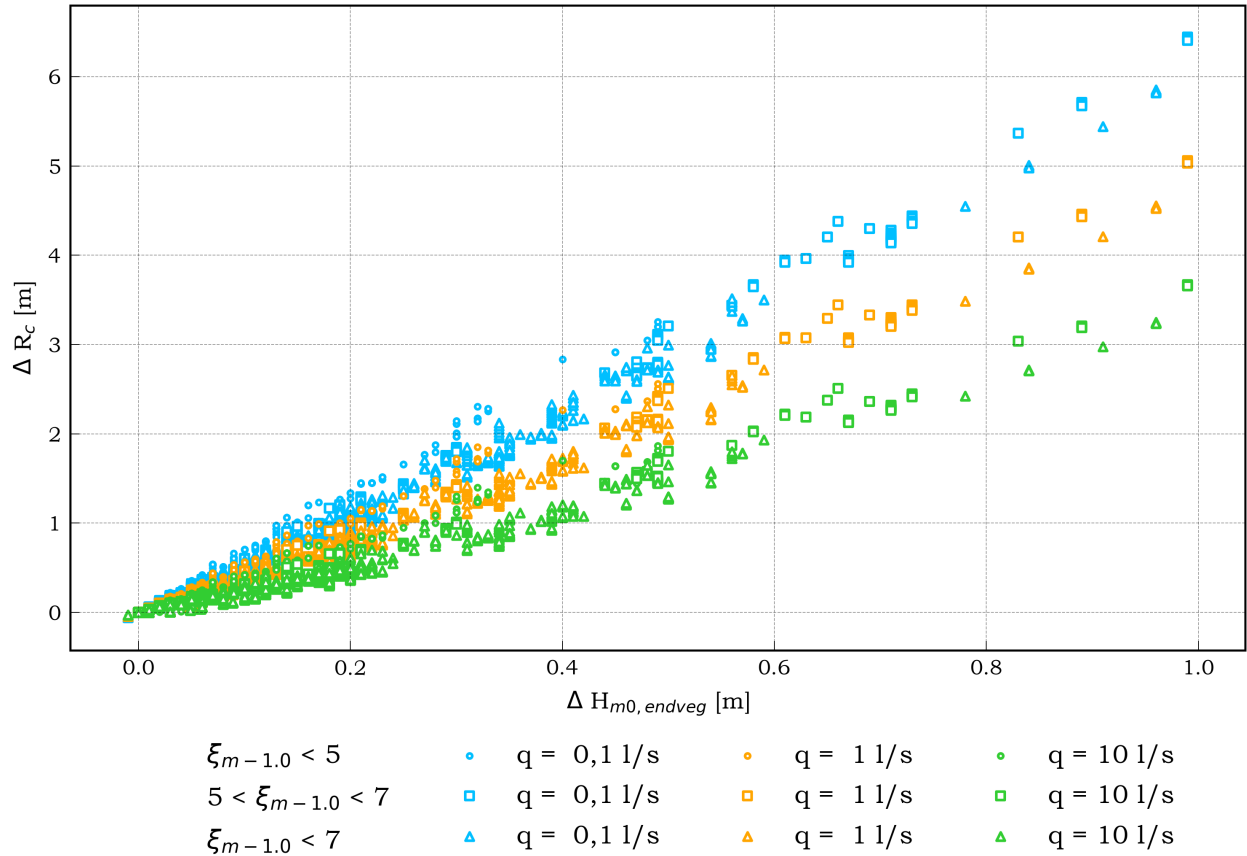


Figure 5.23: Influence of maximum overtopping criterion on crest height reduction by foreshore vegetation

### Crest height reduction per country

The crest height reduction results per country are derived by correlating the transects to a world borders dataset (Sandvik, 2009). Per country the total dike height reduction is calculated according Equation (5.3). Only transects exceeding a minimum wave attenuation threshold of 10 cm are taken into account, because lower wave attenuation results are assumed unreliable.

$$\text{Sum of dike height reduction per country} = \sum_{i=1}^n \Delta R_{c,i} \quad (5.3)$$

with  $n$  = number of transects in country with  $\Delta H_{m0} > 10\text{cm}$

The distribution of the sum of dike height reduction among countries has a bias towards countries with a long coastline, for this reason two other indicators are used to compare countries. The first indicator shows the dike height reduction by foreshore vegetation relative to the country's coastline length. In other words the average dike height reduction per kilometer coastline. In Figure 5.24 the top 15 countries are presented. A high value indicates a high potential of foreshore vegetation, however it remains unknown whether this is caused by a few extensive vegetated areas or a almost continuous, but less extensive, vegetated coast.



The second indicator shows the dike height reduction relative to the coastline length along wave attenuation of at least 10 cm is observed. A small difference between both indicators means a quite continuous vegetated coast. At the other hand, a large difference indicates the presence of a few extensive vegetated areas. A table with results for all countries in alphabetic order can be found in Appendix D.6.

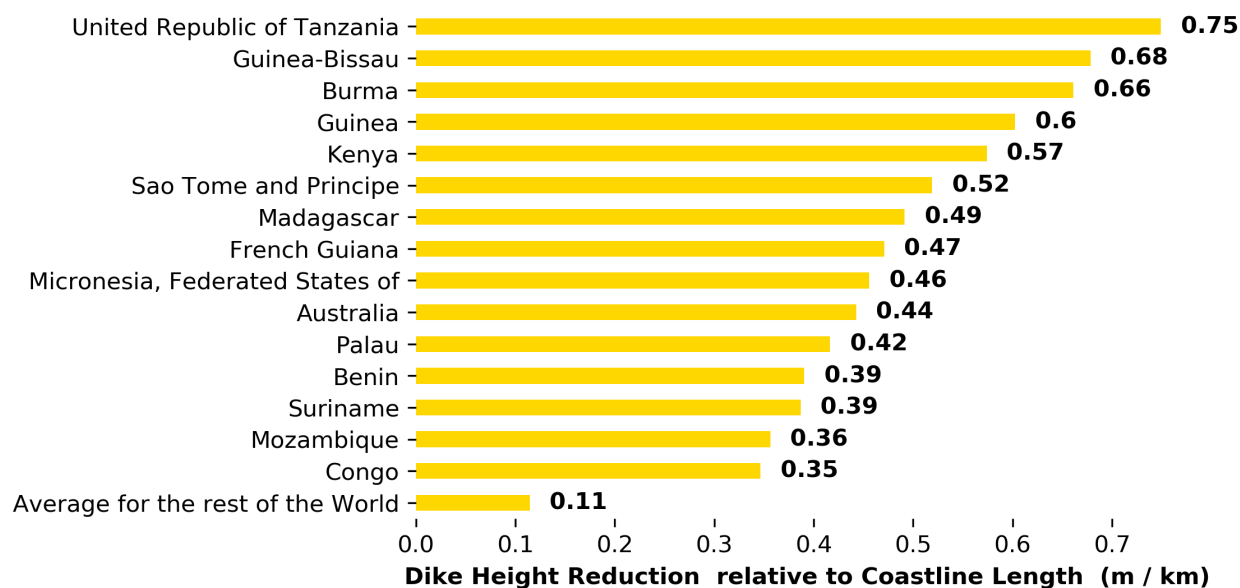


Figure 5.24: Top 15 countries with largest potential dike height reduction by foreshore vegetation relative to coastline length

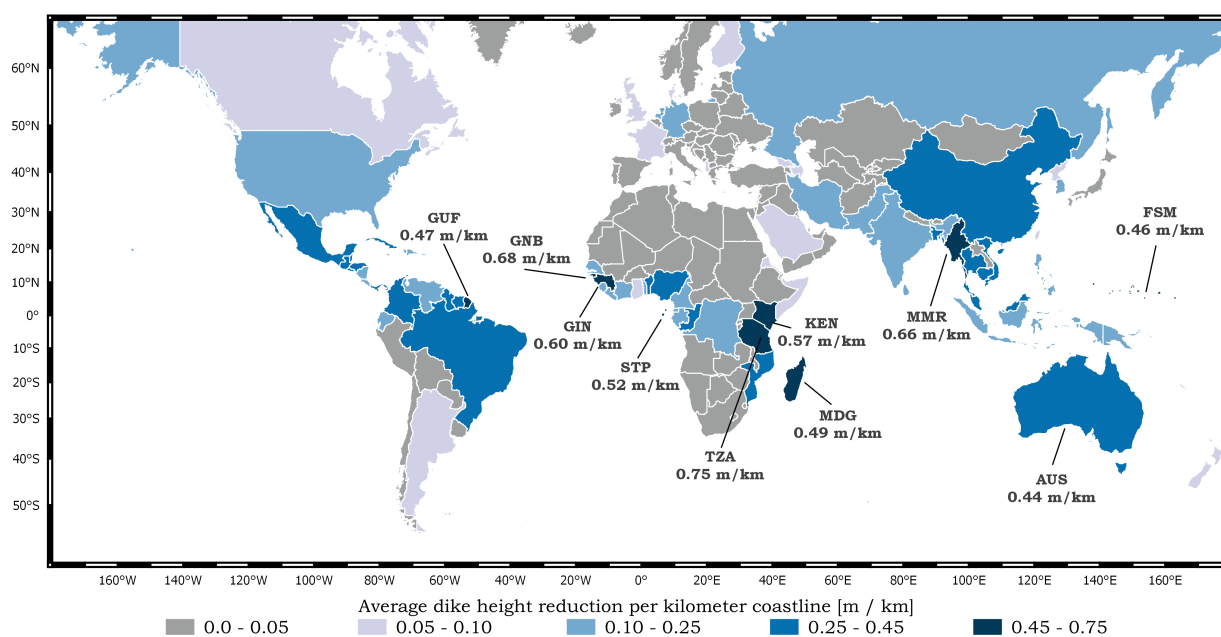


Figure 5.25: Global potential dike cost reduction by foreshore vegetation.

### 5.3. Social impact of flood hazard reduction by foreshore vegetation

The outcomes of the global assessment show that present coastal vegetation can play a role in protecting world's coastline from flooding, solely based on wave damping by wave-vegetation interaction. The truth value of coastal vegetation would be revealed by further translation of the results in terms of reduced population affected and reduced damage costs related to flood events. This translation is outside the scope of this research, but a first step is made towards the social impact of coastal vegetation on a global scale.

#### Wave reduction in the low elevation coastal zone

This step aims to identify vulnerable coastal areas and making a link with the wave attenuation results from the global assessment. Low elevation coastal zones (LECZ) are defined as the contiguous area along the coast that is less than 10 m above sea level. Almost two-thirds of urban settlements with populations greater than 5 million fall, at least partly, in this zone (McGranahan et al., 2007). In addition, analysis on urban expansion indicated that urban land expansion has been occurring faster in this zone than in other areas. It is exactly this zone, the LECZ, which is assumed to be vulnerable for flooding. Using the LECZ Urban-Rural Population map version 2 (30 arcs seconds) (CIESIN, 2013) an indication is given for which areas coastal vegetation is more beneficial. This map is made based on population data from the Global Rural-Urban Mapping Project (GRUMP)v1 and Gridded Population of the World (GPW) v3 in combination with elevation data from the Shuttle Radar Topography Mission (SRTM).

For every transect in the study area is checked if it intersects with rural or urban area in the LECZ. The results are presented in Figure 5.26 and in Table 5.7. The most vegetated transects are situated in front of rural areas. In total about 28 % of the vegetated transects situated in rural area have a potential to reduce the incoming wave height with at least 20 centimeters. For urban areas this percentages is 10 %.

$\Delta H_{m0}$ [m]	0.0 - 0.10	0.10 - 0.20	0.20 - 0.30	0.30 - 0.40	0.40 - 0.50	0.50 - 0.75	0.75 - 1.00	> 1
<i>Urban area</i>								
Amount of transects [-]	5931	4463	3587	1177	549	494	129	45
Percentage of vegetated transects [%]	3.8	2.9	2.3	0.8	0.4	0.3	0.1	< 0.1
<i>Rural area</i>								
Amount of transects [-]	39357	25852	22536	8386	4152	5323	2146	1322
Percentage of vegetated transects [%]	25.5	16.8	14.6	5.4	2.7	3.5	1.4	0.9
<i>LECZ not populated</i>								
Amount of transects [-]	2670	1074	507	185	86	133	50	31
Percentage of vegetated transects [%]	1.7	0.7	0.3	0.1	0.1	0.1	< 0.1	< 0.1

Table 5.7: Distribution of transects over wave attenuation bins

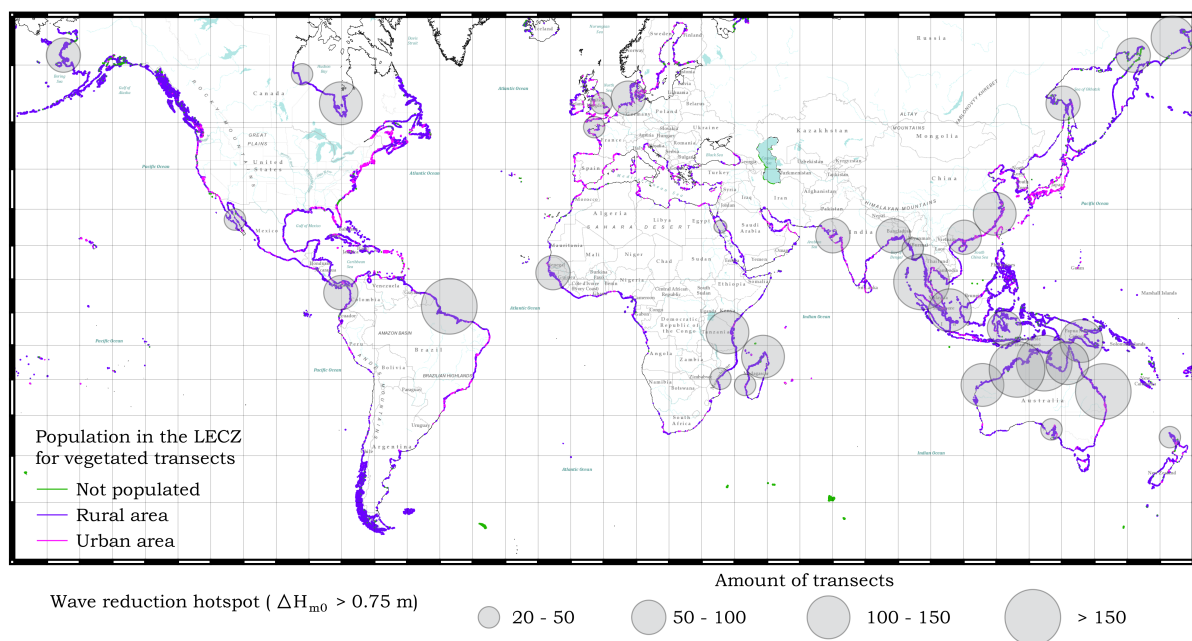


Figure 5.26: Global hotspots of wave damping by foreshore vegetation in urban and rural areas

### Human development index

As can be observed in Figure 5.26 most wave reduction hotspots are not situated in Western countries. The results of the global flood hazard assessment are compared with the human development index (HDI). This gives insight in the relation between the wave damping potential of foreshore vegetation and the development level per country. The HDI is a combined index taking into account life expectancy, education and standard of living and is published on a yearly basis by the United Nations Development Programme (UNDP, 2016). It is assumed that a country with a lower human development index is possibly less capable to take measures against flooding, e.g. due to lacking governmental strength, knowledge or financial resources. The distribution of the human development index and the wave reduction hotspots are presented in Figure 5.27.

Especially Guinea-Bissau, Guinea and countries at the South-East coast of Africa, e.g. Mozambique and Madagascar have high potential according to this comparison. Countries in Asia have overall a medium or high human development index, which also underlines the importance of the role of vegetation in these countries. In addition the hotspots in Figure 5.27 are based on absolute wave reduction results, but even more hotspots would be situated especially in South-East Asia if the relative wave attenuation was plotted.

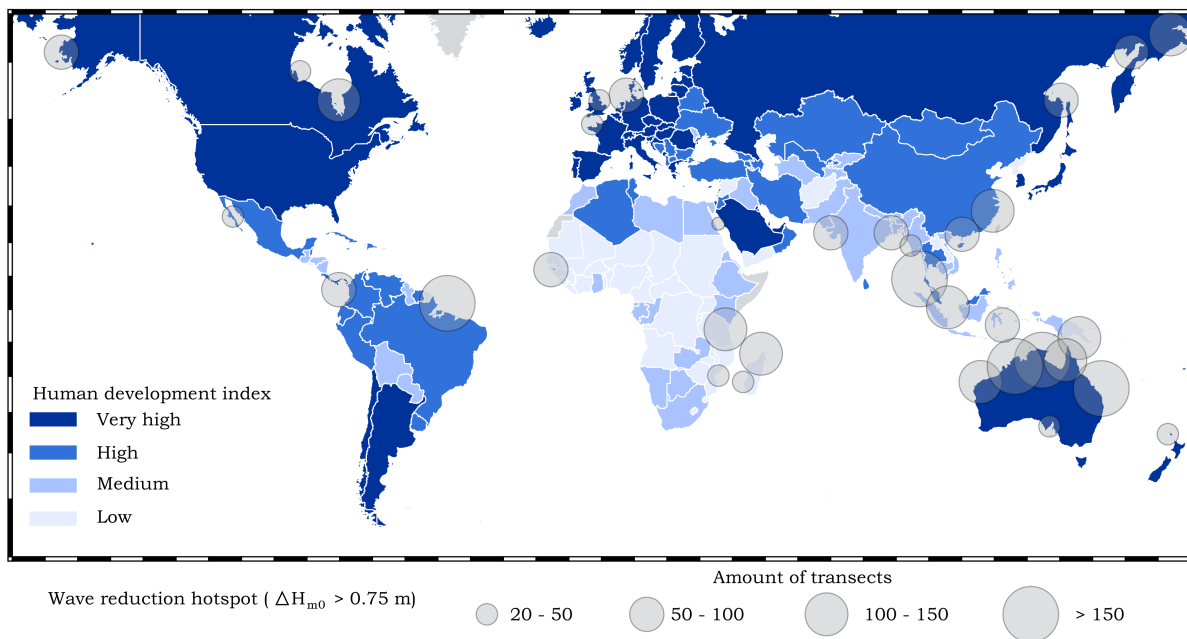


Figure 5.27: Global hotspots of wave damping by foreshore vegetation and human development index

### Financial impact of flood hazard reduction by foreshore vegetation

Making use of foreshore vegetation in combination with a new (existing) dike can save initial (maintenance) costs, because the dike height can be reduced. The dike height reduction results presented in Section 5.2 are summed up per country. Next the potential reduction costs are calculated by multiplying the summed dike height reduction with a unit price per m per km. The price per meter dike height per kilometer is based on Hillen et al. (2010), corrected for inflation and linked to the human development index (HDI). In total four different unit prices are used, one for every state of human development. Using this approach takes into account price differences between countries. The approach is described in more detail in Appendix D.6. As presented in Figure 5.28 large Western countries benefit potentially the most in absolute terms. The appearance of these countries in the top 10 is explained by their long coastline and high unit dike price. The appearance of Indonesia in the top 10 indicates a large potential, because for Indonesia a lower unit price is used, related to the medium HDI score.

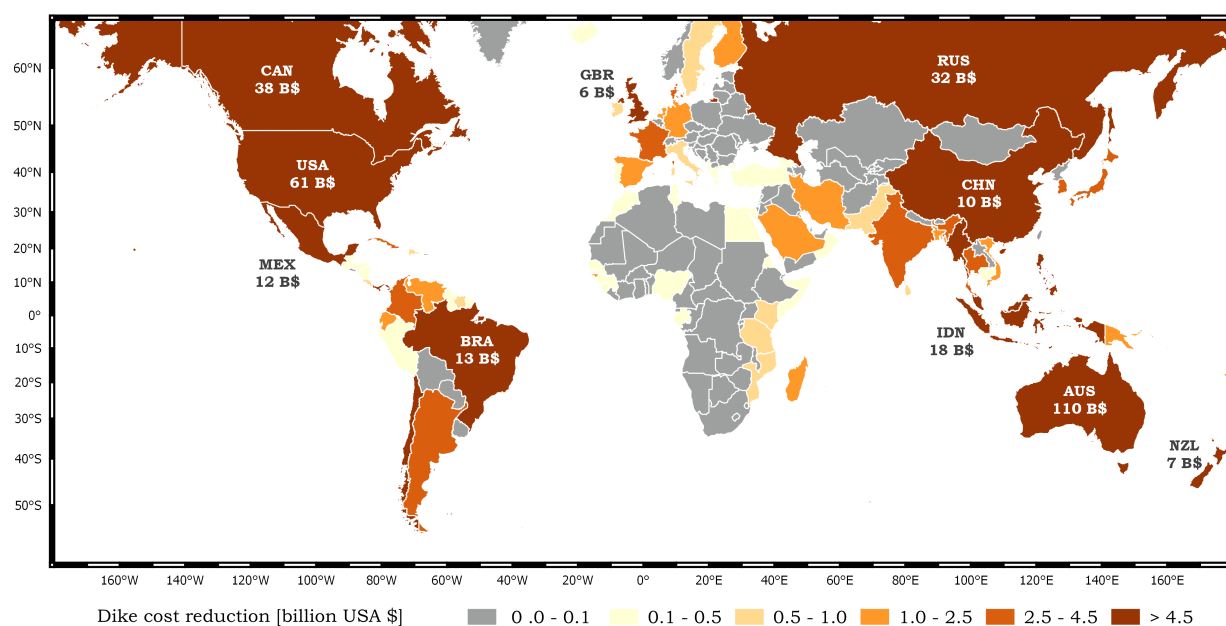


Figure 5.28: Global potential dike cost reduction by foreshore vegetation with labeled top 10.

Per country the dike cost reduction is divided by the gross domestic product (GDP). The indicator shows what percentage of the country's GDP can potentially be saved when foreshore vegetation is used as complementary flood hazard reduction measure. The results in Figure 5.29 show that mainly countries with a lower or medium HDI benefit potentially the most, because the potential savings are large in relation to their GDP. Countries which are part of the Small Island Developing States (SIDS) especially stand out. SIDS appear in the top 10 because these countries have a low GDP, are well vegetated and are mostly islands which induces a relatively long coastline length. Construction of flood prevention structures is probably financially not feasible, as these states deal with limited resources and remoteness. This underlines the importance of present coastal vegetation at the SIDS, as it will at least lower wave impact.

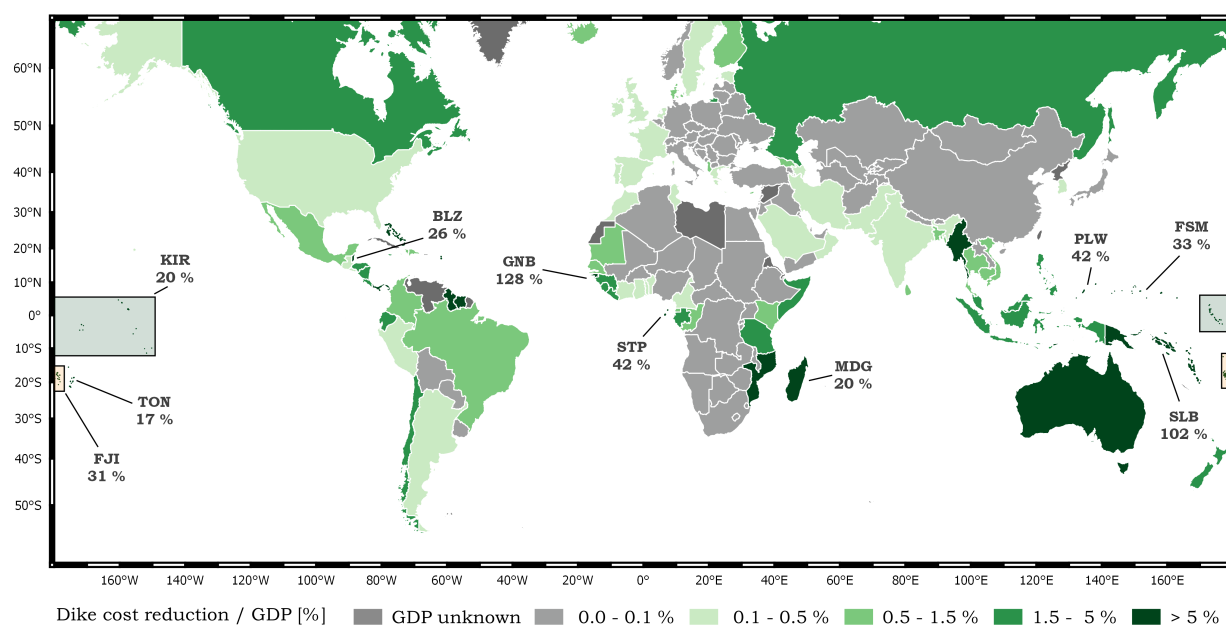


Figure 5.29: Global potential dike cost reduction by foreshore vegetation relative to GDP with labeled top 10.



# III

## Local framework



## Case study Eastern and Western Scheldt

The model approach and results of the global flood hazard assessment are presented in Chapters 4 and 5. Performing a global study induces an error for multiple reason, e.g. due to the use of global bathymetry data which has a relatively coarse resolution. On account of the spatial scale of the study a larger error is expected and assumed acceptable in comparison to local case studies. In the local framework the performance of the global flood hazard assessment is assessed based on a case study.

### 6.1. Site characteristics

The Eastern Scheldt and Western Scheldt are water bodies situated in the South of the Netherlands. The wave environment is classified as storm wave environment. In reality the Eastern Scheldt is closed off from sea during extreme storm conditions by the Eastern Scheldt barrier, which was constructed as part of the Deltaworks. In the global flood hazard assessment the presence of hydraulic structures is not included, so for research purposes the barrier is assumed to be absent. The study area contains in total 278 transects of which 38 are vegetated. An overview of the study area is presented in Figure 6.1.

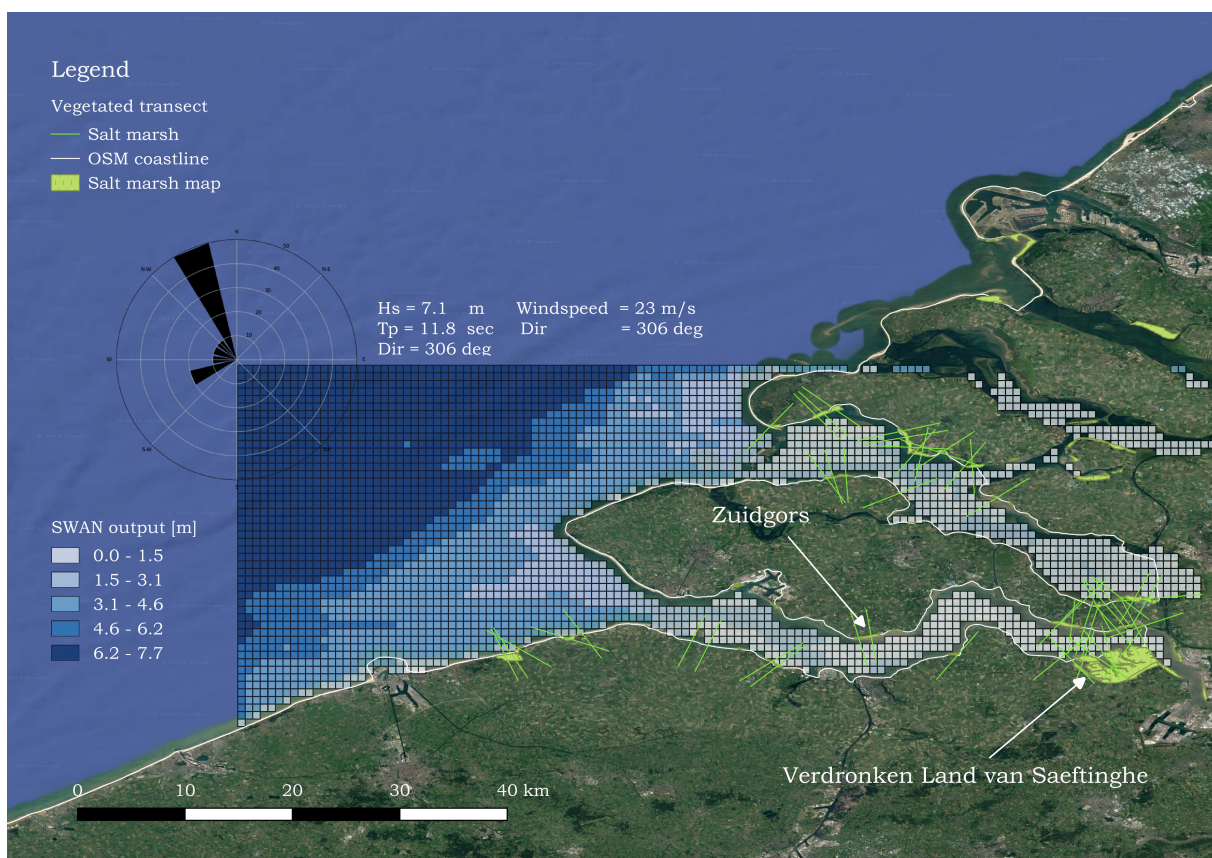


Figure 6.1: Overview of case study area with the SWAN output projected



### 6.1.1. Bathymetry and elevation

An accurate foreshore profile is key for determining wave attenuation by foreshore vegetation. Better bathymetry and elevation data is used in the local framework to get insight in the effect of input uncertainty on the wave damping results. The expected effect is large, because the water depth, which mainly depends on the profile data, is very important for wave propagation in shallow areas. Second, determination of the end of the foreshore in the global assessment is based on assumptions, described in Section 4.3. Because the location of the dike protecting the hinterland is not represented in the global data sets. However the dike is clearly visible in local elevation data, which makes it possible to derive correctly the end of the foreshore.

The profile is based on data from a Digital Topography Model (DTM), which consists of bathymetry data from Vaklodingen (resolution 20 m) and elevation data from the AHN (DEM of the Netherlands, resolution of 25 m).

### 6.1.2. Hydrodynamic boundary conditions

The used ERA-Interim derived wave and wind boundary conditions and water levels from the GTSM model for this location are shown in Table 6.1. Figure ?? gives an overview of the study site and the derived wave heights.

Return period	1	2	5	10	25	50	100	250	500	1000
Hs (m)	4.6	5.0	5.5	5.9	6.4	6.7	7.1	7.6	7.9	8.3
Tp (s)	9.4	9.8	10.4	10.7	11.2	11.5	11.8	12.2	12.5	12.7
Water level (m +MSL)	3.7	4.0	4.3	4.5	4.8	5.0	5.2	5.5	5.7	5.9
Wind speed (m/s)	19.0	19.8	20.8	21.5	22.2	22.7	23.1	23.5	23.9	24.1

Table 6.1: Boundary conditions from ERA-Interim

## 6.2. Model approach

The model approach in the local framework differs on various aspects from the approach used in the global assessment:

- Better bathymetry and elevation data source
- Use of the numerical model SWAN to simulate wave propagation from offshore to nearshore
- Different foreshore definition algorithm
- Use of the numerical model XBeach for wave propagation over the foreshore

Extensions are written for the algorithm used in the global assessment, in order to implement the above mentioned differences in model approach. The extensions work as communication line between the main algorithm and the numerical models SWAN and XBeach.

### 6.2.1. Nearshore wave propagation

Instead of the depth limited approach, the numerical model SWAN is used in stationary mode to calculate the wave propagation from offshore to nearshore. The calculation is made for all nine return periods, as defined in Chapter 3, using ERA-I data points which are often situated tens of kilometers from the coast.

A curvilinear grid is used with a grid size of 0.01 degrees, about 1 km. Bathymetry is derived from EMODNET. The water depth is corrected extreme water levels, which are derived from the GTSM model.

Wind and wave boundary conditions are derived from ERA-I. A wave direction of 306 ° is used based on the fifteen highest wave events in the available ERA-I data. The wind direction is assumed to be equal to the wave direction. A parametric JONSWAP spectrum shape is used, using a peak enhancement factor of 3.3 and directional spreading of 20 degrees.

Output is written for every grid point also containing coordinate information in the EPSG 4326 reference frame. Holding coordinate information makes it possible for the algorithm to find the SWAN based wave conditions corresponding to a transect. First, the coordinates of the start of the foreshore are calculated. Next, the corresponding SWAN wave conditions are found based on shortest distance between the start of the foreshore and the SWAN grid points.

### 6.2.2. Derivation of foreshore location

The derivation of the foreshore is comparable with method 2 in the global framework, described in Section 4.3. Several differences exist, which have in general the purpose of locating the dike and to make sure the end of the foreshore is situated at the toe of the dike.

First points are selected between a minimum and maximum threshold. The thresholds are -2 m +MSL and the extreme water level with a return period of 2 years respectively, similar to the values used in the global assessment. Next, the slope of every grid point is determined also similar to the global approach.

Second the accumulated maximum is calculated for every grid point based on all the points in the profile. This step aims to automatically identify high points in the profile, e.g. dike. This function simply checks for every point if it is situated higher or lower in relation to the accumulated maximum. If the elevation of the grid point is higher than the accumulated maximum, the accumulated maximum is replaced by this value. In estuaries quite complicated coastline configurations can be found, resulting in profiles which cross tidal flats or start at another bank. The accumulated maximum function handles this by resetting its value once the profile crosses -5 m +MSL. In this way not one, but several high peaks can be identified. Combining the selected points between thresholds, the accumulated maximum and the slope information for grid points creates patches.

The patches are checked based on continuity, using a minimum data length and maximum gap length. The minimum data length threshold is lowered for the case study, because of the high accuracy of the DTM data. Eventually the foreshore location is derived from the last valid patch. In order to get better alignment with the global run results a last check is performed. If the start of the foreshore based on GIE is situated between the derived start of the foreshore and the end of the foreshore, the start of the foreshore based on GIE is used.

In general four different configurations can be found, which can be distinguished based on:

- if the transect starts on open water or on the other bank
- if the transect crosses SLRP2

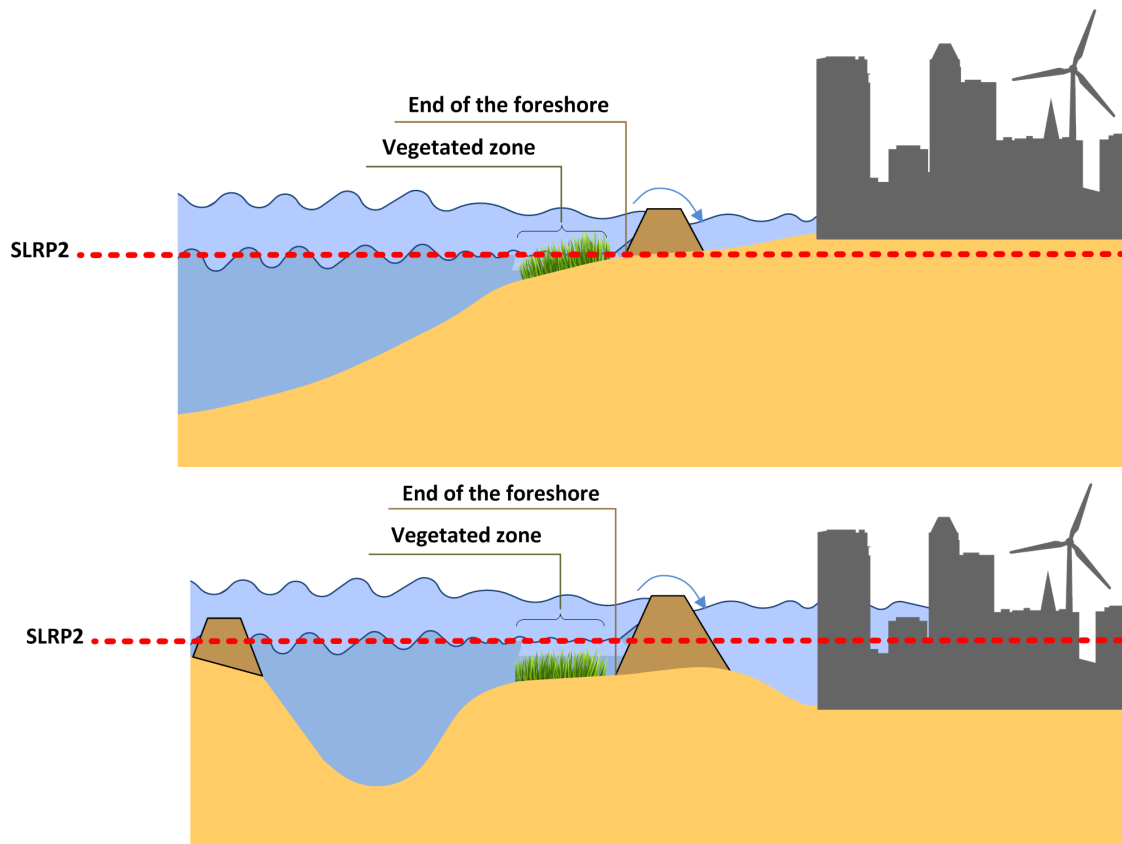


Figure 6.2: Examples of transect configuration

Start at open water and intersection between MG profile and SLRP2 (above)  
 Start at other bank and no intersection between MG profile and SLRP2 (below)

### 6.2.3. Foreshore wave propagation

Once the foreshore profile is derived and the wave boundary conditions are known, wave propagation over the foreshore is calculated. In the global assessment the look-up table is used to determine wave attenuation of the foreshore. In the local framework numerical XBeach simulations are performed for each individual transect based on the actual derived profile. If vegetation is present on the foreshore two calculations are made, with vegetation and without vegetation, in order to determine wave attenuation by foreshore vegetation.

XBeach is run for the 1D transects in surfbeat mode, described in Section 2.4.2. The settings are in line with the settings used to derive the values in the look-up table. The simulated time is 2700 seconds and a computational grid of 10 meters is used. The breaking parameter is set to 0.55, which is the same as in the look-up table. The wave direction is assumed to be perpendicular to the OSM coastline, which is the worst case scenario.

## 6.3. Results

A total of 278 transects is used in the study, of which 38 were vegetated. All the vegetated transects are confirmed by the salt marshes map (vegetation cover method 1). The distribution of the wave height at start of the vegetated zone, the wave period, the water depth in front of the vegetated zone, the vegetation width and the foreshore slope is studied and compared with the global flood hazard assessment results. These parameters are chosen, because they are used as input for the look-up table. A detailed overview of the distributions and the error between the local and global runs can be found in Appendix E.1. In Table 6.2 the mean and standard deviation of the errors is shown. A positive value means that the global run overestimates the parameter.

The wave height is continuously overestimated, due to the depth averaged approach. The wave period is not transformed from offshore to nearshore resulting in a large error. Despite the use of global datasets the mean error for water depth and vegetation width is quite small. The standard deviation for vegetation width is large, because the global method fails sometimes to identify a vegetated transect. This happens in case the derived foreshore is situated too far inland.

The depth is quite accurate when the foreshore is derived based on GIE data. However, the deviation between GEBCO and Vakkoddingen is considerable. The foreshore slope shows a large mean error and standard deviation. This is largely because the dike location is not represented in global data, resulting in a transect which is too long. In the Netherlands the land behind the dike is situated below MSL. If the foreshore is derived too far inland, a negative slope can be derived, for which automatically a slope of 2000 is assigned.

Parameter	Mean of error ( $\mu$ )	Sigma of error ( $\sigma$ )
$H_{m0}$ at the start of the vegetated zone [m]	1.12	0.64
$T_p$ [s]	7.88	1.54
Water depth at the start of the vegetated zone[m]	0.73	1.46
Vegetation width [m]	-17	126
Foreshore slope [1/slope]	586	741

Table 6.2: Mean and standard deviation of the error between output from the global framework and local framework

### 6.3.1. Wave attenuation by foreshore vegetation

In the local framework the nearshore wave height is determined using the numerical model SWAN and by applying the depth limited approach, which is used in the global assessment. For both nearshore wave heights determination methods the corresponding wave propagation over the foreshore is calculated using XBeach. This gives insight in the error between the local and global framework and the sensitivity to the calculation approach. In Figure 6.3 the wave attenuation results of the global run and the two runs in the local framework are presented.

The XBeach output based on a 'Depth limited + XBeach' run is situated between the results of the two other runs. This indicates that the error between the local and global framework is partly induced by uncertainty in the profile and partly by the depth limited approach. For several transects the results of the 'Depth limited + XBeach' and the 'Global run' simulations show a good match. This means that the look-up table is able to represent the XBeach simulations, in case the profile is determined correctly.

The difference between the 'Global run' and the 'Depth limited + XBeach' simulations represent model uncertainty induced by the look-up table and input uncertainty by the use of global bathymetry and elevation data. In addition, the difference between the 'Depth limited + XBeach' and 'SWAN + XBeach' simulations represent the model uncertainty solely induced by the depth limited approach.

Overall, the output from the 'SWAN + XBeach' simulation in comparison to the 'Global run' shows a large absolute error in wave attenuation with a magnitude of roughly 1.5 -2. The RMSE for the 'Global run' and the 'Depth limited + XBeach' simulations in comparison to the 'SWAN + XBeach' run is 0.25 m and 0.15 m respectively. In other words, overall a deviation of 0.10 m is induced by uncertainty related to the profile data and 0.15 m is induced by the depth limited approach. These outcomes show that using global datasets induces an error. In addition, using the depth limited approach in an sheltered area like the Western Scheldt induces an overestimation of wave attenuation by foreshore vegetation.

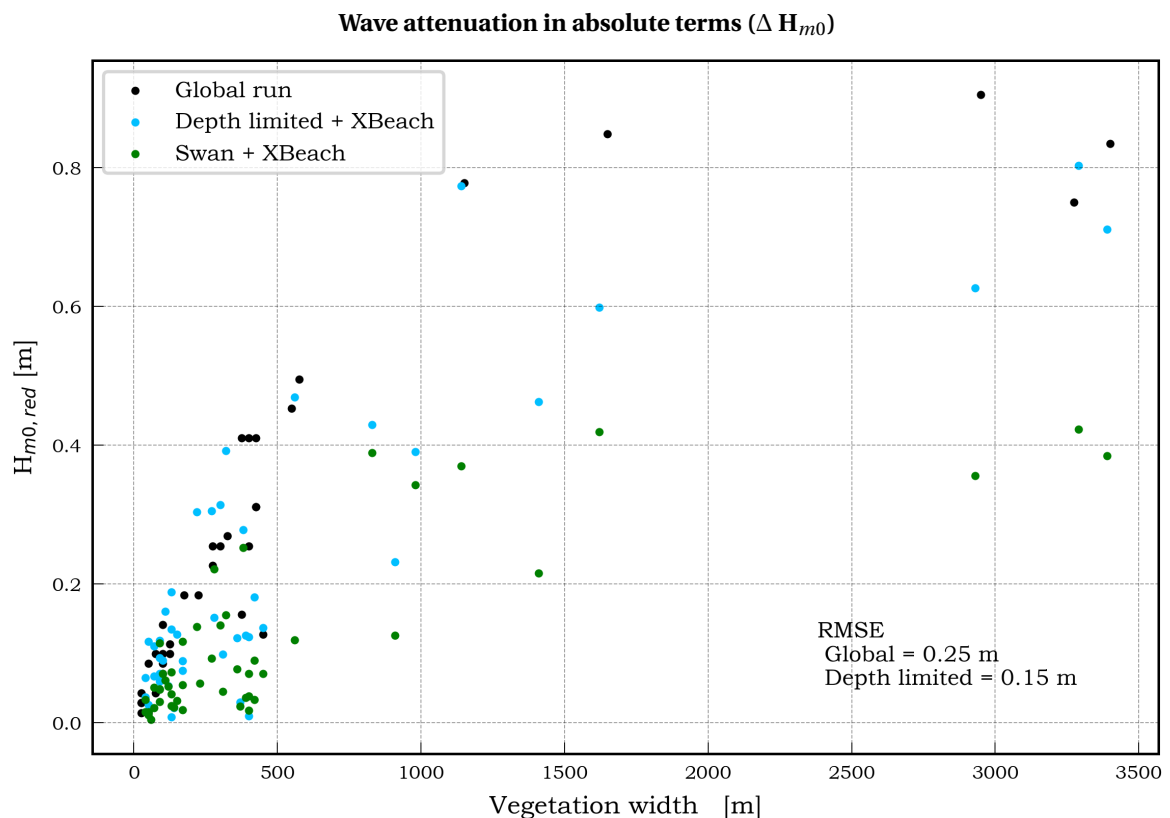


Figure 6.3: Wave attention in absolute terms versus vegetation width for global and local framework

### 6.3.2. Wave attenuation by foreshore vegetation in relative terms

Besides the comparison of the wave attenuation results in absolute terms, several dimensionless indicators of wave attenuation by foreshore vegetation are studied, described Appendix E.1. Wave transmission and wave attenuation relative to the incoming wave height show a reasonable fit.

For vegetation widths below 2000 m wave transmission is overestimated in the global run. For larger vegetation widths the global model tends to underestimate wave damping. The look-up table uses a maximum vegetation width of 2000 m, this explains the change from overestimating to underestimating wave transmission around 2000 m. The average error in wave transmission between the 'Global run' and the 'SWAN + XBeach' simulations is bounded between +/- 20 %.

The best match is observed for the indicator wave damping relative to the incoming wave height at the begin of the vegetated zone. This dimensionless measure is plotted in Figure 6.4. Wave transmission includes the combined effect of wave breaking, bottom friction and wave vegetation interaction included. However, wave damping relative to the incoming wave shows which percentage of the incoming is damped by vegetation, i.o. reduced wave transmission by vegetation. Thus focuses solely on wave-vegetation interaction.

The RMSE error of the 'Global run' and the 'Depth limited + XBeach' run in comparison to the 'SWAN + XBeach' based run is respectively 7.5 % and 5.8 %. Thus 1.7 % deviation induced by profile uncertainty and model uncertainty induced by the look-up table. The 5.8 % deviation induced by the depth limited approach again shows the costs of the use of this approach in sheltered areas. Overall, the results show that the global model is able to give a good approximation of wave damping relative to the incoming wave height.

**Wave attenuation relative to incoming wave height in front of vegetated zone ( $\Delta H_{m0} / H_{m0, \text{start veg}}$ )**

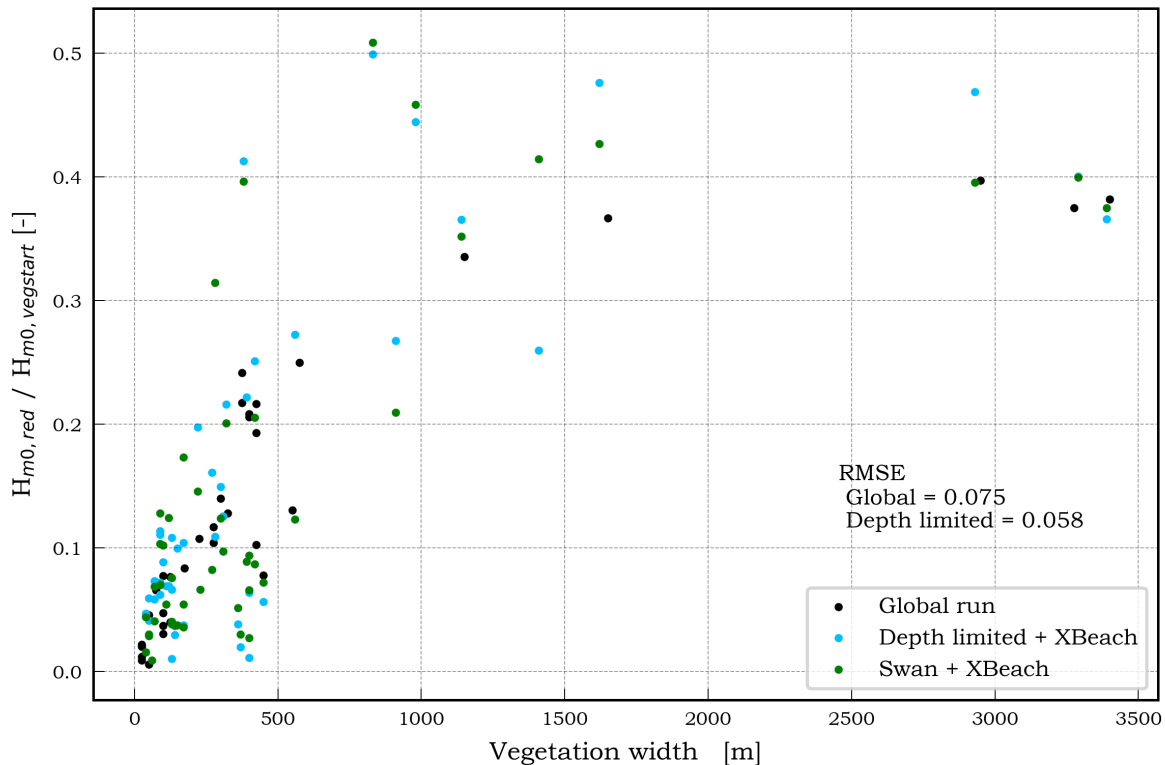


Figure 6.4: Wave attenuation relative to wave height at the start of the vegetated zone versus vegetation width for global and local framework

## 6.4. Morris sensitivity analysis

For a vegetated transect at the Verdrongen Land van Saeftinghe and at Zuidgors a sensitivity analysis is performed according the Morris approach, described in Appendix B. The method is especially applicable to assess sensitivity if only a limited amount of model simulations is preferred, because the model has high computational costs. Approximately 10-100 model outcomes are needed per assessed parameter in order to obtain a reliable result (Pianosi et al., 2016).

The Verdrongen Land van Saeftinghe and Zuidgors are chosen, because they have different foreshore slopes and vegetation widths. The transects at Zuidgors contains a small vegetation stretch (300 m) and has a relatively steep slope (1:251). The transect at the Verdrongen Land van Saeftinghe is well vegetated (3290 m) and a mild slope (1:1637).

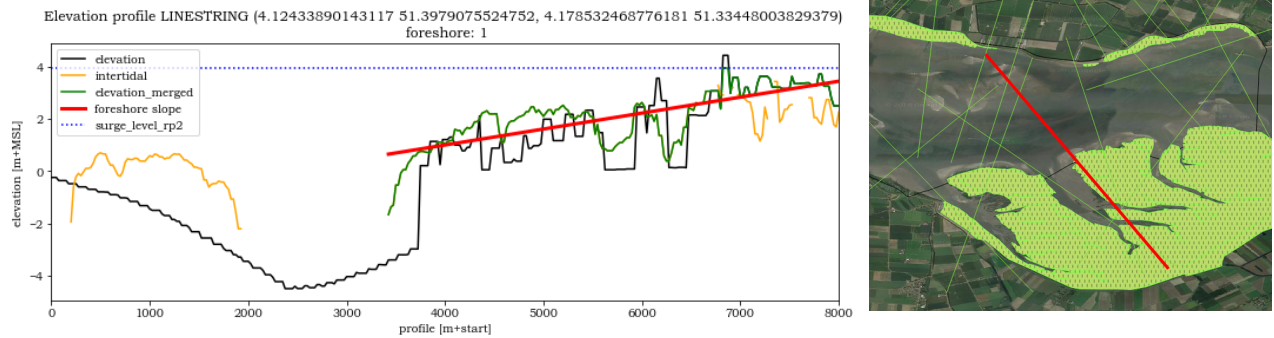


Figure 6.5: Alignment of transect and derived profile at the Verdrongen Land van Saeftinghe in the global framework

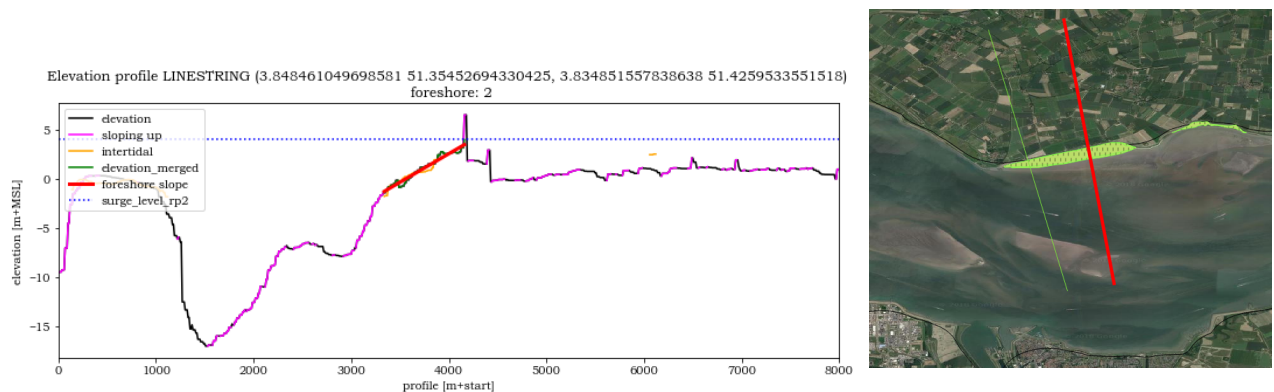


Figure 6.6: Alignment of transect and derived profile at Zuidgors in the local framework

### 6.4.1. Model approach

The sensitivity analysis is performed for both a global framework and local framework giving a 1 in 100 years storm conditions. For the global framework the exact same method and datasets are used as in the global flood hazard assessment. In the local framework local data is used and the simulations are performed using SWAN and XBeach, as described in Section 6.2.

The input bounds for the global run are based on the difference between the global and local framework, as shown in Table 6.2. For the local framework the bounds are determined on literature and on inaccuracies in the data sources. An overview of the input parameters for both frameworks can be found in Appendix E.1. The results for the global framework and local framework are based on roughly 700 and 450 simulations respectively.

### 6.4.2. Results

#### Verdronken Land van Saeftinghe

##### Global framework

The wave period is according the performed sensitivity analysis the most influential parameter. This results is observed, because the offshore wave period is used in the sheltered case study area, where lower wave period are expected. Longer waves are harder to attenuate, so it is a conservative approach. The depth at the start of the vegetated zone is often overestimated in the global assessment, due to uncertainties in the global datasets. This overestimation results in combination with the depth limited approach into an overestimation of wave attenuation. The same holds for the water level, however the accompanied input uncertainty does not result in an overestimation, but a spreading around the mean. Deviations in the vegetation width and foreshore slope are minor, because the chosen transect has an extensive vegetation width and a very mild slope.

##### Local framework

The biophysical parameters which are used to model vegetation are included in the sensitivity analysis in the local framework. The stem density, stem height and stem diameter are together with the water level the most influential. The results show that vegetation state is very important for the wave damping capacity of foreshore vegetation. However, input uncertainty of the drag coefficient is of less importance.

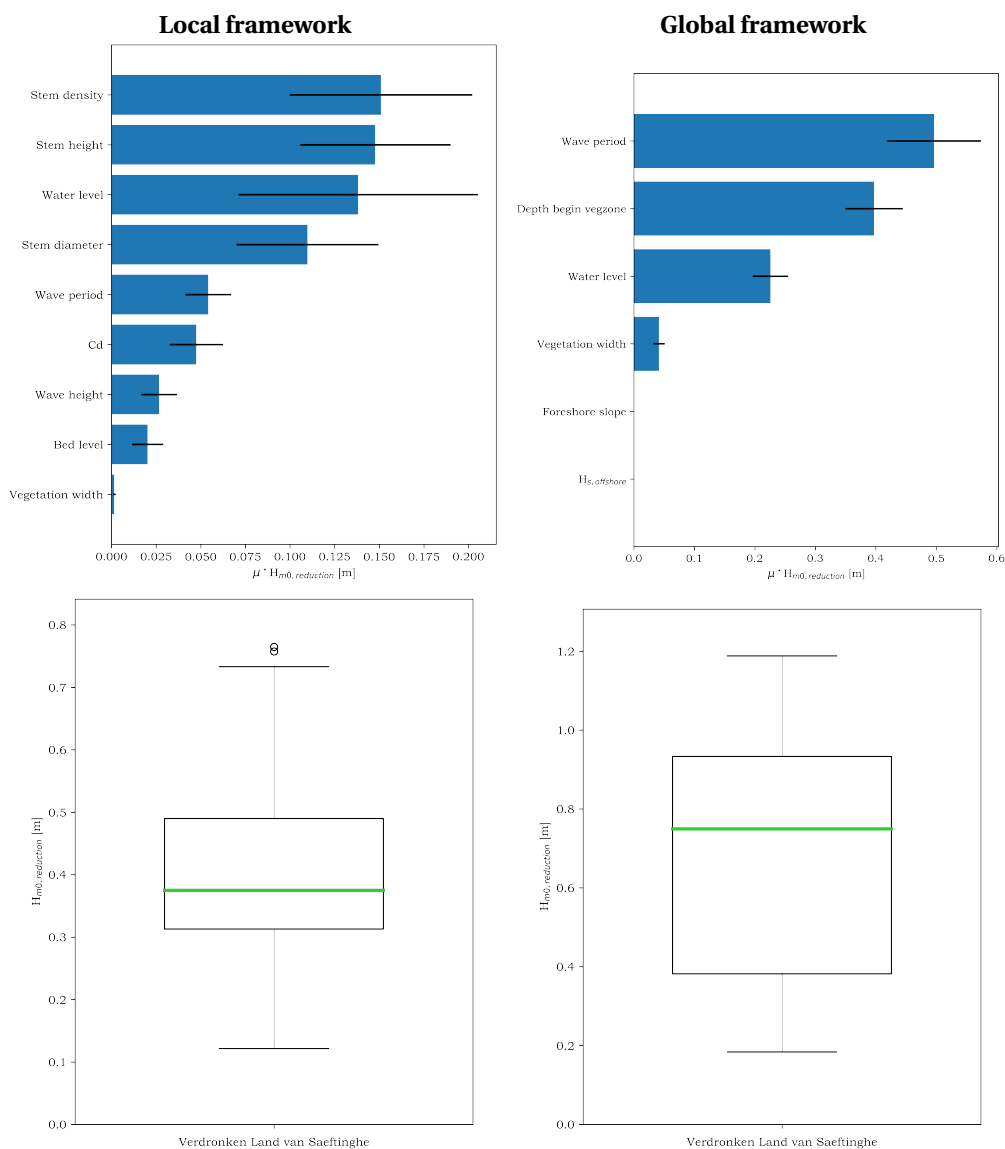


Figure 6.7: Bar plots (above) with influence of input uncertainty on wave attenuation. Box plots (below) with spreading of wave attenuation due to input uncertainty for transect at the Verdronken Land van Saeftinghe.

## Zuidgors

### Global framework

At Zuidgors uncertainty in the foreshore slope and the vegetation width are important, which is in contradiction to the results for the transect at the Verdrongen Land van Saeftinghe. On a steeper slope less wave energy is lost by wave-vegetation interaction, as more wave energy is lost due to depth induced breaking. Deviations in the foreshore slope will change the balance between those wave dissipating mechanisms. As presented earlier, most attenuation by vegetation is observed in the first hundreds of meters of the vegetation zone. This explains the sensitivity to deviations of the vegetation width at Zuidgors, where a less extensive vegetation zone is present.

### Local framework

The sensitivity analysis results show more influence of vegetation related parameters in comparison with the results for the Verdrongen Land van Saeftinghe.

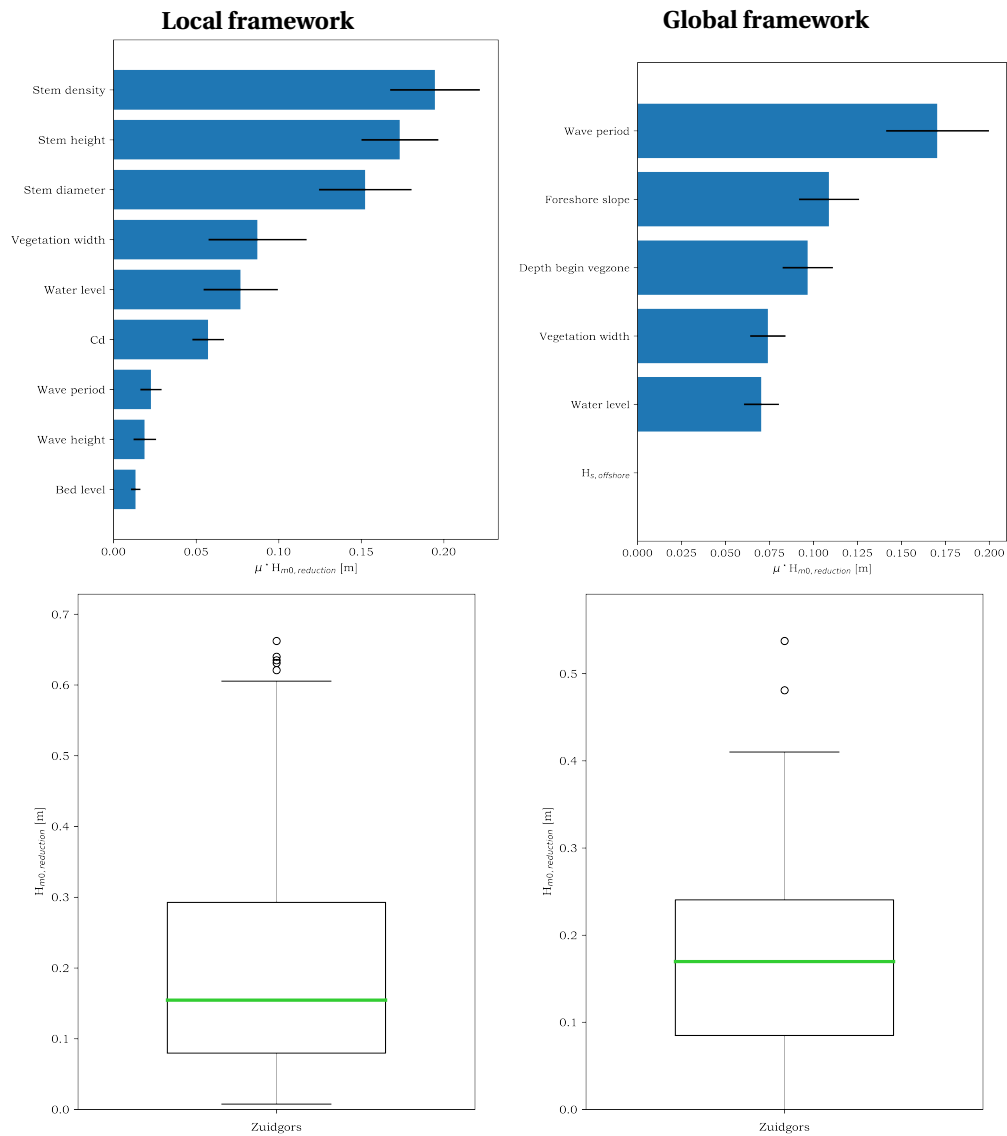


Figure 6.8: Bar plots (above) with influence of input uncertainty on wave attenuation. Box plots (below) with spreading of wave attenuation due to input uncertainty for transect at Zuidgors.

### 6.4.3. Conclusion

Both presented locations are situated in the same estuary, but differ mainly in vegetation width and foreshore slope. The outcomes of the sensitivity analysis in the global framework show that the wave period is the most influential parameter. This is explained by the use of the offshore wave period at the start of the vegetated zone. With this approach the global run results tend to be conservative, because longer waves are harder to attenuate. In the local framework biophysical parameters are included and the accompanied uncertainty is the most influential. Overall, the sensitivity analysis results show that for a steeper and less extensive vegetated transect vegetation characteristics become more important relative to the hydrodynamic boundary conditions.





# IV

## Interpretation



## Discussion

In this research a global assessment is performed to get insight in the global potential of wave damping by foreshore vegetation in vegetated foreshore dike systems. This global scale requires the use of datasets with global coverage, which have in general a lower resolution and accuracy, as described in Chapter 3. The global model uses different methods e.g. for the determination of the foreshore, because several different coastal configurations can be found globally. In this chapter the input data, calculation methods and results are evaluated for different steps in the study.

### 7.1. Determination of foreshore profiles

This research focuses on wave attenuation by vegetation on the foreshore, thus determination of the foreshore is an important step in the whole calculation procedure. GEE intertidal elevation (GIE) and a merged set of MERIT and GEBCO (MG) are used as input, described in Chapter 3. The foreshore is determined for each individual transect using four different foreshore determination methods, which are explained in Chapter 4.

#### 7.1.1. Input data

The merged MG set has coverage over the full transect, but has a coarse resolution (MERIT 3 arc-seconds, GEBCO 30 arc-seconds) and a low vertical accuracy (MERIT ~2 m, GEBCO ~10 m). The GEBCO data points which are available near the coast showed large deviations in comparison to the actual bathymetry. This error is originated by interpolation which is used in the GEBCO set between sounding data and satellite data (Becker et al., 2009). The MERIT data is available with a reasonable accuracy, but is lacking the vertical accuracy in forested areas (Yamazaki et al., 2017). This vertical deviation in order of meters can make the difference between flooding and no flooding.

Besides these inaccuracies, both separate sets are not directly applicable in the coastal zone, because this area is often missing in the sets. This gap is specifically important, because the foreshore is situated in the intertidal zone. The gap between MERIT and GEBCO is filled using linear interpolation towards the OSM coastline assuming it represents Mean Sea Level (MSL).

On the other hand, GIE has a high resolution and vertical accuracy, yet often positively identifies inland water or land as intertidal zone. The set is derived from Landsat and Sentinel2 satellite imagery, which results into an increased chance of missing the highest and lowest area of the intertidal zone, due to less available cloud free images for these areas. Furthermore, the set contains speckle noise, specifically in areas with a small tidal range. These inaccuracies make it more difficult to determine an accurate foreshore profile.

### 7.1.2. Foreshore methods

#### Transect alignment

Wave attenuation by foreshore vegetation is studied on a global scale using transects which are aligned perpendicular to the Open Street Map (OSM) coastline, which is a common approach used in global studies. The position of the OSM coastline is sometimes situated in front of e.g. a marsh and sometimes at the end of a marsh. In this study the transects have a length of 8 km, in order to capture the most foreshores. Most banks along estuaries are included in the OSM coastline. However, some developers of the OSM coastline deem that estuaries are not part of the coastal system. The largest deviation is observed at the Rio de la Plata estuary near Buenos Aires, Argentina, which is not part of the OSM coastline.

All transects which are situated completely on water or land are not processed. The starting point of most of the transects is on open sea and the ending point on land. However, in estuaries specifically, different configurations can be observed, e.g. transects which start on land cross several sand banks, or end in water. The foreshore method is aimed to recognize these configurations and determine the correct foreshore location. In Figure 7.1 the complex configuration of the OSM coastline at the Ganges-Brahmaputra Delta is presented.

#### Foreshore method 1 (GIE based)

The first foreshore determination method is based on GIE. The other three methods use MG. Validity checks on the GIE data and are performed for every transect to remove earlier mentioned inaccuracies. These checks are tested for various profiles world wide, but specifically in the UK which is used as pilot study area. The first check aims to remove points which are falsely identified as intertidal zone. The hinterland should be elevated higher than the derived extreme water level with a return period of two years (SLRP2). Thus, this check works inefficiently in low-lying areas coping with higher extreme water levels, e.g. the Netherlands. The second check removes speckle noise mainly for transects facing open ocean. This check is less important than the first check, because the final profile is established based on the last valid patch. The last check aims to remove speckle noise nearshore, which is often present in areas with a small tidal range, e.g. the Mediterranean Sea. In these areas a wide and mild sloped foreshore is derived when nearshore noise is not filtered. After performing a case study for the Mediterranean Sea, Appendix E.2, it seems that the noise filter threshold used in the global assessment was set too low for efficient filtering.

After the validity checks, gaps between the valid data patches are interpolated when the gap is smaller than a certain gap length threshold. Furthermore, data patches which are smaller than a data length threshold are removed. In the global run the gap length threshold was 250 m and the data length threshold was 100 m. The result is that one or more profile patches along the profile is marked as valid GIE data. The foreshore profile is determined based on the last patch. The last patch is chosen as foreshore location, because e.g. for transects in estuaries sandbanks should be omitted. However, this approach can result in an inaccurate foreshore location when noise in the hinterland is not filtered correctly and the last patch is situated inland. This is observed during the research for some transects in low-lying areas.



Figure 7.1: Alignment of the OSM coastline at the Ganges-Brahmaputra Delta

### Foreshore methods 2,3,4 (MG based)

The foreshore is determined using MG when not enough valid GIE data points are available for a transect. For the foreshore determination based on MG, points between a low and high threshold are selected. These thresholds can be set manually before the model runs. For the global run a low threshold of  $-2 \text{ m} + \text{MSL}$  and a high threshold corresponding to an extreme water level with a return period of 2 years are chosen. The low threshold should be an estimate of the start of the intertidal zone. The global use of a single low threshold might seem undesirable, but is justified taking into account the large vertical inaccuracies in the bathymetry and the very rare occurrence of salt marshes and mangroves below  $-2 \text{ m} + \text{MSL}$ . Choosing a lower value will result in more data points, but will on average result in a steeper slope. The highest threshold is chosen assuming the end of the foreshore has no elevation larger than the chosen extreme water level. The value will be generally slightly larger than HAT, which makes it possible to include parts of the upper marsh if present.

The patches created in the second method based on MG are comparable with the patches in foreshore method 1. In the third method the starting point of the foreshore coincides with the first upcrossing of the profile through  $-2 \text{ m} + \text{MSL}$ . The fourth method is used when no start or end of the foreshore can be determined. In this way the MG based methods are directly an indication of transect reliability.

A pitfall of the MG based methods occurs in areas with a small tidal range. These areas contain transects which are often not vegetated and are therefore not the main focus of this study. These transects have often a limited amount of data points, e.g. 2 points, below MSL to construct the foreshore. This can result a very mild slope in combination with a small foreshore width. This combination can be seen as an indication of absence of a substantial foreshore.

Another pitfall occurs in mangroves areas due to the lack of MERIT performance in forested areas. Although the elevation in MERIT is corrected for tree presence, still transects exist where the mangroves map indicates mangroves presence, but MERIT indicates an elevation of  $10 \text{ m} + \text{MSL}$ . It is possible that the vegetation indicated in the mangroves map is in reality of another tree type. Another possibility is that the elevation in MERIT overestimates the elevation, because it measures the canopies as the surface. This final argument seems more acceptable, because the 90% confidence interval for the mean error for MERIT is 9 m in flat forested areas. This problem is handled by assuming the highest threshold as elevation (for the global run the extreme water level with a return period of two years) in case MERIT's elevation exceeds the highest elevation threshold. This assumption is unlikely to still overestimate the elevation, resulting in an underestimation of the wave damping potential by mangroves.

A third pitfall for the MG based methods occurs when in reality a dike or another flood defence structure is present. The structure is not present in the elevation set, due to the 3 arc-seconds ( $\sim 90 \text{ m}$ ) resolution. In these cases the end of the foreshore might not be situated at the structure's toe, but far more inland. The error is largest for areas characterized by a low-lying hinterland and high extreme water levels, because it is hard to find an end of the foreshore in these cases using MG.

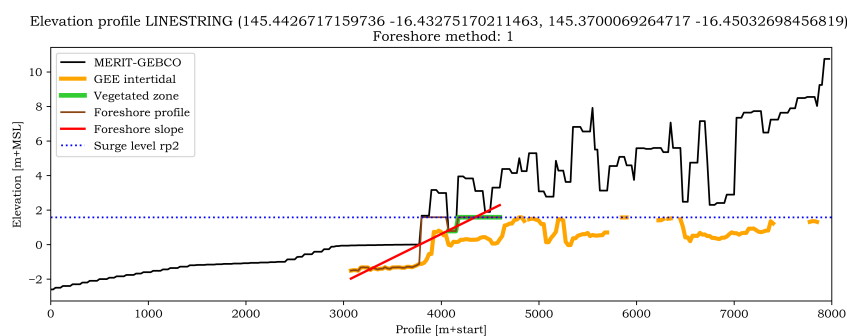


Figure 7.2: Alignment of transect derived using MG, for which MERIT measures the canopies of the mangroves.

### Foreshore extension based on vegetation map

The foreshore is extended in case the end of the foreshore, based on one of the foreshore methods ends earlier than the vegetation in the salt marshes map or mangroves map. This extension is implemented to include the whole vegetated zone as presented in the vegetation maps. This is useful if foreshore method 1 is used, because GIE lacks in the low and high intertidal zone. Furthermore, the extension makes it possible to include mangroves for areas where MG overestimates the elevation. In this case, the derived profile often has a very mild slope, because the elevation for the extended part of the profile is set to a constant elevation equal to SLRP2.

Difficulties occur in case a transect is aligned in such a way that it e.g. crosses two marshes situated at both sides of a populated land body. The elevation of the middle of the land body most likely exceeds the surge level by far. It is because of this reason that in reality no waves ever reach the determined end of the foreshore, this can only occur if the whole land body is submerged. This situation is simulated in the global assessment as a transect with a very mild slope, and with a consecutive vegetation zone with a width consisting of the sum of the two vegetated zones. In this case the slope estimation is too mild and the vegetation width is too large. How frequent this phenomenon occurs is not studied, but is observed in a few occasions.

### Conclusion

The foreshores based on GIE has the potential of having a better accuracy, but the multiple noise factors are a major drawback. When a wrong foreshore is determined based on GIE, it is often far from reality. The most common observed erroneous transects have a very mild slope or are situated far inland. The width of these erroneous transects differs depending on the amount of speckle noise. The largest drawback of the MG based foreshores is the lack of vertical accuracy. Overall both methods are least accurate in areas with a small tidal range. In these areas GIE data contains often speckle noise in the nearshore and MG data only contains a few useful data points.

## 7.2. Determination of the vegetated zone

Once the foreshore is determined, several vegetation data sources, described in Chapter 3, are used to determine vegetation presence and the corresponding vegetation type. The VegGEE set is used to scan for vegetation presence along the profile. VegGEE is an excellent set to determine the transition from bare tidal flat to vegetated zone. Yet, the set is quite sensitive and could indicate e.g. algae as vegetation. Following, the corresponding type is determined based on the mangroves map, salt marsh map, Corine Land Cover (CLC) or GlobCover. Coverage of the CLC cover type map is limited to Europe, which indicates a difference in reliability between transects inside and outside Europe.

### Europe

The salt marsh map and CLC for Europe are used to determine the corresponding cover type. Due to the full coverage in Europe of CLC is it most unlikely to incorrectly indicate a transect as vegetated while it is non vegetated in reality. This is only possible in case the information in the salt marsh map or CLC is outdated or inaccurate, but this situation was not observed during the study. When a foreshore is situated too far inland the VegGEE set will most likely indicate vegetation presence, but the combination of the cover data sources will correctly indicate that no intertidal vegetation is present.

### Outside Europe

The mangroves map, salt marshes map and GlobCover are used as cover type sources outside Europe. The mangroves and salt marshes map are based on information from various sources complemented with satellite data. This induces the risk of outdated classification, yet in Europe no false indications are observed in the salt marsh map. However, few cases were observed in which the mangroves map falsely indicated mangroves presence. It is possible that in this case the mangroves were cut. Although false indications are observed, it seems to occur rarely and the uncertainties are minor in comparison to uncertainties in the GlobCover set. The data in GlobCover has a coarse resolution (300 m) and is very sparse. The data has no full coverage, but is spread as speckles over the coastal zone. For this reason it is often that no data is found along the transect. In these cases the cover type is determined based on latitude. In addition, when data is found, it is often incorrect e.g. salt marshes are indicated as trees. The combination of VegGEE, which is very sensitive, and GlobCover results in a high chance of false indication of intertidal vegetation. As long as the foreshore is determined correctly the error is probably reasonable. The combination is used during the study, because several locations have no alternative, e.g. in Chile.



### 7.3. Hydrodynamics

Wave boundary conditions are derived from ERA-Interim (ERA-I) reanalysis. For the FAST project a peak over threshold analysis is performed for a selection of ERA-I points which are situated nearshore. The results are projected on Dynamic and Interactive Vulnerability Assessments (DIVA) points. In the global assessment the DIVA point closest to the transect is chosen. This DIVA point is situated often relatively close to the assessed transect, but the actual data is originated from the ERA-I point, which is situated approximately tens of kilometers offshore. The extreme water levels are derived from the Global Tide and Surge Model (GTSM). The results from the GTSM model are again projected on the DIVA points, only the distance between the GTSM model output and the DIVA points is projected in kilometers.

#### 7.3.1. Extreme water levels

The extreme water levels derived from GTSM have a high accuracy. The uncertainty fit is below 10 % for half of world's coastline and only larger than 25 % for 4% of the coastline (Muis et al., 2016). The largest uncertainty is found in areas with relatively low extremes, e.g. the Mediterranean Sea. Local configurations, e.g. funnel shaped estuaries, can result in large extreme water levels. The performance of the GTSM model in these settings is not tested during this research. The results of the global study can overestimate the wave damping effect of vegetation, when the water level is in reality higher than assumed based on the GTSM model.

#### 7.3.2. Wave propagation

The wave characteristics from ERA-I are available on a  $0.75^\circ \times 0.75^\circ$  grid. The dataset tends to underestimate tropical cyclone waves, due to the large grid size (Shanas and Kumar, 2015). The global study wave propagation from offshore to nearshore is based on a depth limited criterium and foreshore wave propagation is based on a set of earlier performed XBeach runs. In the local framework a combination of SWAN and XBeach runs is used to describe wave propagation from offshore to nearshore and foreshore wave propagation respectively.

##### Determination of nearshore wave height

The depth limited breaker criterion is compared with SWAN calculations for the Western Scheldt Estuary, the Netherlands and Chesapeake Bay, the United States of America, presented in Appendix C. The case studies showed that the depth limited approach overestimates the wave height at beginning of the transect with a magnitude of several meters. The results of the study are in line with the research of Janssen (2016), in which the use of a depth limited approach was also studied. However, this study only compared the use of SWAN and the depth limited approach at several buoy locations. In addition, the present study showed to which extent the depth limited approach influences the final wave attenuation results, presented in Chapter 6. For the vegetated transects in the Western Scheldt the significant wave height at the start of the vegetated zone was overestimated on average by 1.1 m with a standard deviation of 0.6 m. For the same case the RMSE between use of the depth limited criterion and SWAN was 0.15 m in terms of significant wave height reduction by foreshore vegetation. This is considerable knowing the maximum wave height reduction was for this case roughly 0.6 m. The difference between the two approaches increases for increasing water depth at the start of the vegetated zone. Furthermore it is expected that the difference decreases for transects which face open sea. However, intertidal vegetation is often situated in sheltered areas, because plants are here protected from large wave impact. In other words, the differences between the two approaches are large at locations where one might expect wave attenuation by foreshore vegetation. For this reason it is suggested to interpret the results of the global assessment by taking these deviations into account.

##### Foreshore wave propagation

The foreshore wave propagation in the global assessment is determined using a set of earlier performed XBeach runs, described in Section 4.5. The step size between the different values for a parameter in the conditions used for the XBeach pre-runs determines the accuracy. For example, when a wave height of 1.2 m is found at the start of the vegetated zone, a value of 1.0 m will be used in the look-up table. This deviation has a maximum of half of a step size. In most cases this will result into a wave height and water level deviation of 0.25 m as a maximum. This might seem large, e.g. 25% difference maximum for a wave height of 1 m, but it is assumed to be reasonable taking into account the other uncertainties in the assessment.

The model runs in the local framework and the look-up table runs are conducted using XBeach surfbeat, including the influence of infragravity waves. The settings for both frameworks were identical. The use of XBeach stationary is tested in an earlier stage of the study. The combination of XBeach stationary and the depth limited approach was unsatisfactory, because depth induced breaking was directly induced at the beginning of the transect. The use of a phase resolving model such as XBeach non-hydrostatic or SWASH is not computational feasible and has no extra advantage considering the enormous spatial scale of the research.

### Influence of vegetation characteristics

Two vegetation types are used in the global assessment: salt marshes and mangroves. These types are schematized by a stem density, stem height, stem diameter and a drag coefficient. In reality deviations between different salt marsh and mangrove species exist, described Section 2.5. One could argue that the choice for static vegetation schematizations results in a large deviation from reality. In the global assessment conservative vegetation schematizations are used. Even during winter, salt marshes in Northern Europe will seldom be more sparse than the schematizations used in this study. Temporary influences are not significant for mangroves, but differences exist between species and age. Although different vegetation characterizations are studied based on a case study for Queensland, Australia, no different zonations are studied.

It is incorrect to use a static drag coefficient, because the value depends on the vegetation characteristics and the hydrodynamic conditions. Although the biophysical characteristics are static, in theory the drag coefficient should change over the course of different hydraulic conditions. However, the use of a static drag coefficient is commonly used in the field of hydraulic engineering. In addition, a dynamic drag coefficient in combination with the look-up table is not easily implemented in a global framework. Even if a sensitivity study would be implemented in the local framework, it would show that the deviation in the drag coefficient is minor, compared to profile uncertainties and uncertainty in vegetation characterization.

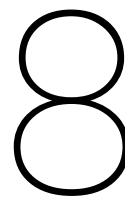
The performance of vegetation under extreme conditions is rarely studied, which implies that less is known about e.g. uprooting of vegetation. The research by [Vuik et al. \(2017\)](#) gives insight in this phenomenon. Possible biomass loss during extreme conditions and the influence of the corresponding storm duration is not implemented in the global assessment. This implies that the results might be overestimating wave damping by foreshore vegetation. This mainly relates to salt marshes, as they are more prone to biomass loss than mangroves during extreme conditions.

## 7.4. Dike location and schematization

Dikes and other flood defense structures are too small to be distinguished in the MG data set and without the existence of a global dike map, the presence of a dike remains unknown. The assumed dike location at the end of the foreshore depends on the determination method of the foreshore and the quality of the global data sources. The assumed dike profile has an inner and outer slope of 1:3, no berm and no protective cover, e.g. grass. A critical overtopping rate of 1 l/s/m is used, which is realistic for the assumed profile. However, it induces an overestimation of the effect of vegetation if in reality a well maintained grass cover is present.

Furthermore, vegetated fields can in some occasions be classified as very shallow foreshores, for which the traditional overtopping formulations do not necessarily apply ([Hofland et al., 2017](#)). In addition, the hydraulic conditions do not correspond exactly to the presented return periods, because no correlation between wave heights and extreme water levels is considered. In reality, the mutual probability of occurrence of an e.g. 1/100 years wave height and 1/100 years water level smaller than 1/100 years.

In the global assessment the presence of a dike is assumed somewhere along the transect. However, the number of people living in the hinterland, the corresponding economic value and the elevation of the hinterland is not considered. In reality this is important input when determining if a dike should be built to protect the hinterland from flooding. Building a dike along the whole coastline is unrealistic and induces an overestimation of the presented potential dike cost reduction. The goal of this research was not to come up with dike designs, but to map wave damping by foreshore vegetation on a global scale. The translation to dike cost reduction is made to express the added value of foreshore vegetation. The use of monetary values make the outcomes understandable for people outside the field of hydraulic engineering.



## Conclusion

In this research a global assessment is performed using open source global datasets to reveal the wave damping potential of present coastal vegetation to reduce flood hazard in coastal areas. Wave attenuation is calculated by assessing roughly 500.000 individual transects along the world's coastline.

### **In which areas worldwide is wave attenuation by foreshore vegetation the largest?**

According to the global assessment results, roughly 30 % of the world's coastline is vegetated, of which more than half has a vegetation width larger than 100 m and 5 % has a vegetation width exceeding 1000 m. When defining a significant wave height reduction of at least 30 cm to be substantial, then along 5 % of world's coastline substantial wave attenuation is observed for a storm return period of 100 years. This corresponds to roughly 15 % of the vegetated transects in the study area. Hot spots where wave attenuation in absolute terms exceeds 75 cm are found along James Bay in Canada, the coast of Columbia, Brazil, Guinea, Tanzania, Mozambique, Madagascar, India, Bangladesh, Myanmar, Thailand, Vietnam, China, Indonesia, Papua New Guinea, Australia and a few locations in the UK and France. The use of an absolute measure of wave attenuation resulted in a focus towards areas where high offshore significant wave heights are observed, because it is harder to achieve 0.95 m wave damping on a significant wave height of 1.00 m, than on a significant wave height of 3.00 m.

The reduction in wave transmission along the vegetated field on a transect is used as a measure of wave attenuation in relative terms. This measure indicates hotspots along the Gulf of Mexico and overall highlights areas in South-East Asia where extensive mangrove fields can be found. Evaluation of over 150 000 vegetated transects showed that mangroves and salt marshes are able to reduce wave transmission by a maximum of roughly 60 % and 40 % respectively. This result was found both for an exposed wave environment and a sheltered wave environment. However, in an exposed environment the maximum was reached in about 1000 m and in a sheltered environment after roughly 500 m. The obtained maximum wave transmission reductions depend on the characterization of vegetation in the model. In other words, for a more sparse characterization lower reduced wave transmission results would be obtained and vice-versa for a more dense characterization.

### **Where do people worldwide potentially benefit the most of wave attenuation by foreshore vegetation?**

The results of the global assessment are linked to data of the LECZ Urban-Rural population map ([CIESIN, 2013](#)), which showed that 28 % and 10 % of the vegetated transects in rural and urban areas respectively have a potential to reduce the incoming wave height with at least 20 centimeters. Another correlation is studied during the research using the human development index ([UNDP, 2016](#)). The results show that especially for countries at the South-East coast of Africa and in Asia coastal vegetation can have an important role, because countries with a low or medium human development index are likely to have less governmental strength, knowledge, or financial resources to take measures against flooding.

The dike height reduction results are summed per country and are translated to monetary values using an unit price per meter dike height per kilometer which is related to the HDI per country. The results show that Tanzania, Guinea-Bissau and Burma are the top 3 countries having the largest potential dike height reduction by foreshore vegetation relative to their coastline length, with a maximum of 0.75 m/km dike height reduction. Together Australia, The United States of America and Canada can potentially save 208 billion USA dollar, due to reduced dike investment or maintenance costs. The total dike reduction cost relative to the Gross Domestic Product (GDP) underlines the importance of coastal vegetation for Small Islands Development States (SIDS). Countries such as the Solomon Islands and the Federated States of Micronesia deal with limited resources and remoteness. For this reason, taking flood prevention measures is unattractive from an economic point of view. Under this assumption present coastal vegetation will, at least, lower wave impact.

### **How is uncertainty in flood hazard reduction due to wave attenuation by foreshore vegetation apportioned over the input parameters?**

In the global study datasets are used that have global coverage. These datasets have typically larger errors than datasets that are normally used for local studies. The datasets can be split in three categories (1) bathymetry and elevation data, (2) hydrodynamic data and (3) vegetation data. The datasets used in the global assessment are described in Chapter 3. Most of the input data uncertainty is induced by the global bathymetry and elevation data. The GEE Intertidal Elevation (GIE) set (20-30 m resolution,  $\sim 1$  m vertical accuracy) which provides profile data in the intertidal zone often falsely indicates land or open sea as intertidal zone. Validation checks are performed to identify and remove erroneous data. In total the set provided profile data for 24,5 % of the transects. For the other transects, the foreshore profile is derived using data from MERIT-GEBCO (MG). The MG data set is the result of merging GEBCO (30 arc-seconds resolution, tens of meters vertical accuracy) and MERIT (3 arc-seconds resolution, 2 meters vertical accuracy) datasets. The uncertainties in the profile input data are larger than the input uncertainty in the hydrodynamic data and vegetation data. However, also these sets have their drawbacks, e.g. the ERA-I wave data underestimates tropical cyclones. Furthermore the salt marsh map and mangroves map, which are the main vegetation cover type data sources, are based on various sources originated from different years. This induces the chance that in some cases e.g. mangroves are cut and mangrove present is falsely assigned based on data on mangroves map. Last, GlobCover data is speckled and often assigns false vegetation types.

In addition, uncertainty is induced by the model approach, which can be split in four parts (1) foreshore determination, (2) determination of vegetation width and type, (4) determination of nearshore wave characteristics and (3) determination of wave attenuation over the foreshore. In the local framework the performance of the global model is assessed by comparison case study results for the Western Scheldt, The Netherlands, derived with numerical calculations made with detailed bathymetry and elevation data. The significant wave height at the start of the vegetated zone was overestimated on average by 1.1 m with a standard deviation of 0.6 m. Wave height reduction by foreshore vegetation was overestimated with a RMSE of 0.15 m. The induced error is the largest for sheltered areas which have high extreme water levels, because the incoming wave is not or only partly depth limited in this case. Despite the error in absolute terms, the global model performed well in relative terms. The global reduced wave transmission results showed a RMSE of 7.5 % in comparison to the local framework results.

Based on a case study for the coastline of Queensland, Australia, it is found that the variation of wave attenuation capability can be large for different salt marshes states, related to seasonal influences. The results show a decrease in mean wave transmission from 22 % to 4 %, due to reduced biomass. For mangroves an increase of wave transmission reduction of 15 % is observed with respect to the vegetation characterization used in the global assessment.

Last, a sensitivity analysis is performed using the Morrison approach for both the global and local framework. In the global assessment, the wave period is the most influential parameter in sheltered areas. Assuming no change of the wave period from offshore to nearshore results in an underestimation of the wave attenuation. Next the profile parameters are the most influential, because they have a large influence on the water depth of the vegetated field. For extensive vegetated transects the vegetation width is of less importance, because most attenuation by salt marsh vegetation is observed in the first kilometer. The uncertainty in the extreme water level is not the most influential, despite a strong dependency of the wave propagation on the water depth. This is explained by good performance of the GTSM model relative to the profile data. In the local framework the bed level data is more accurate, resulting in more relative influence of the water level. In the sensitivity analysis for the local framework also the salt marsh characterization parameters are included. The stem density has the most influence on wave attenuation, followed by the stem height, because they come with large uncertainties due to seasonal influences. Overall, the sensitivity analysis results show that for a steeper and less extensive vegetated transect, vegetation characteristics become more important relative to the hydrodynamic boundary conditions.

## Recommendations

This recommendations chapter consists of two parts. First, it addresses topics which will explain the potential increase in accuracy of the global flood hazard assessment. This chapter concludes with a view on the implementation of foreshore vegetation as additional coastal defence measure.

### Technical recommendations

#### Determination of the foreshore

Correct determination of the foreshore profile is extremely important for the accuracy of the study. The global assessment revealed weaknesses of the global data sets. The use of GEBCO for an application which focuses on the intertidal zone is not ideal, but the best available option for most of the transect locations. The GIE dataset is developed specially for the FAST project and has great potential. During the research the author of the GIE set shared several preliminary results of an improved GIE set, which were very promising. The present algorithm is designed in such a way that no changes are necessary once the new GIE dataset is published. The use of MERIT is at that point still necessary, because the new set will still have limited coverage, high in the intertidal zone. The resolution and vertical accuracy of MERIT are much better in comparison to GEBCO, which means that the use of MERIT complementary to GIE is not seen as a large limitation. Without the publication of a new GIE set there are a few measures which can be taken to improve the foreshore determination:

- **GIE threshold**

The GIE threshold to filter noise on the sea was set to 10 centimeters for the global assessment. Based on the results this value was too low to effectively filter erroneous data, see Appendix D.3.2. Increasing this value to approximately 30 centimeters will most likely remove most of the noise

- **Improvement of foreshore methods based on MG**

Incorrect foreshore determinations are observed in case the profile has multiple or no intersections with the extreme water level with a return period of two years (SLRP2). In case of multiple intersections it is not advised to use the last patch for foreshore determination, but rather using the first intersecting patch instead. Transects that start on land should be recognized in order to make the recipe work. In case of no intersection with SLRP2, a better foreshore is determined using the highest point after the start of the foreshore. With the use of vegetation maps and the extension function there is a small chance of missing vegetation along the transect. After performing the global assessment, a pilot version of this improved foreshore determination function was developed and tested for several locations, but not used globally.

- **Implement local digital terrain models (DTMs)**

For an increasing number of countries (open source) DTM data is available. Hosting this data on the existing GeoServer and using these local DTMs in the assessment will improve the results. This will especially improve the results for low lying areas, as the present algorithm needs an intersection between the profile and SLRP2 to effectively filter GIE noise in the hinterland.

#### Vegetation

The next step in the assessment is the determination of vegetation presence and type. The determination and characterization of foreshore vegetation can be further improved in several ways:

- **Use of salt marshes and mangroves map**

In the present script the foreshore is extended based on the salt marshes and mangroves map. Using the GIE set induces the chance of determining a foreshore which is situated in the hinterland. Redefining the beginning of the foreshore based on the vegetation maps in these cases can prevent determination of inaccurate foreshores.

- **Use of multiple salt marsh states**

The research showed that seasonal changes can influence the wave attenuation results significantly. Using several salt marsh states e.g. based on latitude and longitude will give more realistic results. A more sophisticated option is to use the satellite derived LAI to determine the biomass and next assign the vegetation properties.

### Wave propagation

#### Determination of nearshore wave height

Comparison between the global and local framework showed that for wave height and wave period model, uncertainty is dominant over input uncertainty for sheltered areas in the global assessment. This is mainly induced by the depth limited approach used to estimate the nearshore wave height. Implementing the use of the numerical model SWAN in combination with MG and wave characteristics from ERA-I, will result in more accurate results. The following upscaling implementation is suggested; after determination of the foreshore profile the availability of SWAN output data at an acceptable distance from the beginning of the vegetated zone can be checked. If no output data is available, the following steps can be performed:

- 1. Determination of tile number, based on the grid of ERA-I ( $0.75^\circ \times 0.75^\circ$ )
- 2. Loading of bathymetry and elevation data from MG dataset
- 3. Loading of wave and wind boundary conditions from ERA-I dataset
  - Significant wave height
  - Wave period
  - Dominant wave direction
  - Wind speed
- 4. Creation of curvilinear grid with a grid size of roughly 30 arc-seconds
- 5. Creation matching depth file based on grid and MG data
- 6. Preparation of input file for SWAN calculation
- 7. Start of SWAN calculation
- 8. Retrieving and saving of output

The retrieved output can directly be used for evaluation of the transect. This approach can be looped over several return periods. It is important that the depth is corrected for increasing water levels for higher return periods based on the GTSM data. The most difficult aspect will be the determination of the dominant wave direction. This data can be prepared in advance or in the calculation itself. During the research it was found that in some occasions no clear dominant direction can be distinguished from the ERA-I data. Furthermore, in some cases the dominant direction is not landward directed. Different approaches to deal with these situations should be investigated.

#### Enlargement of look-up table

More accurate results can be obtained if more conditions are represented in the look-up table. It is suggested to reduce the step size for water depths lower than 2 m and wave heights around 1 meter, because the present step size of 0.5 m is still quite coarse. Another option is to downscale the look-up table by linear interpolation between the present data points. A sensitivity analysis is difficult to perform with the present look-up data, because the step sizes are often too large to represent input uncertainty well. In order to use the look-up table to perform a sensitivity analysis, smaller steps are mainly suggested for a wide range of water levels and wave heights and also for the other look-up table parameters.

### Reliability of global assessment

The performed global assessment pointed out areas where foreshore vegetation can contribute to flood hazard reduction. The quality of the VegGEE dataset and the salt marshes and mangroves maps made it possible to obtain a good overview of extensive vegetated transects. However, the magnitude of wave attenuation in absolute terms remains uncertain. The wave attenuation results relative to the incoming wave height seem more trustworthy, but this statement is only based on one case study for a sheltered area. Large deviations in absolute terms were expected for this location. The reliability of the global model is qualitatively assessed by studying the distribution of the foreshore methods and the used vegetation cover type sources. A more solid approach is to perform a series of case studies for various places around the world. This gives the possibility to determine the reliability in a quantitative way with a solid base. Another option is to set up a scoring table which includes various uncertainty sources. For example, a transect which uses GlobCover will then get a low score based on the vegetation type determination method. The total score qualitatively indicates the reliability of the transect.



## Realistic view on the implementation of foreshore vegetation

The results of the performed global flood hazard reduction assessment show the effect of foreshore vegetation in terms of wave attenuation, reduced dike height and the potential social impact. The results show in which countries and, more in general, in which areas wave damping by foreshore vegetation is the most beneficial.

Salt marshes are found outside the tropics, mainly in countries that are well developed (high to very high HDI). Coastal cities in these countries have a large economic value. Large potential losses stimulate to choose for a high protection level against floods. Giving a higher protection level, the present knowledge gap addressing the behavior of salt marshes under extreme conditions becomes more important. Furthermore, urban expansion resulted in degradation of salt marshes near coastal cities. For this reason it is unlikely that governments will accept salt marshes as an added coastal defence measure on the short term, solely based on the wave damping capacity during extreme events.

In rural areas more extensive vegetated areas are found during the study. In addition, it is likely that rural areas have a lower protection level against flooding. Extensive vegetation width and a lower protection level decrease the uncertainty corresponding to the use of salt marshes as added coastal defence. For this reason the implementation of salt marshes is more likely in rural areas.

Although not researched in this study, salt marshes can accumulate sediments and counterattack the impact of sea level rise. Combining the positive effects can result in an integral solution which counters sea level rise, reduces wave loads on the dike and in addition provides habitat for various animals.

Mangroves are found in the tropics. The results of the global assessment show that mangroves attenuate waves more effectively. In addition, larger vegetation widths are found for mangroves in comparison to salt marshes. Furthermore, mangroves are less sensitive for uprooting and are less subjected to seasonal influences. This makes mangroves more attractive as a coastal defence measure from a technical point of view.

In general, countries in the tropics are less developed than countries outside the tropics. The results from the global assessment show that mainly countries in South-East Africa, North-West Africa, South-East Asia and Oceania benefit the most from foreshore vegetation as added coastal defence. In particular the Northern coast of Australia, although not densely populated and very high developed. In addition, the Small Island Developing States (SIDS) are particularly standing out. These countries have a low Gross Domestic Product (GDP) and are well vegetated, resulting in a high potential dike cost reduction relative to their GDP. Construction coastal defence structures is most likely to be financially unfeasible. Present coastal vegetation will at least lower the wave impact and probably delay submergence of these vulnerable states.

In conclusion, mangroves attenuate waves more efficiently in comparison to salt marshes. Furthermore, the implementation of foreshore vegetation is more likely in rural areas than in urban areas. In addition, the implementation of salt marshes is prevented by knowledge gaps concerning behavior during extreme events and long term resilience. Despite these knowledge gaps, based on the performed analysis it can be concluded that foreshore vegetation has a high potential to mitigate flood hazard globally.





# V

## References



# Bibliography

- Adam, P. *Saltmarsh ecology*. Cambridge University Press, 1990.
- Allen, J. R. Morphodynamics of Holocene salt marshes: A review sketch from the Atlantic and Southern North Sea coasts of Europe. *Quaternary Science Reviews*, 19(12):1155–1231, 2000. ISSN 02773791. doi: 10.1016/S0277-3791(99)00034-7.
- Altomare, C., Suzuki, T., Chen, X., Verwaest, T., and Kortenhaus, A. Wave overtopping of sea dikes with very shallow foreshores. *Coastal Engineering*, 116:236–257, 2016. ISSN 03783839. doi: 10.1016/j.coastaleng.2016.07.002. URL <http://dx.doi.org/10.1016/j.coastaleng.2016.07.002>.
- Anderson, C. M. and Treshow, M. A review of environmental and genetic factors that affect height in *Spartina alterniflora* Loisel. (salt marsh cord grass). *Estuaries and Coasts*, 3(3):168–176, 1980.
- Anderson, M. E. and Smith, J. M. Wave attenuation by flexible, idealized salt marsh vegetation. *Coastal Engineering*, 83:82–92, 2014. ISSN 03783839. doi: 10.1016/j.coastaleng.2013.10.004. URL <http://dx.doi.org/10.1016/j.coastaleng.2013.10.004>.
- Anderson, M., Smith, J., and McKay, S. Wave dissipation by vegetation, CHETN-I-82. *US Army Corps of Engineers Engineer Research and Development Center: Vicksburg, MS.*, (September):22 pp, 2011. URL <http://repository.tudelft.nl/view/hydro/uuid:17f2915f-bb57-47f9-8e85-67ff0c82510c/>.
- Asano, T., Deguchi, H., and Kobayashi, N. Interaction between water waves and vegetation. In *Coastal Engineering 1992*, pages 2709–2723. 1992.
- Augustin, L. N., Irish, J. L., and Lynett, P. Laboratory and numerical studies of wave damping by emergent and near-emergent wetland vegetation. *Coastal Engineering*, 56(3):332–340, 2009. ISSN 03783839. doi: 10.1016/j.coastaleng.2008.09.004. URL <http://dx.doi.org/10.1016/j.coastaleng.2008.09.004>.
- Battjes, J. and Stive, M. Calibration and verification of a dissipation model for random breaking waves. *Journal of Geophysical Research: Oceans*, 90(C5):9159–9167, 1985.
- Becker, J., Sandwell, D., Smith, W., Braud, J., Binder, B., Depner, J., Fabre, D., Factor, J., Ingalls, S., Kim, S., et al. Global bathymetry and elevation data at 30 arc seconds resolution: Srtm30\_plus. *Marine Geodesy*, 32(4):355–371, 2009.
- Borsje, B. W., van Wesenbeeck, B. K., Dekker, E., Paalvast, P., Bouma, T. J., van Katwijk, M. M., and de Vries, M. B. How ecological engineering can serve in coastal protection. *Ecological Engineering*, 37(2):113–122, 2011. ISSN 09258574. doi: 10.1016/j.ecoleng.2010.11.027. URL <http://dx.doi.org/10.1016/j.ecoleng.2010.11.027>.
- Bouma, T. J., van Belzen, J., Balke, T., Zhu, Z., Airoldi, L., Blight, A. J., Davies, A. J., Galvan, C., Hawkins, S. J., Hoggart, S. P., Lara, J. L., Losada, I. J., Maza, M., Ondiviela, B., Skov, M. W., Strain, E. M., Thompson, R. C., Yang, S., Zanuttigh, B., Zhang, L., and Herman, P. M. Identifying knowledge gaps hampering application of intertidal habitats in coastal protection: Opportunities & steps to take. *Coastal Engineering*, 87:147–157, 2014. ISSN 03783839. doi: 10.1016/j.coastaleng.2013.11.014.
- Bradley, K. and Houser, C. Relative velocity of seagrass blades : Implications for wave attenuation in low-energy environments. *Journal of Geophysical Research: Earth Surface*, 114(November 2007):1–13, 2009. doi: 10.1029/2007JF000951.
- Brinkman, R. M. *Wave attenuation in mangrove forests: An investigation through field and theoretical studies*. PhD thesis, James Cook University, 2006.
- Cain, J. L. and Cohen, R. A. Using sediment alginate amendment as a tool in the restoration of *Spartina alterniflora* marsh. *Wetlands ecology and management*, 22(4):439–449, 2014.
- Campolongo, F., Tarantola, S., and Saltelli, A. Tackling quantitatively large dimensionality problems. *Computer physics communications*, 117(1-2):75–85, 1999.
- Campolongo, F., Cariboni, J., and Saltelli, A. An effective screening design for sensitivity analysis of large models. *Environmental modelling & software*, 22(10):1509–1518, 2007.

- Chaisson, C. Factors Influencing Stem Density of Creekbank *Spartina alterniflora* in a New England Salt Marsh. *Botany Honors Papers*, 3, 2012.
- CIESIN. Low elevation coastal zone urban-rural population and land area estimates. <http://sedac.ciesin.columbia.edu/data/set/lec2-urban-rural-population-land-area-estimates-v2/docs>, 2013.
- Coppenolle, R. v., Schwarz, C., and Temmerman, S. Contribution of Mangroves and Salt Marshes to Nature-Based Mitigation of Coastal Flood Risks in Major Deltas of the World. *Estuaries and Coasts*, 2018. doi: 10.1007/s12237-018-0394-7Contribution.
- Craft, C., Clough, J., Ehman, J., Joye, S., Park, R., Pennings, S., Guo, H., and Machmuller, M. Forecasting the effects of accelerated sea-level rise on tidal marsh ecosystem services. *Frontiers in Ecology and the Environment*, 7(2):73–78, 2009.
- Crain, C. M., Silliman, B. R., Bertness, S. L., and Bertness, M. D. Physical and biotic drivers of plant distribution across estuarine salinity gradients. *Ecology*, 85(9):2539–2549, 2004. ISSN 1939-9170. doi: 10.1890/03-0745. URL <http://dx.doi.org/10.1890/03-0745>.
- Cronk, J. K. and Fennessy, M. S. *Wetland plants: biology and ecology*. CRC press, 2001.
- Cunha, S. R., Asmus, M., and Costa, C. PRODUCTION DYNAMICS OF *Spartina alterniflora* SALT MARSHES IN THE ESTUARY OF PATOS LAGOON (RS, BRAZIL): A SIMULATION MODEL APPROACH. *Brazilian Journal of Aquatic Science and Technology*, 9(2):75–85, 2005. doi: 10.14210/bjast.v9n2.p75-85.
- Dalrymple, R. A., Kirby, J. T., and Hwang, P. A. Wave Diffraction Due To Areas of Energy-Dissipation. *Journal of Waterway Port Coastal and Ocean Engineering-Asce*, 110(1):67–79, 1984.
- Dame, R. E. and Kenny, P. D. Variability of *Spartina alterniflora* primary production in the euhaline North Inlet estuary. *Marine Ecology - Progress Series*, 32:71–80, 1986. ISSN 0171-8630. doi: 10.3354/meps032071. URL <http://www.int-res.com/articles/meps/32/m032p071.pdf>.
- Dijkema, K. S. Geography of salt marshes in europe. *Zeitschrift fur Geomorphologie*, 31(4):489–499, 1987.
- Dijkstra, J. T. and Uittenbogaard, R. E. Modeling the interaction between flow and highly flexible aquatic vegetation. *Water Resources Research*, 46(12):1–14, 2010. ISSN 00431397. doi: 10.1029/2010WR009246.
- Dubi, A. and Tørum, A. Wave damping by kelp vegetation. In *Coastal Engineering 1994*, pages 142–156. 1995.
- EEA, E. E. A. Corine land cover - part 1: Methodology, 2016. URL <https://www.eea.europa.eu/publications/COR0-landcover>.
- EurOtop. *European Manual for the Assessment of Wave Overtopping*. Pullen, T., Allsop, N.W.H., Bruce, T., Kortenhaus, A., Schuttrumpf, H., van der Meer, J.w., 2007.
- EurOtop. *Manual on wave overtopping of sea defences and related structures. An overtopping manual largely based on European research, but for worldwide application*. Van der Meer, J.W., Allsop, N.W.H., Bruce, T., De Rouck, J., Kortenhaus, A., Pullen, T., Schuttrumpf, H., Troch, P., Zanuttigh, B., 2016.
- Feagin, R. A., Irish, J. L., Möller, I., Williams, A. M., Colón-Rivera, R. J., and Mousavi, M. E. Short communication: Engineering properties of wetland plants with application to wave attenuation. *Coastal Engineering*, 58(3):251–255, 2011. ISSN 03783839. doi: 10.1016/j.coastaleng.2010.10.003. URL <http://dx.doi.org/10.1016/j.coastaleng.2010.10.003>.
- Giri, C., Ochieng, E., Tieszen, L. L., Zhu, Z., Singh, A., Loveland, T., Masek, J., and Duke, N. Status and distribution of mangrove forests of the world using earth observation satellite data. *Global Ecology and Biogeography*, 20(1): 154–159, 2011.
- Gordon, D. and Cranford, P. Export of organic matter from macrotidal salt marshes in the upper bay of fundy, canada. *Oceanographic Literature Review*, 9(42):735, 1995.
- Güneralp, B., Güneralp, I., and Liu, Y. Changing global patterns of urban exposure to flood and drought hazards. *Global Environmental Change*, 31:217–225, 2015. ISSN 09593780. doi: 10.1016/j.gloenvcha.2015.01.002.
- Hillen, M. M., Jonkman, S. N., Kanning, W., Kok, M., Geldenhuys, M. A., and Stive, M. J. F. Coastal defence cost estimates: Case study of the Netherlands, New Orleans and Vietnam. *Communications on Hydraulic and Geotechnical Engineering*, (April), 2010. URL <http://repository.tudelft.nl/view/ir/uuid:604825d4-f218-40fc-b3b5-5f4280b2338d/>.

- Hinkel, J., Lincke, D., Vafeidis, A. T., Perrette, M., Nicholls, R. J., Tol, R. S. J., Marzeion, B., Fettweis, X., Ionescu, C., and Levermann, A. Coastal flood damage and adaptation costs under 21st century sea-level rise. *Proceedings of the National Academy of Sciences*, 111(9):3292–3297, 2014. ISSN 0027-8424. doi: 10.1073/pnas.1222469111. URL <http://www.pnas.org/lookup/doi/10.1073/pnas.1222469111>.
- Hofland, B., Chen, X., Altomare, C., and Oosterlo, P. Prediction formula for the spectral wave period  $T_{m-1,0}$  on mildly sloping shallow foreshores. *Coastal Engineering*, 123(February):21–28, 2017. ISSN 03783839. doi: 10.1016/j.coastaleng.2017.02.005.
- Holthuijsen, L. H. *Waves in oceanic and coastal waters*. Cambridge university press, 2010.
- Horstman, E. M., Dohmen-Janssen, C. M., Narra, P. M., van den Berg, N. J., Siemerink, M., and Hulscher, S. J. Wave attenuation in mangroves: A quantitative approach to field observations. *Coastal Engineering*, 94:47–62, 2014. ISSN 03783839. doi: 10.1016/j.coastaleng.2014.08.005. URL <http://dx.doi.org/10.1016/j.coastaleng.2014.08.005>.
- Hu, Z., Suzuki, T., Zitman, T., Uittewaal, W., and Stive, M. Laboratory study on wave dissipation by vegetation in combined current – wave flow. *Coastal Engineering*, 88:131–142, 2014. ISSN 0378-3839. doi: 10.1016/j.coastaleng.2014.02.009. URL <http://dx.doi.org/10.1016/j.coastaleng.2014.02.009>.
- Jadhav, R. S., Chen, Q., and Smith, J. M. Spectral distribution of wave energy dissipation by salt marsh vegetation. *Coastal Engineering*, 77:99–107, 2013. ISSN 03783839. doi: 10.1016/j.coastaleng.2013.02.013. URL <http://dx.doi.org/10.1016/j.coastaleng.2013.02.013>.
- Jadhav, R. and Chen, Q. Field Investigation of Wave Dissipation Over Salt Marsh Vegetation During Tropical Cyclone. *Coastal Engineering Proceedings*, pages 1–11, 2012. URL <http://journals.tdl.org/icce/index.php/icce/article/view/6575>.
- Janssen, M. Flood hazard reduction by mangroves. Master's thesis, Delft University of Technology, 2016.
- Jongman, B., Ward, P. J., and Aerts, J. C. Global exposure to river and coastal flooding: Long term trends and changes. *Global Environmental Change*, 22(4):823–835, 2012. ISSN 09593780. doi: 10.1016/j.gloenvcha.2012.07.004. URL <http://dx.doi.org/10.1016/j.gloenvcha.2012.07.004>.
- Kirwan, M. L. and Megonigal, J. P. Tidal wetland stability in the face of human impacts and sea-level rise. *Nature*, 504(7478):53–60, 2013. ISSN 0028-0836. doi: 10.1038/nature12856. URL <http://www.nature.com/doi/10.1038/nature12856>.
- Kirwan, M. L., Guntenspergen, G. R., and Morris, J. T. Latitudinal trends in *Spartina alterniflora* productivity and the response of coastal marshes to global change. *Global Change Biology*, 15(8):1982–1989, 2009. ISSN 13541013. doi: 10.1111/j.1365-2486.2008.01834.x.
- Kirwan, M. L., Guntenspergen, G. R., D'Alpaos, A., Morris, J. T., Mudd, S. M., and Temmerman, S. Limits on the adaptability of coastal marshes to rising sea level. *Geophysical Research Letters*, 37(23), 2010. ISSN 00948276. doi: 10.1029/2010GL045489.
- Knutson, P. L., Brochu, R. A., Seelig, W. N., and Inskeep, M. Wave damping in *Spartina alterniflora* marshes. *Wetlands*, 2(1):87–104, 1982.
- Kobayashi, N., Raichle, A., and Asano, T. Wave attenuation by vegetation. *Journal of Waterway, Port, Coastal, and Ocean Engineering*, 119(1):30–48, 1993.
- Lana, P. d. C., Guiss, C., and Disaró, S. T. Seasonal variation of biomass and production dynamics for above- and belowground components of a *Spartina alterniflora* marsh in the euhaline sector of Paranaguá Bay (SE Brazil). *Estuarine, Coastal and Shelf Science*, 32(3):231–241, 1991. ISSN 02727714. doi: 10.1016/0272-7714(91)90017-6.
- Mandelbrot, B. How long is the coast of Britain? statistical self-similarity and fractional dimension. *science*, 156(3775):636–638, 1967.
- Maza, M., Lara, J. L., and Losada, I. J. A coupled model of submerged vegetation under oscillatory flow using Navier-Stokes equations. *Coastal Engineering*, 80:16–34, 2013. ISSN 03783839. doi: 10.1016/j.coastaleng.2013.04.009. URL <http://dx.doi.org/10.1016/j.coastaleng.2013.04.009>.
- McFadden, L., Spencer, T., and Nicholls, R. J. Broad-scale modelling of coastal wetlands: What is required? *Hydrobiologia*, 577(1):5–15, 2007. ISSN 00188158. doi: 10.1007/s10750-006-0413-8.

- McGranahan, G., Balk, D., and Anderson, B. The rising tide: assessing the risks of climate change and human settlements in low elevation coastal zones. *Environment and Urbanization*, 19(1):17–37, 2007. ISSN 0956-2478. doi: 10.1177/0956247807076960. URL <http://journals.sagepub.com/doi/10.1177/0956247807076960>.
- Mcowen, C., Weatherdon, L., Bochove, J.-W., Sullivan, E., Blyth, S., Zockler, C., Stanwell-Smith, D., Kingston, N., Martin, C., Spalding, M., and Fletcher, S. A global map of saltmarshes. *Biodiversity Data Journal*, 5:e11764, 2017. ISSN 1314-2828. doi: 10.3897/BDJ.5.e11764. URL <http://bdj.pensoft.net/articles.php?id=11764>.
- Mendez, F. J. and Losada, I. J. An empirical model to estimate the propagation of random breaking and nonbreaking waves over vegetation fields. *Coastal Engineering*, 51(2):103–118, 2004. ISSN 03783839. doi: 10.1016/j.coastaleng.2003.11.003.
- Méndez, F. J., Losada, I. J., and Losada, M. A. Hydrodynamics induced by wind waves in a vegetation field. *Journal of Geophysical Research: Oceans*, 104(C8):18383–18396, 1999. ISSN 01480227. doi: 10.1029/1999JC900119. URL <http://doi.wiley.com/10.1029/1999JC900119>.
- Moller, I. Quantifying saltmarsh vegetation and its effect on wave height dissipation : Results from a UK East coast saltmarsh. *Estuarine, Coastal and Shelf Science*, 69:337–351, 2006. doi: 10.1016/j.ecss.2006.05.003.
- Möller, I., Spencer, T., and French, J. R. Wild wave attenuation over saltmarsh surfaces: Preliminary results from Norfolk, England. *Journal of Coastal Research*, 12(4):1009–1016, 1996. ISSN 07490208. URL <http://discovery.ucl.ac.uk/136152/>.
- Möller, I. and Spencer, T. Wave dissipation over macro-tidal saltmarshes: Effects of marsh edge typology and vegetation change. *Journal of Coastal Research*, 36(36):506–521, 2002. ISSN 0749-0208. doi: 10.1016/S0749-0208(02)00083-2. URL <http://www.mendeley.com/research/wave-dissipation-macrotidal-saltmarshes-effects-marsh-edge-typology-vegetation-change/>.
- Möller, I., Kudella, M., Rupprecht, F., Spencer, T., Paul, M., Wesenbeeck, B. K. V., Wolters, G., Jensen, K., Bouma, T. J., Miranda-lange, M., and Schimmels, S. Wave attenuation over coastal salt marshes under storm surge conditions. *Nature Geoscience*, 7(September):727–732, 2014. doi: 10.1038/NGEO2251.
- Morris, J. T., Sundareswarar, P. V., Nietch, C. T., Kjerfve, B., and Cahoon, D. R. Responses of coastal wetlands to rising sea level. *Ecology*, 83(10):2869–2877, 2002. ISSN 0012-9658. doi: 10.1890/0012-9658(2002)083[2869:ROCWTR]2.0.CO;2.
- Morris, M. D. Factorial sampling plans for preliminary computational experiments. *Technometrics*, 33(2):161–174, 1991.
- Muis, S., Güneralp, B., Jongman, B., Aerts, J. C., and Ward, P. J. Flood risk and adaptation strategies under climate change and urban expansion: A probabilistic analysis using global data. *Science of the Total Environment*, 538: 445–457, 2015a. ISSN 18791026. doi: 10.1016/j.scitotenv.2015.08.068. URL <http://dx.doi.org/10.1016/j.scitotenv.2015.08.068>.
- Muis, S., Verlaan, M., Winsemius, H., and Ward, P. A first global-scale hindcast of extreme sea levels induced by extra-tropical storms. In *EGU General Assembly Conference Abstracts*, volume 17, 2015b.
- Muis, S., Verlaan, M., Winsemius, H. C., Aerts, J. C., and Ward, P. J. A global reanalysis of storm surges and extreme sea levels. *Nature communications*, 7, 2016.
- Murray, N. J., Phinn, S. R., Clemens, R. S., Roelfsema, C. M., and Fuller, R. A. Continental scale mapping of tidal flats across east asia using the landsat archive. *Remote Sensing*, 4(11):3417–3426, 2012.
- Nairn, R. B. *Prediction of cross-shore sediment transport and beach profile evolution*. PhD thesis, Imperial College London (University of London), 1990.
- Neumeier, U. Quantification of vertical density variations of salt-marsh vegetation. *Estuarine, Coastal and Shelf Science*, 63(4):489–496, 2005. ISSN 02727714. doi: 10.1016/j.ecss.2004.12.009.
- Nicholls, R. J. Coastal megacities and climate change. *GeoJournal*, 37(3):369–379, 1995. ISSN 03432521. doi: 10.1007/BF00814018.
- Niedermeier, A., Hoja, D., and Lehner, S. Topography and morphodynamics in the german bight using sar and optical remote sensing data. *Ocean Dynamics*, 55(2):100–109, 2005.



- Norton, J. An introduction to sensitivity assessment of simulation models. *Environmental Modelling and Software*, 69:166–174, 2015. ISSN 13648152. doi: 10.1016/j.envsoft.2015.03.020. URL <http://dx.doi.org/10.1016/j.envsoft.2015.03.020>.
- NRCS, N. R. C. S. *National Soil Survey Handbook: Glossary of landform and geologic terms*. United States Department of Agriculture, 2007.
- Owen, M. Design of seawalls allowing for wave overtopping. *Report Ex*, 924:39, 1980.
- Ozeren, Y., Asce, A. M., Wren, D. G., Asce, M., Wu, W., and Asce, M. Experimental Investigation of Wave Attenuation through Model and Live Vegetation. *Journal of Waterway, Port, Coastal, Ocean Engineering*, 140(5):1–12, 2014. doi: 10.1061/(ASCE)WW.1943-5460.0000251.
- Paul, M. and Amos, C. L. Spatial and seasonal variation in wave attenuation over *Zostera noltii*. *Journal of Geophysical Research*, 116:1–16, 2011. doi: 10.1029/2010JC006797.
- Pennings, S. C. and Bertness, M. D. Salt marsh communities. *Marine community ecology*, pages 289–316, 2001.
- Pianosi, F., Beven, K., Freer, J., Hall, J. W., Rougier, J., Stephenson, D. B., and Wagener, T. Sensitivity analysis of environmental models: A systematic review with practical workflow. *Environmental Modelling and Software*, 79:214–232, 2016. ISSN 13648152. doi: 10.1016/j.envsoft.2016.02.008. URL <http://dx.doi.org/10.1016/j.envsoft.2016.02.008>.
- Puijalon, S., Bouma, T. J., Douady, C. J., Groenendaal, J. V., Anten, N. P. R., Martel, E., and Bornette, G. Plant resistance to mechanical stress : evidence of an avoidance – tolerance trade-off. *New Phytologist*, 191:1141–1149, 2011.
- Pye, K. and French, P. *Erosion and Accretion Processes on British Salt Marshes. Volume One: Introduction: Saltmarsh process and morphology*, volume 1. Cambridge Environmental Research Consultants, 1993. ISBN 1 873 702 00 2.
- Reed, D. J. The response of coastal marshes to sea-level rise: Survival or submergence? *Earth Surface Processes and Landforms*, 20(1):39–48, 1995.
- Roelvink, D., Reniers, A., van Dongeren, A., van Thiel de Vries, J., McCall, R., and Lescinski, J. Modelling storm impacts on beaches, dunes and barrier islands. *Coastal Engineering*, 56(11-12):1133–1152, 2009. ISSN 03783839. doi: 10.1016/j.coastaleng.2009.08.006. URL <http://dx.doi.org/10.1016/j.coastaleng.2009.08.006>.
- Roelvink, R. A. V. T. d. V. J. L. J. M. R., D. *XBeach Model Description and Manual*. Unesco-IHE, Deltares and Delft University of Technology, 2010. version 6.
- Rogers, J. N., Parrish, C. E., Ward, L. G., and Burdick, D. M. Assessment of Elevation Uncertainty in Salt Marsh Environments using Discrete-Return and Full-Waveform Lidar. *Journal of Coastal Research*, 76:107–122, 2016. ISSN 0749-0208. doi: 10.2112/SI76-010. URL <http://www.bioone.org/doi/10.2112/SI76-010>.
- Rothmaler, W. Pflanzenwachstum auf versalzten boden. 2001. URL <http://www.halophyten.uni-osnabrueck.de/>. Accessed: 1 - nov - 2017.
- Ruessink, B., Walstra, D., and Southgate, H. Calibration and verification of a parametric wave model on barred beaches. *Coastal Engineering*, 48(3):139 – 149, 2003. ISSN 0378-3839. doi: [https://doi.org/10.1016/S0378-3839\(03\)00023-1](https://doi.org/10.1016/S0378-3839(03)00023-1). URL <http://www.sciencedirect.com/science/article/pii/S0378383903000231>.
- Rupprecht, F., Möller, I., Evans, B., Spencer, T., and Jensen, K. Biophysical properties of salt marsh canopies - Quantifying plant stem flexibility and above ground biomass. *Coastal Engineering*, 100:48–57, 2015. ISSN 03783839. doi: 10.1016/j.coastaleng.2015.03.009. URL <http://dx.doi.org/10.1016/j.coastaleng.2015.03.009>.
- Rupprecht, F., Möller, I., Paul, M., Kudella, M., Spencer, T., van Wesenbeeck, B. K., Wolters, G., Jensen, K., Bouma, T. J., Miranda-Lange, M., and Schimmels, S. Vegetation-wave interactions in salt marshes under storm surge conditions. *Ecological Engineering*, 100:301–315, 2017. ISSN 09258574. doi: 10.1016/j.ecoleng.2016.12.030. URL <http://dx.doi.org/10.1016/j.ecoleng.2016.12.030>.
- Saltelli, A., Ratto, M., Andres, T., Campolongo, F., Cariboni, J., Gatelli, D., Saisana, M., and Tarantola, S. *Global sensitivity analysis: the primer*. John Wiley & Sons, 2008.
- Sandvik, B. World borders dataset, 2009. URL <http://thematicmapping.org/>. accessed 8 june 2018.
- Schierbeck, V. H., Gerrit J. *Introduction to bed, bank and shore protection, 2nd edition*. VSSD, 2012.

- Scott, D. B., Frail-Gauthier, J., and Mudie, P. J. *Coastal wetlands of the world: geology, ecology, distribution and applications*. Cambridge University Press, 2014.
- Seymour, R. J., Tegner, M. J., Dayton, P. K., and Parnell, P. E. Storm wave induced mortality of giant kelp, *Macrocystis pyrifera*, in southern California. *Estuarine, Coastal and Shelf Science*, 28:277–292, 1989. ISSN 02727714. doi: 10.1016/0272-7714(89)90018-8. URL <http://www.sciencedirect.com/science/article/pii/0272771489900188>.
- Shanas, P. and Kumar, V. S. Trends in surface wind speed and significant wave height as revealed by era-interim wind wave hindcast in the central bay of bengal. *International Journal of Climatology*, 35(9):2654–2663, 2015.
- Songy, G. Wave attenuation by global coastal salt marsh habitats. Master's thesis, Delft University of Technology, 2016.
- Spalding, M., McIvor, A., Tonneijck, H., F Tol, S., and van Eijk, P. Mangroves for coastal defence. Technical report, Wetlands International and The Nature Conservancy, 2014. Guidelines for coastal managers and policy makers.
- Suzuki, T., Zijlema, M., Burger, B., Meijer, M. C., and Narayan, S. Wave dissipation by vegetation with layer schematization in SWAN. *Coastal Engineering*, 59(1):64–71, 2011. ISSN 03783839. doi: 10.1016/j.coastaleng.2011.07.006. URL <http://dx.doi.org/10.1016/j.coastaleng.2011.07.006>.
- SWAN, t. *SWAN User Manual Cycle III version 41.10 AB*, 2017. available from <http://www.swan.tudelft.nl>.
- SWASH, t. *SWASH User manual version 4.01 A*, 2017. available from <http://swash.sourceforge.net>.
- Tschirky, P., Hall, K., and Turcke, D. Wave attenuation by emergent wetland vegetation. In *Coastal Engineering 2000*, pages 865–877. 2001.
- UNDESA. *World Urbanization Prospects*. 2014. ISBN 9789211515176. doi: 10.4054/DemRes.2005.12.9. URL <http://esa.un.org/unpd/wup/Highlights/WUP2014-Highlights.pdf>.
- UNDP. Un human development report 2016. <http://hdr.undp.org/en/2016-report>, 2016.
- van Belzen, B. T. S. M. Z. L. Y. L., J. Salt marshes in europe and temporal variability. 2013. URL [http://www.coastalwiki.org/w/images/8/86/Figure\\_salt-marsh\\_zonation.JPG](http://www.coastalwiki.org/w/images/8/86/Figure_salt-marsh_zonation.JPG). Accessed: 9 - oct - 2017.
- van der Meer, B. T., Jentsje. New Physical Insights and Design Formulas on Wave Overtopping at Sloping and Vertical Structures. *Journal of Waterway, Port, Coastal, and Ocean Engineering*, 140(6):04014025, 2014. ISSN 0733-950X. doi: 10.1061/(ASCE)WW.1943-5460.0000221. URL [http://ascelibrary.org/doi/10.1061/\(ASCE\)WW.1943-5460.0000221](http://ascelibrary.org/doi/10.1061/(ASCE)WW.1943-5460.0000221).
- van der Wal, D., Morris, E., Smith, G., and Hendriksen, G. D3.3 3.5 3.9 geo-spatial data products. Technical report, Deltares, 2016. FAST deliverable.
- Van Gent, M. Physical model investigations on coastal structures with shallow foreshores: 2d model tests with single and double-peaked wave energy spectra. *H3608*, 1999.
- van Griensven, A., Meixner, T., Grunwald, S., Bishop, T., Diluzio, M., and Srinivasan, R. A global sensitivity analysis tool for the parameters of multi-variable catchment models. *Journal of Hydrology*, 324(1-4):10–23, 2006. ISSN 00221694. doi: 10.1016/j.jhydrol.2005.09.008.
- van Rooijen, A., van Thiel de Vries, J., McCall, R., van Dongeren, A., Roelvink, J., and Reniers, A. Modeling of wave attenuation by vegetation with XBeach. *E-proceedings of the 36th IAHR World Congress*, page 7, 2015.
- van Wesenbeeck, B. and Dijkstra, J. D 5.4 prototype linkage of general rules for engineering requirements of dike design. Technical report, Deltares, 2017. FAST deliverable.
- Van Wesenbeeck, B. K., Mulder, J. P. M., Marchand, M., Reed, D. J., De Vries, M. B., De Vriend, H. J., and Herman, P. M. J. Damming deltas: A practice of the past? Towards nature-based flood defenses. *Estuarine, Coastal and Shelf Science*, 140:1–6, 2014. ISSN 02727714. doi: 10.1016/j.ecss.2013.12.031. URL <http://dx.doi.org/10.1016/j.ecss.2013.12.031>.
- Vuik, V., Jonkman, S. N., Borsje, B. W., and Suzuki, T. Nature-based flood protection: The efficiency of vegetated foreshores for reducing wave loads on coastal dikes. *Coastal Engineering*, 116:42–56, 2016. ISSN 03783839. doi: 10.1016/j.coastaleng.2016.06.001. URL <http://dx.doi.org/10.1016/j.coastaleng.2016.06.001>.

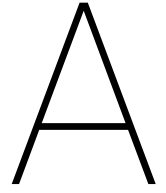
- Vuik, V., Heo, H. Y. S., Zhu, Z., Borsje, B. W., and Jonkman, S. N. Stem breakage of salt marsh vegetation under wave forcing : a field and model study. (Manuscript submitted for publication), 2017.
- Wu, W. C. and Cox, D. T. Effects of wave steepness and relative water depth on wave attenuation by emergent vegetation. *Estuarine, Coastal and Shelf Science*, 164:443–450, 2015. ISSN 02727714. doi: 10.1016/j.ecss.2015.08.009. URL <http://dx.doi.org/10.1016/j.ecss.2015.08.009>.
- Yamazaki, D., Ikeshima, D., Tawatari, R., Yamaguchi, T., O'Loughlin, E., Neal, J. C., Sampson, C. C., Kanae, S., and Bates, P. D. A high accuracy map of global terrain elevations. *Geophysical Research Letters*, 2017.
- Yang, S. L., Shi, B. W., Bouma, T. J., Ysebaert, T., and Luo, X. X. Wave Attenuation at a Salt Marsh Margin : A Case Study of an Exposed Coast on the Yangtze Estuary. *Estuaries and Coasts*, 35:169–182, 2011. doi: 10.1007/s12237-011-9424-4.
- Zhang, R. S., Shen, Y. M., Lu, L. Y., Yan, S. G., Wang, Y. H., Li, J. L., and Zhang, Z. L. Formation of *Spartina alterniflora* salt marshes on the coast of Jiangsu Province, China. *Ecological Engineering*, 23(2):95–105, 2004. ISSN 09258574. doi: 10.1016/j.ecoleng.2004.07.007.



# VI

## Appendices





# Vegetated foreshore dike systems

## Derivation Dalrymple's formulation

As waves propagate through salt marshes they lose energy due to work done on the vegetation. (Dalrymple et al., 1984) produced a formulation for wave energy dissipation by vegetation.

Wave energy conservation when only including dissipation by wave-vegetation interaction reads:

$$\frac{\partial(Ec_g)}{\partial x} = -\epsilon_D \quad (\text{A.1})$$

In which  $E$  = wave energy/unit area =  $0.5 \rho g a^2$ ,  $\rho$  = fluid density,  $g$  = gravity,  $a$  = wave amplitude,  $c_g$  = wave group velocity =  $n \cdot c$ ,  $n = \frac{1}{2} \frac{1 + 2kh}{\sinh 2kh}$ ,  $c = \sqrt{(g/k) \tanh kh}$ ,  $k$  = wave number =  $\frac{2\pi}{L}$ ,  $L$  = wave length,  $h$  = water depth and  $\epsilon_D$  = energy dissipation.

By neglecting inertia, only dissipation due to drag force is considered. The waves lose energy due to the work done on the vegetation. The dissipation term is described by:  $\epsilon_D = F_{drag} \cdot u$ . Integration over the effective depth gives:

$$\epsilon_D = \int_{-h}^{s-h} \frac{1}{2} \rho C_D A u |u| \cdot u \, dz \cdot N = B a^3 \quad (\text{A.2})$$

In which  $C_D$  = drag coefficient,  $A$  = area,  $u$  = horizontal velocity due to wave motion,  $h$  = water depth,  $s$  = stem height and  $N$  = the number of plants / per unit area.

With use of linear wave theory,  $B$  can be described by:

$$B = 2\rho \frac{C_D}{3\pi} \frac{D}{k} \frac{(\sinh^3 ks + 3 \sinh ks)}{3 \cosh^3 kh} \left( \frac{gk^3}{\sigma} \right) \left( \frac{1}{b^2} \right) \quad (\text{A.3})$$

In which:  $b$  = spacing between plants.

The solution for A.1 is:

$$\frac{a}{a_0} = \frac{1}{1 + \alpha x} \quad (\text{A.4})$$

In which:

$$\alpha = \frac{2C_D}{3\pi} \left( \frac{D}{b} \right) \left( \frac{a_0}{b} \right) (\sinh^3 ks + 3 \sinh ks) \left[ \frac{4k}{3 \sinh kh (\sinh 2kh + 2kh)} \right] \quad (\text{A.5})$$



## Influence factors wave overtopping

### Influence factors for wave run-up and wave overtopping formulas

In the presented wave run-up and overtopping formulas several influence factors are included (EurOtop, 2016). Below an overview of the several factors which will be discussed.

When an influence factor is absent a value of 1.0 has to be considered. If an influence is present an value smaller

Influence factors	
$\gamma_f$	influence factor for roughness elements on a slope
$\gamma_\beta$	influence factor for oblique wave attack
$\gamma_b$	influence factor for a berm
$\gamma_v$	influence factor for a wall on a slope
$\gamma^*$	combined influence factor for a storm wall on a slope

Table A.1: Overview of influence factors used in wave run-up and wave overtopping formulations (EurOtop, 2016)

than 1.0 is used, resulting in a decrease of wave-up or wave overtopping.  $\gamma_v$  and  $\gamma^*$  are only used in the wave overtopping formula. The influence factors for roughness and a berm, respectively  $\gamma_f$  and  $\gamma_b$  are equal for both wave run-up and overtopping. The influence factor for oblique wave attack  $\gamma_\beta$  differs.

### Roughness influence factor, $\gamma_f$

This factor includes the influence of roughness on the seaward slope. This typically will be grass, asphalt, loose rocks or block revetment systems.

Reference type	$\gamma_f$
Concrete	1.0
Asphalt	1.0
Grass	1.0
Basalt / basaltion	0.90
Placed revetment blocks	0.90
one layer riprap	0.70
double layer riprap	0.55

Table A.2: Surface roughness factors

For grass the recommended value of 1.0 is shown in table A.2, but decrease on run-up is measured on grass slopes for  $H_{m0} < 0.75$  m.

$$\gamma_{f,grass} = 1.15 H_{m0}^{0.5} \quad (A.6)$$

### Oblique wave attack influence factor, $\gamma_\beta$

The angle of wave attack  $\beta$  is defined at the toe of the structure. Oblique, instead of perpendicular incoming waves, result in a decrease of wave run-up and overtopping.

for wave run-up:

$$\begin{aligned} \gamma_\beta &= 1 - 0.22|\gamma_\beta| & \text{for: } 0^\circ < \beta < 80^\circ \text{ (short crested waves)} \\ \gamma_\beta &= 0.824 & \text{for: } |\beta| > 80^\circ \end{aligned}$$

for wave overtopping:

$$\begin{aligned} \gamma_\beta &= 1 - 0.0033|\gamma_\beta| & \text{for: } 0^\circ < \beta < 80^\circ \text{ (short crested waves)} \\ \gamma_\beta &= 0.736 & \text{for: } |\beta| > 80^\circ \end{aligned}$$

### Berm influence factor, $\gamma_b$

If well placed, a berm can reduce wave run-up and wave overtopping. The most effective position is the still water line. A position  $2H_{m0}$  below or  $Ru_{2\%}$  above SWL has no influence.

$$\gamma_b = 1 - \frac{B_b}{L_b} \left[ 0.5 + 0.5 \cos \left( \pi \frac{h_B}{x} \right) \right] \quad (A.7)$$

Where  $B_b$ = width of the berm,  $L_b$  is length of the berm,  $h_B$ =berm depth,  $x=Ru_{2\%}$  for berm above SWL and  $x=2H_{m0}$  for berm below SWL.  $\gamma_b$  is limited to a value of 0.6.

Formulations for  $\gamma_v$  and  $\gamma^*$  are not presented, because walls on a slope/crest are not considered.

# B

## Sensitivity analysis methods

A definition of sensitivity analysis (SA) is: "The study of how uncertainty in the output of a model can be apportioned to different sources of uncertainty in the model input" (Saltelli et al., 2008). Although similarities exist, a SA should not be mistaken with a uncertainty analysis (UA). An UA aims to quantify the uncertainty of the final outcome of the model, while a SA focuses to point output uncertainty back to different input factors.

### Sensitivity analysis characteristics

#### Type of sensitivity analysis

A large division among methods is made based on local or global input character. A local SA considers input variation around a certain user specified value, while a global SA includes the total range of possible variability (van Griensven et al., 2006). The latter results in a more robust analysis avoiding focussing only on local behaviour, downside is the size of the model evaluation set.

#### Sampling method

Two main sampling strategies exist:

- **One-at-a-time (OAT)** in which one input factor is varying a time, while other input factors are kept constant.
- **All-at-a-time (AAT)** all factors vary simultaneously

A Local SA is often performed using a OAT sampling approach. A global SA can both use OAT or AAT sampling. The main advantage of AAT is the insight of interaction between factors. The disadvantage is the extensive sampling set which is needed for AAT SA, which can make this approach less suitable together with computational costly numerical models (Pianosi et al., 2016).

### Sensitivity analysis methods

Overtime several SA methods are developed which can be distinguished e.g. based on the method of sensitivity assessment, sampling method and purpose. In line with the research questions as proposed in section 1, the purpose of the SA is ranking of input factors based on their contribution to the output variability. An overview of the methods is given in figure B.1.

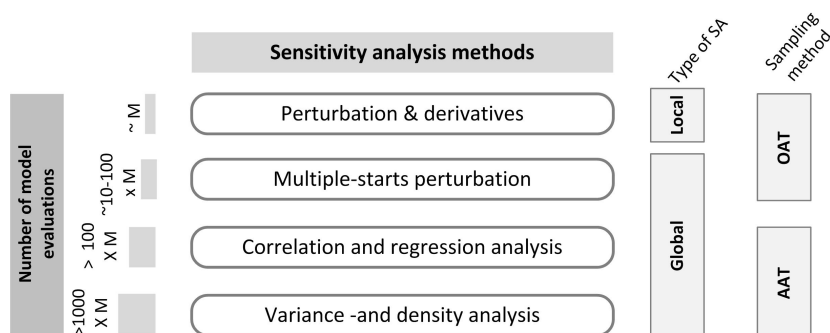


Figure B.1: Overview of sensitivity methods (modified from (Pianosi et al., 2016))

### Perturbation & derivatives

Vary every input parameter OAT from their value and assess impacts via visual inspection, i.e. input/output scatter plots. Quantitative approach can be used in case the output is defined as a scalar. The sensitivity of each input factor can be defined using the partial derivative at the nominal factor. Rescaling makes it possible to compare sensitivity among factors with different units.

$$S_i(\bar{x}) = \frac{\partial g}{\partial x_i} \Big|_{\bar{x}} c_i \quad (\text{B.1})$$

If the output function  $g$  is not differentiable an estimation with Taylor expansions is commonly used. Using finite differences gives:

$$\hat{S}_i(\bar{x}) = \frac{g(\bar{x}_1, \dots, \bar{x}_i + \Delta_i, \dots, \bar{x}_M) - g(\bar{x}_1, \dots, \bar{x}_i, \dots, \bar{x}_M)}{\Delta_i} c_i \quad (\text{B.2})$$

This simple -and computationally low approach gives only information about sensitivity around a certain point. If each parameter is varied just once, only  $M + 1$  model runs are needed. In case second order derivatives are included insight in factor interaction is gained.

### Multiple-starts perturbation

An extension on the former method computes varying outputs for multiple points instead for one single point. Methods in this category are i.e. the Elementary Effect Test (EET) and Distributed Evaluation of Local Sensitivity Analysis (DELSA). The most common method is the EET by (Morris, 1991) which is further elaborated here. Out of the possible input space  $r$  sample trajectories are sampled for  $M$  input factors. The influence of an individual input factor is defined via the elementary effect of this factor, comparable with equation B.2, only now averaged over the different trajectories. The elementary effect (EE) averaged over  $r$  is described as (Saltelli et al., 2008):

$$\mu_i = \frac{1}{r} \sum_{j=1}^r EE_i^j \quad (\text{B.3})$$

With  $i = 1, 2, \dots, M$ ,  $j = 1, 2, \dots, r$  and  $EE_i$  described by:

$$EE_i = \frac{Y(X_1, X_2, \dots, X_{i-1}, X_i + \Delta, \dots, X_M) - Y(X_1, X_2, \dots, X_M)}{\Delta} \quad (\text{B.4})$$

Including different trajectories shifts the analysis from a local to a more global perspective. Furthermore, insight can be given in the degree of interaction of factors. A high standard deviation  $\sigma$  of a factor implies that the value of a particular EE is strongly effected by the choice of the sample point. This means that the standard deviation  $\sigma$  combines in this case non-linear behaviour and interaction between factors.

$$\sigma_i^2 = \frac{1}{r-1} \sum_{j=1}^r (EE_i^j - \mu)^2 \quad (\text{B.5})$$

Using only  $\mu$  as sensitivity measure can fail to identify important factors. (Campolongo et al., 2007) proposed use of  $\mu_*$  which considers the absolute value  $|EE_i^j|$  in equation B.3.

### Sample strategy

By choosing an effective strategy this method includes a large range of variation, but keeps the computational costs low. Different sampling strategies are proposed overtime. (Morris, 1991) suggested a method of  $r$  trajectories with each  $(M + 1)$  points, resulting in a total of  $r(M + 1)$  sample points. First, a base vector  $\mathbf{x}^*$  is randomly generated out the input space which is defined as a  $M$ -dimensional unit cube with  $p$  levels. The first trajectory,  $\mathbf{x}^{(1)}$  is created by increasing/decreasing one component in  $\mathbf{x}^*$  by the step size  $\Delta$ . The trajectory,  $\mathbf{x}^{(1)}$ , is the base for  $\mathbf{x}^{(2)}$  which is obtained by again one manipulation. This continues till  $\mathbf{x}^{(M+1)}$ .

The choice of  $p$  (discretization grid level),  $\Delta$  (step size) and  $r$  (amount of trajectories) is key for an effective sampling strategy. (Saltelli et al., 2008) suggests  $p$  to be even and  $\Delta = p / [2(p - 1)]$ . A high value of  $p$  should be coupled with a high value of  $r$ , otherwise a lot of levels will not be covered. This sampling approach works for uniform distributions. In case of a nonuniform distribution samples should be taken from the inverse cumulative distribution function which is divided into quantiles (Campolongo et al., 1999). Other sample strategies exist, i.e. Latin Hypercube (LH) OAT is a strategy, which the starting trajectory is not randomly generated by via LH sampling. LH sampling is characterized by the objective to sample each factor at least over a minimum amount of levels, and that the sample points are equally distributed over the levels.

### Correlation and regression analysis

These methods are based on a large data set generated by a Monte Carlo simulation. A correlation SA considers the correlation between input and output variables as sensitivity measure. Different correlation definitions can be used based on the degree of non-linearity between the input/output. In a regression SA the least-squares estimate of the regression coefficient is used a sensitivity measure. A range of regression methods is available, from linear to non-linear methods. Approximately  $> 100 \times k$  model evaluations are needed (Pianosi et al., 2016).

### Variance -and density based analysis

Variance SA studies the influence of input uncertainty on the variance of the output. This global approach captures the whole range of input space and gives knowledge on interaction among factors. Downside is the high associated computational costs. A distinction is made between first-order and higher-order effects. First-order effects measure the individual contribution of a input factor to the output variance. If interaction effects are significantly, higher-order measures are suggested (Pianosi et al., 2016). Different calculation methods are available, i.e. The Sobol' method and the computational more effective Fourier amplitude sensitivity testing method (FAST-method) (Norton, 2015). The total computational costs depends on the amount of included parameters. The total cost of Sobol' method is  $N(M + 2)$  in which  $M$  are the amount of input factors and  $N$  is the sample base, which is in order of few hundreds to a few thousands (Saltelli et al., 2008).

Density based SA consider the variation in the output probability density function (PDF) when removing uncertainty in the input. Variance and density based SA need approximately  $> 1000 \times M$  model evaluations (Pianosi et al., 2016). Considering this high number of model evaluations these methods are probably not suitable and are not elaborated further.

### Reliability analysis

Reliability is defined as the probability that a limit state function which depends on a set of random variables is in a safe region. In other words, the likelihood that a system, i.e. a vegetated foreshore dike system, continues to function under specified conditions. The reliability is modelled by a limit state function  $g(\mathbf{X})$ , which describes load (S) and resistance (R). The function  $g(\mathbf{X})$  depends on the description of R and S and the set of random variables  $\mathbf{X}$ . Each variable, e.g. dike height, has its own variability described by a probability density function (*pdf*). If the joint *pdf* of the random variables  $\mathbf{X}$  is  $f_{\mathbf{x}}(\mathbf{x})$ , the reliability is computed by:

$$P\{g(\mathbf{X}) > 0\} = \int_{g(\mathbf{X}) > 0} f_{\mathbf{x}}(\mathbf{x}) d\mathbf{x} \quad (\text{B.6})$$

In contrast to the earlier presented sensitivity analyses, a reliability analysis (RA) gives insight in the probability of failure of a system instead of uncertainty contribution of individual parameters. A common RA method is the First Order Reliability Analysis (FORM).

#### FORM

The FORM estimates the reliability by assuming independence between variables, simplifying the joint *pdf*,  $f_{\mathbf{x}}(\mathbf{x})$  and linearising  $g(\mathbf{X})$  using a first order Taylor expansion. Without these simplifications the integral in equation B.6 is hard to solve due to: 1. high number of included random variables, 2. the joint pdf  $f_{\mathbf{x}}(\mathbf{x})$  is nonlinear and 3. wave propagating and other hydrodynamic processes are also nonlinear.

The set  $\mathbf{X}$  of random variables are all transformed to a set  $\mathbf{U}$  of standard normal distributed variables. This Rosenblatt transformation makes use of the fact that the cumulative distribution function (cdf) remains the same. The transformation can be linear or nonlinear, depending on the original distribution. The linearisation of  $g(\mathbf{U})$  is performed in the point with the highest probability density, called the Most Probable Point (MPP). This point is iteratively by searching the minimal distance between the limit state function and the origin of the variable space. This minimum distance  $\beta$  is called the reliability index. The reliability is given by:  $\Phi(\beta)$ . Besides the reliability, FORM gives insight in the sensitivity to the input parameters. Further mathematical equations can be found in appendix B.

### Applicability to flood hazard assessment

In line of this research the limit state function should represent the wave processes, wave-vegetation interaction and wave overtopping, as presented in figure 1.1. The limit state should be in this case a linearization of the wave action balance as presented in 2.24 and the wave overtopping formulation. To which extends this linearization holds should be checked based on numerical runs. The advantage is that wave processes, sensitivity and probability of failure are calculated in one module.

## First Order Reliability Method

The MPP is found by searching for  $\min \|u\|$  subject to  $g(\mathbf{u})=0$ .

In which:

$$\|u\| = \sqrt{u_1^2 + u_2^2 + \dots u_n^2} = \sum_{i=1}^n u_i^2 \quad (\text{B.7})$$

MPP point search is very difficult to solve analytically, for this reason numerical methods are available to get to the MPP point, which are not further elaborated here.

The approximation of the limit state function,  $g(\mathbf{U})$ , at the MPP is given by:

$$L(\mathbf{U}) = \sum_{i=1}^n \frac{\partial g(\mathbf{U})}{\partial U_i} \Big|_{\mathbf{u}^*} (\mathbf{U}_i - \mathbf{u}_i^*) = a_0 + \sum_{i=1}^n a_i U_i \quad (\text{B.8})$$

where:

$$a_0 = - \sum_{i=1}^n \frac{\partial g(\mathbf{U})}{\partial U_i} \Big|_{\mathbf{u}^*} \quad (\text{B.9})$$

and:

$$a_i = \frac{\partial g(\mathbf{U})}{\partial U_i} \Big|_{\mathbf{u}^*} \quad (\text{B.10})$$

The mean and standard deviation of  $L(\mathbf{U})$  are given by:

$$\mu_L = a_0 \quad (\text{B.11})$$

$$\sigma_L = \sqrt{\sum_{i=1}^n a_i^2} = \sqrt{\sum_{i=1}^n \left( \frac{\partial g(\mathbf{U})}{\partial U_i} \Big|_{\mathbf{u}^*} \right)^2}$$

The probability of failure is given by:

$$p_f \approx PL(\mathbf{U}) < 0 = \Phi \left( \frac{-\mu_L}{\sigma_L} \right) = \Phi \left( \sum_{i=1}^n \alpha_i u_i^* \right) \quad (\text{B.12})$$

where:

$$\alpha_i = \frac{\frac{\partial g}{\partial U_i} \Big|_{\mathbf{u}^*}}{\sqrt{\sum_{i=1}^n \left( \frac{\partial g}{\partial U_i} \Big|_{\mathbf{u}^*} \right)^2}} \quad (\text{B.13})$$

# Offshore to nearshore wave transformation methods

## Hydrodynamics

The boundary conditions derived from ERA-Interim wave data are still off shore conditions. These conditions are not valid at the begin of the transects. Especially in sheltered areas is expected that differences between offshore and nearshore conditions might be increasing due to i.e. refraction. For three study areas several wave transformation methods are compared.

The first method is based on depth limited breaking. At the begin of the transect is checked whether the wave can physically exist at this point using a breaker index of 0,55. The second option uses the method developed by Bretschneider, in which the wave characteristics are calculated based on the wind speed and fetch length. The third considered method uses the numerical model SWAN. A coarse grid is used for numerical calculations, In light of the global approach of the study and upscaling possibilities. The performance of the methods are compared for a range of return periods in order to be able to identify a possible trend towards higher return periods.

## Chesapeake Bay

For the study ERA boundary conditions derived by the FAST project team are used, Table C.1. Although the wave height, peak wave period and wind speed are known for a range of return periods, the corresponding wind directions are unknown. In absence of these data the Mean Wave Direction (MWD) is used, in case of Chesapeake Bay 144°.

Return period	1	2	5	10	25	50	100	250	500	1000
Hs (m)	3.6	4.0	4.5	4.9	5.5	6.0	6.5	7.3	8.0	8.7
Tp (s)	11.4	12.2	13.2	13.9	14.8	15.4	16.0	16.8	17.4	17.9
Wind speed (m/s)	17.3	18.4	19.7	20.7	22.0	22.9	23.8	25.0	25.9	26.7

Table C.1: Boundary conditions from ERA-Interim

In Figure C.1 an overview is presented of the study location. For comparison between the different methods several output locations are selected at NOAA buoy locations. The fetches used for the Bretschneider method are represented by the black arrows, of which the direction is equal to the MWD. Significant wave height output results for a return period of 100 years is also plotted.



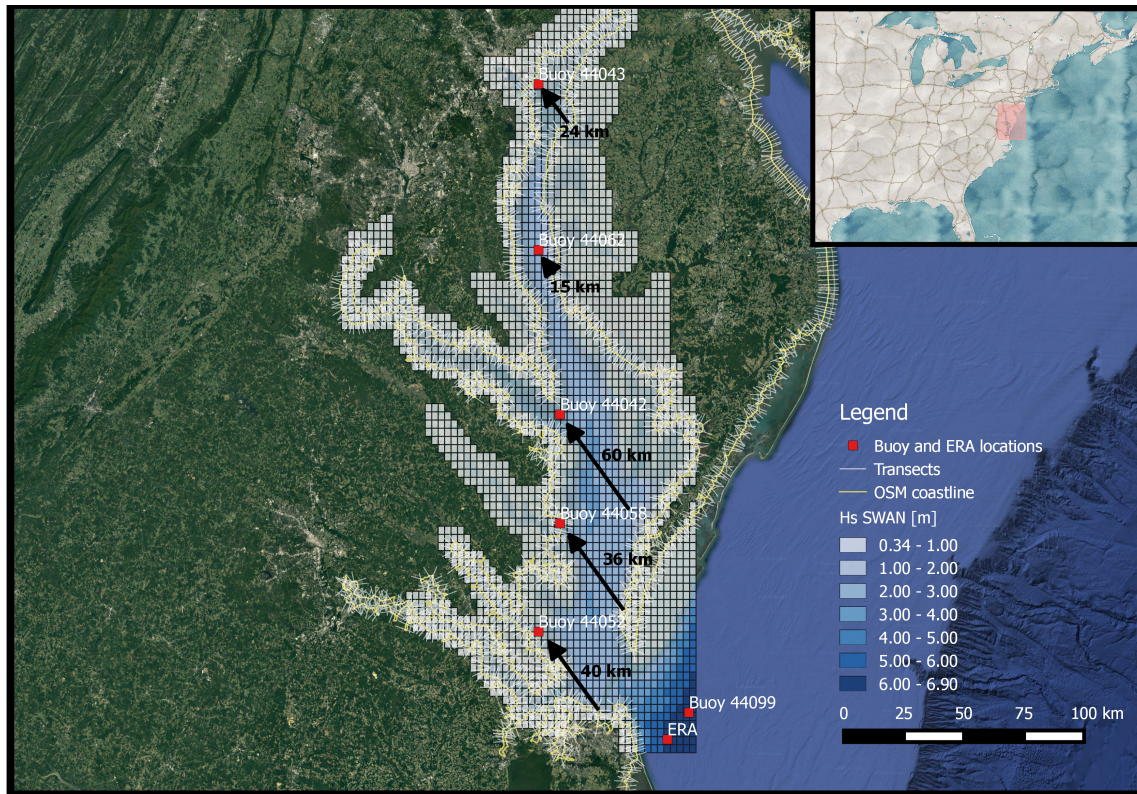


Figure C.1: Overview of Chesapeake Bay, USA

### SWAN

A range of stationary SWAN runs is performed with varying grid size and bathymetric data. Four different grid sizes are tested:  $0.03^\circ$ ,  $0.04^\circ$ ,  $0.05^\circ$  and  $0.06^\circ$ . Results show deviations of significant wave height in order of ten centimetres. Overall a coarser grid resulted in a lower estimation of the significant wave height. The different bathymetry sources are GEBCO and NOAA's Coastal Relief Model (CRM) with a higher resolution. The largest deviations are observed at buoy 44043, probably because the buoy is situated far north in the estuary and close to the bank where GEBCO might be inaccurate.

### Comparison

For the different return periods the RMSE is calculated in which the depth limited approach and Bretschneider approach are compared with the SWAN output. The average RMSE values over the locations are presented in Table C.2. Both methods give an overestimation of the wave height in comparison with the SWAN results. The depth limited approach has the largest RMSE with values exceeding 2 meter. Looking at the differences over the return periods, it seems that the RMSE increases for higher return periods. Despite the wave height inaccuracies it is yet unclear to which extend these errors influence wave damping calculations for the Chesapeake Bay.

Return period	1	2	5	10	25	50	100	250	500	1000
Depth limited versus SWAN										
RMSE [m]	1.6	1.7	1.9	1.9	2.0	2.0	2.0	2.2	2.3	2.5
RMSE [m] excluding buoy 44062	1.6	1.7	1.7	1.8	1.8	1.7	1.7	1.7	1.8	1.9
Bretschneider versus SWAN										
RMSE [m]	0.5	0.5	0.6	0.7	0.7	0.8	0.8	0.9	1.0	1.0

Table C.2: Significant wave height RMSE for depth limited -and Bretschneider approach versus SWAN



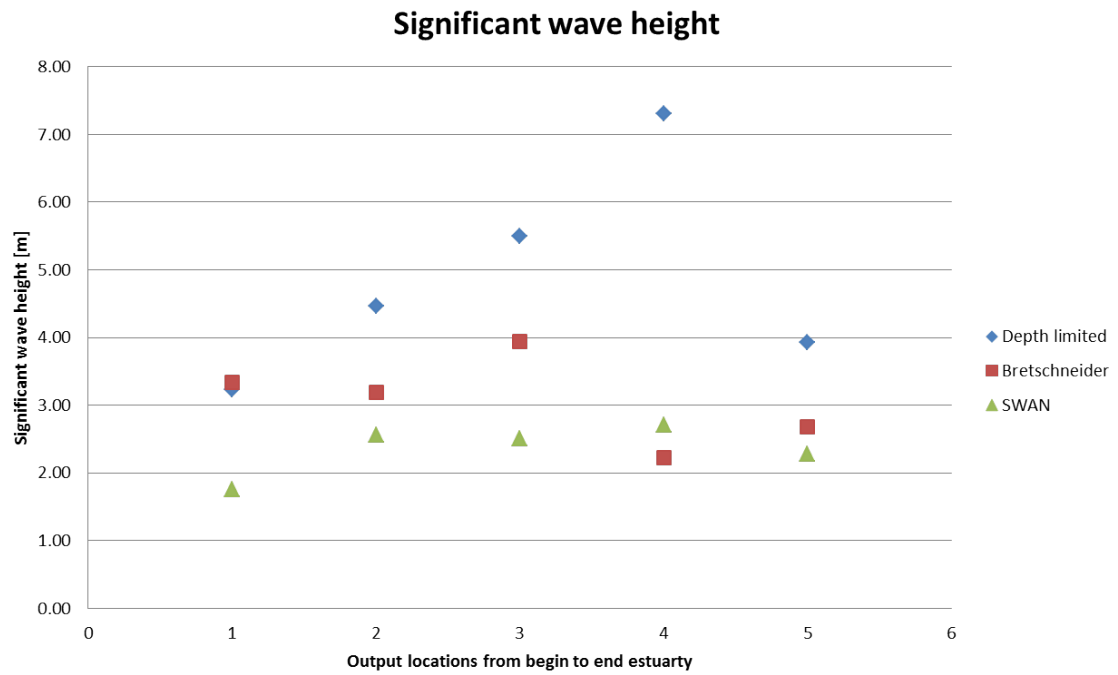


Figure C.2:  $H_s$  for 250 year return period at output locations for Chesapeake Bay, USA

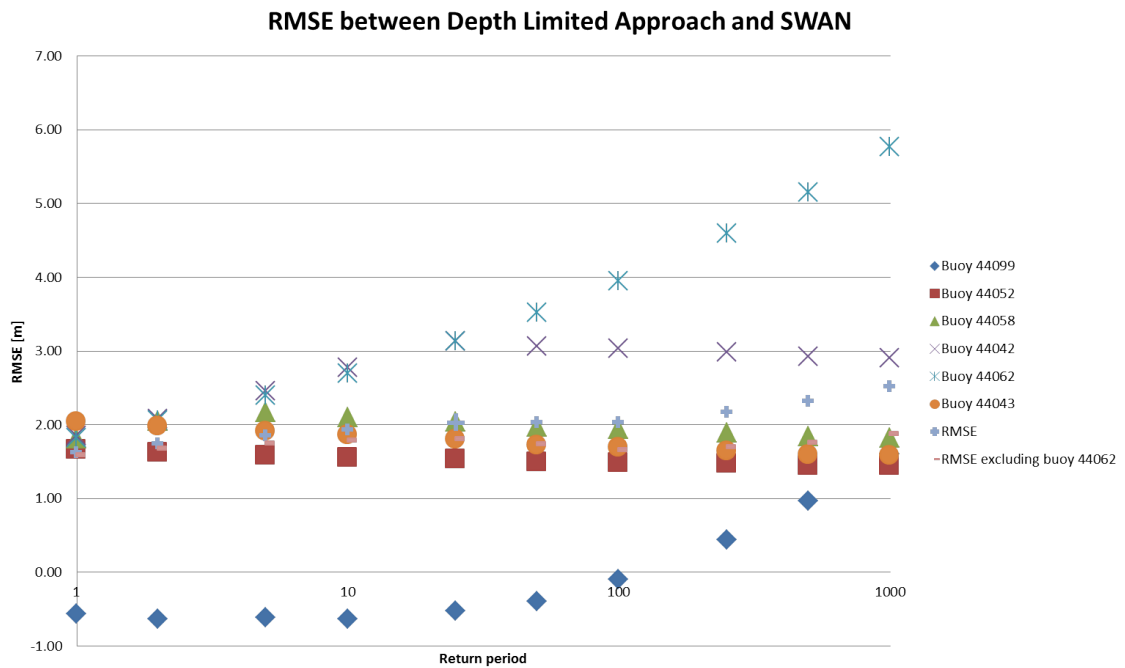


Figure C.3: RMSE over different return periods and output locations for Chesapeake Bay, USA

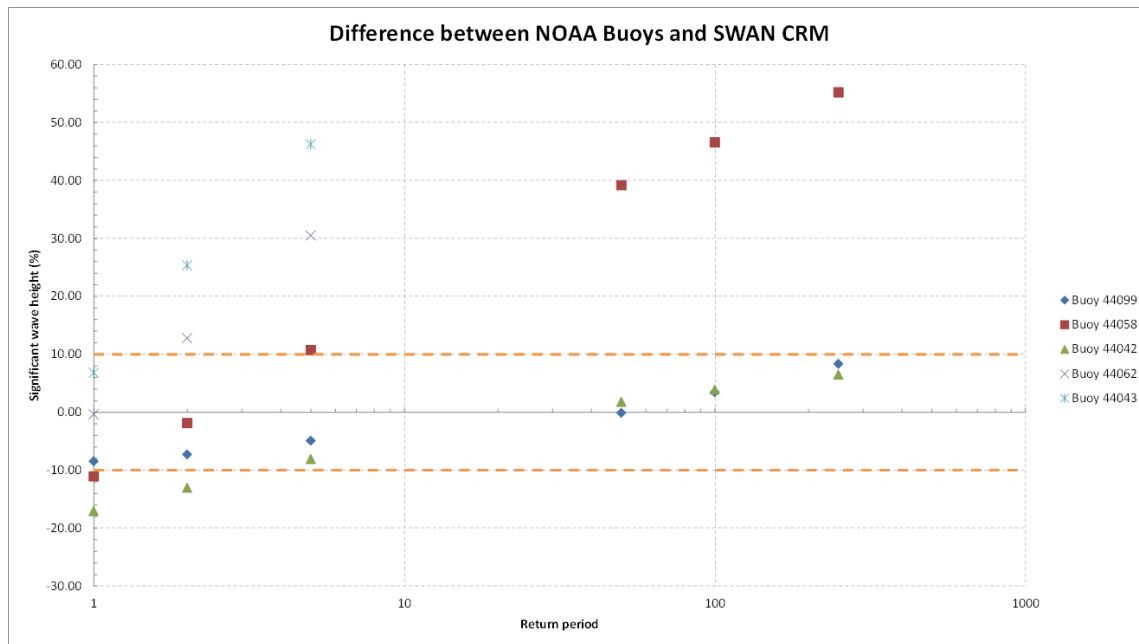


Figure C.4: Error in terms of percentage between SWAN and wave buoys for different return periods for Chesapeake Bay, USA

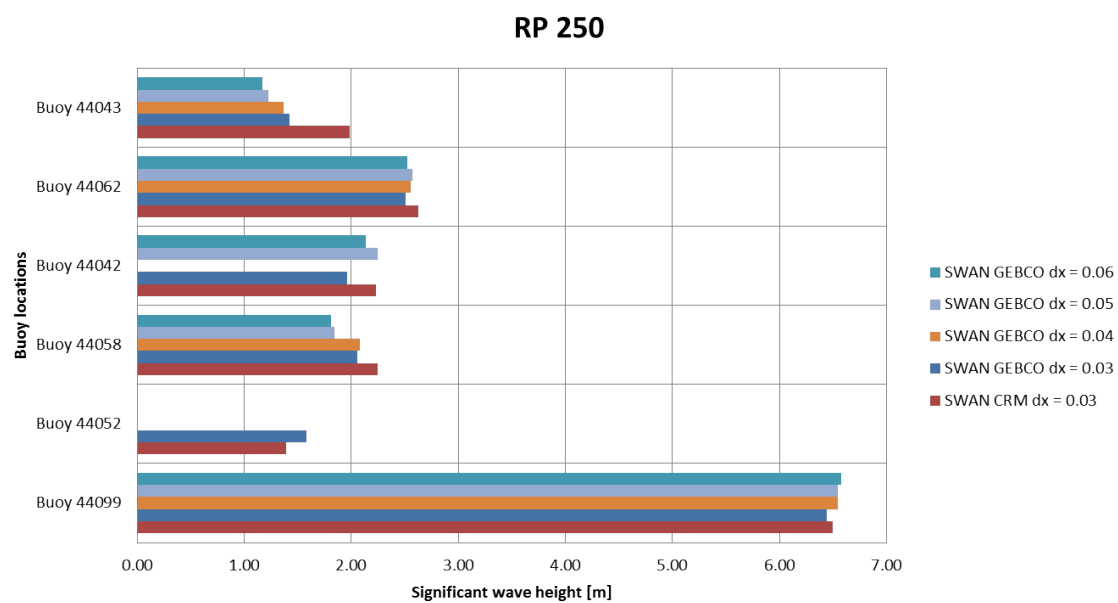


Figure C.5: Influence of grid size on SWAN wave height calculations for Chesapeake Bay, USA

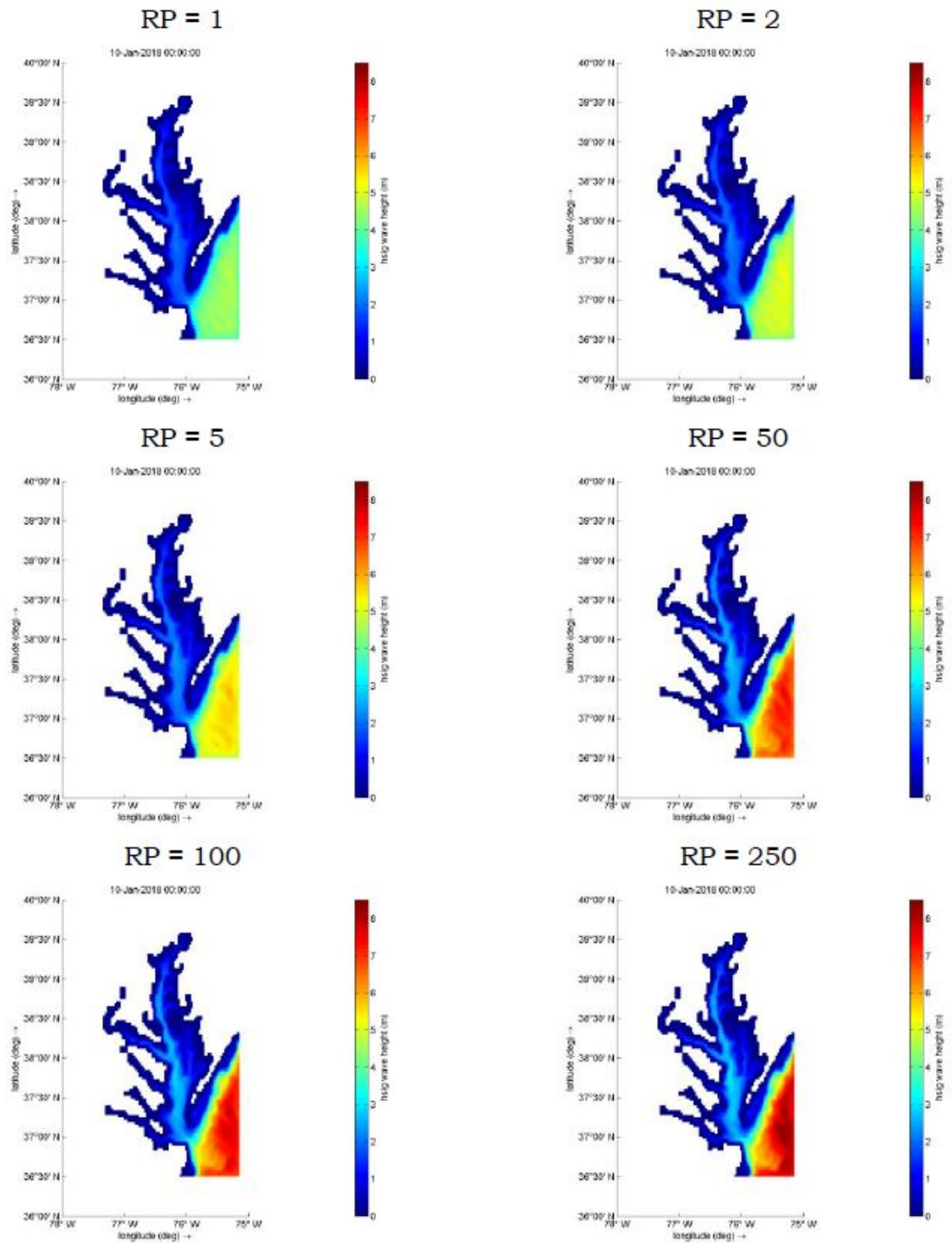


Figure C.6: Overview of SWAN wave height calculations for Chesapeake Bay, USA

### Western Scheldt

The used ERA-Interim derived wave -and wind boundary conditions and water levels from the GTSM model for this location are shown in Table C.3. The wave direction used is the MWD of  $217^\circ$ . Figure C.7 gives an overview of the study site and the wave height for a return period of 100 years based on a SWAN calculation using bathymetry from EMODNET with a grid size of  $0.01^\circ$ .

Return period	1	2	5	10	25	50	100	250	500	1000
Hs (m)	4.6	5.0	5.5	5.9	6.4	6.7	7.1	7.6	7.9	8.3
Tp (s)	9.4	9.8	10.4	10.7	11.2	11.5	11.8	12.2	12.5	12.7
Water level (m +MSL)	3.7	4.0	4.3	4.5	4.8	5.0	5.2	5.5	5.7	5.9
Wind speed (m/s)	19.0	19.8	20.8	21.5	22.2	22.7	23.1	23.5	23.9	24.1

Table C.3: Boundary conditions from ERA-Interim

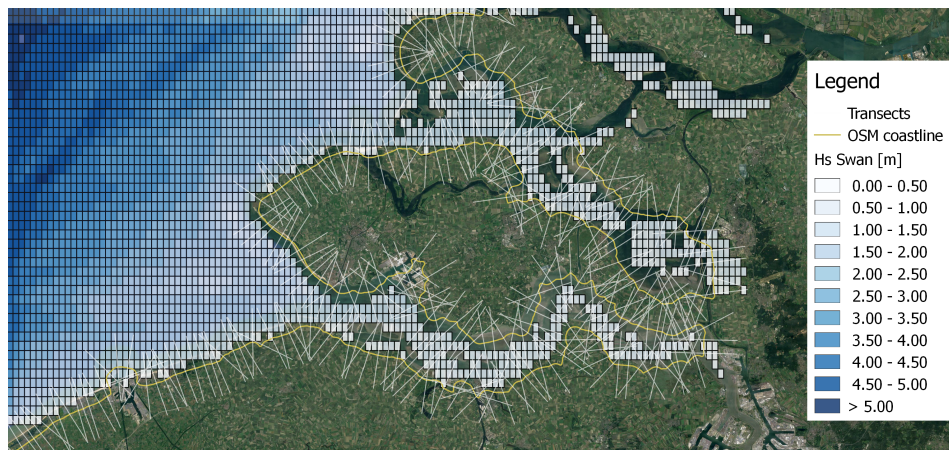


Figure C.7: Significant wave height for return period of 100 years, Western Scheldt



In figure C.8, C.9 are the nearshore wave heights presented corresponding to the transects in the study area. The difference between the methods is even larger than for the Chesapeake Bay. One reason is the higher water level which makes depth limiting breaking less likely to occur. Furthermore underestimates SWAN probably the wave height, because it uses the mean wave direction.

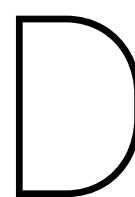


Figure C.8: Significant wave height from SWAN at begin of the transect for return period of 100 years, Western Scheldt



Figure C.9: Significant wave height according the depth limited approach at begin of the transect for return period of 100 years, Western Scheldt





## Global flood hazard assessment



### D.1. Hydrodynamic boundary conditions

The offshore wave height and the extreme water levels obtained in step 2 are visually presented in figure D.1 and D.17.

#### Offshore wave height

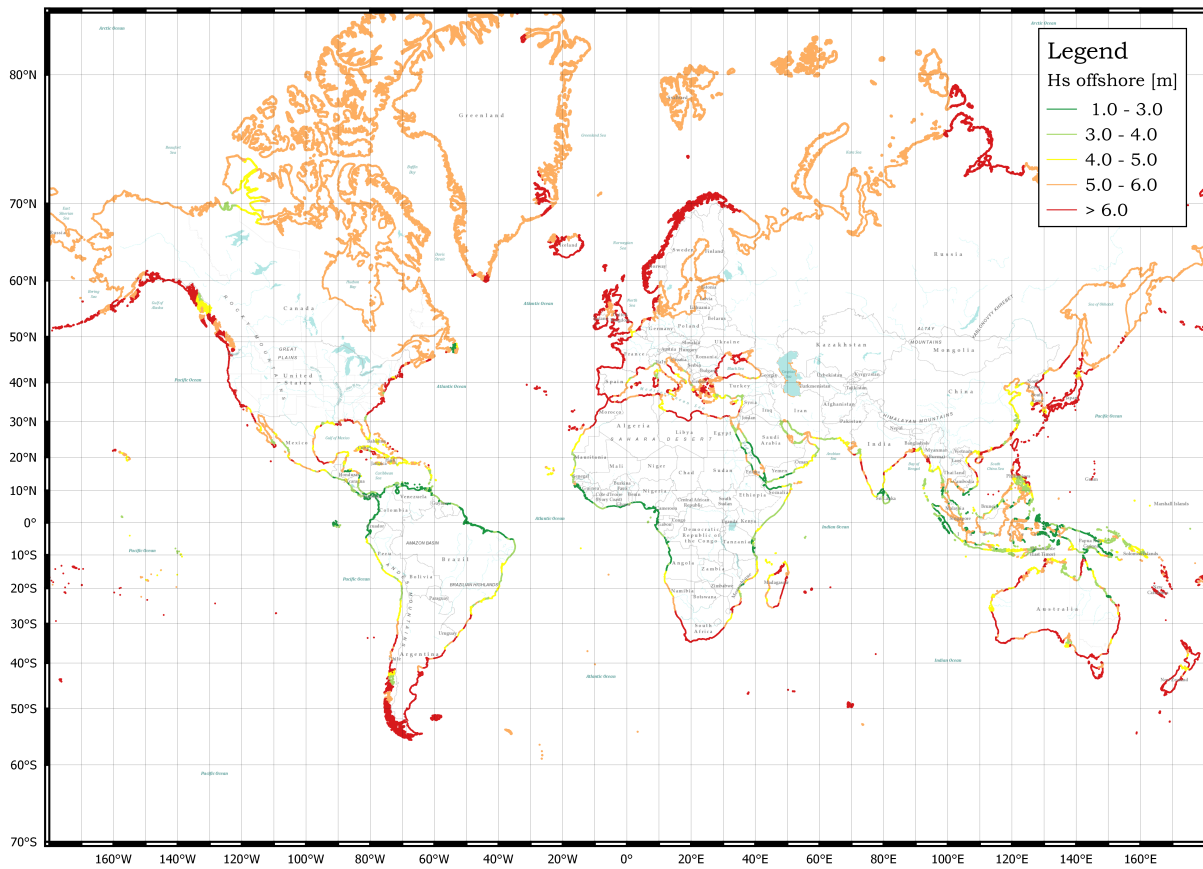


Figure D.1: World map of offshore significant wave heights derived from ERA-I for return period of 100 years

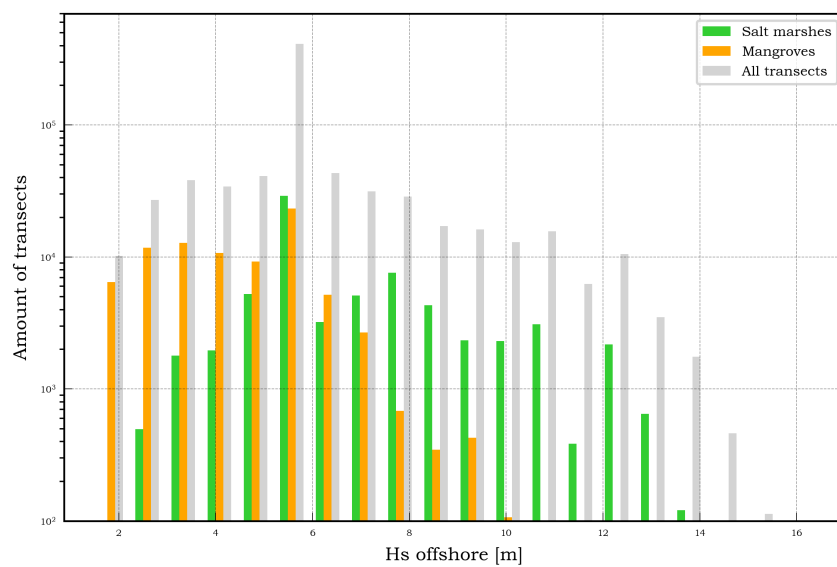


Figure D.2: Variation of offshore wave height amongst vegetated transects in relation to vegetated transects

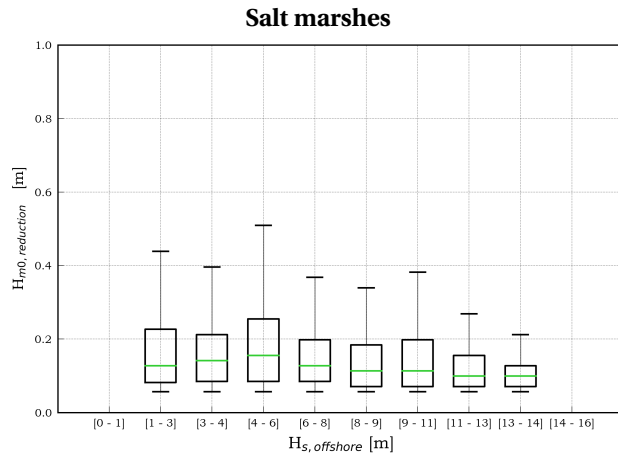


Figure D.3: Effect of offshore significant wave height on wave attenuation in absolute terms by salt marshes

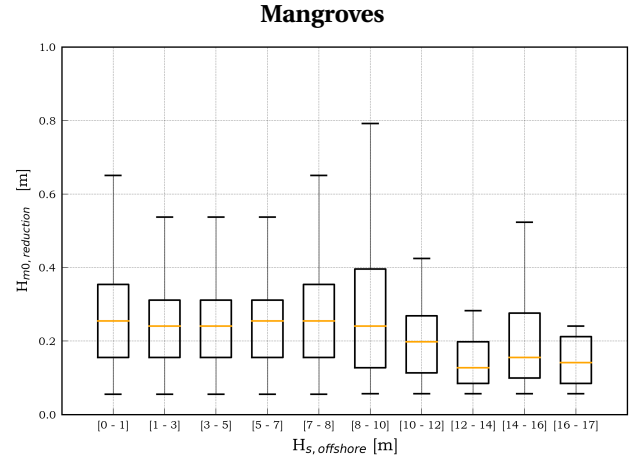


Figure D.4: Effect of offshore significant wave height on wave attenuation in absolute terms by mangroves

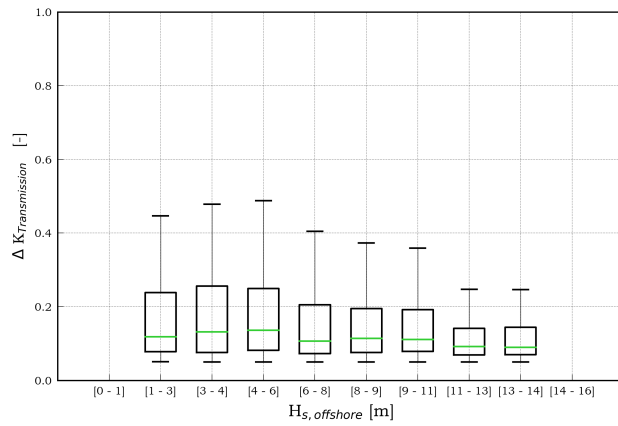


Figure D.5: Effect of offshore significant wave height on wave transmission reduction by salt marshes

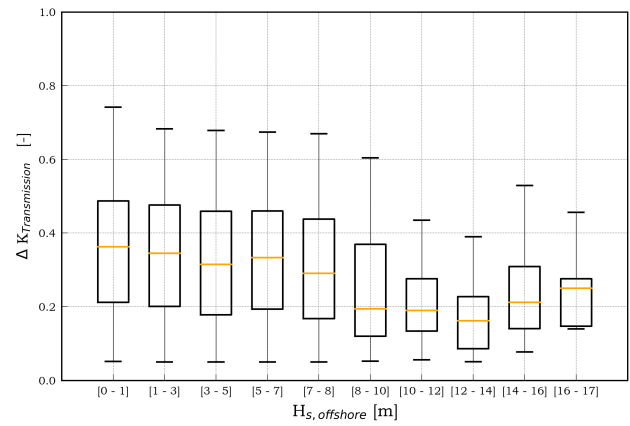


Figure D.6: Effect of offshore significant wave height on wave transmission reduction by mangroves

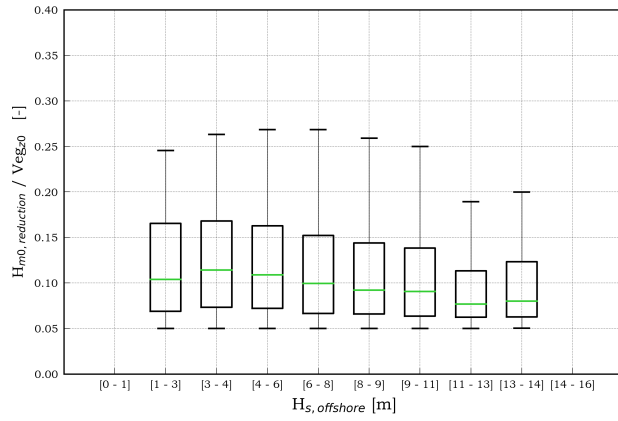


Figure D.7: Effect of offshore significant wave height on wave attenuation by salt marshes relative to depth in front of vegetated zone

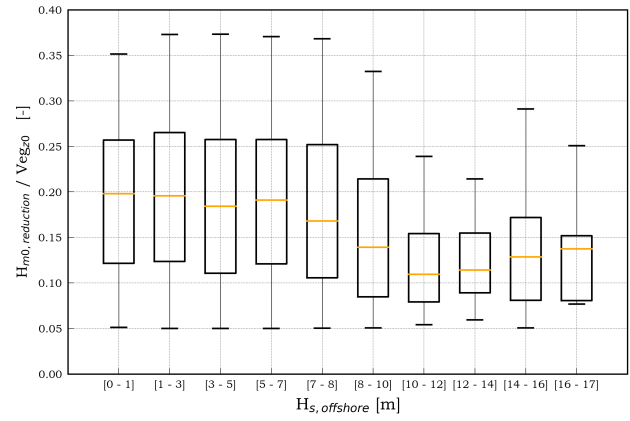


Figure D.8: Effect of offshore significant wave height on wave attenuation by mangroves relative to depth in front of vegetated zone

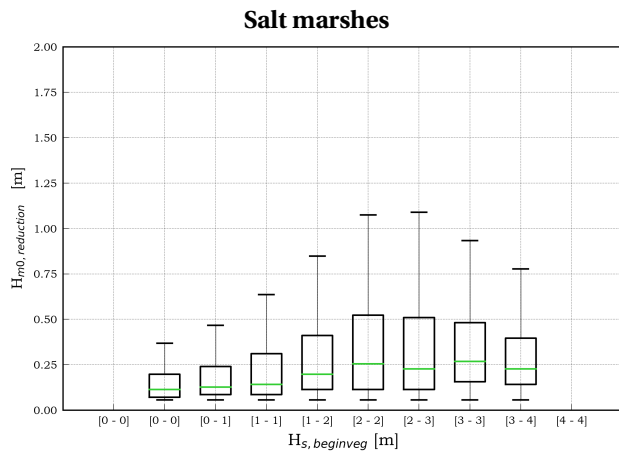


Figure D.9: Effect of significant wave height at begin of vegetated zone on wave attenuation in absolute terms by salt marshes

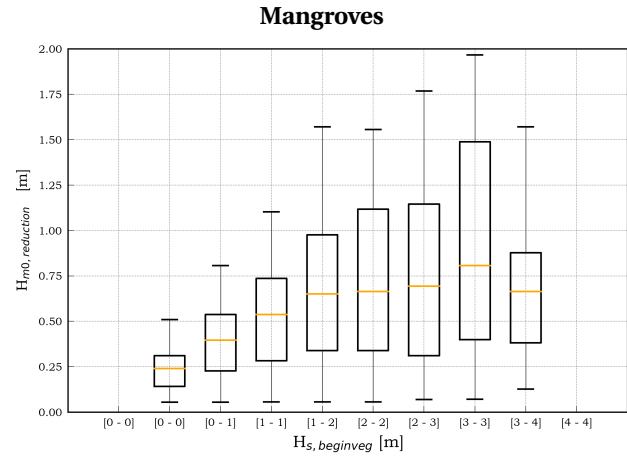


Figure D.10: Effect of significant wave height at begin of vegetated zone on wave attenuation in absolute terms by mangroves

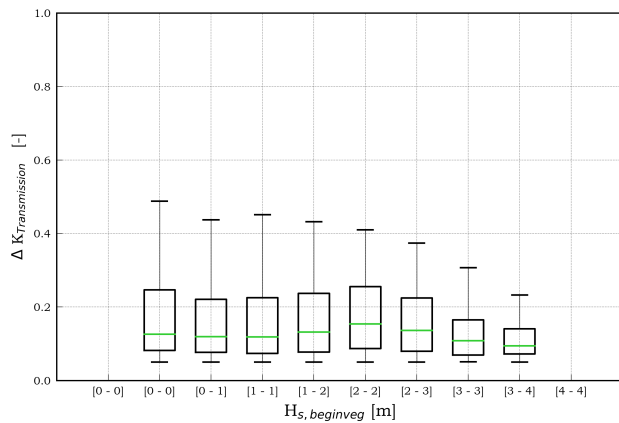


Figure D.11: Effect of significant wave height at begin of vegetated zone on wave transmission reduction by salt marshes

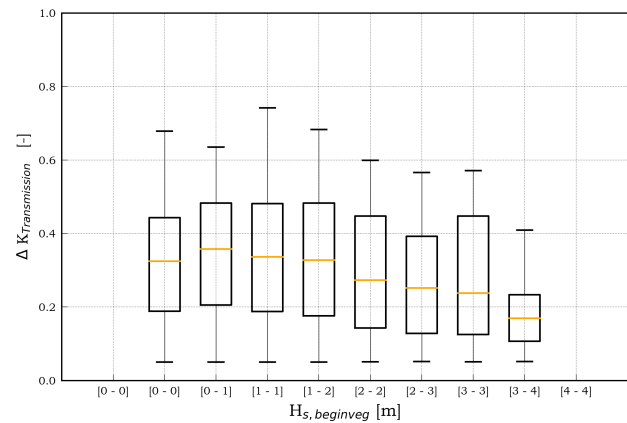


Figure D.12: Effect of significant wave height at begin of vegetated zone on wave transmission reduction by mangroves

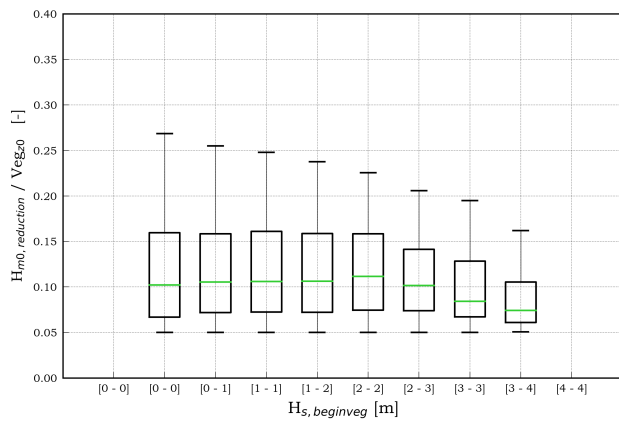


Figure D.13: Effect of significant wave height at begin of vegetated zone on wave attenuation by salt marshes relative to depth in front of vegetated zone

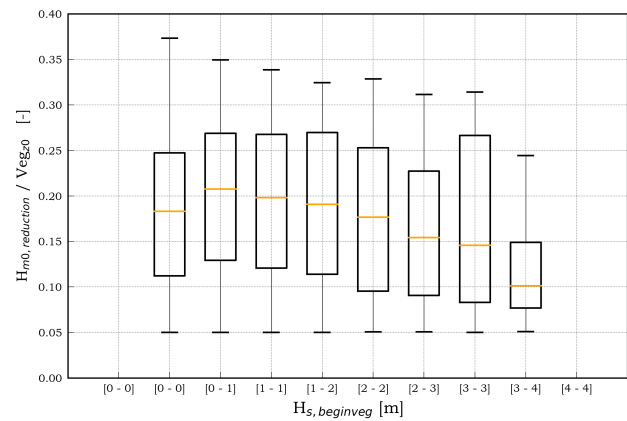


Figure D.14: Effect of significant wave height at begin of vegetated zone on wave attenuation by mangroves relative to depth in front of vegetated zone

## Offshore wave period

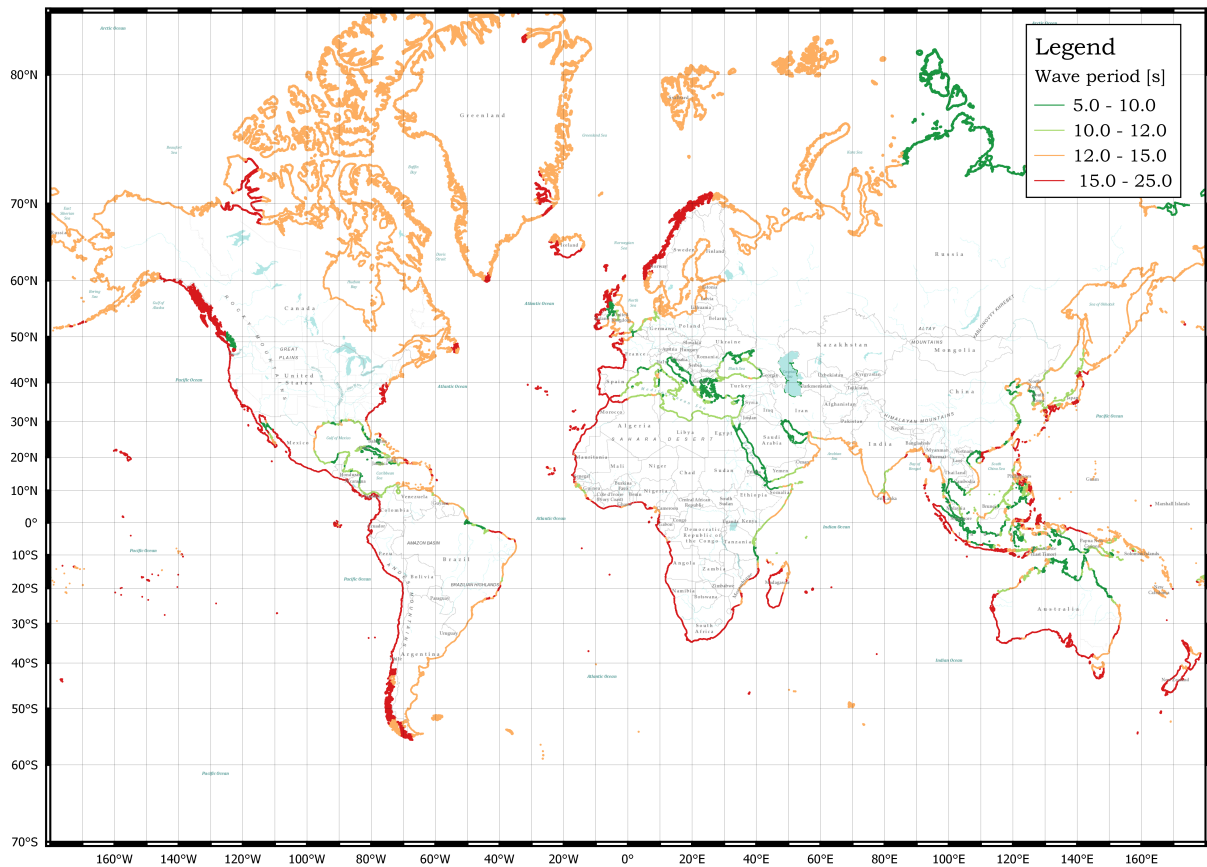


Figure D.15: Global spatial distribution of wave periods for a return period of 100 years

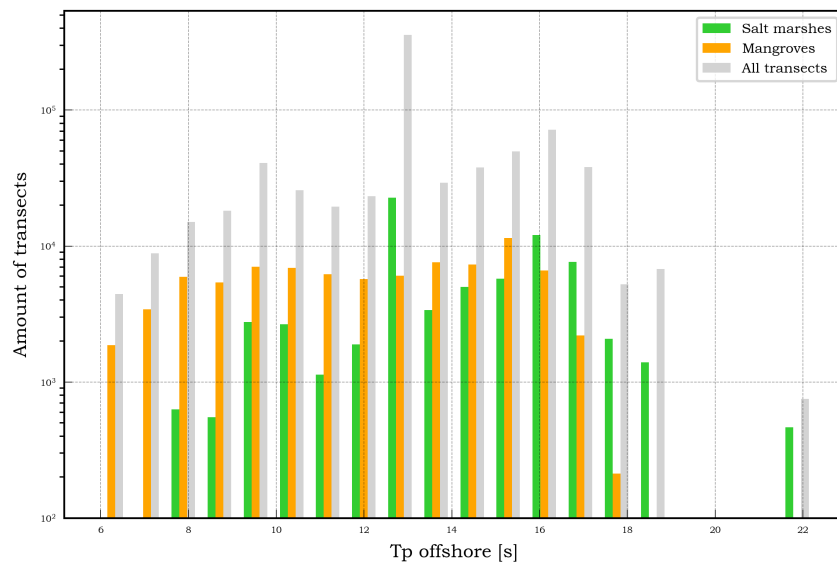


Figure D.16: Variation of offshore wave period amongst vegetated transects in relation to all transects

## Extreme water level

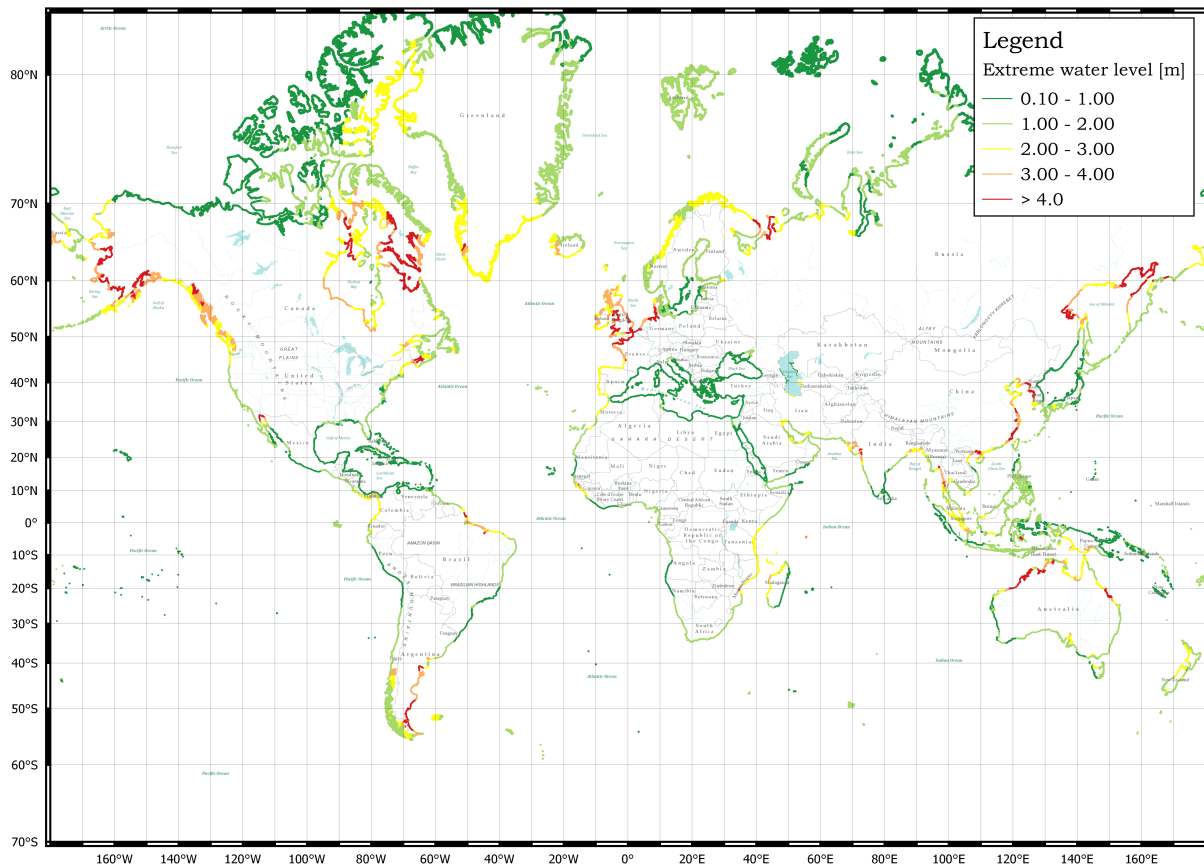


Figure D.17: World map of extreme water levels derived from GTSM for return period of 100 years

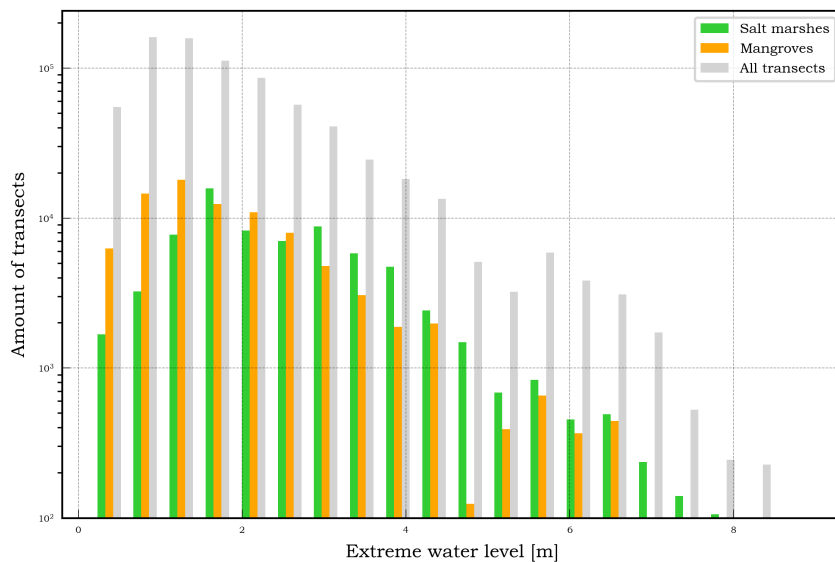


Figure D.18: Variation of offshore wave height amongst vegetated transects in relation to all transects

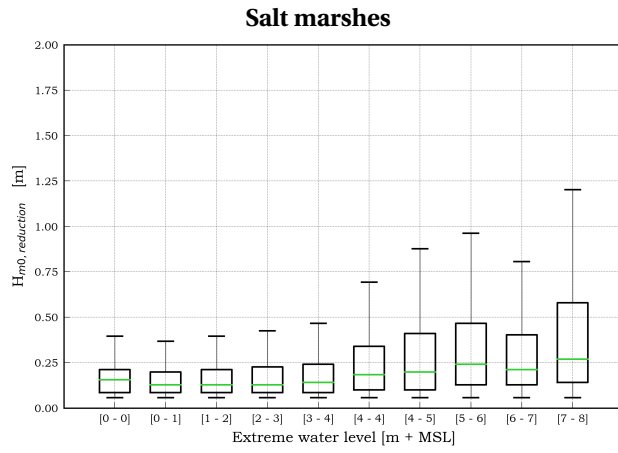


Figure D.19: Effect of water level on wave attenuation in absolute terms by salt marshes

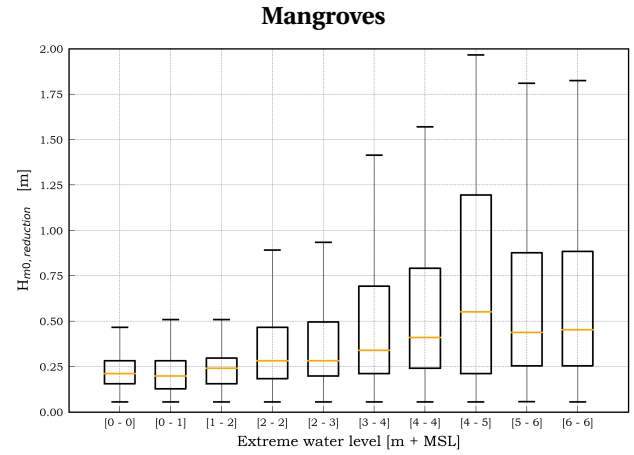


Figure D.20: Effect of water level on wave attenuation in absolute terms by mangroves

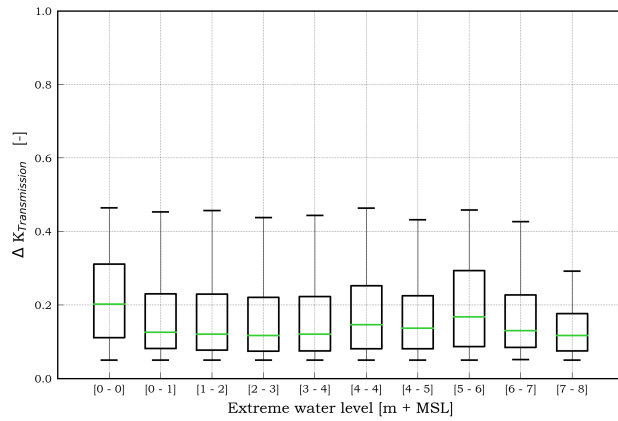


Figure D.21: Effect of water level on wave attenuation by salt marshes relative to incoming wave height

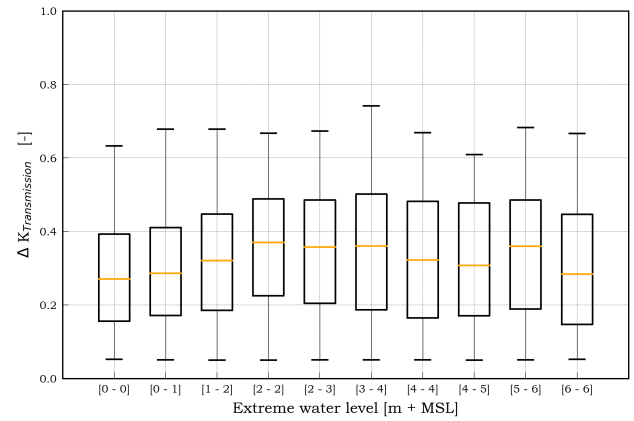


Figure D.22: Effect of water level on wave attenuation by mangroves relative to incoming wave height

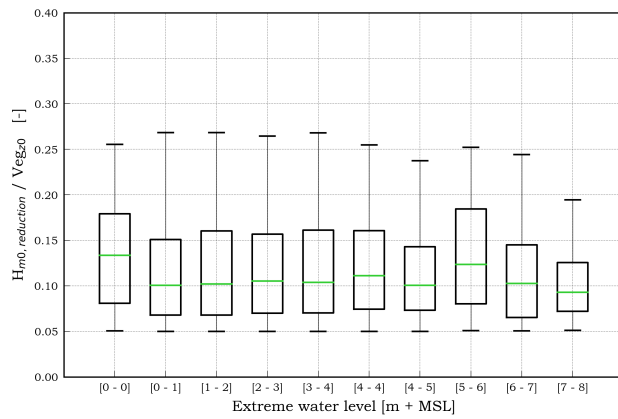


Figure D.23: Effect of water level on wave attenuation by salt marshes relative to depth in front of vegetated zone

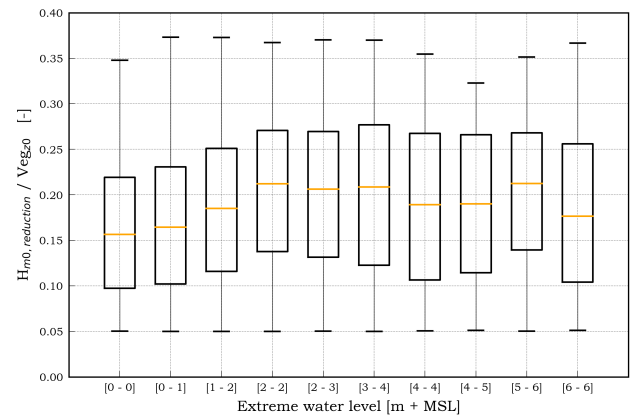


Figure D.24: Effect of water level on wave attenuation by mangroves relative to depth in front of vegetated zone

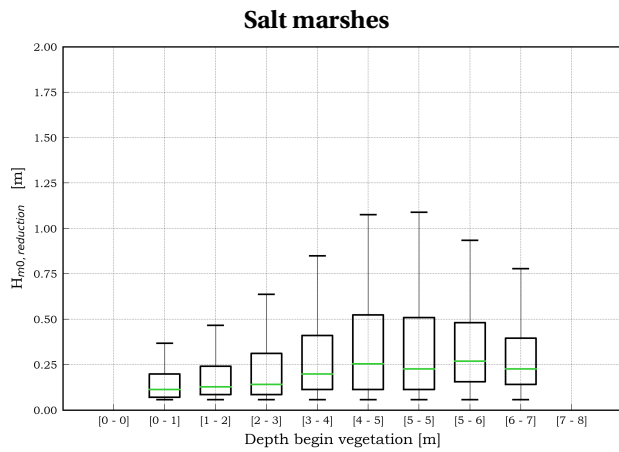


Figure D.25: Effect of water depth in front of vegetated zone on wave attenuation in absolute terms by salt marshes

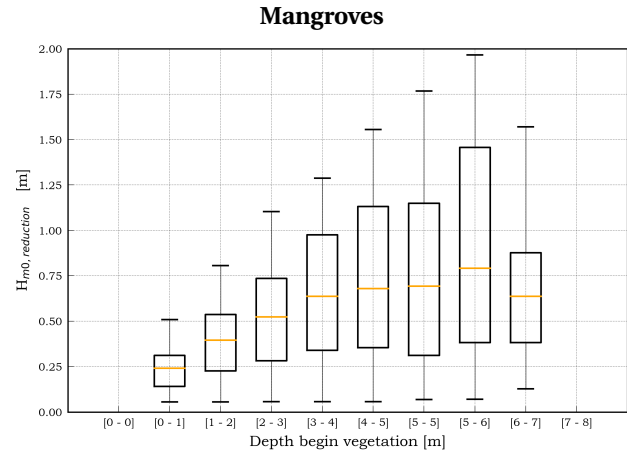


Figure D.26: Effect of water depth in front of vegetated zone on wave attenuation in absolute terms by mangroves

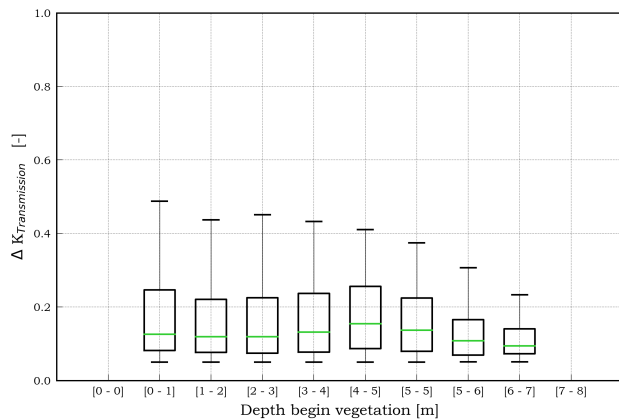


Figure D.27: Effect of water depth in front of vegetated zone on wave attenuation by salt marshes relative to incoming wave height

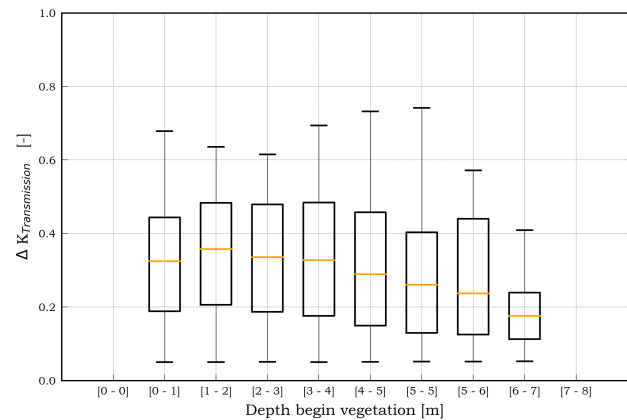


Figure D.28: Effect of water depth in front of vegetated zone on wave attenuation by mangroves relative to incoming wave height

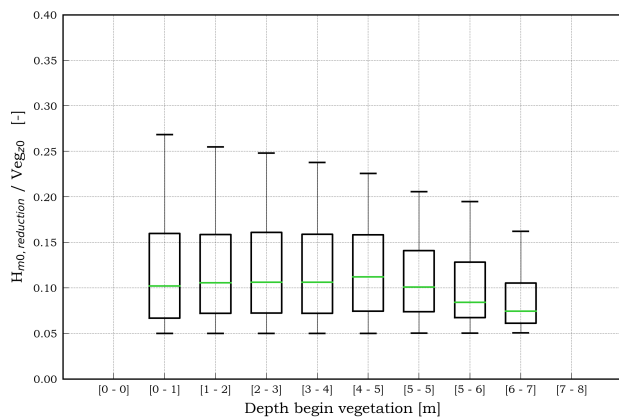


Figure D.29: Effect of water depth in front of vegetated zone on wave attenuation by salt marshes relative to depth in front of vegetated zone

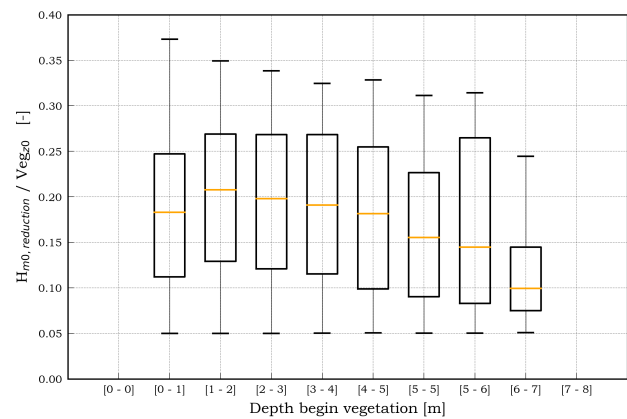


Figure D.30: Effect of water depth in front of vegetated zone on wave attenuation by mangroves relative to depth in front of vegetated zone

D.2. Vegetation width

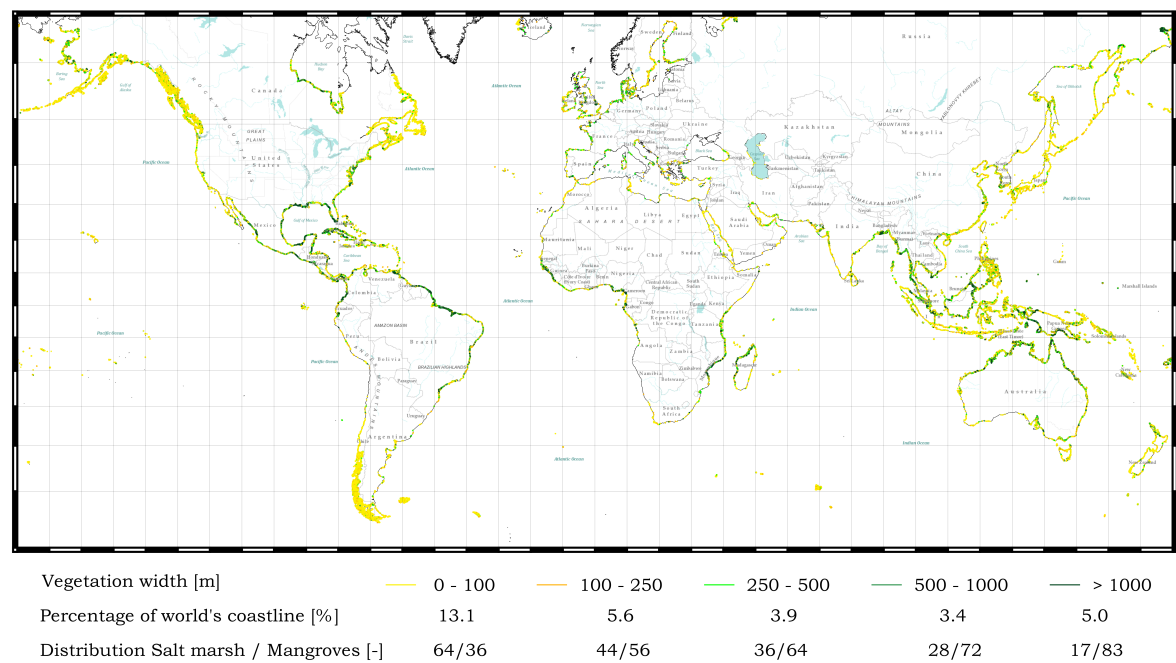


Figure D.31: Global spatial distribution of vegetation width

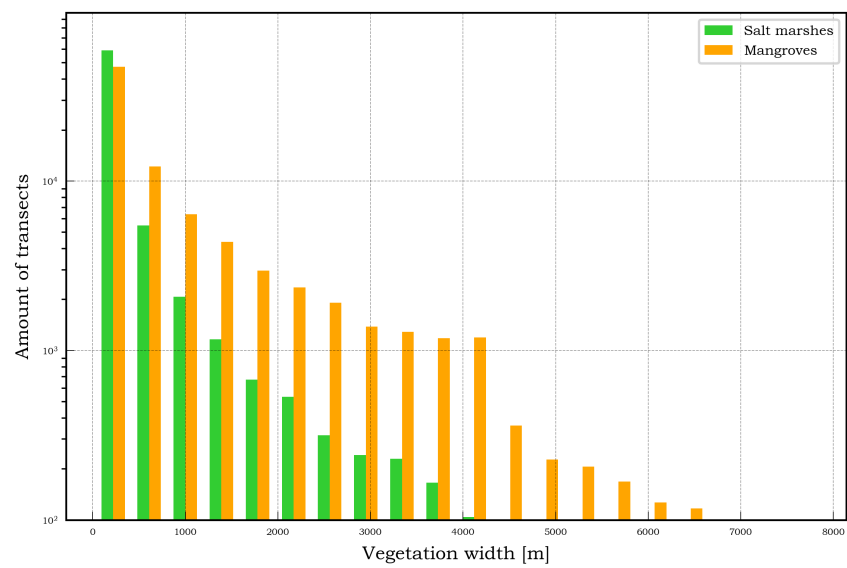


Figure D.32: Variation of vegetation width amongst vegetated transects



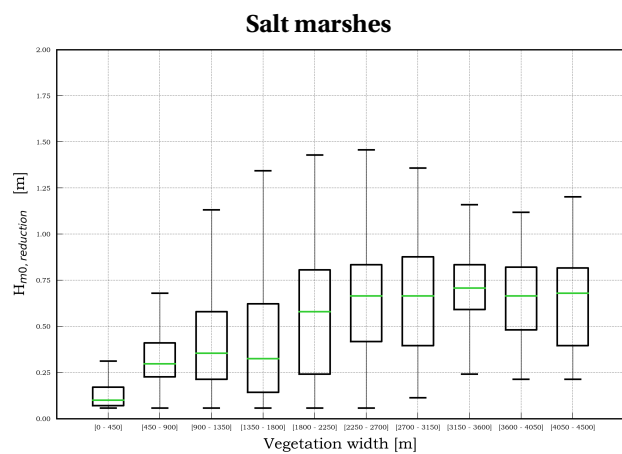


Figure D.33: Effect of vegetation width on wave attenuation in absolute terms by salt marshes

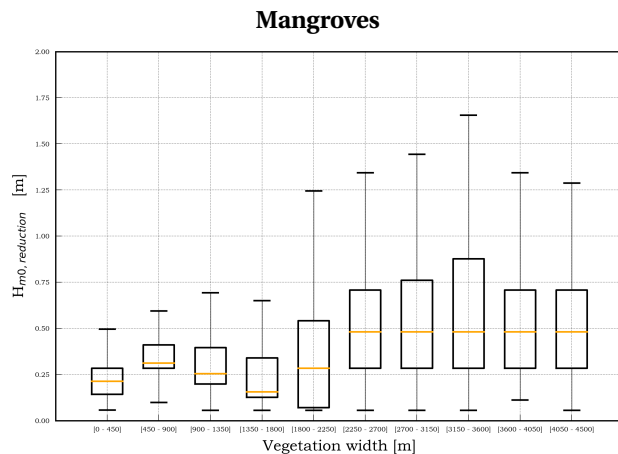


Figure D.34: Effect of vegetation width on wave attenuation in absolute terms by mangroves

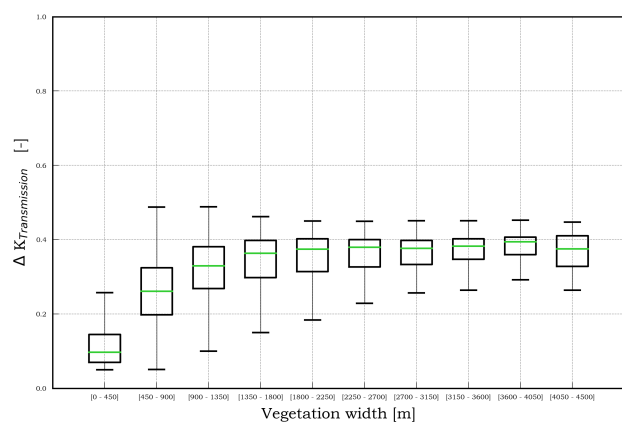


Figure D.35: Effect of vegetation width on wave attenuation by salt marshes relative to incoming wave height

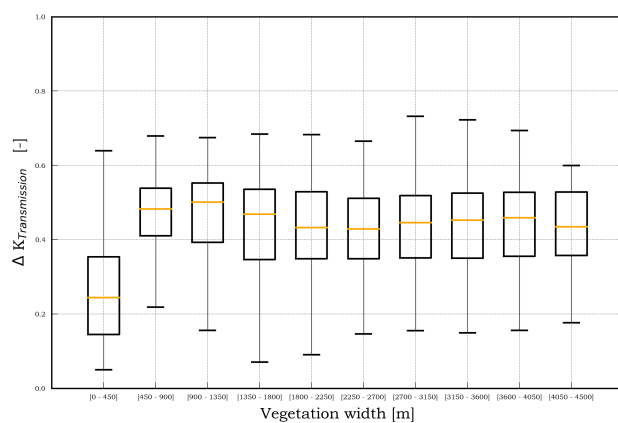


Figure D.36: Effect of vegetation width on wave attenuation by mangroves relative to incoming wave height

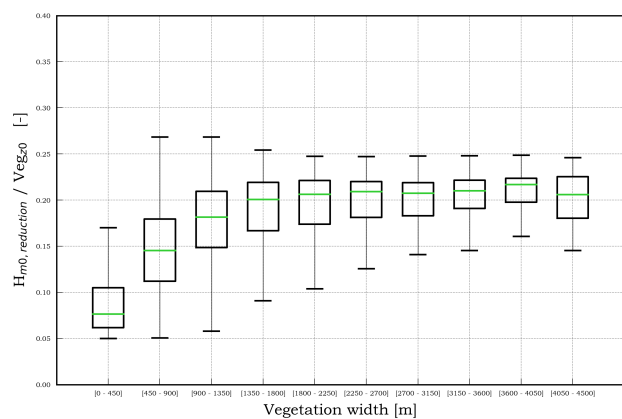


Figure D.37: Effect of vegetation width on wave attenuation by salt marshes relative to depth in front of vegetated zone

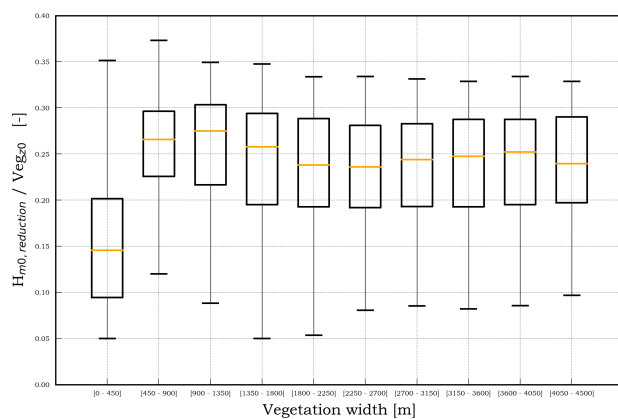


Figure D.38: Effect of vegetation width on wave attenuation by mangroves relative to depth in front of vegetated zone

## Wave attenuation in exposed and sheltered wave environment

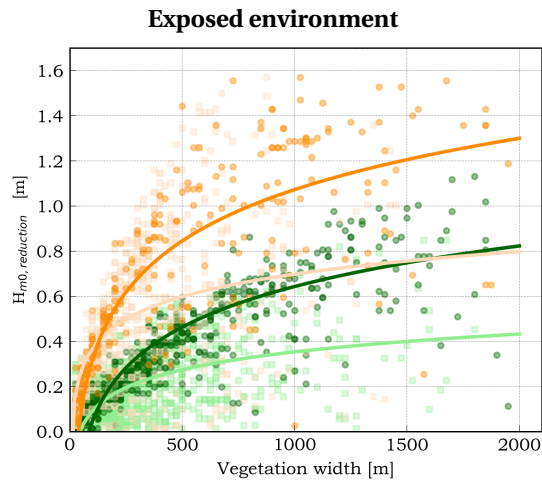


Figure D.39: Wave reduction over vegetated field in exposed environment

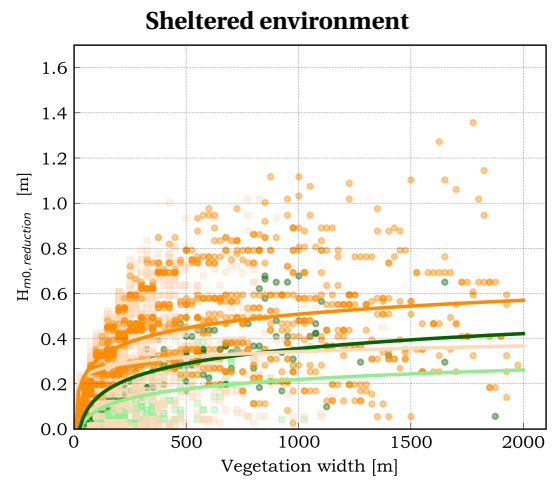


Figure D.40: Wave reduction over vegetated field in sheltered environment

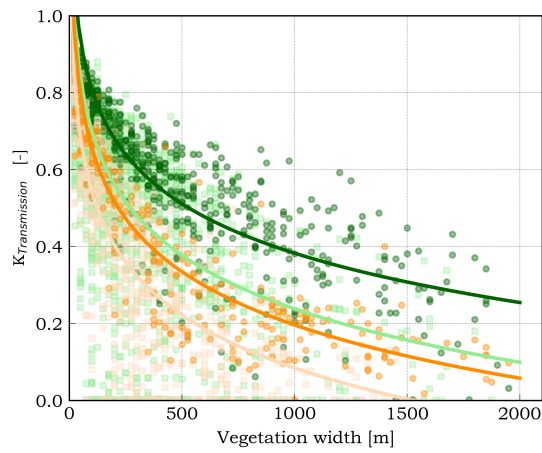


Figure D.41: Wave transmission over vegetated field in exposed environment

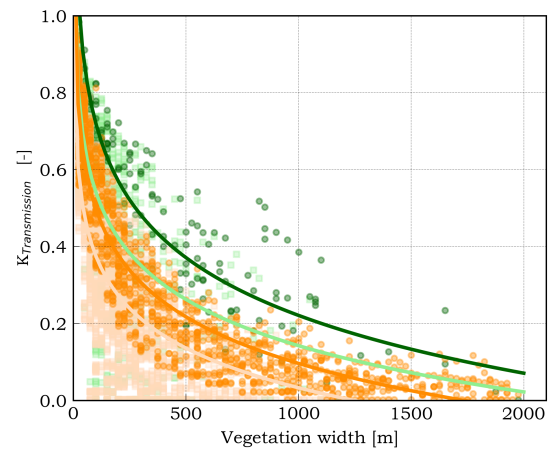


Figure D.42: Wave transmission over vegetated field in sheltered environment

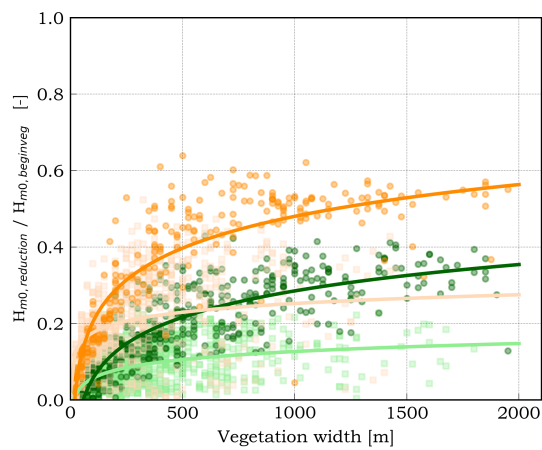


Figure D.43: Wave attenuation relative to incoming wave height in exposed environment

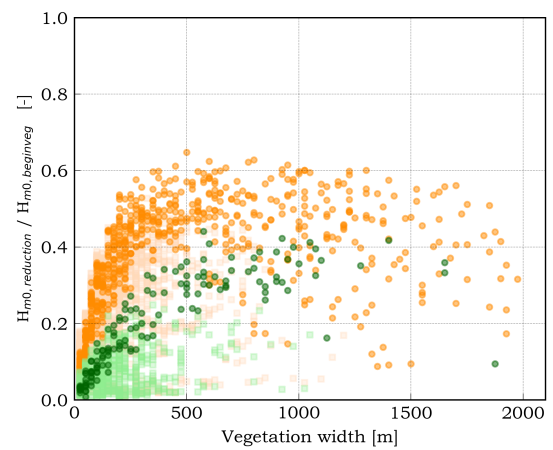
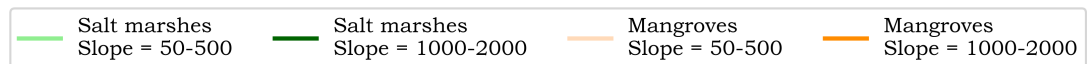


Figure D.44: Wave attenuation relative to incoming wave height in sheltered environment



### D.3. Foreshore slope

#### D.3.1. Foreshore slopes in global flood hazard assessment

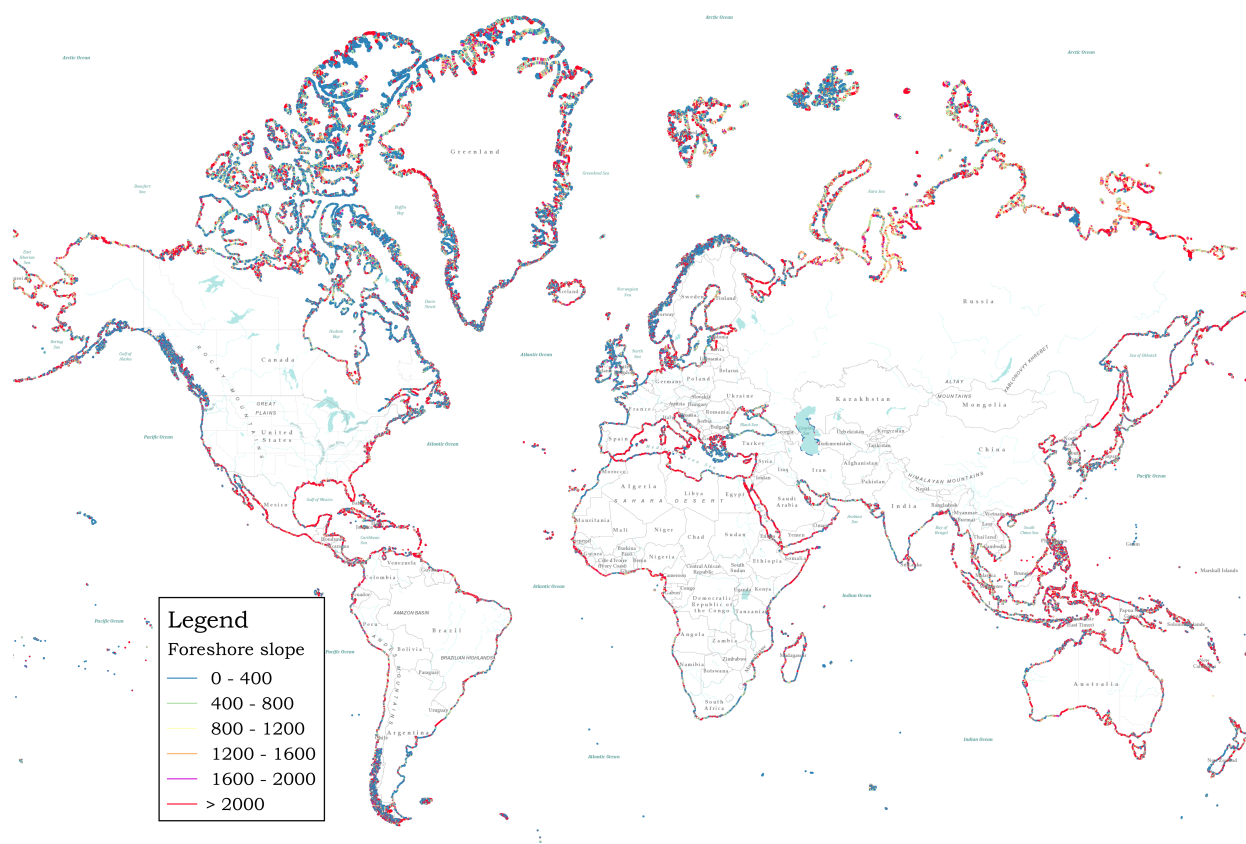


Figure D.45: Global spatial distribution of foreshore slopes

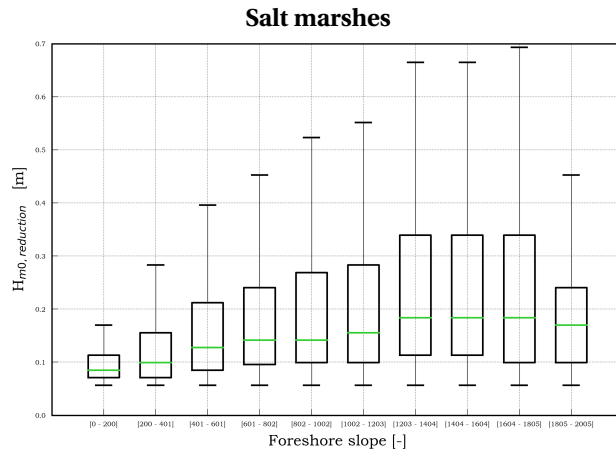


Figure D.46: Effect of foreshore slope on wave attenuation in absolute terms by salt marshes

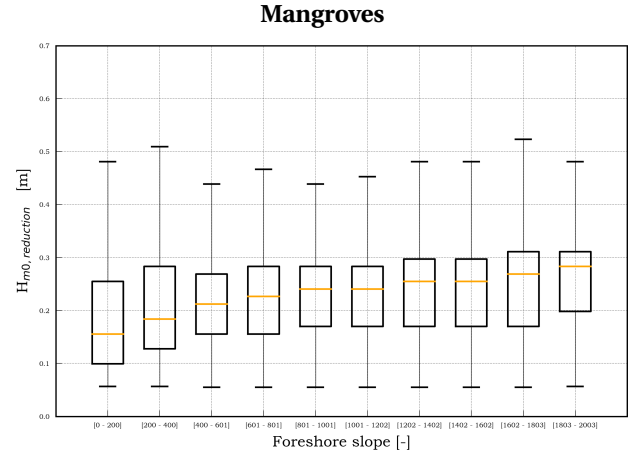


Figure D.47: Effect of foreshore slope on wave attenuation in absolute terms by mangroves

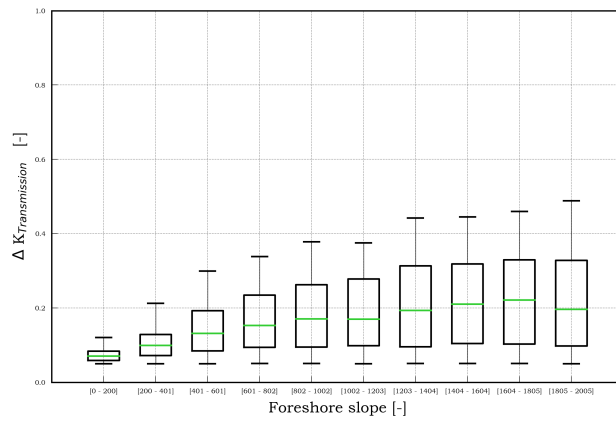


Figure D.48: Effect of foreshore slope on wave attenuation by salt marshes relative to incoming wave height

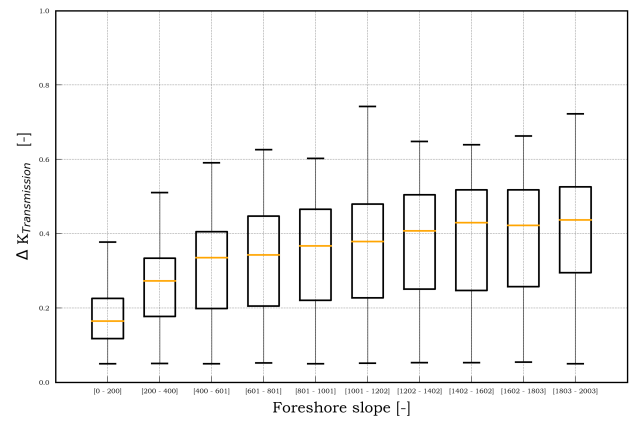


Figure D.49: Effect of foreshore slope on wave attenuation by mangroves relative to incoming wave height

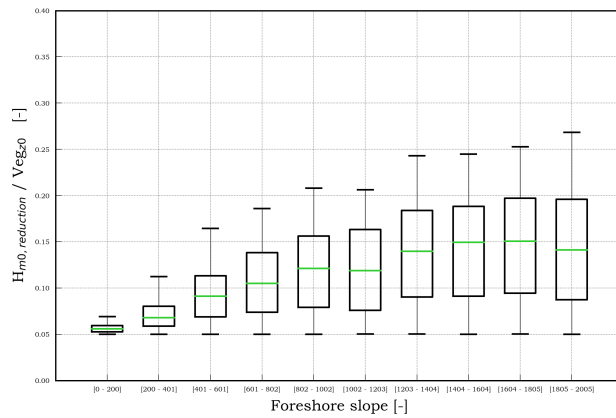


Figure D.50: Effect of foreshore slope on wave attenuation by salt marshes relative to depth in front of vegetated zone

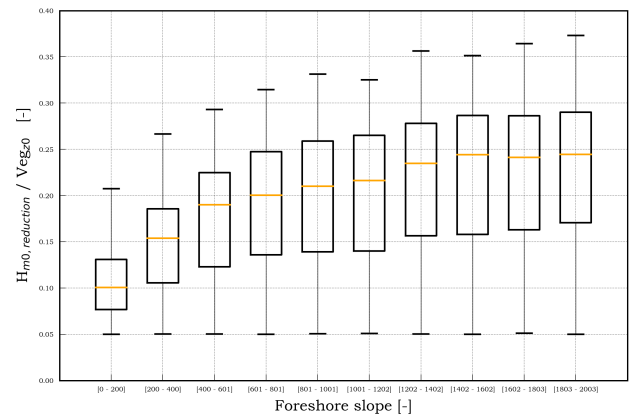


Figure D.51: Effect of foreshore slope on wave attenuation by mangroves relative to depth in front of vegetated zone

### D.3.2. Foreshore slopes in Mediterranean sea

The results of the global assessment showed a large quantity of transects derived using foreshore method 1 with a foreshore slope of 1:2000 and a large foreshore width. This unexpected result was further studied. The occurrence of the mild slopes is partly explained by the lacking performance of the GIE set in areas with a small tidal range. In these areas speckle noise is present, which indicates open sea as intertidal zone. The GIE threshold should remove this noise from the set, but the threshold of 0.10 m used in the global assessment was not sufficient. Simulations for the Mediterranean sea are performed with different threshold to study this phenomenon. The use of a higher threshold gives a shift towards the use of foreshore method 2, see figure D.56.

In figure D.52 an example transect is presented. The profile determined in the global run is shown in figure D.53. This profile is not correct derived, due to noise in the GIE as mentioned earlier. In figure D.54 the profile with an increased threshold of 0.25 m is presented. This transect has multiple crossings with the surge level with a return period of 2 years, which results in multiple patches. In this case is the profile not correct derived, because it should not be based on the last patch.



Figure D.52: Overview example transect in the Mediterranean Sea

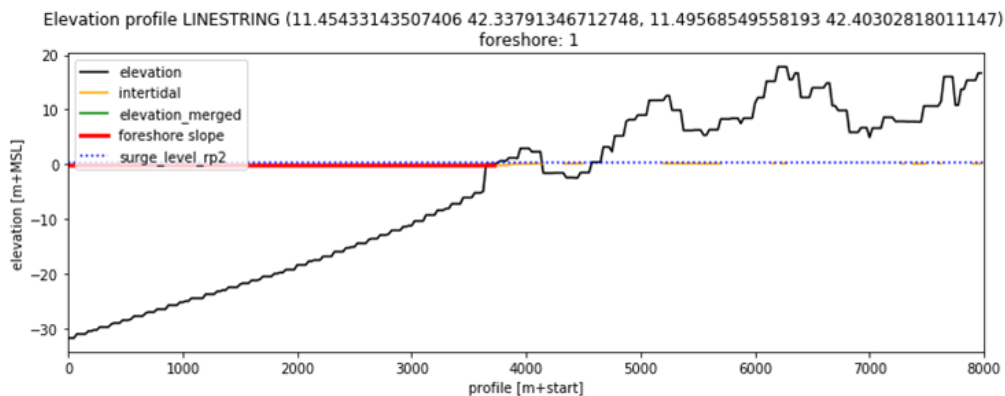


Figure D.53: Derived profile of example transect using GIE threshold of 10 centimeters

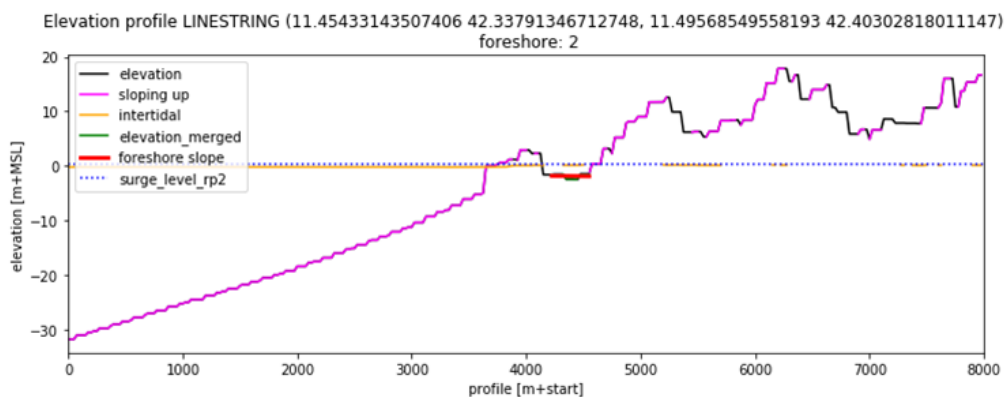


Figure D.54: Derived profile of example transect using GIE threshold of 25 centimeters

The absence of an intersection with the surge level for a return period of 2 years or having multiple intersection also contributes to the high amount of mild slopes. After performing the global assessment an adaption of the algorithm is tested which recognizes these situations and uses the highest point in case of no intersection, or the first intersection in case of multiple intersection. This method is referred to as the accumax function, because it uses the accumulated elevation over the profile. In figure D.55 the resulting profile with derived with implementation of the accumax function is shown.

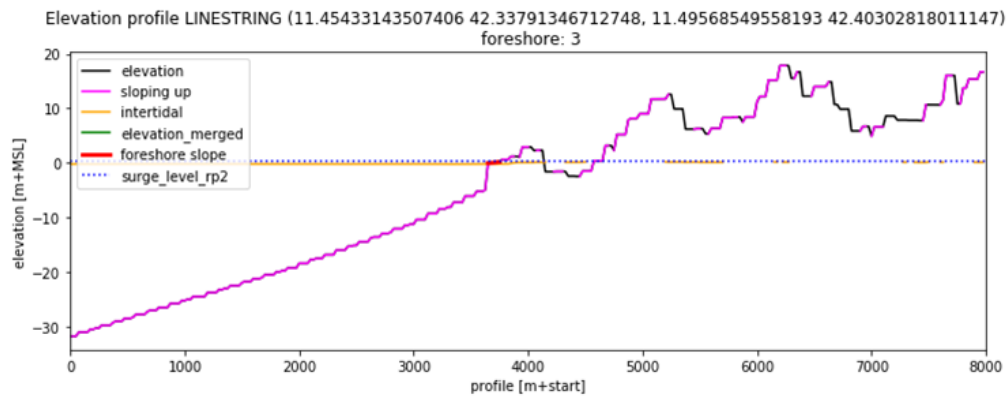


Figure D.55: Derived profile of example transect using GIE threshold of 25 centimeters and accumax function

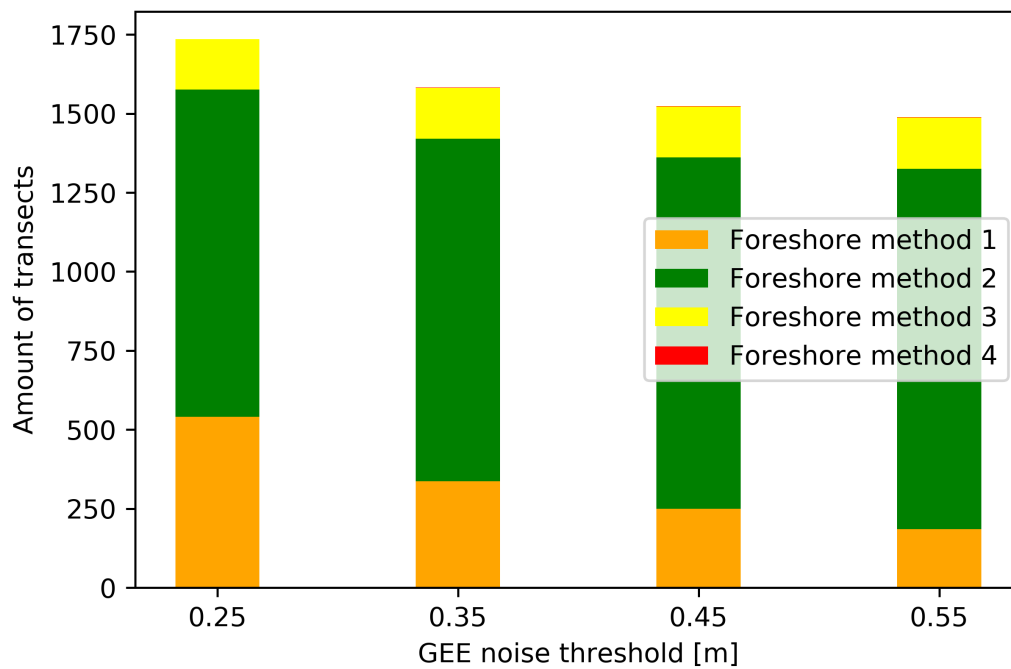


Figure D.56: Distribution of transects among foreshore determination methods for different GIE thresholds

## D.4. Wave attenuation

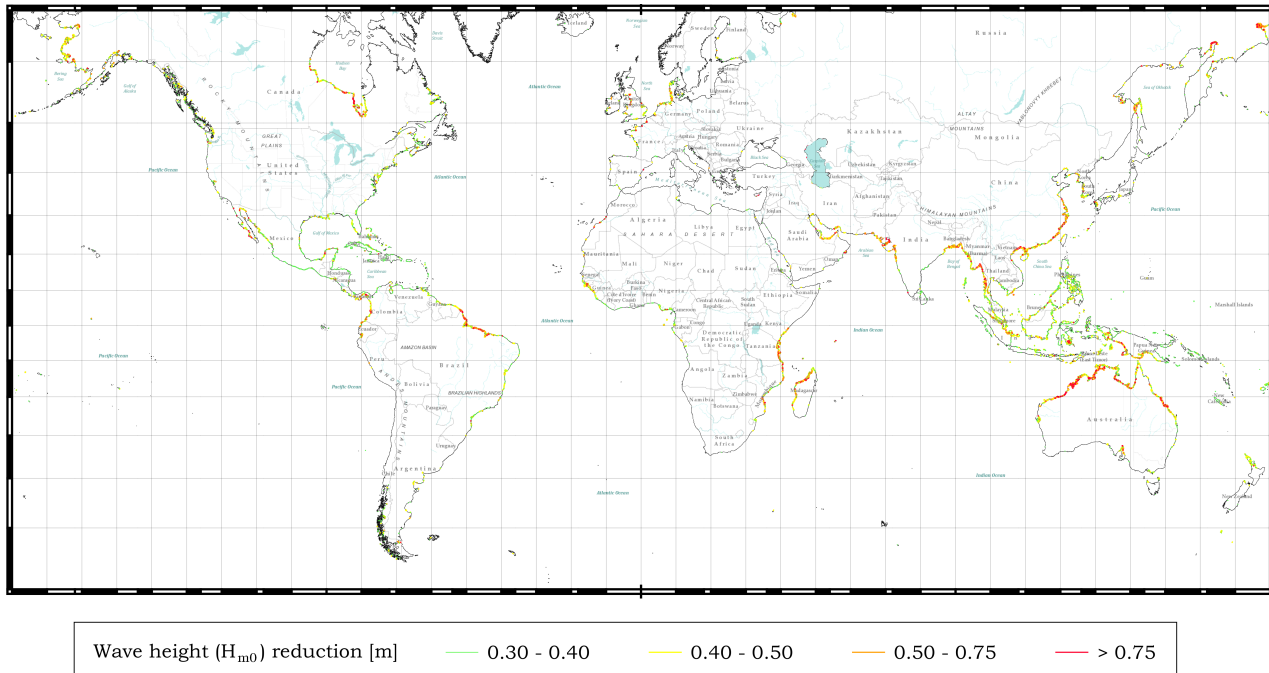


Figure D.57: Global potential of wave damping by foreshore vegetation for a return period of 100 years

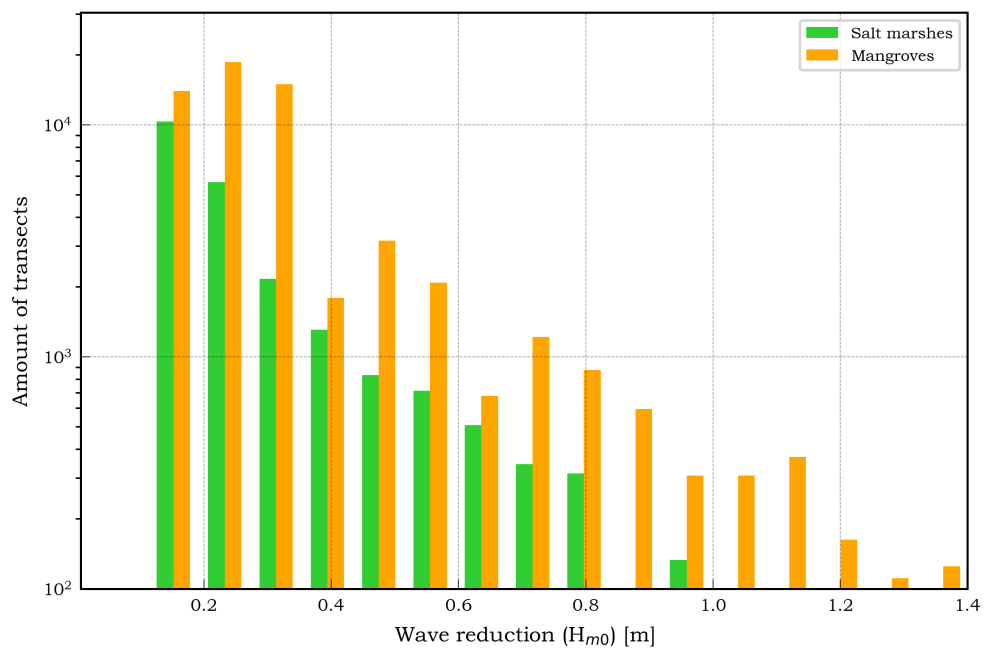


Figure D.58: Variation of wave attenuation amongst vegetated transects

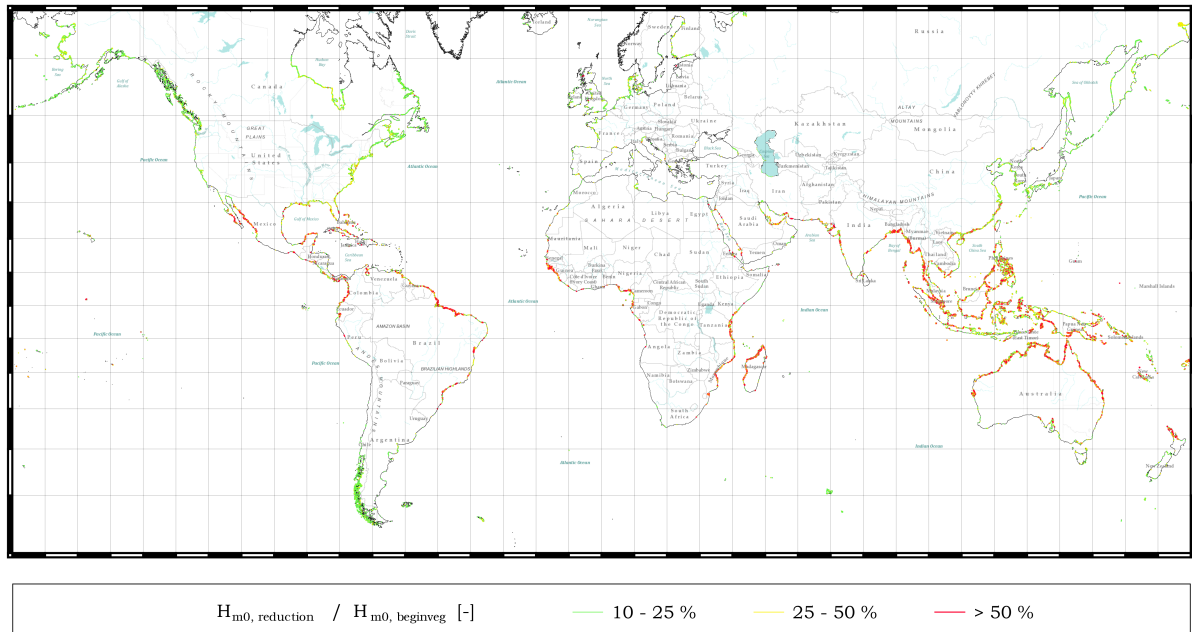


Figure D.59: Global potential of wave damping in relative terms by foreshore vegetation for a return period of 100 years



## D.5. Crest height reduction

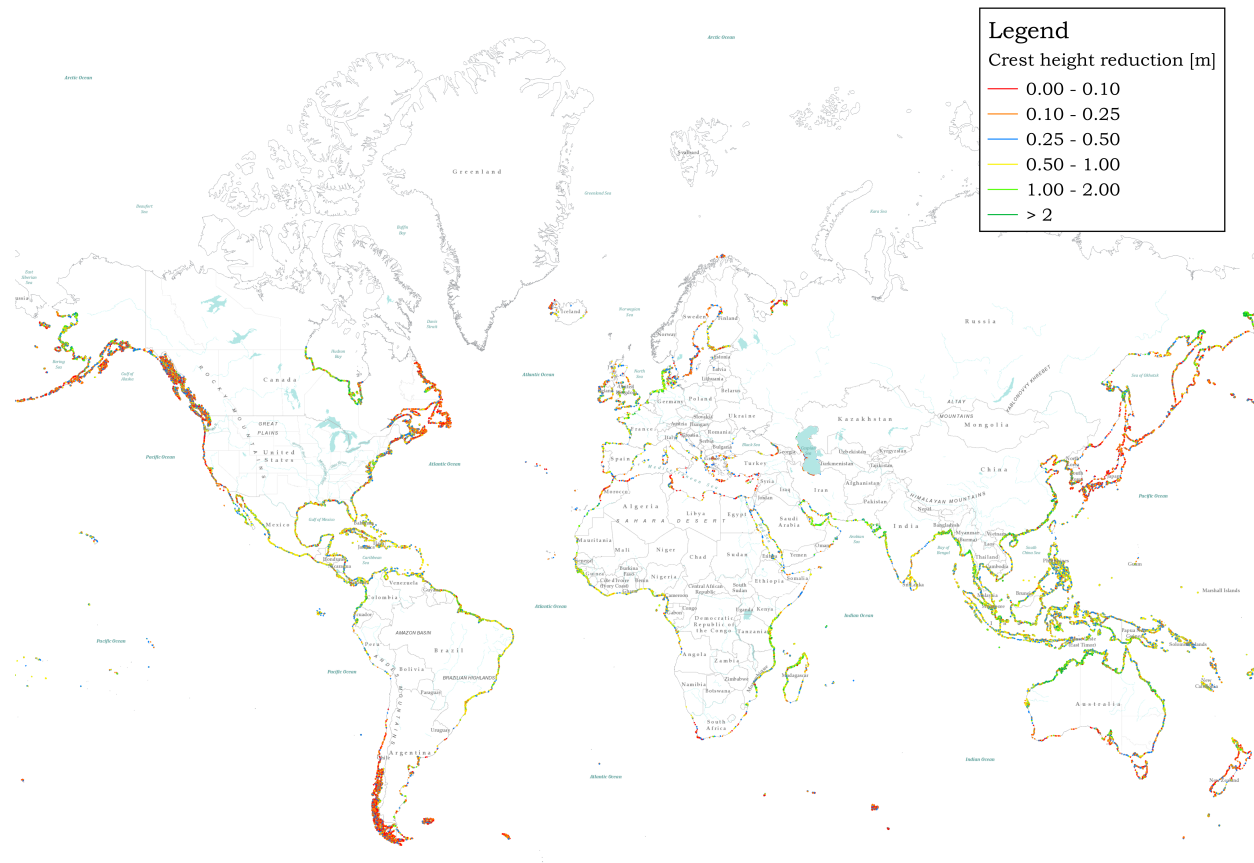


Figure D.60: Global potential of crest height reduction by foreshore vegetation for a return period of 100 years

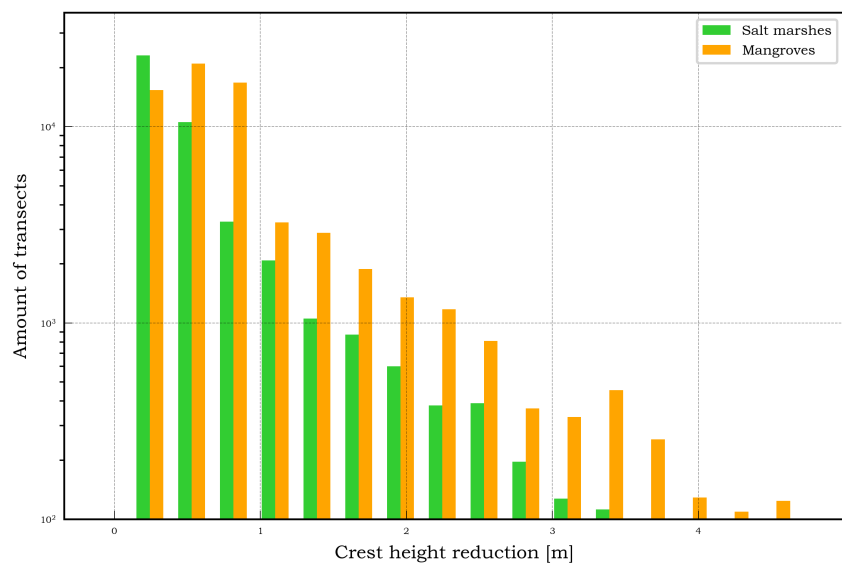


Figure D.61: Variation of crest height reduction amongst vegetated transects

## D.6. Crest height reduction results per country

In this section is first described how the crest height reduction indicators per country are calculated. Next, an overview of the results per country are presented in alphabetic order.

Dike height reduction per country is calculated according equation D.1. Only transects with wave attenuation results larger than 10 centimeters are taken into account.

$$\text{Sum of dike height reduction per country} = \sum_{i=1}^n \Delta R_{c,i} \quad (\text{D.1})$$

with  $n$  = number of transects in country with  $\Delta H_{m0} > 10\text{cm}$

The coastline length per country (CL1) is given by the sum of transects per country, because the the distance between transects is roughly 1 kilometer. The effective coastline length (CL2) is calculated by the sum of transects along wave attenuation exceeding 10 centimeters is observed.

Average unit costs per meter dike height per kilometer are based on research of [Hillen et al. \(2010\)](#). The values for rural areas are used and are corrected for inflation and expressed in USA dollars.

The Netherlands:	10.5	million USA \$ m/km
Viet Nam:	2.2	million USA \$ m/km

Based on these unit prices four unit prices are derived, each corresponding to a class of the human development index.

Very high HDI:	10.5	million USA \$ m/km
High HDI:	5.0	million USA \$ m/km
Medium HDI:	2.2	million USA \$ m/km
Low HDI:	1.0	million USA \$ m/km

Dike cost reduction per country is calculated by:

$$\text{Dike cost reduction} = \text{Sum of dike height reduction per country} \times \text{Unit price} \quad (\text{D.2})$$

# Afghanistan



# Chile

Country name	Human Development Index	Gross Domestic Product (GDP)	
	[·]	[USA Dollars]	
Afghanistan	Low development	\$	19,469,022,208
Aland Islands	Not published		Not published
Albania	High development	\$	11,863,865,978
Algeria	High development	\$	159,049,096,745
American Samoa	High development	\$	658,000,000
Andorra	Very high development	\$	2,858,517,699
Angola	Low development	\$	95,335,111,741
Anguilla	Not published		Not published
Antarctica	Not published		Not published
Antigua and Barbuda	High development	\$	1,460,144,704
Argentina	Very high development	\$	545,476,103,427
Armenia	High development	\$	10,572,298,342
Aruba	Not published		Not published
Australia	Very high development	\$	1,204,616,439,828
Austria	Very high development	\$	390,799,991,147
Azerbaijan	High development	\$	37,847,715,736
Bahamas	High development	\$	11,240,000,000
Bahrain	Very high development	\$	32,179,069,149
Bangladesh	Medium development	\$	221,415,162,446
Barbados	High development	\$	4,529,050,000
Belarus	High development	\$	47,407,217,531
Belgium	Very high development	\$	467,955,709,818
Belize	High development	\$	1,741,100,000
Benin	Low development	\$	8,583,031,398
Bermuda	Not published		Not published
Bhutan	Medium development	\$	2,212,638,830
Bolivia	Medium development	\$	33,806,395,514
Bosnia and Herzegovina	High development	\$	16,910,277,134
Botswana	Medium development	\$	15,581,137,274
Bouvet Island	Not published		Not published
Brazil	High development	\$	1,796,186,586,414
British Indian Ocean Territory	Not published		Not published
British Virgin Islands	Not published		Not published
Brunei Darussalam	Very high development	\$	11,400,653,732
Bulgaria	High development	\$	53,237,882,473
Burkina Faso	Low development	\$	11,693,235,542
Burma	Medium development	\$	63,225,097,051
Burundi	Low development	\$	3,007,029,030
Cambodia	Medium development	\$	20,016,747,754
Cameroon	Low development	\$	32,217,497,470
Canada	Very high development	\$	1,535,767,736,946
Cape Verde	Medium development		Not published
Cayman Islands	Not published		Not published
Central African Republic	Low development	\$	1,756,124,677
Chad	Low development	\$	9,600,761,474
Chile	Very high development	\$	247,027,912,574

Figure D.62: Human development index and GDP Afghanistan - Chile

Country name	Sum dike height reduction	Total coastline length (CL1) *	Vegetated coastline length (CL2)**
	[m]	[km]	[km]
Afghanistan	0	0	0
Aland Islands	1	262	2
Albania	21	281	32
Algeria	1	954	2
American Samoa	0	50	0
Andorra	0	0	0
Angola	44	1226	74
Anguilla	0	25	0
Antarctica	0	0	0
Antigua and Barbuda	15	97	21
Argentina	257	3835	271
Armenia	0	0	0
Aruba	4	45	7
Australia	10449	23596	8353
Austria	0	0	0
Azerbaijan	12	191	22
Bahamas	362	1891	548
Bahrain	6	105	9
Bangladesh	681	1995	577
Barbados	1	60	2
Belarus	0	0	0
Belgium	0	67	0
Belize	91	312	150
Benin	29	74	42
Bermuda	0	0	0
Bhutan	0	0	0
Bolivia	0	0	0
Bosnia and Herzegovina	0	20	0
Botswana	0	0	0
Bouvet Island	0	16	0
Brazil	2678	7963	2812
British Indian Ocean Territory	0	0	0
British Virgin Islands	3	43	5
Brunei Darussalam	24	117	39
Bulgaria	0	259	0
Burkina Faso	0	0	0
Burma	2352	3557	1911
Burundi	0	0	0
Cambodia	100	399	180
Cameroon	96	498	151
Canada	3614	60077	4348
Cape Verde	0	419	0
Cayman Islands	10	64	21
Central African Republic	0	0	0
Chad	0	0	0
Chile	559	28103	845

Figure D.63: Crest height reduction results Afghanistan - Chile

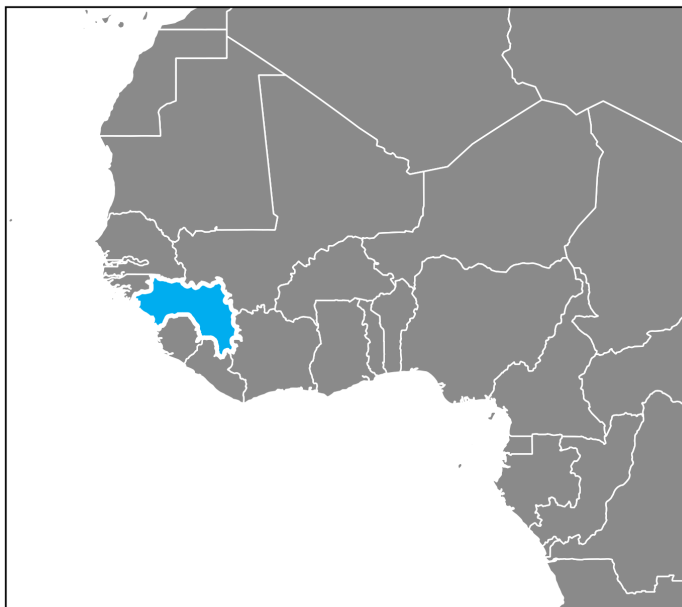
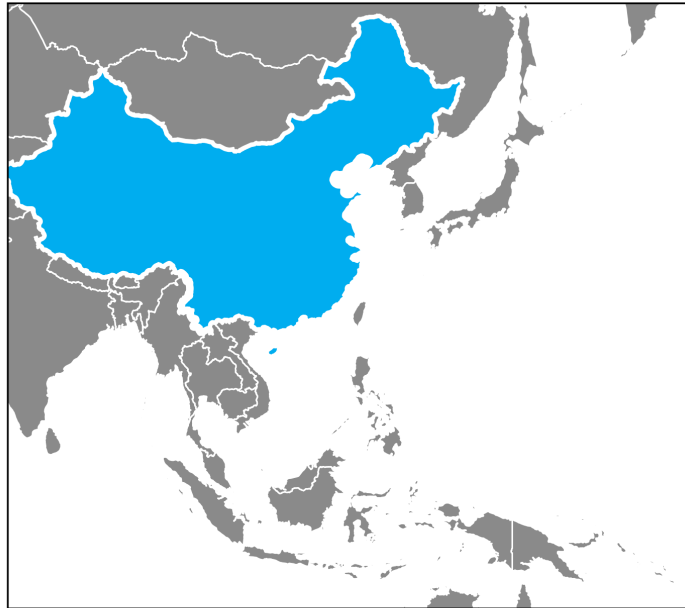
\* Approximated coastline length calculated by sum of transects per country

\*\* Coastline length along wave attenuation of at least 10 centimeters is observed

\*\*\* Dike costs reduction per country is calculated by multiplying the sum of dike height reduction per country with an unit dike price which depends on the human development index of the country

$\Delta R_c / CL1$	$\Delta R_c / CL2$	Dike costs reduction***		Dike costs reduction / GDP	
[m/km]	[m/km]	[millions USA Dollars]		[% of GDP]	
0.00	0.00	0.0		0.00	
0.00	0.51	1.0		GDP unknown	
0.07	0.64	102.8		0.87	
0.00	0.37	3.7		0.00	
0.00	0.00	0.0		0.00	
0.00	0.00	0.0		0.00	
0.04	0.60	44.1		0.05	
0.00	0.00	0.0		GDP unknown	
0.00	0.00	0.0		GDP unknown	
0.15	0.71	74.6		5.11	
0.07	0.95	2695.8		0.49	
0.00	0.00	0.0		0.00	
0.09	0.57	4.0		GDP unknown	
0.44	1.25	109710.4		9.11	
0.00	0.00	0.0		0.00	
0.07	0.57	62.2		0.16	
0.19	0.66	1811.1		16.11	
0.06	0.70	66.6		0.21	
0.34	1.18	1498.9		0.68	
0.02	0.64	6.4		0.14	
0.00	0.00	0.0		0.00	
0.00	0.00	0.0		0.00	
0.29	0.60	453.3		26.04	
0.39	0.69	28.9		0.34	
0.00	0.00	0.0		GDP unknown	
0.00	0.00	0.0		0.00	
0.00	0.00	0.0		0.00	
0.00	0.00	0.0		0.00	
0.00	0.00	0.0		0.00	
0.00	0.00	0.0		GDP unknown	
0.34	0.95	13391.7		0.75	
0.00	0.00	0.0		GDP unknown	
0.07	0.63	3.1		GDP unknown	
0.21	0.62	255.8		2.24	
0.00	0.00	0.0		0.00	
0.00	0.00	0.0		0.00	
0.66	1.23	5175.2		8.19	
0.00	0.00	0.0		0.00	
0.25	0.55	219.5		1.10	
0.19	0.64	96.3		0.30	
0.06	0.83	37950.8		2.47	
0.00	0.00	0.0		GDP unknown	
0.16	0.48	10.1		GDP unknown	
0.00	0.00	0.0		0.00	
0.00	0.00	0.0		0.00	
0.02	0.66	5869.3		2.38	

**China**



**Guinea**

Country name	Human Development Index	Gross Domestic Product (GDP)
	[·]	[USA Dollars]
China	High development	\$ 11,199,145,157,649
Christmas Island	Not published	Not published
Cocos (Keeling) Islands	Not published	Not published
Colombia	High development	\$ 282,462,551,367
Comoros	Low development	\$ 616,654,490
Congo	Medium development	\$ 8,553,154,580
Cook Islands	Not published	Not published
Costa Rica	High development	\$ 57,435,507,212
Cote d'Ivoire	Low development	\$ 36,372,613,023
Croatia	Very high development	\$ 50,714,957,391
Cuba	High development	Not published
Cyprus	Very high development	\$ 20,047,013,274
Czech Republic	Very high development	\$ 195,305,084,919
Democratic Republic of the Congo	Low development	\$ 37,917,704,900
Denmark	Very high development	\$ 306,899,653,410
Djibouti	Low development	Not published
Dominica	High development	\$ 581,484,032
Dominican Republic	High development	\$ 71,583,553,488
Ecuador	High development	\$ 98,613,972,000
Egypt	Medium development	\$ 332,698,041,031
El Salvador	Low development	\$ 26,797,470,000
Equatorial Guinea	Medium development	\$ 10,684,804,794
Eritrea	Medium development	Not published
Estonia	Very high development	\$ 23,337,907,619
Ethiopia	Medium development	\$ 72,374,224,249
Falkland Islands (Malvinas)	Not published	Not published
Faroe Islands	Not published	Not published
Fiji	High development	\$ 4,703,632,978
Finland	Very high development	\$ 238,677,672,282
France	Very high development	\$ 2,465,453,975,282
French Guiana	Low development	Not published
French Polynesia	Not published	Not published
French Southern and Antarctic Lands	Not published	Not published
Gabon	Medium development	\$ 14,213,558,130
Gambia	Low development	\$ 907,652,510
Georgia	High development	\$ 14,378,016,729
Germany	Very high development	\$ 3,477,796,274,497
Ghana	Medium development	\$ 42,689,783,734
Gibraltar	Not published	Not published
Greece	Very high development	\$ 192,690,813,127
Greenland	Not published	Not published
Grenada	High development	\$ 1,056,188,593
Guadeloupe	Not published	Not published
Guam	Not published	\$ 5,793,000,000
Guatemala	Medium development	\$ 68,763,255,964
Guernsey	Not published	Not published
Guinea	Low development	\$ 8,200,248,003

Figure D.64: Human development index and GDP

China - Guinea
























































































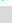
























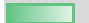
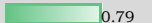










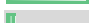
























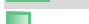














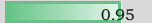













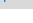













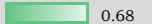





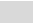






Country name	Sum dike height reduction	Total coastline length (CL1) *	Vegetated coastline length (CL2)**
	[m]	[km]	[km]
China	 2066	 7959	 1692
Christmas Island	4	13	3
Cocos (Keeling) Islands	0	0	0
Colombia	 520	 1617	 588
Comoros	3	228	7
Congo	 43	 125	 44
Cook Islands	2	53	3
Costa Rica	 183	 857	 231
Cote d'Ivoire	 46	 323	 66
Croatia	3	1744	7
Cuba	 841	 3261	 1493
Cyprus	 12	 474	 9
Czech Republic	0	0	0
Democratic Republic of the Congo	 22	 127	 31
Denmark	 315	 3709	 351
Djibouti	5	223	9
Dominica	0	83	0
Dominican Republic	 120	 882	 179
Ecuador	 400	 1760	 473
Egypt	 49	 2229	 87
El Salvador	 74	 243	 90
Equatorial Guinea	 37	 272	 58
Eritrea	 71	 938	 117
Estonia	3	1365	7
Ethiopia	0	0	0
Falkland Islands (Malvinas)	 24	 1941	 44
Faroe Islands	0	555	0
Fiji	 288	 1211	 486
Finland	 176	 2772	 258
France	 280	 3197	 295
French Guiana	 138	 294	 149
French Polynesia	 18	 543	 26
French Southern and Antarctic Lands	 25	 1247	 53
Gabon	 166	 845	 263
Gambia	 10	 59	 16
Georgia	 24	 243	 40
Germany	 238	 1901	 166
Ghana	 36	 365	 54
Gibraltar	0	2	0
Greece	 23	 6089	 47
Greenland	0	 14857	0
Grenada	4	68	6
Guadeloupe	 18	 203	 26
Guam	4	90	6
Guatemala	 78	 269	 130
Guernsey	0	28	0
Guinea	 278	 462	 296

Figure D.65: Crest height reduction results China - Guinea

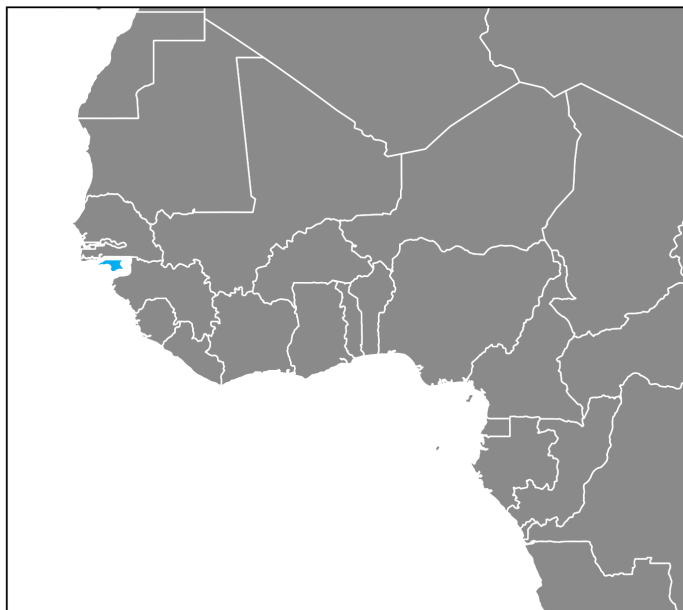
\* Approximated coastline length calculated by sum of transects per country

\*\* Coastline length along wave attenuation of at least 10 centimeters is observed

\*\*\* Dike costs reduction per country is calculated by multiplying the sum of dike height reduction per country with an unit dike price which depends on the human development index of the country

$\Delta R_c / CL1$		$\Delta R_c / CL2$		Dike costs reduction***	Dike costs reduction / GDP
[m/km]		[m/km]		[millions USA Dollars]	[% of GDP]
 0.26		 1.22		10332.4	0.09
 0.29		 1.27		3.8	GDP unknown
0.00		0.00		0.0	GDP unknown
 0.32		 0.88		2598.9	0.92
 0.01		 0.44		3.1	0.50
 0.35		 0.98		95.3	1.11
 0.03		 0.56		1.7	GDP unknown
 0.21		 0.79		917.5	1.60
 0.14		 0.69		45.8	0.13
 0.00		 0.46		33.9	0.07
 0.26		 0.56		4207.0	GDP unknown
 0.03		 1.38		130.2	0.65
0.00		0.00		0.0	0.00
 0.18		 0.72		22.4	0.06
 0.08		 0.90		3302.4	1.08
 0.02		 0.53		4.8	GDP unknown
0.00		0.00		0.0	0.00
 0.14		 0.67		598.0	0.84
 0.23		 0.84		1998.1	2.03
 0.02		 0.56		107.5	0.03
 0.30		 0.82		73.6	0.27
 0.14		 0.64		81.4	0.76
 0.08		 0.60		155.6	GDP unknown
 0.00		 0.49		36.3	0.16
0.00		0.00		0.0	0.00
 0.01		 0.53		23.5	GDP unknown
0.00		0.00		0.0	GDP unknown
 0.24		 0.59		1441.2	30.64
 0.06		 0.68		1851.7	0.78
 0.09		 0.95		2942.0	0.12
 0.47		 0.93		138.4	GDP unknown
 0.03		 0.71		18.5	GDP unknown
 0.02		 0.46		24.5	GDP unknown
 0.20		 0.63		365.0	2.57
 0.16		 0.60		9.6	1.06
 0.10		 0.59		118.6	0.82
 0.12		 1.43		2494.6	0.07
 0.10		 0.66		78.4	0.18
0.00		0.00		0.0	GDP unknown
 0.00		 0.49		241.7	0.13
0.00		0.00		0.0	GDP unknown
 0.06		 0.68		20.5	1.94
 0.09		 0.68		17.6	GDP unknown
 0.05		 0.70		4.2	0.07
 0.29		 0.60		172.1	0.25
0.00		0.00		0.0	GDP unknown
 0.60		 0.94		278.4	3.39

**Guinea-  
Bissau**



**Mexico**

Country name	Human Development Index	Gross Domestic Product (GDP)	
	[·]	[USA Dollars]	
Guinea-Bissau	Medium development	\$	1,164,944,510
Guyana	Medium development	\$	3,502,397,094
Haiti	Low development	\$	8,022,638,722
Heard Island and McDonald Islands	Not published		Not published
Holy See (Vatican City)	Not published		Not published
Honduras	Medium development	\$	21,516,938,910
Hong Kong	Very high development	\$	309,403,880,389
Hungary	Very high development	\$	125,816,640,421
Iceland	Very high development	\$	20,304,098,101
India	Medium development	\$	2,263,792,499,341
Indonesia	Medium development	\$	932,259,177,765
Iran (Islamic Republic of)	High development	\$	385,874,474,399
Iraq	Medium development	\$	171,489,001,692
Ireland	Very high development	\$	304,819,018,067
Isle of Man	Not published		Not published
Israel	Very high development	\$	317,744,784,695
Italy	Very high development	\$	1,859,383,610,249
Jamaica	High development	\$	14,056,908,749
Japan	Very high development	\$	4,949,273,341,994
Jersey	Not published		Not published
Jordan	High development	\$	38,654,727,746
Kazakhstan	High development	\$	137,278,320,084
Kenya	Medium development	\$	70,529,014,778
Kiribati	Medium development	\$	181,551,485
Korea	Low development		Not published
Korea	Very high development	\$	1,382,764,027,114
Kuwait	Very high development	\$	110,875,579,087
Kyrgyzstan	Medium development	\$	6,551,287,938
Lao People's Democratic Republic	Low development	\$	15,805,707,154
Latvia	Very high development	\$	27,572,698,482
Lebanon	High development	\$	49,598,825,982
Lesotho	Low development	\$	2,291,321,667
Liberia	Low development	\$	2,101,000,000
Libyan Arab Jamahiriya	Medium development		Not published
Liechtenstein	Very high development		Not published
Lithuania	Very high development	\$	42,773,029,835
Luxembourg	Very high development	\$	58,631,324,559
Macau	Very high development	\$	45,361,678,147
Madagascar	Low development	\$	10,001,193,420
Malawi	Low development	\$	5,433,038,647
Malaysia	High development	\$	296,535,930,381
Maldives	High development	\$	4,224,209,599
Mali	Low development	\$	14,034,980,334
Malta	Very high development	\$	10,999,047,580
Marshall Islands	Not published	\$	194,497,900
Martinique	Not published		Not published
Mauritania	Low development	\$	4,739,298,730
Mauritius	High development	\$	12,168,437,744
Mayotte	Not published		Not published
Mexico	High development	\$	1,046,922,702,461

Figure D.66: Human development index and GDP

Guinea-Bissau - Mexico

Country name	Sum dike height reduction	Total coastline length (CL1) *	Vegetated coastline length (CL2)**
	[m]	[km]	[km]
Guinea-Bissau	679	1000	695
Guyana	100	379	152
Haiti	107	1020	171
Heard Island and McDonald Islands	6	87	13
Holy See (Vatican City)	0	0	0
Honduras	195	681	301
Hong Kong	32	192	39
Hungary	0	0	0
Iceland	21	4687	37
India	1703	7307	1687
Indonesia	8350	33632	11256
Iran (Islamic Republic of)	333	2082	278
Iraq	4	105	2
Ireland	88	2767	119
Isle of Man	0	107	0
Israel	0	146	0
Italy	68	4090	133
Jamaica	65	435	116
Japan	322	10015	463
Jersey	0	44	0
Jordan	0	18	0
Kazakhstan	0	400	0
Kenya	264	460	255
Kiribati	16	108	22
Korea	94	1279	89
Korea	272	2287	313
Kuwait	2	323	3
Kyrgyzstan	0	0	0
Lao People's Democratic Republic	0	0	0
Latvia	0	433	1
Lebanon	0	166	0
Lesotho	0	0	0
Liberia	83	401	127
Libyan Arab Jamahiriya	13	1317	19
Liechtenstein	0	0	0
Lithuania	0	122	0
Luxembourg	0	0	0
Macau	0	4	1
Madagascar	1952	3971	1623
Malawi	0	0	0
Malaysia	972	3541	1423
Maldives	0	0	0
Mali	0	0	0
Malta	0	74	0
Marshall Islands	0	0	0
Martinique	16	137	22
Mauritania	26	590	31
Mauritius	4	167	9
Mayotte	7	73	12
Mexico	2425	9117	3209

Figure D.67: Crest height reduction results      Guinea-Bissau - Mexico

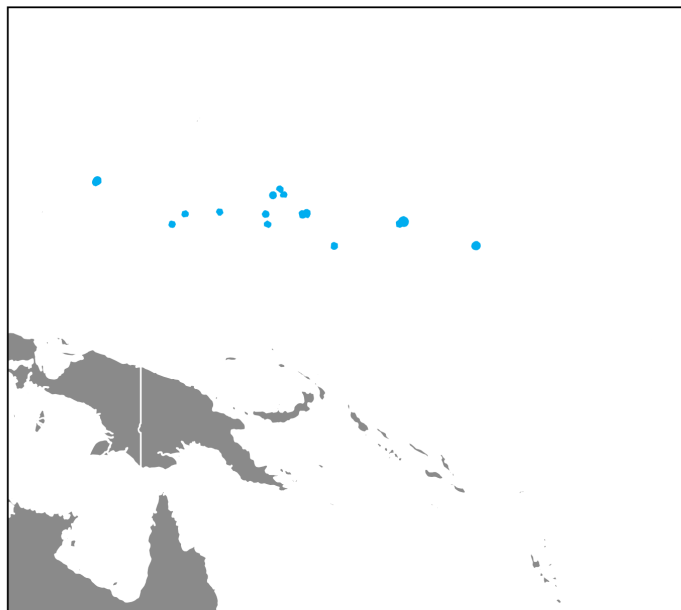
\* Approximated coastline length calculated by sum of transects per country

\*\* Coastline length along wave attenuation of at least 10 centimeters is observed

\*\*\* Dike costs reduction per country is calculated by multiplying the sum of dike height reduction per country with an unit dike price which depends on the human development index of the country

$\Delta R_c / CL1$	$\Delta R_c / CL2$	Dike costs reduction***		Dike costs reduction / GDP
[m/km]	[m/km]	[millions USA Dollars]	[% of GDP]	
0.68	0.98	1492.8	128.15	
0.26	0.66	219.8	6.28	
0.10	0.62	106.7	1.33	
0.07	0.44	5.7	GDP unknown	
0.00	0.00	0.0	GDP unknown	
0.29	0.65	429.5	2.00	
0.17	0.82	335.3	0.11	
0.00	0.00	0.0	0.00	
0.00	0.57	222.3	1.09	
0.23	1.01	3745.6	0.17	
0.25	0.74	18369.2	1.97	
0.16	1.20	1666.6	0.43	
0.03	1.83	8.0	0.00	
0.03	0.74	926.4	0.30	
0.00	0.00	0.0	GDP unknown	
0.00	0.00	0.0	0.00	
0.02	0.51	712.8	0.04	
0.15	0.56	324.5	2.31	
0.03	0.70	3385.6	0.07	
0.00	0.00	0.0	GDP unknown	
0.00	0.00	0.0	0.00	
0.00	0.00	0.0	0.00	
0.57	1.04	581.1	0.82	
0.15	0.74	35.7	19.66	
0.07	1.06	94.4	GDP unknown	
0.12	0.87	2858.6	0.21	
0.01	0.75	23.6	0.02	
0.00	0.00	0.0	0.00	
0.00	0.00	0.0	0.00	
0.00	0.47	4.9	0.02	
0.00	0.00	0.0	0.00	
0.00	0.00	0.0	0.00	
0.21	0.65	82.7	3.94	
0.01	0.69	28.7	GDP unknown	
0.00	0.00	0.0	GDP unknown	
0.00	0.00	0.0	0.00	
0.00	0.00	0.0	0.00	
0.11	0.44	4.6	0.01	
0.49	1.20	1952.2	19.52	
0.00	0.00	0.0	0.00	
0.27	0.68	4860.4	1.64	
0.00	0.00	0.0	0.00	
0.00	0.00	0.0	0.00	
0.00	0.00	0.0	0.00	
0.11	0.71	15.6	GDP unknown	
0.04	0.85	26.4	0.56	
0.03	0.48	21.4	0.18	
0.09	0.55	6.7	GDP unknown	
0.27	0.76	12126.7	1.16	

# Micronesia



# Saudi-Arabia

Country name	Human Development Index	Gross Domestic Product (GDP)	
	[·]	[USA Dollars]	
Micronesia	Medium development	\$	315,179,700
Monaco	Very high development		Not published
Mongolia	High development	\$	11,183,458,131
Montenegro	Very high development	\$	4,374,127,212
Montserrat	Not published		Not published
Morocco	Medium development	\$	103,606,321,693
Mozambique	Low development	\$	11,014,858,592
Namibia	Medium development	\$	10,947,880,690
Nauru	Not published		Not published
Nepal	Medium development	\$	21,131,983,246
Netherlands	Very high development	\$	777,227,541,581
Netherlands Antilles	Not published		Not published
New Caledonia	Not published		Not published
New Zealand	Very high development	\$	184,970,675,763
Nicaragua	Medium development	\$	13,230,844,687
Niger	Low development	\$	7,528,387,858
Nigeria	Low development	\$	404,652,720,165
Niue	Not published		Not published
Norfolk Island	Not published		Not published
Northern Mariana Islands	Not published	\$	1,242,000,000
Norway	Very high development	\$	371,075,238,095
Oman	High development	\$	66,293,368,010
Pakistan	Medium development	\$	278,913,371,202
Palau	High development	\$	310,248,300
Palestine	Medium development		Not published
Panama	Very high development	\$	55,187,700,000
Papua New Guinea	Low development	\$	20,213,214,172
Paraguay	Medium development	\$	27,424,071,383
Peru	High development	\$	192,207,342,005
Philippines	Medium development	\$	304,905,406,845
Pitcairn Islands	Not published		Not published
Poland	Very high development	\$	471,364,408,714
Portugal	Very high development	\$	205,184,480,409
Puerto Rico	Not published	\$	105,034,500,000
Qatar	Very high development	\$	152,451,923,077
Republic of Moldova	Medium development	\$	6,749,515,655
Reunion	Not published		Not published
Romania	Very high development	\$	187,592,037,840
Russia	Very high development	\$	1,283,162,985,989
Rwanda	Low development	\$	8,376,048,905
Saint Barthelemy	Not published		Not published
Saint Helena	Not published		Not published
Saint Kitts and Nevis	High development	\$	909,854,620
Saint Lucia	High development	\$	1,667,078,704
Saint Martin	Not published		Not published
Saint Pierre and Miquelon	Not published		Not published
Saint Vincent and the Grenadines	High development	\$	768,224,227
Samoa	High development	\$	786,356,315
San Marino	Not published	\$	1,590,707,965
Sao Tome and Principe	Medium development	\$	342,781,716
Saudi Arabia	Very high development	\$	646,438,380,560

Figure D.68: Human development index and GDP Micronesia - Saudi-Arabia









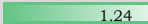












































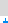









































Country name	Sum dike height reduction	Total coastline length (CL1) *	Vegetated coastline length (CL2)**
	[m]	[km]	[km]
Micronesia	47	104	73
Monaco	0	6	0
Mongolia	0	0	0
Montenegro	0	153	0
Montserrat	1	31	2
Morocco	62	1360	50
Mozambique	802	2252	836
Namibia	1	1066	1
Nauru	0	0	0
Nepal	0	0	0
Netherlands	148	754	96
Netherlands Antilles	5	174	9
New Caledonia	205	1144	336
New Zealand	662	6780	837
Nicaragua	131	728	236
Niger	0	0	0
Nigeria	379	1286	550
Niue	5	45	8
Norfolk Island	0	14	0
Northern Mariana Islands	1	142	2
Norway	0	11264	0
Oman	52	1528	51
Pakistan	258	1138	169
Palau	26	62	41
Palestine	0	34	0
Panama	536	1905	651
Papua New Guinea	1683	7389	2446
Paraguay	0	0	0
Peru	62	1797	98
Philippines	2403	11245	3796
Pitcairn Islands	0	17	0
Poland	0	545	0
Portugal	26	1077	40
Puerto Rico	73	396	122
Qatar	77	402	72
Republic of Moldova	0	0	0
Reunion	2	141	3
Romania	7	157	9
Russia	3033	24291	2315
Rwanda	0	0	0
Saint Barthelemy	0	13	0
Saint Helena	1	108	3
Saint Kitts and Nevis	1	59	2
Saint Lucia	5	74	8
Saint Martin	1	10	1
Saint Pierre and Miquelon	0	62	0
Saint Vincent and the Grenadines	1	52	2
Samoa	10	256	16
San Marino	0	0	0
Sao Tome and Principe	65	125	57
Saudi Arabia	180	2402	236

Figure D.69: Crest height reduction results Micronesia - Saudi-Arabia

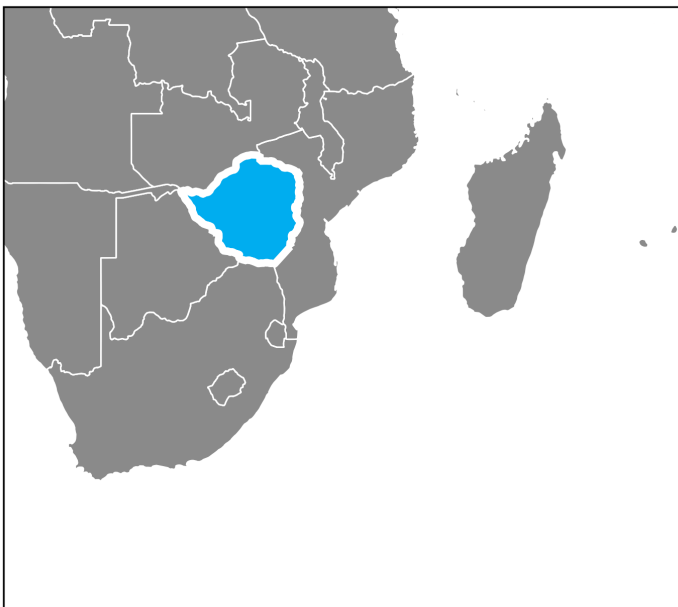
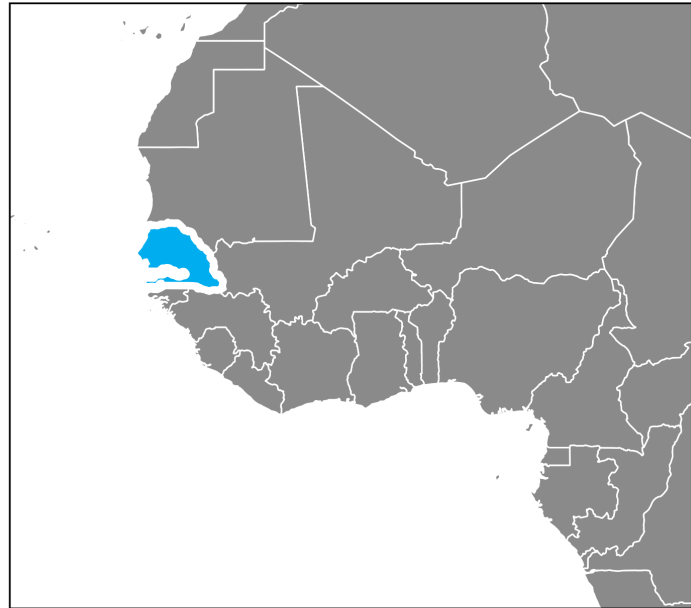
\* Approximated coastline length calculated by sum of transects per country

\*\* Coastline length along wave attenuation of at least 10 centimeters is observed

\*\*\* Dike costs reduction per country is calculated by multiplying the sum of dike height reduction per country with an unit dike price which depends on the human development index of the country

$\Delta R_c / CL1$	$\Delta R_c / CL2$	Dike costs reduction***	Dike costs reduction / GDP
[m/km]	[m/km]	[millions USA Dollars]	[% of GDP]
 0.46	 0.65	104.3	 33.09
0.00	0.00	0.0	GDP unknown
0.00	0.00	0.0	0.00
0.00	0.00	0.0	0.00
 0.03	 0.49	1.0	GDP unknown
 0.05	 1.24	136.3	 0.13
 0.36	 0.96	802.5	 7.29
 0.00	 0.59	1.3	0.01
0.00	0.00	0.0	GDP unknown
0.00	0.00	0.0	0.00
 0.20	 1.54	1552.5	 0.20
 0.03	 0.52	4.7	GDP unknown
 0.18	 0.61	204.6	GDP unknown
 0.10	 0.79	6955.7	 3.76
 0.18	 0.56	288.6	 2.18
0.00	0.00	0.0	0.00
 0.29	 0.69	378.9	 0.09
 0.12	 0.65	5.2	GDP unknown
0.00	0.00	0.0	GDP unknown
 0.01	 0.45	0.9	 0.07
0.00	0.00	0.0	0.00
 0.03	 1.02	261.1	 0.39
 0.23	 1.52	566.9	 0.20
 0.42	 0.63	129.1	 41.61
0.00	0.00	0.0	GDP unknown
 0.28	 0.82	5628.1	 10.20
 0.23	 0.69	1683.2	 8.33
0.00	0.00	0.0	0.00
 0.03	 0.63	309.0	 0.16
 0.21	 0.63	5287.2	 1.73
0.00	0.00	0.0	GDP unknown
0.00	0.00	0.0	0.00
 0.02	 0.64	268.7	 0.13
 0.19	 0.60	73.4	 0.07
 0.19	 1.07	808.1	 0.53
0.00	0.00	0.0	0.00
 0.01	 0.55	1.7	GDP unknown
 0.05	 0.79	74.8	0.04
 0.12	 1.31	31841.6	 2.48
0.00	0.00	0.0	0.00
0.00	0.00	0.0	GDP unknown
 0.01	 0.41	1.2	GDP unknown
 0.01	 0.41	4.1	 0.45
 0.07	 0.67	27.0	 1.62
 0.07	 0.72	0.7	GDP unknown
0.00	0.00	0.0	GDP unknown
 0.02	 0.55	5.5	 0.72
 0.04	 0.61	49.1	 6.24
0.00	0.00	0.0	0.00
 0.52	 1.14	142.7	 41.64
 0.07	 0.76	1890.8	 0.29

**Senegal**



**Zimbabwe**

Country name	Human Development Index	Gross Domestic Product (GDP)	
	[·]	[USA Dollars]	
Senegal	Low development	\$	14,683,697,631
Serbia	High development	\$	38,299,854,688
Seychelles	High development	\$	1,427,323,889
Sierra Leone	Low development	\$	3,736,588,554
Singapore	Very high development	\$	296,975,678,610
Slovakia	Very high development	\$	89,768,598,023
Slovenia	Very high development	\$	44,708,598,649
Solomon Islands	Medium development	\$	1,202,125,000
Somalia	Not published	\$	6,217,000,000
South Africa	Medium development	\$	295,456,189,492
South Georgia South Sandwich Islands	High development		Not published
Spain	Very high development	\$	1,237,255,019,654
Sri Lanka	High development	\$	81,321,876,307
Sudan	Low development	\$	95,584,380,032
Suriname	High development	\$	3,278,425,328
Svalbard	Not published		Not published
Swaziland	Low development	\$	3,720,649,375
Sweden	Very high development	\$	514,459,972,806
Switzerland	Very high development	\$	668,851,296,244
Syrian Arab Republic	Low development		Not published
Taiwan	Not published		Not published
Tajikistan	Medium development	\$	6,951,657,159
Thailand	High development	\$	407,026,127,310
The former Yugoslav Republic of Macedonia	High development	\$	10,051,659,161
Timor-Leste	Medium development	\$	1,782,974,000
Togo	Low development	\$	4,399,995,987
Tokelau	Not published		Not published
Tonga	High development	\$	401,562,006
Trinidad and Tobago	High development	\$	21,894,706,041
Tunisia	High development	\$	42,062,549,395
Turkey	High development	\$	863,711,710,427
Turkmenistan	Medium development	\$	36,179,885,714
Turks and Caicos Islands	Not published		Not published
Tuvalu	Not published	\$	34,218,878
Uganda	Low development	\$	24,078,931,933
Ukraine	High development	\$	93,270,479,389
United Arab Emirates	Very high development	\$	348,743,265,705
United Kingdom	Very high development	\$	2,650,850,178,102
United Republic of Tanzania	Low development	\$	47,340,071,107
United States	Very high development	\$	18,624,475,000,000
United States Minor Outlying Islands	Not published		Not published
United States Virgin Islands	Not published		Not published
Uruguay	High development	\$	52,419,720,714
Uzbekistan	High development	\$	67,220,335,570
Vanuatu	Medium development	\$	773,502,896
Venezuela	High development		Not published
Viet Nam	Medium development	\$	205,276,172,135
Wallis and Futuna Islands	Not published		Not published
Western Sahara	Not published		Not published
Yemen	Low development	\$	37,733,919,936
Zambia	Medium development	\$	21,063,989,683
Zimbabwe	Low development	\$	16,619,960,402

Figure D.70: Human development index and GDP Senegal - Zimbabwe


























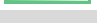




















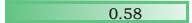





















Country name	Sum dike height reduction	Total coastline length (CL1) *	Vegetated coastline length (CL2)**
	[m]	[km]	[km]
Senegal	103	600	148
Serbia	0	0	0
Seychelles	30	106	29
Sierra Leone	120	520	193
Singapore	17	82	23
Slovakia	0	0	0
Slovenia	1	34	1
Solomon Islands	555	2685	930
Somalia	115	2194	128
South Africa	32	2216	56
South Georgia South Sandwich Islands	11	700	20
Spain	120	3729	178
Sri Lanka	166	1017	261
Sudan	12	492	24
Suriname	108	279	152
Svalbard	0	0	0
Swaziland	0	0	0
Sweden	58	5038	128
Switzerland	0	0	0
Syrian Arab Republic	0	112	0
Taiwan	65	762	87
Tajikistan	0	0	0
Thailand	547	2047	835
The former Yugoslav Republic of Macedonia	0	0	0
Timor-Leste	51	449	75
Togo	7	46	12
Tokelau	0	0	0
Tonga	14	152	22
Trinidad and Tobago	33	338	58
Tunisia	40	983	78
Turkey	44	4195	92
Turkmenistan	0	230	0
Turks and Caicos Islands	23	116	36
Tuvalu	0	0	0
Uganda	0	0	0
Ukraine	0	2082	0
United Arab Emirates	434	751	299
United Kingdom	566	9923	555
United Republic of Tanzania	882	1178	718
United States	5787	46325	7623
United States Minor Outlying Islands	0	0	0
United States Virgin Islands	8	92	13
Uruguay	0	167	0
Uzbekistan	0	0	0
Vanuatu	52	1398	100
Venezuela	398	2615	588
Viet Nam	689	2149	673
Wallis and Futuna Islands	7	30	9
Western Sahara	33	738	24
Yemen	21	1622	34
Zambia	0	0	0
Zimbabwe	0	0	0

Figure D.71: Crest height reduction results Senegal - Zimbabwe

\* Approximated coastline length calculated by sum of transects per country

\*\* Coastline length along wave attenuation of at least 10 centimeters is observed

\*\*\* Dike costs reduction per country is calculated by multiplying the sum of dike height reduction per country with an unit dike price which depends on the human development index of the country

$\Delta R_c$ / CL1		$\Delta R_c$ / CL2		Dike costs reduction***	Dike costs reduction / GDP
[m/km]		[m/km]		[millions USA Dollars]	[% of GDP]
	0.17		0.70	102.9	0.70
	0.00		0.00	0.0	0.00
	0.28		1.04	150.3	10.53
	0.23		0.62	119.9	3.21
	0.20		0.73	175.5	0.06
	0.00		0.00	0.0	0.00
	0.02		0.61	6.4	0.01
	0.21		0.60	1220.4	101.52
	0.05		0.90	115.3	1.85
	0.01		0.58	71.2	0.02
	0.02		0.53	53.4	GDP unknown
	0.03		0.67	1259.9	0.10
	0.16		0.64	831.1	1.02
	0.02		0.49	11.8	0.01
	0.39		0.71	539.9	16.47
	0.00		0.00	0.0	GDP unknown
	0.00		0.00	0.0	0.00
	0.01		0.45	610.5	0.12
	0.00		0.00	0.0	0.00
	0.00		0.00	0.0	GDP unknown
	0.09		0.75	65.5	GDP unknown
	0.00		0.00	0.0	0.00
	0.27		0.66	2735.7	0.67
	0.00		0.00	0.0	0.00
	0.11		0.69	113.3	6.35
	0.16		0.62	7.4	0.17
	0.00		0.00	0.0	GDP unknown
	0.09		0.63	69.3	17.27
	0.10		0.58	167.3	0.76
	0.04		0.52	202.4	0.48
	0.01		0.48	219.2	0.03
	0.00		0.00	0.0	0.00
	0.20		0.64	23.1	GDP unknown
	0.00		0.00	0.0	0.00
	0.00		0.00	0.0	0.00
	0.00		0.00	0.0	0.00
	0.58		1.45	4560.5	1.31
	0.06		1.02	5938.7	0.22
	0.75		1.23	882.5	1.86
	0.12		0.76	60761.9	0.33
	0.00		0.00	0.0	GDP unknown
	0.09		0.62	8.1	GDP unknown
	0.00		0.00	0.0	0.00
	0.00		0.00	0.0	0.00
	0.04		0.52	115.4	14.91
	0.15		0.68	1992.0	GDP unknown
	0.32		1.02	1516.5	0.74
	0.25		0.82	7.4	GDP unknown
	0.04		1.38	33.1	GDP unknown
	0.01		0.61	20.9	0.06
	0.00		0.00	0.0	0.00
	0.00		0.00	0.0	0.00

## D.7. Pilot study results for look-up table

To get insight in the possible foreshore configurations and boundary conditions a pilot study is performed for the United Kingdom and sampled transects world wide.

### Pilot study based on transect for the United Kingdom

The UK is chosen because the coastline shows various configurations and multiple salt marsh areas are present. This pilot study contained roughly 6800 transects. Based on output a step of 0.50 m is chosen in the look-up table for the significant wave height and water level. In the look-up table vegetation width has a small step size of 25 m for small widths, because the most transects have a vegetation width below 300 m. Furthermore accuracy for small vegetation widths is more important, because most wave attenuation takes place in the first meters [Möller et al. \(2014\)](#). The foreshore slope distribution shows an almost negligible amount of transects with very mild slopes (foreshore slope < 1/2000). For this reason the look-up table has smaller step sizes for steep slopes than for very mild slopes.

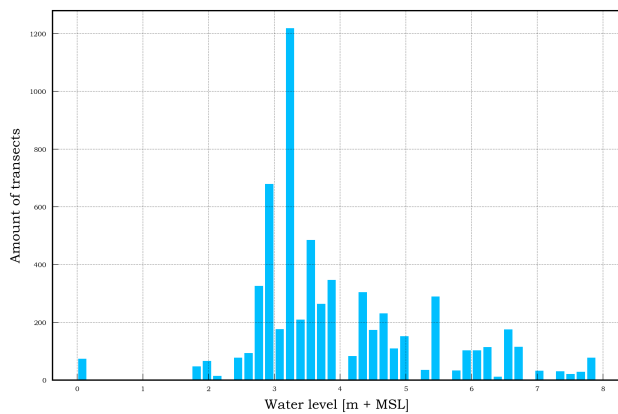


Figure D.72: Distribution of extreme water levels for UK pilot study for return period of 100 years

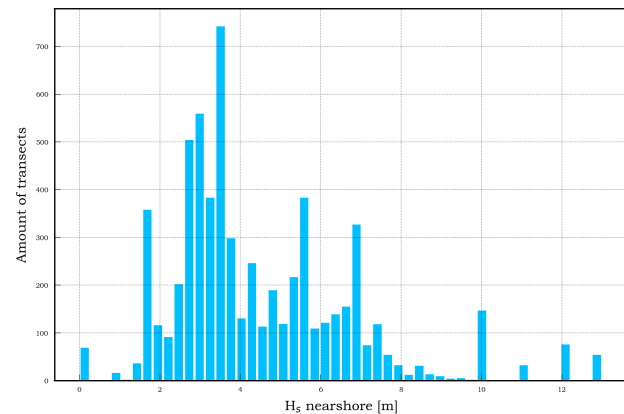


Figure D.73: Distribution of nearshore wave height for UK pilot study for return period of 100 years

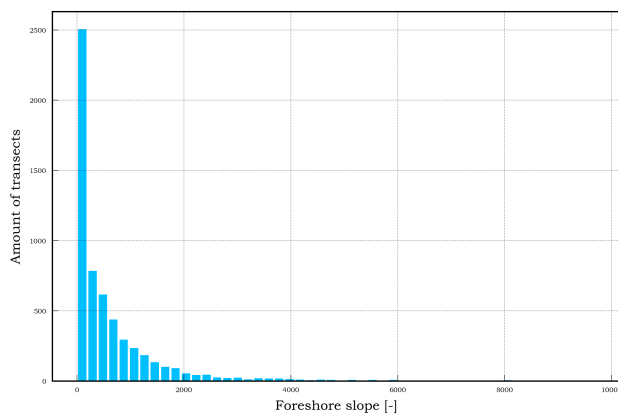


Figure D.74: Distribution of foreshore slope for UK pilot study

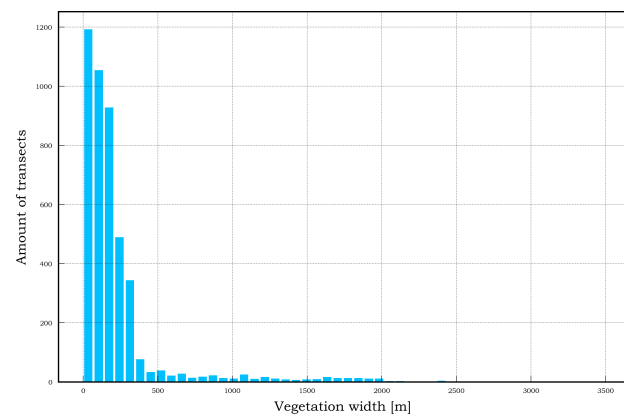


Figure D.75: Distribution of vegetation width for UK pilot study

### Pilot study based on sampled transects worldwide

From all transect which describe world's coastline a sample is taken, resulting in a sample set of about 3500 vegetated transects. The world pilot study is performed for all nine return periods, in contrast to the UK pilot run which is performed for one return period. This approach is chosen to test the algorithm over all return periods and to get a good insight in the hydraulic boundary conditions world wide.

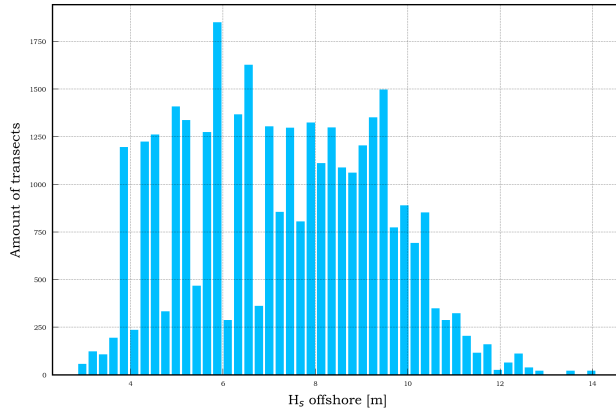


Figure D.76: Distribution of offshore wave height based on pilot study for all return periods

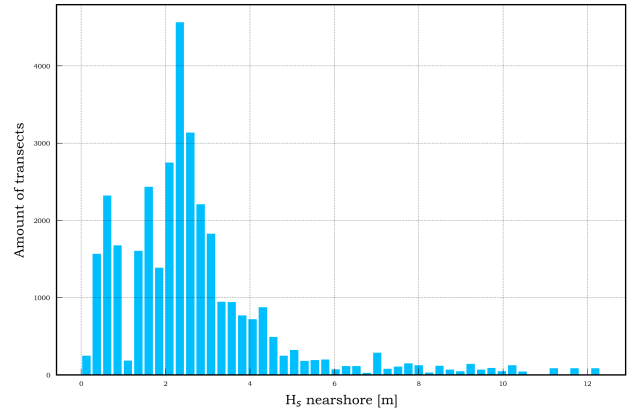


Figure D.77: Distribution of nearshore wave height based on pilot study for all return periods

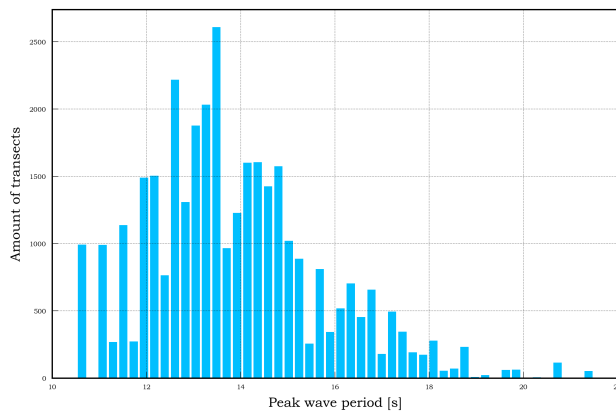


Figure D.78: Distribution of offshore wave period based on pilot study for all return periods

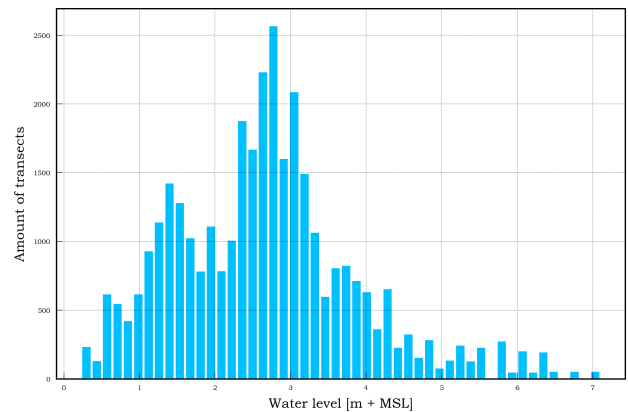


Figure D.79: Distribution of extreme water levels based on pilot study for all return periods





E

Case studies

## E.1. Western Scheldt, The Netherlands

### Distribution and difference between local and global framework for input parameters

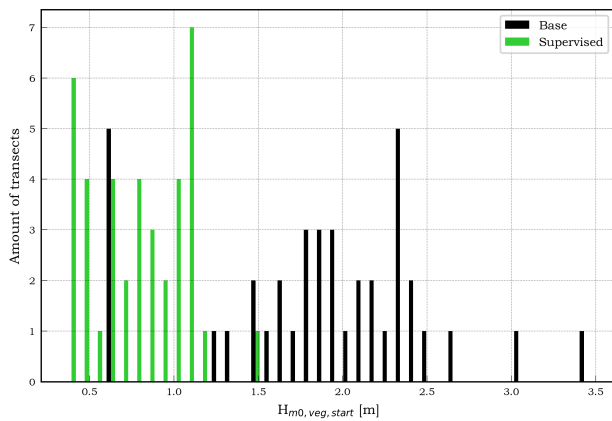


Figure E.1: Distribution of  $H_{m0}$  at begin of the vegetated zone for the global and supervised framework

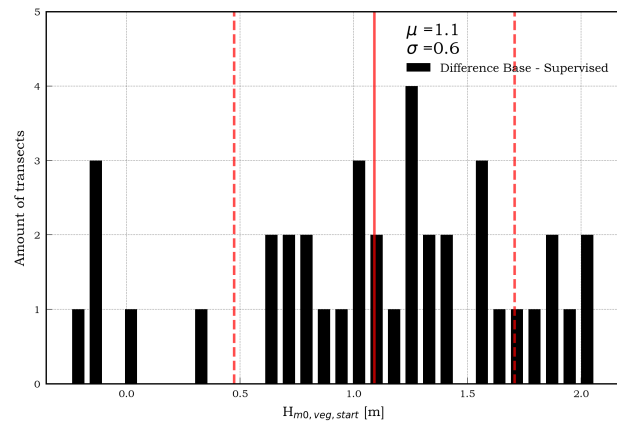


Figure E.2: Difference in  $H_{m0}$  at begin of the vegetated zone between the global and supervised framework

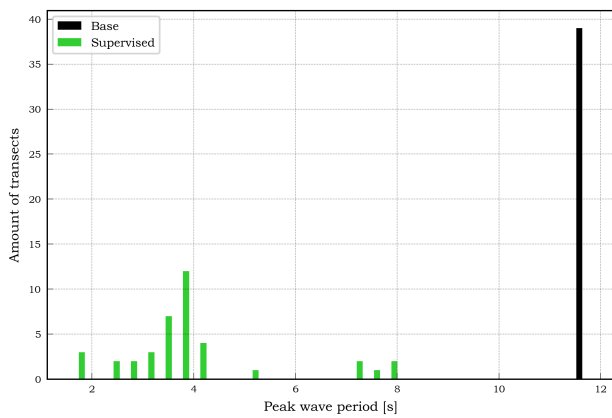


Figure E.3: Distribution of the wave period at begin of the vegetated zone for the global and supervised framework

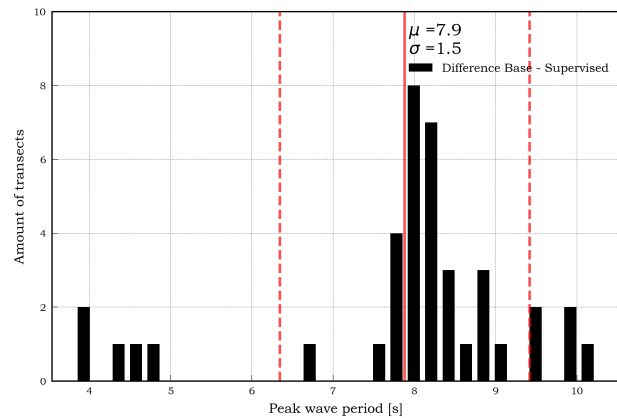


Figure E.4: Difference in wave period at begin of the vegetated zone between the global and supervised framework

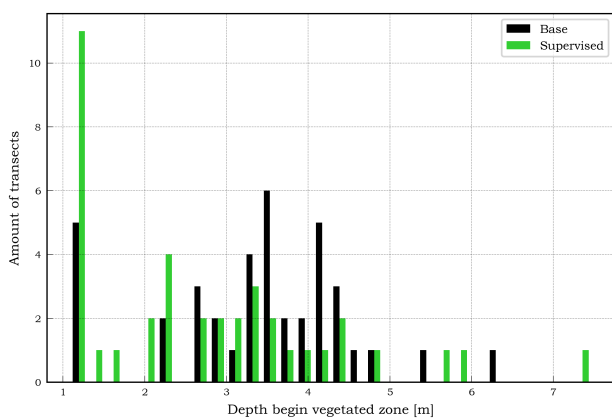


Figure E.5: Distribution of the water depth at begin of the vegetated zone for the global and supervised framework

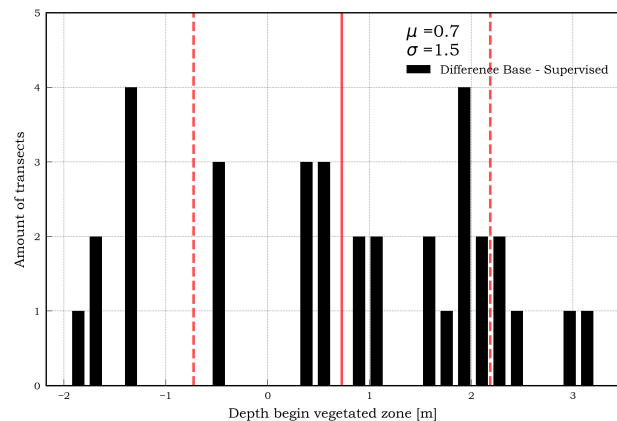


Figure E.6: Difference in water depth at begin of the vegetated zone between the global and supervised framework

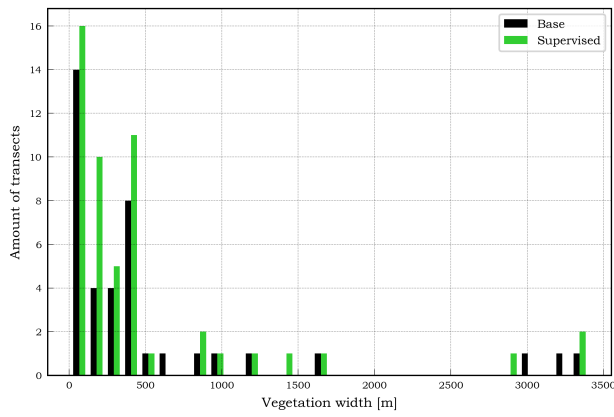


Figure E.7: Distribution of vegetation width for the global and supervised framework

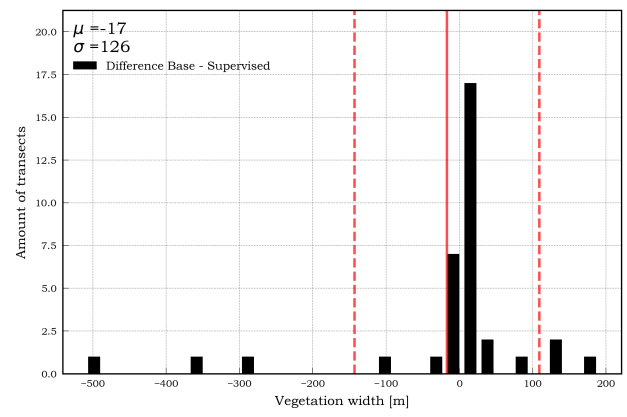


Figure E.8: Difference in vegetation width between the global and supervised framework

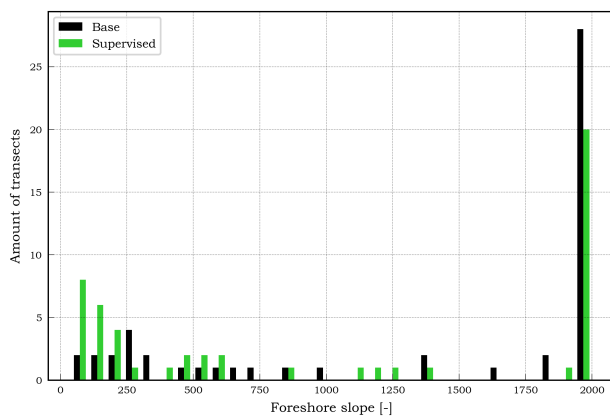


Figure E.9: Distribution of foreshore slopes for the global and supervised framework

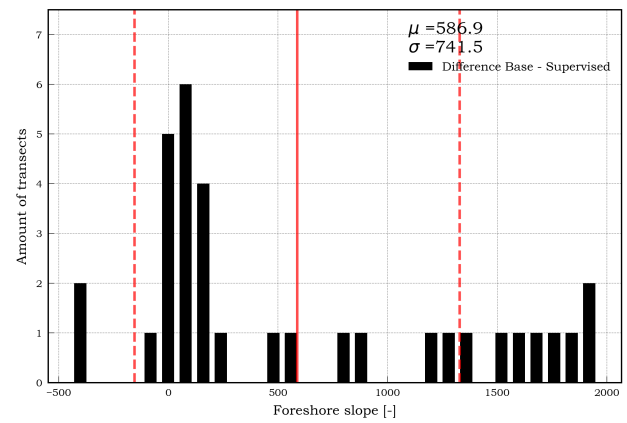


Figure E.10: Difference in foreshore slope between the global and supervised framework

## Results of different model approaches

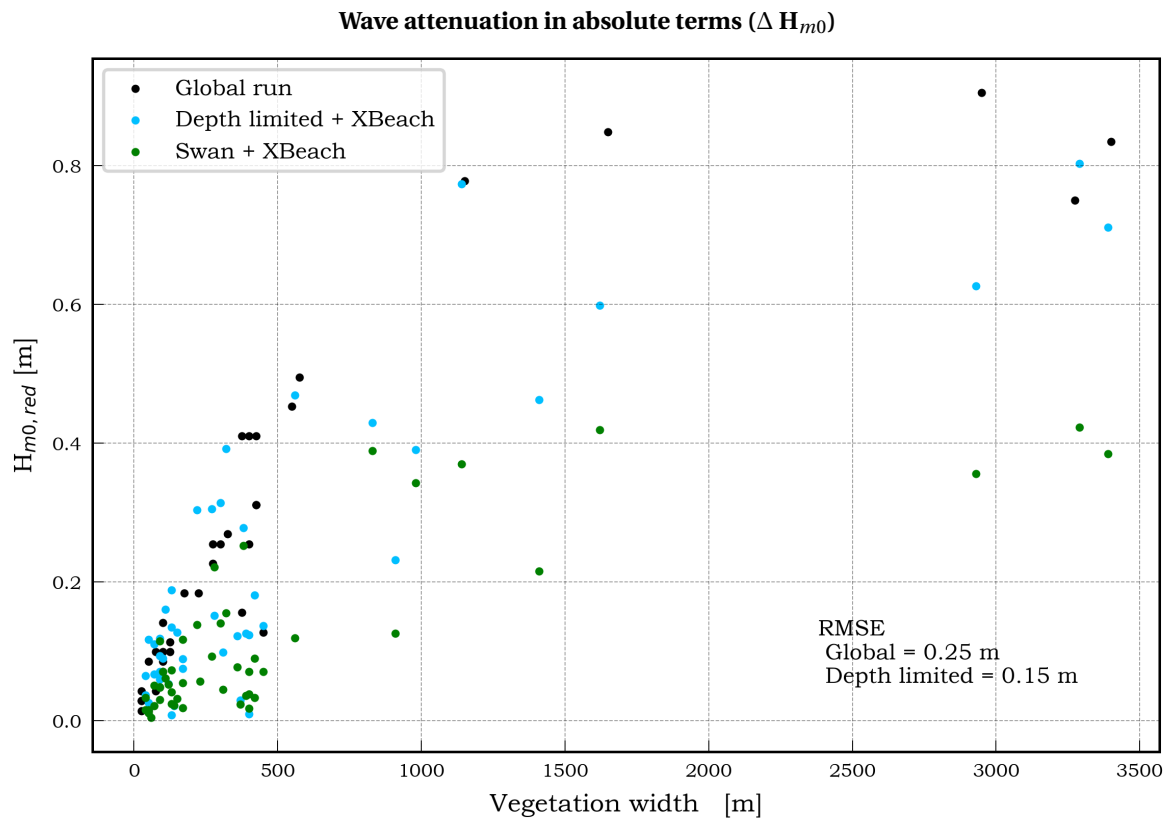


Figure E.11: Wave attenuation in absolute terms versus vegetation width for global and supervised framework

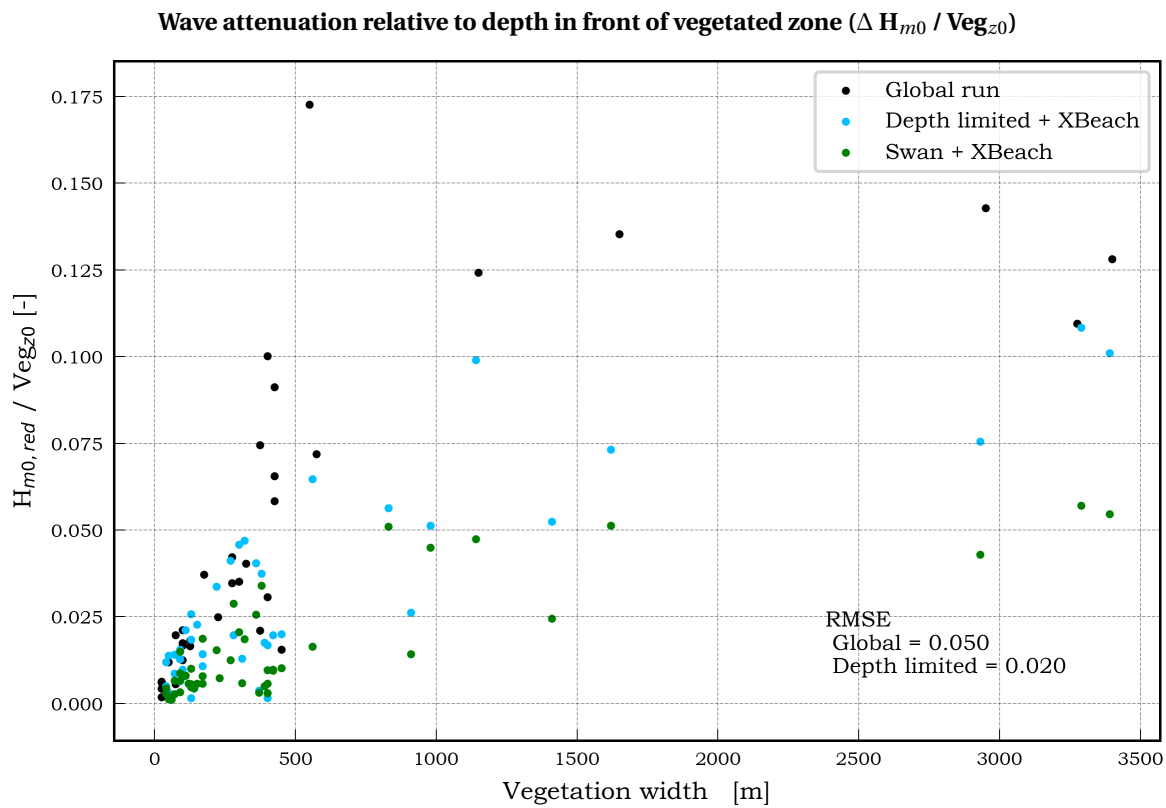


Figure E.12: Wave attenuation relative to water depth at start of the vegetated zone versus vegetation width for global and supervised framework

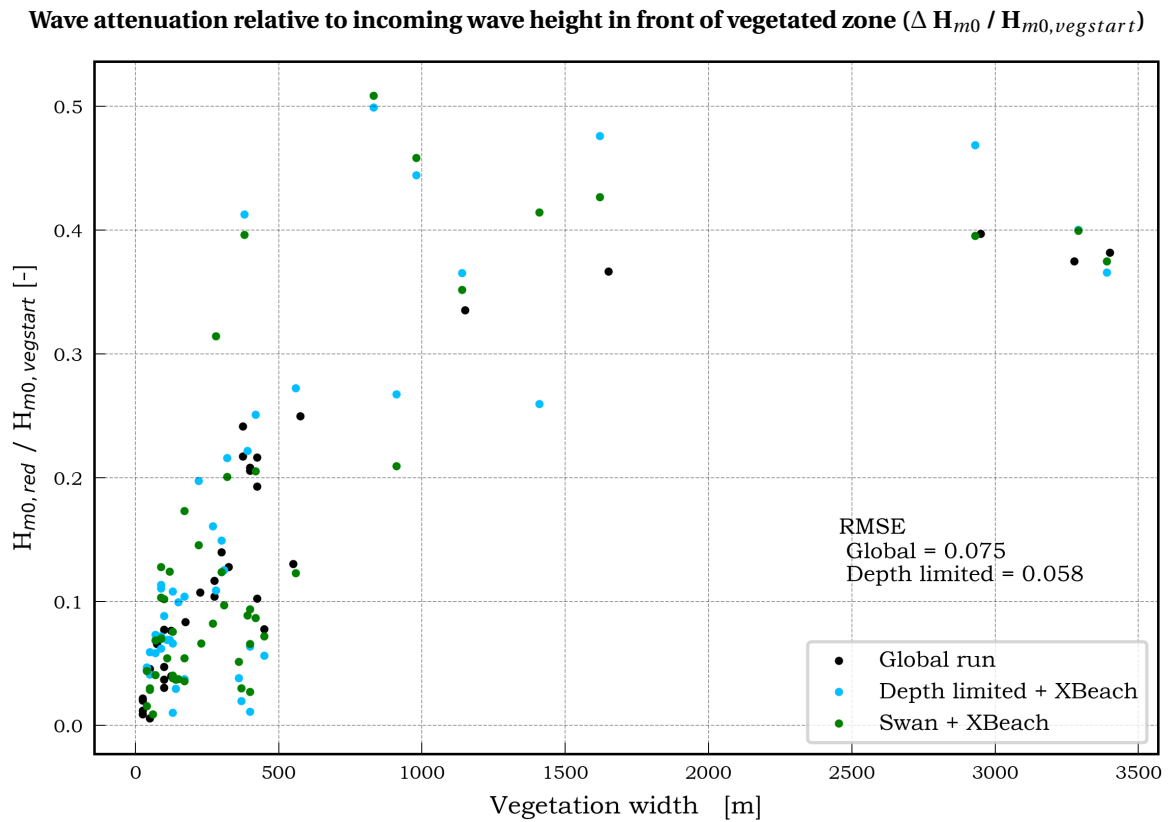


Figure E.13: Wave attenuation relative to wave height at the start of the vegetated zone versus vegetation width for global and supervised framework

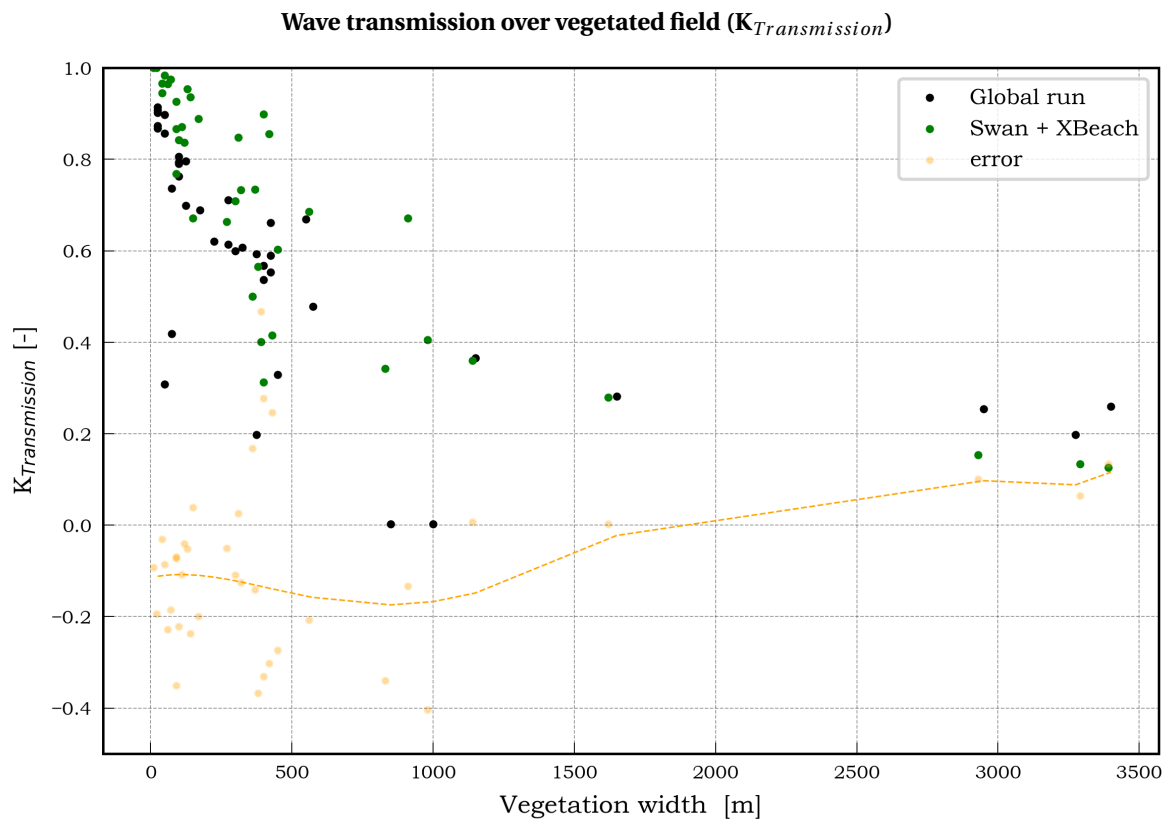


Figure E.14: Wave transmission versus vegetation width for global and supervised framework

## Sensitivity analysis

### Verdrunken Land van Saeftinghe

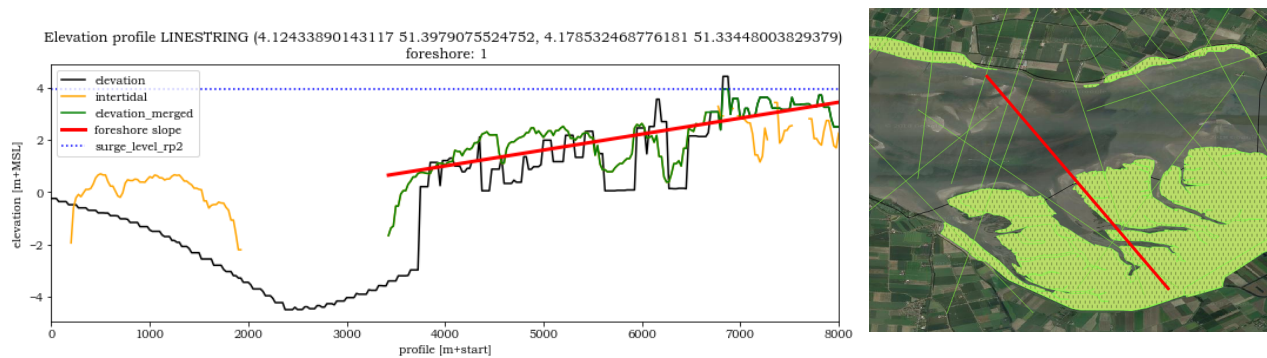


Figure E.15: Alignment of transect and derived profile at the Verdrunken Land van Saeftinghe in the global framework

### Input parameters sensitivity analysis local framework

	Water level [m +MSL]	$H_{s,beginveg}$ [m]	Wave period [s]	Bed level [m]
Local framework	5.24	1.36	3.6	-
Lower bound	4.45	1.21	3.3	- 0.10
Upper bound	6.03	1.49	4.0	+ 0.10

Table E.1: Mean and standard deviation of the error between output of the global and local framework

	Vegetation width [m]	Stem density [ $1/m^2$ ]	Stem diameter [mm]	Stem height [m]	$C_D$ [-]
Local framework	3290	1225	1.25	0.30	0.19
Lower bound	3260	300	1.25	0.20	0.15
Upper bound	3320	1225	4.2	0.75	0.23

Table E.2: Mean and standard deviation of the error between output of the global and local framework

### Input parameters sensitivity analysis global framework

	Water level [m + MSL]	$H_{s,offshore}$ [m]	Wave period [s]	Bed level [m]	Foreshore slope [-]	Vegetation width [m]
Global framework	5.24	7.1	11.8	1.60	1637	3275
Lower bound	4.45	6.4	2.4	-0.59	1537	1572
Upper bound	6.03	7.8	11.8	2.33	1737	4781

Table E.3: Mean and standard deviation of the error between output of the global and local framework

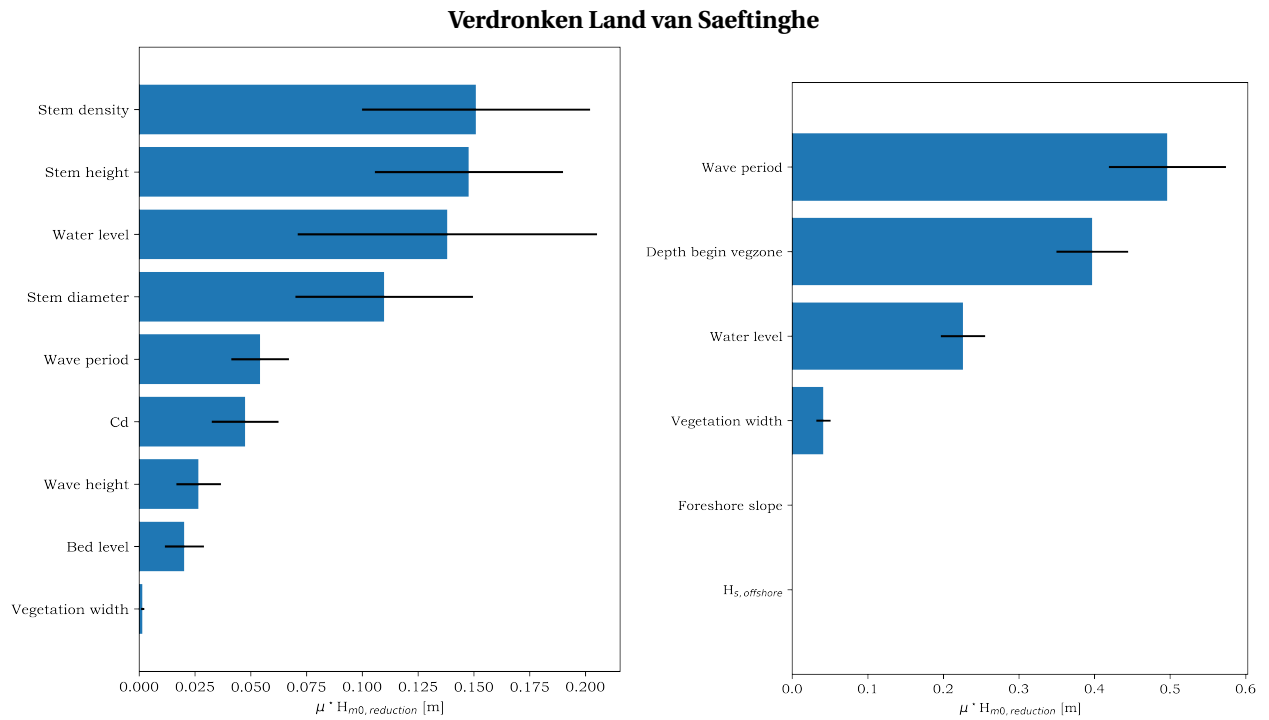


Figure E.16: Bar plot with influence of input uncertainty on wave attenuation for Verdronken Land van Saeftinghe in local framework

Figure E.17: Bar plot with influence of input uncertainty on wave attenuation for Verdronken Land van Saeftinghe in global framework

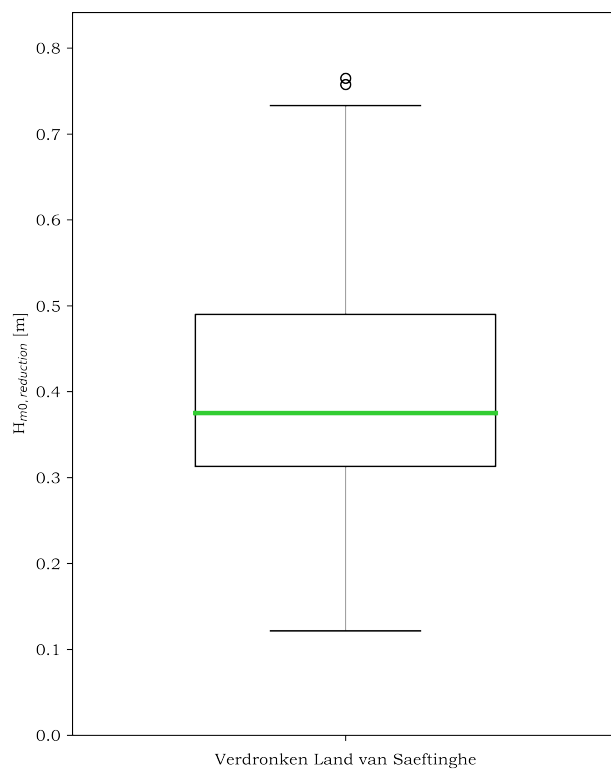


Figure E.18: Boxplot with spreading of wave attenuation due to input uncertainty for Verdronken Land van Saeftinghe in local framework

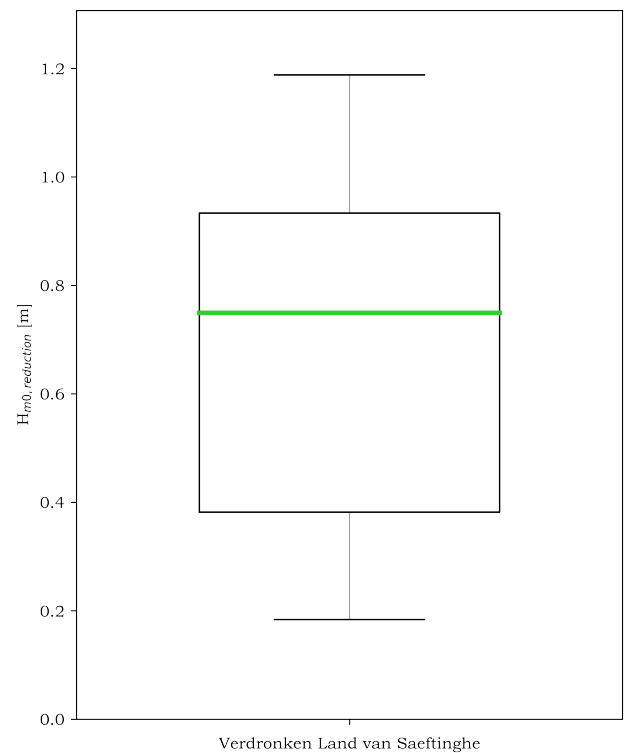


Figure E.19: Boxplot with spreading of wave attenuation due to input uncertainty for Verdronken Land van Saeftinghe in global framework



## Zuidgors

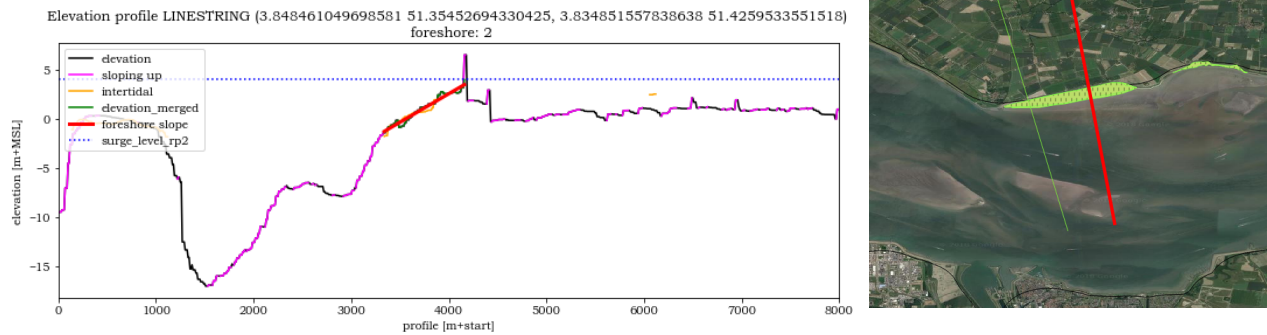


Figure E.20: Alignment of transect and derived profile at Zuidgors in the local framework

## Input parameters sensitivity analysis local framework

	Water level [m +MSL]	$H_{s,beginveg}$ [m]	Wave period [s]	Bed level [m]
Local framework	5.27	1.26	3.6	-
Lower bound	4.48	1.14	3.2	- 0.10
Upper bound	6.07	1.39	3.9	+ 0.10

Table E.4: Mean and standard deviation of the error between output of the global and local framework

	Vegetation width [m]	Stem density [ $1/m^2$ ]	Stem diameter [mm]	Stem height [m]	$C_D$ [-]
Local framework	300	1225	1.25	0.30	0.19
Lower bound	270	300	1.25	0.20	0.15
Upper bound	330	1225	4.2	0.75	0.23

Table E.5: Mean and standard deviation of the error between output of the global and local framework

## Input parameters sensitivity analysis global framework

	Water level [m + MSL]	$H_{s,offshore}$ [m]	Wave period [s]	Bed level [m]	Foreshore slope [-]	Vegetation width [m]
Global framework	5.27	7.1	11.8	1.97	251	300
Lower bound	4.48	6.4	2.4	-0.22	151	144
Upper bound	6.07	7.8	11.8	2.70	351	438

Table E.6: Mean and standard deviation of the error between output of the global and local framework

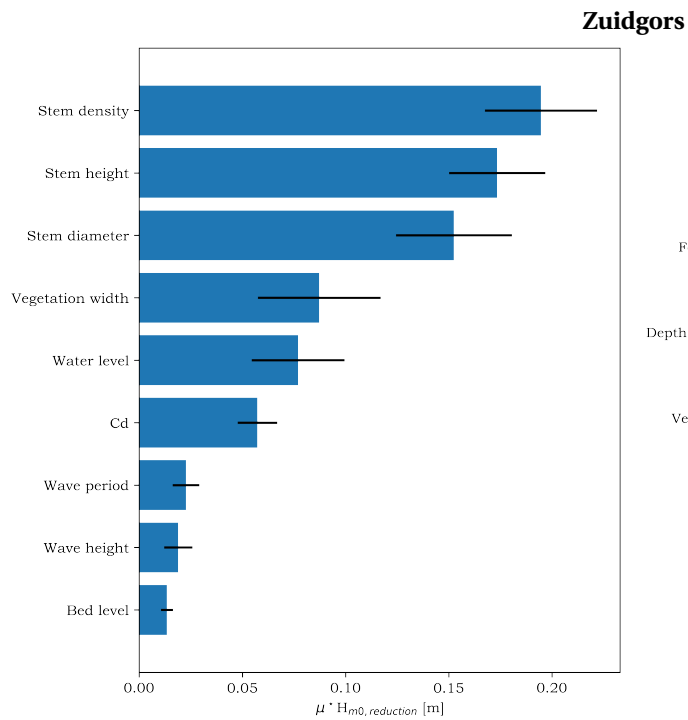


Figure E.21: Bar plot with influence of input uncertainty on wave attenuation for Zuidgors in local framework

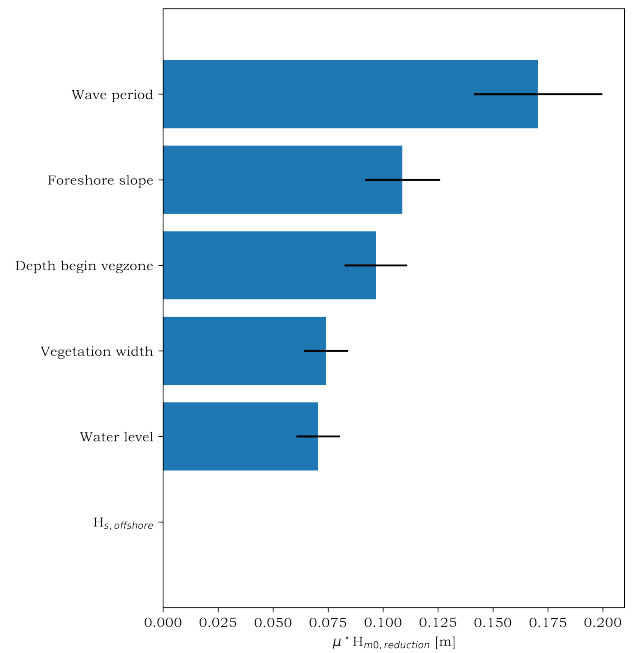


Figure E.22: Bar plot with influence of input uncertainty on wave attenuation for Zuidgors in global framework

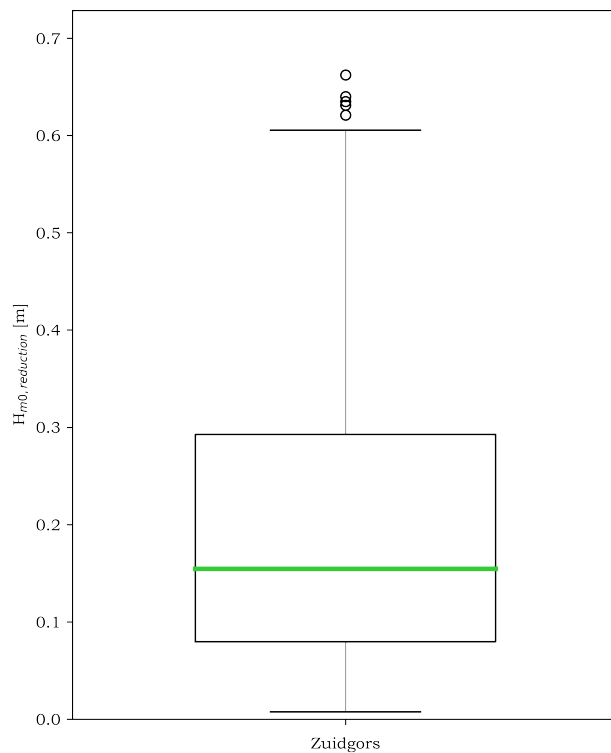


Figure E.23: Boxplot with spreading of wave attenuation due to input uncertainty for Zuidgors in local framework

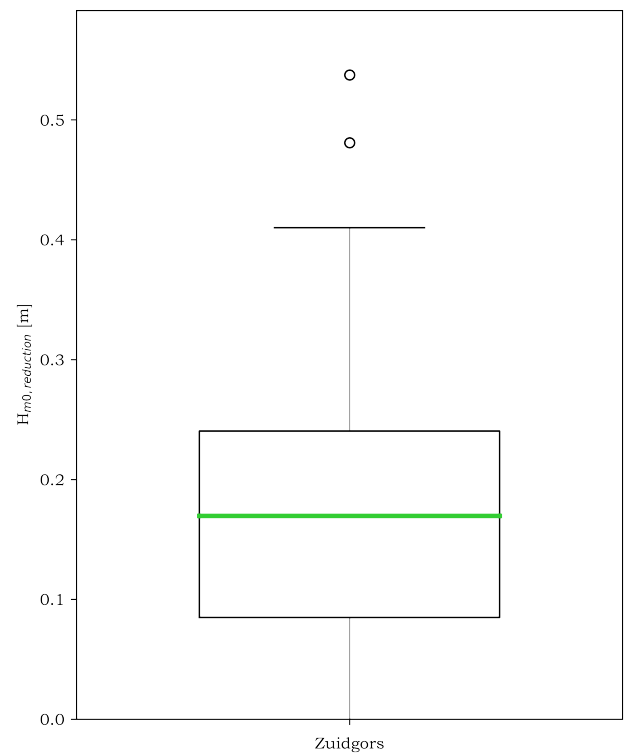


Figure E.24: Boxplot with spreading of wave attenuation due to input uncertainty for Zuidgors in global framework

## E.2. Queensland, Australia

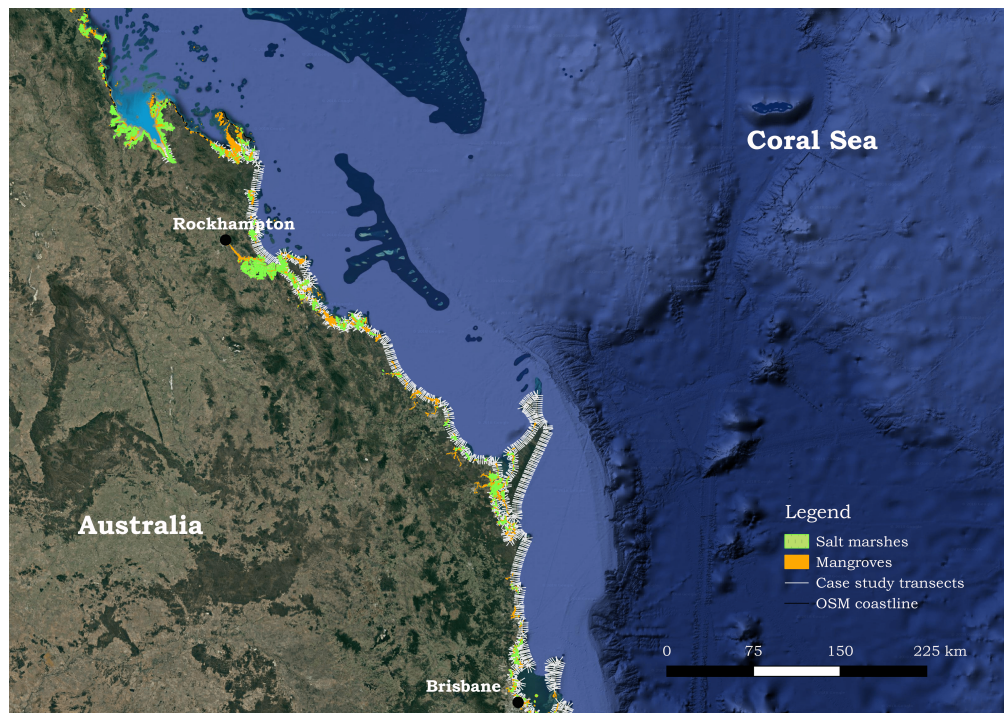


Figure E.25: Overview of case study location at the East coast of Australia

Return period	$H_{s,offshore}$ [m]	$T_p$ [s]	$H_{s,beginveg}$ [m]	Water level [m +MSL]
10 years	4.0	11.4	0.98	2.04
100 years	5.1	12.5	1.07	2.20
1000 years	6.3	13.4	1.17	2.36

Table E.7: Hydraulic boundary conditions for case study at the east coast of Australia

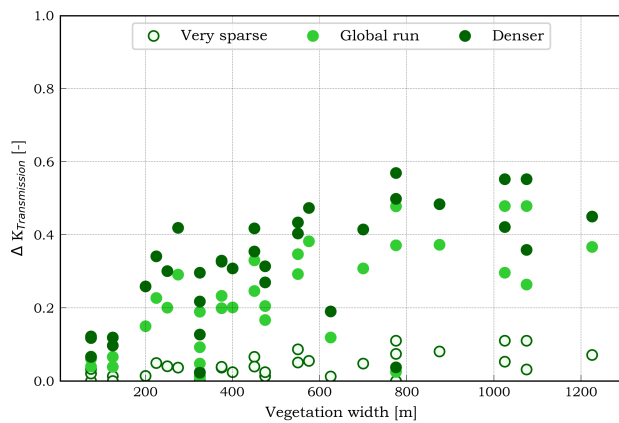


Figure E.26: Reduced wave transmission for different salt marshes characterizations

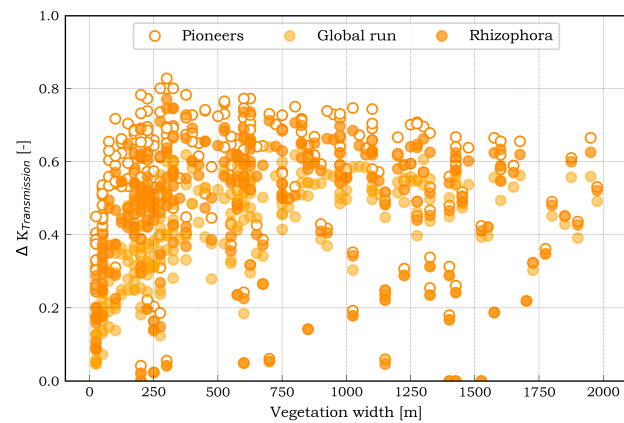


Figure E.27: Reduced wave transmission for different mangrove types

Return period	Salt marshes			Mangroves		
	Very sparse	Global run	Denser	Pioneers	Global run	Rhizophora
10 years	0.040	0.225	0.313	0.528	0.381	0.465
100 years	0.041	0.225	0.314	0.543	0.387	0.476
1000 years	0.041	0.229	0.322	0.561	0.396	0.489

Table E.8: Wave transmission difference for various vegetation characterizations over three return periods

## Vegetation characterization in numerical models

In this appendix an overview is given of the several vegetation types which are used during the research. The salt marsh states are determined using various literature sources, see section 2.5. The *Pioneers* and *Rhizophora* mangroves types are based on work of [Janssen \(2016\)](#). The *Global run* types used in the global assessment are based on [van Wesenbeeck and Dijkstra \(2017\)](#).

### Salt marshes

	Stem density [stems/m <sup>2</sup> ]	Stem diameter [mm]	Stem height [m]	Drag coefficient [-]
<i>Very sparse</i>	300	1.25	0.20	0.17
<i>Global run</i>	1225	1.25	0.30	0.19
<i>Denser</i>	1225	1.25	0.50	0.21

Table E1: Salt marsh vegetation characterizations for numerical modeling

### Mangroves

	Stem density [stems/m <sup>2</sup> ]	Stem diameter [mm]	Stem height [m]	Drag coefficient [-]
<i>Pioneers</i>				
section 1	2.10	1000	1.0	0.6
section 2	1.73	1000	1.7	0.5
section 3	1.37	1000	2.3	0.5
section 4	1.00	1000	3.0	0.5
<i>Global run</i>	30	35	3.0	1
<i>Rhizophora</i>				
section 1	0.900	1000	0.167	0.6
section 2	0.743	1000	0.667	0.6
section 3	0.585	1000	1.167	0.6
section 4	0.427	1000	1.667	0.6
section 5	0.270	1000	2.167	0.6
section 6	0.270	1000	5.500	0.882
section 7	0.513	1000	7.167	0.5
section 8	0.757	1000	8.833	0.5
section 9	1.000	1000	10.500	0.5
section 10	0.667	1000	12.167	0.5
section 11	0.333	1000	13.833	0.5

Table E2: Mangrove vegetation characterizations for numerical modeling